Development of solid adsorbent materials for CO_2 capture

Chidi Premie Ogbuka

B.Tech (Hons), AMInstoP, MSc

Thesis submitted to the University of Nottingham for the degree of Doctor of Philosophy

September 2012

Dedication

This work is dedicated to my wife Abuoma Ogbuka, and my children; Jason, Zoe and Nathan

Abstract

The application of solid adsorbents for gas separation in pre-combustion carbon capture from gasification processes has gained attention in recent times. This is due to the potential of the technology to reduce the overall energy penalty associated with the capture process. However, this requires the development of solid adsorbent materials with large selectivity, large adsorption capacity, fast adsorption kinetics for CO_2 coupled with good mechanical strength and thermal stability. In this work, results on CO_2 adsorption performance of three different types of adsorbents; a commercial activated carbon, phenolic resin activated carbons and zeolite templated carbons have been reported at atmospheric and high pressures conditions. The commercial activated carbon was obtained from Norit Carbons UK, the phenolic resin activated carbon was obtained from MAST Carbon Ltd., while the templated carbons were synthesized in the laboratory. A commercial activated carbon was used as bench mark for this study. Surface modification of these carbons was also undertaken and their CO_2 uptake measurements at ambient and high pressure conditions were recorded. The commercial and templated carbons were modified by functionalising with amine group, while the phenolic resin carbon was modified by oxidation.

The textural properties of the adsorbents was examined using the Micromeritics ASAP, while the CO_2 adsorption capacities were conducted using the thermogravimetric analyser (TGA) and the High pressure volumetric analyser (HPVA).

Textural properties of synthesized templated adsorbents were seen to depend on the textural characteristics of the parent material. The β-type zeolite

produced the carbons with the best textural property. Increase in activation temperature and addition of furfuryl alcohol (FA) enhanced the surface area of most of the templated carbons. The textural property of all the adsorbents under study was seen to differently affect the CO_2 uptake capacity at atmospheric (0.1 MPa) and high pressure conditions (up to 4 MPa).

Micropore volume and surface area of the commercial activated carbons, phenolic resin activated carbons, and the templated carbons greatly influenced the adsorption trends recorded at ambient conditions. Total pore volumes positively influenced adsorption trend for templated carbons, but not the phenolic resin activated carbons at ambient and high pressure. This also positively influenced the adsorption trend for the commercial activated carbons, but at ambient conditions only. The surface area and the micropore volume have no effect on the adsorption trends for the templated carbons and the commercial activated carbons at high pressure conditions. However, these played a positive role in the adsorption capacities of the phenolic resin activated carbons at the same experimental conditions.

Micropore volume and surface area of adsorbents play a major role on the adsorption trends recorded for the modified adsorbents at ambient conditions only. No trend was recorded for adsorption capacities at high pressure conditions. Only the oxidized phenolic resin activated carbon showed a positive adsorption trend with respect to total pore volume at high pressure condition. The amine modified commercial activated carbon showed no positive adsorption trend with respect to the total pore volume at both ambient and high pressure conditions, while the amine modified templated carbon showed no adsorption trend with respect to the textural properties at ambient and high pressure conditions.

CO_2 uptake measurements for the modified and unmodified templated carbon and phenolic resin carbon, were observed to be higher than those of the commercial activated carbon at ambient and high pressure conditions. Maximum CO_2 uptake was recorded at 25 ^oC. At ambient pressure, the phenolic resin carbon (MC11) showed the highest CO_2 uptake of approximately 3.3 mmol g^{-1}, followed by the commercial activated carbon (2.4 mmol g^{-1}), then, the templated carbon (2.4 mmol g^{-1}). At high pressure, the templated carbons (β-AC7-2%) showed the highest CO_2 uptake (21.3 mmol g^{-1}), followed by phenolic resin carbon (MC4 - 12.2 mmol g^{-1}), and the commercial activated carbon (6.6 mmol g^{-1}). When samples were modified, the amine modified templated carbon and oxidized phenolic resin carbon showed the highest CO_2 uptake of 2.9 mmol g^{-1} each at ambient pressure, followed by the commercial activated carbon (2.7 mmol g^{-1}). At high pressure conditions, the oxidized phenolic resin carbon showed the highest (10.6 mmol g^{-1}) uptake level, followed by the templated carbon (8.7 mmol g^{-1}), and commercial activated carbon (6.5 mmol g^{-1}).

Affirmation

Conference proceedings

- Performance of zeolite derived activated carbon on pre-combustion CO_2 capture. 5th international conference on Clean Coal Technologies (CCT2011), Zaragoza Spain (8-13th may 2011)
- High pressure CO_2 adsorption on zeolite derived activated carbon and application in gasification. 9th European Conference on Coal Research and its application; ECCRIA9, University of Nottingham, 10-12th September, 2012.

Poster presentations

- CO_2 capture using adsorption: Application in gasification; Centre for Innovation on Carbon Capture and Storage (CICCS) annual conference, University of Nottingham, November 2009
- Modification of activated carbons and its performance on CO_2 adsorption in gasification; MEGS Xmas seminar, University of Birmingham, December, 2010.
- Performance of phenolic resin activated carbon on CO_2 adsorption in gasification; Social science research for a low carbon future: seminar of the Midlands Energy Consortium and Nottingham's Centre for Advanced Studies, April 2010
- Zeolite beta templated carbon and CO_2 uptake in gasification; The Midlands Energy Graduate School II Annual Conference: Uncertainty and Risk in Energy Futures, Nottingham, 8-9th September 2011.
- High pressure CO_2 adsorption on zeolite derived activated carbon and application in gasification: Postgraduate research showcase, Energy

and sustainability research division, University of Nottingham April 2012.

- High pressure CO_2 adsorption on templated carbons. Midlands Energy Graduate School 3rd annual conference: systems thinking in energy, Birmingham, 18-19th September 2012.

Publications

- Preparation of zeolite templated activated carbons by chemical vapour deposition and their application to CO_2 capture. Fuel (to be submitted October 2012)
- High pressure CO_2 uptake on zeolite templated carbons. (in preparation)
- Amine modified templated carbons and high pressure co_2 uptake in gasification (in preparation)

Acknowledgements

I would like to thank the Almighty God for giving me the inspiration and strength to complete my study in good health.

I would like to gratefully acknowledge the financial support from the University of Nottingham throughout the course of this study. Also, I would like to appreciate the financial support of the University of Nottingham graduate school and the Midland Energy Graduate School (MEGS) to undertake conference activities to showcase the results of this research.

I would like to thank my supervisor Professor Trevor Drage for his unflinching support throughout my study. He has always been invaluable in his constructive input to this work. Thanks also to Dr. Ron Perry for his support throughout my laboratory work.

I would like to thank the laboratory technicians; Vikki Archibald, David Mee and Marion Bryce for their technical support throughout my study. I also want to thank the following workshop technicians; Mic,Phil, and Mel for their support.

Finally, I would like to thank my family for their prayers and moral support throughout my study. The support of the senior pastor of God's Vineyard Ministries and his family is greatly appreciated. The following friends are highly appreciated for their support; Salome Farrow, Pastor Chijioke Elekwachi and family, Solomon Ewusi, Suleiman Salawu, Atinuke akinbobola, and all those who have in one way or the other contributed to the success of this work. May God bless you all.

Table of Contents

Dedication i
Abstract ii
Affirmation v
Acknowledgements vii
Table of Contents viii
List of Figures xiii
List of Tables xx
CHAPTER ONE 1
1. Introduction 1
1.1 Aims and objectives 6
Aims 6
Objectives 6
1.2 Thesis structure 7
CHAPTER TWO 8
2 Literature review 8
2.1 Introduction 8
2.2 Systems for CO_2 capture from fossil fuels 10
2.3 Cost reduction and alternative capture technologies 16
2.3.1 Cost reduction 16
2.3.2 Alternative capture technologies 18
2.3.2.1 Membranes for CO_2 Removal 19
2.3.2.2 Ionic Liquids 20
2.3.2.3 Sorption-Enhanced Water Gas Shift 20
2.3.2.4 Chemical-looping combustion 22
2.4 CO_2 capture sorbent 23
2.4.1 Metal Organic Frameworks (MOFs) 24
2.4.2 Zeolites 28
2.4.3 Activated alumina 29
2.4.4 Silica gel 30
2.5 Carbon materials 31

2.5.1 Activated carbons 31
2.5.2 Carbon synthesis 34
2.5.3 Carbon post production treatments 41
2.6 CO_2 cyclic processes 45
2.6.1 Temperature swing adsorption 45
Pressure swing adsorption 46
Vacuum swing adsorption 47
2.7 Summary 48
CHAPTER THREE 49
3 Methods and Experimental 49
3.1 Introduction 49
3.2 Construction of the vertical furnace & reactor for chemical vapour deposition (CVD) 50
3.1 Furnace calibration 52
3.2 Experimental procedure for templated carbon preparation 54
3.2.1 Experimental procedure for zeolite carbonisation 57
3.2.2 Polymerisation of furfuryl alcohol onto zeolite channels 59
3.2.3 Hydrofluoric acid (HF) wash and drying Process 59
3.3 Surface modification of carbons 60
3.3.1 Hydrogenation of templated carbons 60
3.3.2 Nitration of templated carbon 63
3.3.3 Reduction of the Nitro Groups on the Carbon 64
3.4 Oxidation of phenolic resin activated carbons 64
3.5 Pore Structure Characterisation of the Carbons 66
3.5.1 Experimental procedure 67
3.6 Adsorption isotherm 68
3.6.1 Classification of isotherms 68
Type I isotherm 69
Type II isotherm 69
Type III isotherm 69
Type IV isotherm 70
Type V isotherm 70
Type VI isotherm 70
3.6.2 Adsorption hysteresis 70

3.7 Methods for interpreting the adsorption isotherms 71
3.7.1 Langmuir Model 71
3.7.2 Brunauer – Emmett – Teller (B.E.T) model 72
3.7.3 Dubinin-Radushkevich (DR) 74
3.7.4 Density functional theory (DFT)/ non-linear density functional theory (NLDFT) 75
3.8 Flash elemental analyser 76
Experimental procedure 76
3.9 Thermogravimetric analyser 77
3.9.1 TGA experimental procedures 77
Proximate analysis 77
CO_2 uptake tests 78
Temperature programmed desorption (TPD) 78
3.10 Adsorption kinetic models 78
3.10.1 Pseudo-first-order 79
3.10.2 Pseudo-second-order 79
3.10.3 Correlation coefficients and error function 80
3.11 Error analysis 81
3.12 The high pressure volumetric analyser (HPVA) 81
3.12.1 Free space analysis 82
3.12.2 Pre-measurement procedure 83
3.12.2.1 Blank analysis 83
3.12.2.2 Sample loading 83
3.12.2.3 Degas procedure 83
3.12.2.4 Analysis procedure 84
3.12.3 The HPVA experimental procedure 84
CHAPTER FOUR 89
4 Phenolic Resin Activated Carbons for CO_2 Capture in Gasification 89
4.0 Introduction 89
4.1 Elemental analysis and pore structure characterisation of carbons .. 90
4.2 CO_2 Uptake Capacity at atmospheric pressure 94
4.2.1 Effect of total pore volume, surface area and micropore volume on CO_2 adsorption 97
4.2.2 CO_2 Adsorption and temperature 99
4.3 CO_2 uptake at high pressure 101

4.4 Summary 104
CHAPTER FIVE 105
5 Zeolite templated carbons 105
5.1 Introduction 105
5.2 Pore structure properties of the zeolite template 105
5.3 Effects of template and different synthetic conditions on the textural properties of adsorbents 108
5.4 CO_2 capacity measurements at atmospheric pressure 117
5.5 Adsorption kinetic studies 125
5.6 High pressure CO_2 adsorption 129
5.7 Summary 136
CHAPTER SIX 138
6 Influence of carbon surface modification 138
6.1 Introduction 138
6.2 Amine modified commercial activated carbon 139
6.2.1 CO_2 uptake measurements of commercial activated carbon ... 142
6.3 Oxidized phenolic resin activated carbon 149
6.3.1 Chemical and textural properties of Oxidized phenolic resin carbon 149
6.3.2 CO_2 uptake measurements at ambient pressure: influence of textural properties and surface chemistry 152
6.3.3 High pressure CO_2 uptake measurements on oxidized carbons 156
6.4 Amine modified templated carbons 163
6.4.1 Textural properties 163
6.4.2 CO_2 uptake of amine modified templated carbons at ambient pressure 169
6.4.3 Adsorption kinetic studies 175
6.4.4 High pressure CO_2 uptake measurements on amine modified templated carbons 179
6.5 Summary 183
General discussion 185
Chapter Seven 187
7 Conclusions 187
7.1 Overview 187
7.2 Templated carbon synthesis 187

7.3 Caron surface modification 188
7.4 Carbon vapour deposition rig development 188
7.5 Ambient pressure CO_2 adsorption measurements 189
7.6 High pressure CO_2 adsorption measurements 189
Chapter Eight 191
8 Further work 191
8.1 CO_2 capture systems 191
8.2 Templated carbon applications 191
8.3 Recommendations 192
9 References 193
10 Appendices 233
10.1 Appendix 1: Adsorption/desorption isotherms for templated carbons 233
10.2 Appendix 2: Adsorption/desorption isotherms for oxidized carbons 238

List of Figures

Figure 1.1. Probability of exceeding a given global mean temperature increase by 2100 for emission trajectories peaking in 2016 (UNFCCC 2009). 2
Figure 2.1. Typical CCS flowchart (IPCC, 2005). 9
Figure 2.2. Technology options for CO_2 capture (Adapted from IPCC 2005). . 11
Figure 2.3. The SEWGS principle; reaction and adsorption at high pressure (upper) and desorption at low pressure (lower) (ERC, 2010). 21
Figure 2.4 Schematic illustration of secondary building units (SBUs) for MOF-31-39 including linkers and resulting topologies (Jaheon et al., 2001). 27
Figure 2.5 structural illustration of carbon showing a unit cell of graphite (Haris 1997) 32
Figure 2.6. Concept of template carbonisation technique using inorganic porous template. The red and black parts correspond to carbon precursor and carbon respectively (Kyotani, 2006)..... 36
Figure 2.7 illustration of surface modification by attachment of functional groups on carbon surface; (a) amine functional group, (b) nitrogen functional group, (c) oxygen functional group..... 42
Figure 3.1. Experimental method flowchart. 49
Figure 3.2. Schematic of vertical furnace/CVD rig. 51
Figure 3.3. Accurate temperature control profile. 53
Figure 3.4. Flowchart of carbon synthesis route for this study..... 55
Figure 3.5. Setup for synthesis of templated carbons. 55
Figure 3.6. Temperature profile of CVD: (a) CVD at 600 ^{o}C, (b) CVD at 700 ^{o}C. 58
Figure 3.7. Modification steps for activated carbons under study..... 61
Figure 3.8. A schematic of the Hydropyrolysis apparatus. 62
Figure 3.9. Temperature profile for hydrogenation of synthesised carbons. .. 62
Figure 3.10. Setup for the nitration of synthesized carbons. 63
Figure 3.11. BDDT classification of isotherms (Goyal and Bansal, 2005). 69
Figure 4.1. N_2 Adsorption isotherm For MC1, MC2 and MC3 measured at -196 ^{o}C. 92
Figure 4.2. N_2 Adsorption isotherm for MC4, MC5 and MC6 measured at -196 ^{o}C. 93

Figure 4.3. N_2 adsorption isotherms for MC7, MC8 and MC9 measured at -196 °C. 93
Figure 4.4. N_2 adsorption isotherms for MC10 and MC11 measured at -196 °C. 94
Figure 4.5. CO_2 adsorption capacity of the phenolic resin carbons at 25 °C and atmospheric pressure. Error bars are calculated from multiple analysis of the materials. 96
Figure 4.6. CO_2 adsorption capacity in relation to BET surface area at ambient temperature and pressure..... 98
Figure 4.7. CO_2 adsorption capacity in relation to micropore volume at ambient temperature and pressure..... 98
Figure 4.8. CO_2 adsorption capacity in relation to total pore volume at ambient temperature and pressure..... 99
Figure 4.9. CO_2 adsorption at 25, 50, 75, and 100 °C determined by TG analysis. 100
Figure 4.10. Non-isothermal CO_2 capture tests: heating rate of 0.25 °C min^{-1} in 98 mL min^{-1} of CO_2 flow..... 101
Figure 4.11. Correlation of CO_2 uptake capacity and total pore volume measured at 25 °C and 4.1MPa. 102
Figure 4.12. Correlation of CO_2 uptake capacity and surface area measured at 25 °C and 4.1MPa. 103
Figure 4.13. Correlation of CO_2 uptake capacity and micropore volume measured at 25 °C and 4.1MPa. 103
Figure 4.14. CO_2 adsorption isotherm measured at 25 °C and 4.1 MPa..... 104
Figure 5.1. Nitrogen adsorption isotherms for mordenite, β-type and γ-type zeolites measured at -196 °C..... 106
Figure 5.2. Nitrogen adsorption isotherms for β-type zeolite templated carbons measured at -196 °C. 111
Figure 5.3. Nitrogen adsorption isotherms for γ-type zeolite templated carbons measured at -196 °C. 112
Figure 5.4. Nitrogen adsorption isotherms for mordenite templated carbons measured at -196 °C. 112
Figure 5.5. NLDFT pore size distribution for zeolite β templated carbons measured at -196 °C. 113

Figure 5.6. NLDFT pore size distribution for zeolite γ templated carbons measured at -196 °C. 113
Figure 5.7. NLDFT pore size distribution for mordenite templated carbons measured at -196 °C. 114
Figure 5.8. Effect of S_{BET} on CO_2 uptake of studied adsorbents at 25 °C 118
Figure 5.9 Effect of micropore volume on CO_2 uptake of studied adsorbents at 25 °C..... 118
Figure 5.10 Contribution of micropores to CO_2 uptake 119
Figure 5.11 Contribution of mesopores to CO_2 uptake..... 119
Figure 5.12. Errors associated with CO_2 uptake of the different adsorbents at 25 °C..... 122
Figure 5.13. CO_2 adsorption on γ-AC6-5% at 25 °C. The experimental data was fitted by the pseudo-first order and pseudo-second order models. 127
Figure 5.14. CO_2 adsorption on γ-AC6-5% at 40 °C. The experimental data was fitted by the pseudo-first order and pseudo-second order models. 127
Figure 5.15. CO_2 adsorption on γ-AC6-5% at 60 °C. The experimental data was fitted by the pseudo-first order and pseudo-second order models. 128
Figure 5.16. CO_2 adsorption on γ-AC6-5% at 80 °C. The experimental data was fitted by the pseudo-first order and pseudo-second order models. 128
Figure 5.17. Effect of micropore volume on CO_2 uptake capacity of carbons at 4.1 MPa. 131
Figure 5.18. Effect of surface area on CO_2 uptake capacity of studied adsorbents at 4.1 MPa. 132
Figure 5.19. Effect of total pore volume on CO_2 uptake capacity of studied adsorbents at 4.1 MPa. 132
Figure 5.20. CO_2 adsorption isotherms measured at 25 °C. 133
Figure 5.21. CO_2 adsorption isotherms at 40 °C. 133
Figure 5.22. CO_2 uptake of γ-AC7-AC-5% at 25 and 40 °C at high pressure. 134
Figure 5.23. Adsorption comparison at 25 °C between mmol g^{-1} and mmol cm^{-3} at 4.1 bar. 136

Figure 6.1. Nitrogen adsorption isotherm of unmodified and modified commercial activated carbon measured at -196 ^{o}C. 141
Figure 6.2. NLDFT pore size distribution for unmodified and modified commercial activated carbon measured at -196 ^{o}C. 141
Figure 6.3. CO_2 uptake trend for commercial active carbon and modified carbon with respect to micropore volume measured at ambient temperature and pressure. 143
Figure 6.4. CO_2 uptake trend for commercial active carbon and modified carbon with respect to surface area measured at ambient temperature and pressure. 144
Figure 6.5. CO_2 uptake trend for commercial active carbon and modified carbon with respect to total pore volume measured at ambient temperature and pressure. 144
Figure 6.6. Temperature programmed desorption for CL, H_2-NH_2CL_{40}, and H_2-NH_2CL_{50}: heating rate of at 5 ^{o}C min^{-1} in 98 cm^3 min^{-1} of N_2 flow at ambient pressure. 145
Figure 6.7. Non-isothermal CO_2 capture tests: heating rate of 0.25 ^{o}C min^{-1} in 98 mL min^{-1} of CO_2 flow at ambient pressure. 145
Figure 6.8. CO_2 Adsorption isotherm for unmodified and amine modified commercial activated carbon at 25 oC and pressures up to 4.1 MPa. 147
Figure 6.9. CO_2 uptake trend for commercial active carbon with respect to micropore volume measured at 25 ^{o}C and 4.1 MPa. 147
Figure 6.10. CO_2 uptake trend for commercial active carbon with respect to surface area measured at 25 ^{o}C and 4.1 MPa. 148
Figure 6.11. CO_2 uptake trend for commercial active carbon with respect to total pore volume measured at 25 ^{o}C and 4.1 MPa. 148
Figure 6.12. Non-isothermal CO_2 capture tests: heating rate of 0.25 ^{o}C min^{-1} in 98 mL min^{-1} of CO_2 flow. 154
Figure 6.13. CO_2 uptake trend for oxidized carbon with respect to micropore volume measured at ambient temperature and pressure. 155
Figure 6.14. CO_2 uptake trend for oxidized carbon with respect to surface area measured at ambient temperature and pressure. 155
Figure 6.15. CO_2 uptake trend for oxidized carbon with respect to total pore volume measured at ambient temperature and pressure. 156

Figure 6.16. CO_2 adsorption/desorption isotherms for oxidized carbons at 25 ^{o}C and pressures up to 4.1 MPa. 158
Figure 6.17. CO_2 adsorption/desorption isotherms for oxidized carbons at 40 ^{o}C and pressures up to 4.1 MPa. 158
Figure 6.18. Adsorption isotherms for MNA1-1 carbons at 25 and 40 ^{o}C and pressures up to 4.1 MPa. 159
Figure 6.19. CO_2 uptake trend for oxidized carbons with respect to micropore volume measured at 25 ^{o}C and 4.1 MPa..... 161
Figure 6.20. CO_2 uptake trend for oxidized carbon with respect to surface area measured at 25 ^{o}C and 4.1 MPa..... 161
Figure 6.21. CO_2 uptake trend for oxidized carbon with respect to total pore volume measured at 25 and 4.1 MPa..... 162
Figure 6.22. CO_2 uptake trend for oxidized carbon with respect to oxygen content of the adsorbent at 25 ^{o}C and 4.1 MPa. 162
Figure 6.23. Adsorption/desorption profile for amine modified β-type carbons measured at -196 ^{o}C. 164
Figure 6.24. Adsorption/desorption profile for amine modified γ-type carbons measured at 196 ^{o}C. 164
Figure 6.25. Pore distribution profile for amine modified β–type carbons measured at -196 ^{o}C. 165
Figure 6.26. Pore distribution profile for amine modified γ-type carbons measured at -196 ^{o}C. 165
Figure 6.27. Thermal stability profile of amine modified adsorbents; heating rate 10 ^{o}C min^{-1} in nitrogen; 50 ^{o}C min^{-1} in air..... 167
Figure 6.28. CO_2 uptake of amine modified templated carbons measured at ambient pressure conditions..... 171
Figure 6.29. CO_2 uptake trend for amine modified templated carbons with respect to micropore volume measured at ambient pressure conditions. 171
Figure 6.30. CO_2 uptake trend for amine modified templated carbons with respect to surface area measured at ambient pressure conditions... 172
Figure 6.31. CO_2 uptake trend for amine modified templated carbons with respect to total pore volume measured at ambient pressure conditions. 172

Figure 6.32. TPD profile for amine modified β-type adsorbents during heating in 98 mL min^{-1} of N_2 flow at a heating rate of 5 ^oC min^{-1} up to 105 ^oC. 173
Figure 6.33. TPD profile for amine modified γ-type adsorbents during heating in 98 mL min^{-1} of N_2 flow at a heating rate of 5 ^oC min^{-1} up to 105 ^oC. 174
Figure 6.34. CO_2 adsorption on NH_2-γ-AC6-5% at 25 ^oC. The experimental data was fitted by the pseudo-first order and pseudo-second order models. 177
Figure 6.35. CO_2 adsorption on NH_2-γ-AC6-5% at 40 ^oC. The experimental data was fitted by the pseudo-first order and pseudo-second order models. 177
Figure 6.36. CO_2 adsorption on NH_2-γ-AC6-5% at 60 ^oC. The experimental data was fitted by the pseudo-first order and pseudo-second order models. 178
Figure 6.37. CO_2 adsorption on NH_2-γ-AC6-5% at 80 ^oC. The experimental data was fitted by the pseudo-first order and pseudo-second order models. 178
Figure 6.38. adsorption isotherm of amine modified templated carbons measured ambient temperature and 4.1 MPa. 180
Figure 6.39. Correlation of equilibrium CO_2 uptakes at 4.1MPa with micropore volume for selected amine modified templated carbons. 181
Figure 6.40. Correlation of equilibrium CO_2 uptakes at 4.1MPa with surface area for selected amine modified templated carbons. 182
Figure 6.41. Correlation of equilibrium CO_2 uptakes at 4.1MPa with total pore volume for selected amine modified carbons. 182
Figure 10.1. CO_2 uptake of γ-PFA-AC7-5% at 25 and 40 ^oC at high pressure. 233
Figure 10.2. CO_2 uptake of β-AC6-5% at 25 and 40 ^oC at high pressure. ... 234
Figure 10.3. CO_2 uptake of β-PFA-AC6-5% at 25 and 40 ^oC at high pressure. 234
Figure 10.4. CO_2 uptake of β-PFA-AC6+AC7-5% at 25 and 40 ^oC at high pressure. 235
Figure 10.5. CO_2 uptake of β-PFA-AC7-5% at 25 and 40 ^oC at high pressure. 235

Figure 10.6. CO_2 uptake of β-AC7-5% at 25 and 40 ^oC at high pressure. ... 236
Figure 10.7. CO_2 uptake of β-AC6-2% at 25 and 40 ^oC at high pressure. ... 236
Figure 10.8. CO_2 uptake of β-PFA-AC7-2% at 25 and 40 ^oC at high pressure. 237
Figure 10.9. CO_2 adsorption isotherms for MAP-1 carbons at 25 and 40 ^oC and pressures up to 4.1 MPa. 238
Figure 10.10. Adsorption isotherms for MAP-3 carbons at 25 and 40 ^oC and pressures up to 4.1 MPa. 238
Figure 10.11. Adsorption isotherms for MAP-24 carbons at 25 and 40 ^oC and pressures up to 4.1 MPa. 239
Figure 10.12. Adsorption isotherms for MNA1-24 carbons at 25 and 40 ^oC and pressures up to 4.1 MPa. 239
Figure 10.13. Adsorption isotherms for MNA16-1 carbons at 25 and 40 ^oC and pressures up to 4.1 MPa. 240
Figure 10.14. Adsorption isotherms for MNA16-3 carbons at 25 and 40 ^oC and pressures up to 4.1 MPa. 240
Figure 10.15. Adsorption isotherms for MAM carbons at 25 and 40 ^oC and pressures up to 4.1 MPa. 241

List of Tables

Table 2.1. Typical gas conditions. 12
Table 2.2. Key components for each catpure option. 17
Table 2.3. Projected levelised generation costs of the carbon capture components in £/MWh (Edward et al., 2007). 18
Table 2.4. CO_2 uptake of some MOFs. 26
Table 2.5. Pore sizes in a carbon material (IUPAC, 2012). 33
Table 2.6. Summary of some carbon synthesis base materials and techniques. 37
Table 2.7 Chemical modification in carbons 44
Table 3.1. Carbon synthesis matrix. 56
Table 3.2. TGA results from burn off operation of zeolite/carbon composite. . 60
Table 3.3. abbreviations and interpretation of symbols used in Equations 3.21-3.30. 87
Table 4.1 pore structutre properties of activated phenolic resin carbons measured at -196 ^{o}C. 91
Table 4.2 Ultimate analysis of the phenolic resin activated carbons. 92
Table 4.3. CO_2 uptake capacities of phenolic resin carbons at 25 ^{o}C, atmospheric pressure and 100% CO_2 concentration. 95
Table 4.4. Five different runs for MC11 showing different CO_2 uptake at 25^{o}C. 96
Table 5.1. Properties zeolites used for this study. 107
Table 5.2 Porosity characterisation of zeolites used for this study. 107
Table 5.3 Porosity characterisation of the templated carbons 109
Table 5.4 Results of ultimate analysis of templated carbons calculated by dry ash free basis 110
Table 5.5. CO_2 Uptake of adsorbents measure at ambient pressure conditions. 121
Table 5.6. CO_2 uptake for selected templated carbons at 25, 40, 60 and 80 ^{o}C measured at atmospheric pressure. 124
Table 5.7. Comparison of CO_2 uptake capacities at ambient conditions between this study and literatures. 125
Table 5.8. Kinetic model parameters for the CO_2 adsorption on templated carbon (γ-AC6-5%)) at different temperatures. 129

Table 6.1. Textural properties of amine modified activated carbon measured at -196 °C..... 139
Table 6.2. Ultimate analysis for the R2030 and amine modified adsorbents 140
Table 6.3. CO_2 uptake capacities of CL and amine modified commercial activated carbons at ambient pressure. 143
Table 6.4. CO_2 uptake capacities of CL and amine modified commercial activated carbons at higher pressures up to 4.1 MPa. 146
Table 6.5. Textural properties of oxidized phenolic carbons. 151
Table 6.6. Ultimate analysis calculated by dry ash free basis. 151
Table 6.7. CO_2 uptake of oxidized phenolic resin carbons at ambient conditions. 153
Table 6.8. CO_2 uptake measurements for the oxidized carbons at 4.1 MPa. 157
Table 6.9. Textural properties of amine modified carbons. 168
Table 6.10. Ultimate analysis of amine modified adsorbents (dry ash free). 168
Table 6.11. CO_2 uptake of amine modified adsorbents at 25 °C..... 170
Table 6.12. Kinetic model parameters for the CO_2 adsorption on templated carbon (NH_2-γ-AC6-5%)) at different temperatures. 179
Table 7.1. Summary of maximum CO_2 uptake of studied adsorbents at ambient and high pressure conditions. 190

CHAPTER ONE

1. Introduction

The level of CO_2 in the atmosphere has risen by more than a third since the industrial revolution (Pachauri et al., 2007), and is currently increasing faster than ever before. CO_2 constitutes about 380 parts per million (i.e. 0.038%) of the world's atmosphere (Imtiaz-Ul-Islam et al., 2011). The concentration is rising by 2 to 3 parts per million every year (Goodall, 2007). An increase in global mean temperature of up to 5.8 °C could result if the current growth in demand for fossil fuels is not controlled (DTI, 2005). Though in the Copenhagen accord, there was a call to hold the global mean temperature below 2 ^{o}C. The emissions trajectory projection (Figure 1.1) has indicated a 50-80% probability of exceeding the 2 ^{o}C target by 2100.

For the United Kingdom (UK), this will mean a greater likelihood of heat waves, greater risk of flooding and more water stress in the southern and eastern parts. While in developing countries, particularly the poorest ones, this would worsen food security, water availability and health, as well as accelerate biodiversity losses (UNFCCC 2009).

Greenhouse gases; CO_2 NO_x, SO_x, Freon, ozone, methane and nitrous oxide are mainly responsible for global warming. CO_2 contributes approximately 60% to the overall climate change (Goodall, 2007).

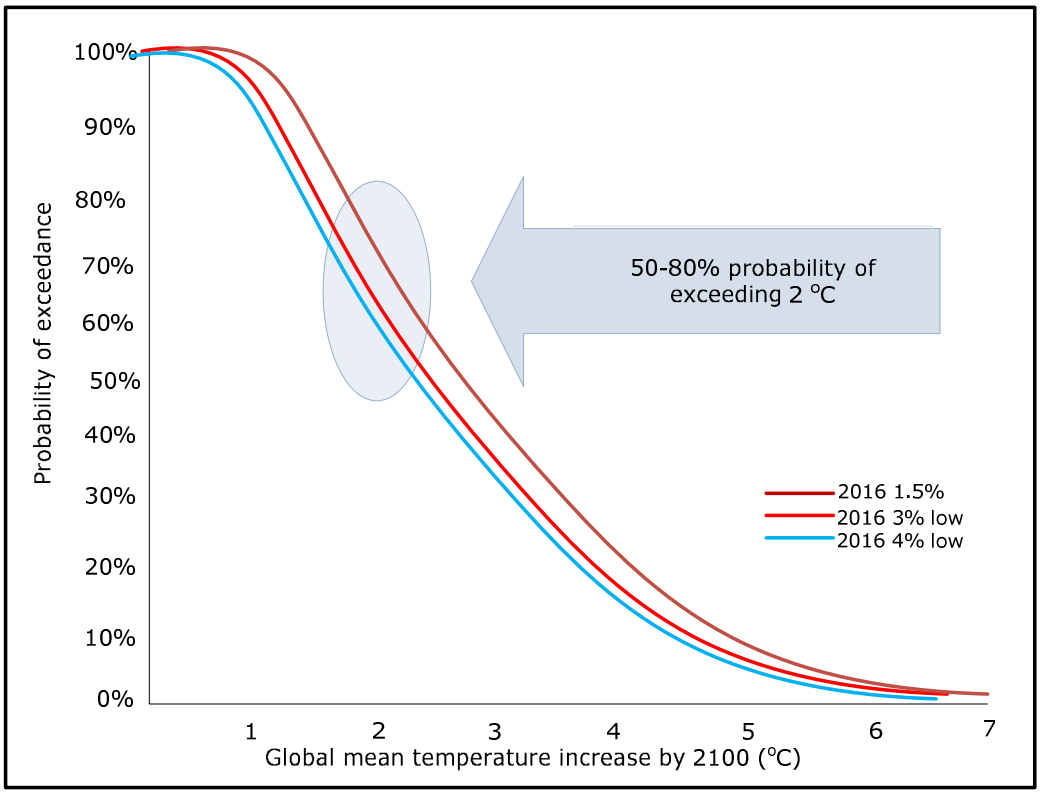

Figure 1.1. Probability of exceeding a given global mean temperature increase by 2100 for emission trajectories peaking in 2016 (UNFCCC 2009).

The Kyoto Protocol (Caplan, 2001; Kojima, 1994), Copenhagen Climate Summit (UNFCCC, 2009), and Carbon Capture and Storage (CCS) legal regulatory workshop held in South Africa (IEA, 2011), all called for international concerted efforts to reduce the amount of CO_2 emitted during domestic, and mostly, commercial and industrial processes. The European Commission in 2008 set new CO_2 emission targets for Britain and other EU member states for an 80% cut by 2050 compared to 2020 levels (OPSI, 2008; DECC, 2012c). Despite all these, global emissions of anthropogenic carbon dioxide hit their highest level in 2010, with the growth driven mainly by booming coal-reliant emerging economies. CO_2 emissions rose by 5.9 percent to 30.6 billion tonnes in 2010 alone (Mohammad et al., 2011). Although, large

gains in energy efficiency are undoubtedly possible and more renewable generation capacity will certainly be deployed, the trend of continued use and dependence on fossil fuels for power generation is very unlikely to reverse in the period to 2050. This implies that the large reductions in CO_2 emissions needed by 2050 will require a major deployment of Carbon Abatement Technologies (CATs) on a world scale (DECC, 2012c).

CATs are a group of innovative technologies that enable large power plants to operate with substantially reduced CO_2 emissions. This means they can be part of the solution to climate change, whilst still making a major contribution to the security of electricity supply. CATs have the potential to reduce carbon emissions from fossil-fuel power stations by up to 90% (TSB, 2009). The application of CATs significantly improves the efficiency of conversion processes in power plants and reduces the amount of fuel consumed during power generation. It also offers technologies that enable fuel switching to lower carbon alternatives such as co-firing with biomass or waste, and finally CCS technologies.

On the international front, the International Energy Agency (IEA) identified three key actions for CCS regulatory development to support CCS. These are; mandate for Organisation for Economic Co-operation and Development (OECD) countries to establish frameworks for CCS demonstration by 2011, while non-OECD countries with CCS potential are given up to 2015; mandate for large scale deployment by 2020; and framework for countries to address international legal issues associated with CCS by 2012 (DoE, 2011). Although significant progress has been made to date towards these goals, there is the urgent need to intensify efforts to meet the greenhouse gas (GHG) reduction targets to avoid damaging the climate. CCS has been identified as one of the

key technologies for application if fossil fuel is to be used for power generation.

CCS is a mitigation technology essential in tackling global climate change, and ensuring a secure energy supply. CCS technology captures carbon dioxide from fossil fuel power stations. The CO_2 captured is then transported via pipelines and stored safely offshore in deep underground structures such as depleted oil and gas reservoirs, and deep saline aquifers. Currently, two hundred and thirty four CCS laboratory and demonstration projects are on-going around the world (APGTF, 2011).

The cost of CCS technology depends on factors such as fuel prices, capital cost of plant, and cost to meet potential regulatory requirements like monitoring etc. However, the cost of employing a full CCS system for electricity generation from a fossil-fired power plant is dominated by the cost of capture. Most energy and economic modelling reported to date suggests that the deployment of CCS systems starts to be significant when carbon prices begin to reach approximately £25-30 per tonne of CO_2 (IPCC, 2005). Studies have also suggested the potential of CCS to address up to 38 Mt of CO_2 emissions per annum in 2030 (decreasing to 37 Mt by 2050), at the costs of between £30 and £150 per tonne of CO_2 abated (DECC, 2012a). The application of capture will add about 5 to 30% parasitic energy losses, 35 to 110 % increase in capital cost, and 30 to 80% increases in electricity cost (Miller, 2011). In effect, it will add about 1.8 to 3.4 US£ct kWh^{-1} to the cost of electricity from a pulverised coal power plant, 0.9 to 2.2 US£ct kWh^{-1} to the cost for electricity from an integrated gasification combined cycle coal power plant, and 1.2 to 2.4 US£ct kWh^{-1} from a natural gas combined cycle power plant (IPCC, 2005) .

The size of the future market for CCS depends mostly on the degree of CO_2 removal and the stringency of the assumed climate stabilization target. The higher the CO_2 emission in the baseline, the more emissions reductions are required to achieve a given level of allowable emissions, and the larger the market for CCS. The present state of short and long term cost implication of CCS has been undertaken. Özge and Reichelstein (2011) have estimated an upper limit for investment in CCS technology for OECD countries to be from £350 to 440 billion over the next 30 years. This estimate was made with the assumption that all new power plant installations will be equipped with CCS. An overall loss of 30% efficiency has been estimated for CCS (HCSTC, 2006). Also, new technological developments and benefits derived from increasing experience and economies of scale could collectively reduce the costs of CCS.

If the UK is to remain amongst the leading nations in CCS technology now and in the future, there is need for widespread deployment of all key CCS technologies. Pre-combustion carbon capture is one major processes/technologies option available. It has the potential for increased power efficiency and reduced cost/energy penalty associated with power generation, and invariably lead to costs reduction in CCS (DECC, 2012c). Whilst solvent based technologies (pre and post carbon capture) and cryogenic separation (oxyfuel) are the most developed for CCS application and the closest to market and deployment. The energy penalties associated with these technologies has led to research and development of a range of alternative, or second and third generation CO_2 capture technologies (Figueroa et al., 2008). Examples of which include, advanced solvents, solid adsorbents, membranes, ionic liquids, SEWGS (Sorption-Enhanced Water-Gas Shift) as well as novel combustion technologies such as chemical looping, Oxygen

Transport Membranes (OTM) cycles. In this research work, efforts have been focused on the development of novel adsorbents that could lead to effective cost reduction in power generation using pre-combustion carbon capture as the lead process/technology.

This work is aimed at producing activated carbons, and screening them for application on pre-combustion carbon capture. Three different carbons will be screened and their physical properties be related to their CO_2 uptake capacity. This research has the potential to produce solid materials with ability to reduce cost associated with power generation.

1.1 Aims and objectives

Aims

The aim of this research work is to develop solid adsorbents that will reduce the cost associated with carbon capture and storage in fossil fuel power plants.

Objectives

The objectives of this work are to:

- Synthesize templated carbons using zeolite as templates.
- Modify synthesized templated carbons with amine based solution and investigate the effect of surface chemistry on adsorption capacity.
- Design and fabricate a chemical vapour deposition rig for use in carbon synthesis.
- Ascertain the CO_2 uptake capacity of oxygen modified activated carbon.
- Ascertain the CO_2 uptake capacity of a commercial activated carbon.
- To characterise the chemical properties and pore structure of the carbons and relate these properties to their CO_2 uptake capacity.

- To determine the CO_2 uptake capabilities of the carbons at low and higher pressures, and identify their trend with surface area, micropore volume, and total pore volume

1.2 Thesis structure

This thesis is divided into seven chapters. Chapter One introduces and discusses the need to mitigate CO_2 and the government's effort towards this. It also presents the aims and objectives of this work. Chapter Two covers the literature review. In this chapter, a detailed literature on systems for CO_2 capture from fossil fuels is discussed, paying more attention to the current state of CCS. Chapter Three covers the fundamental techniques used in obtaining results presented in this thesis. It also presents the working principles of the analytical equipment used, and description of chemical vapour deposition apparatus built during the course of this work.

Chapter Four presents the results obtained by analysing phenolic resin activated carbons. In this chapter, the chemical and textural properties, and the CO_2 uptake capacity of the adsorbents were discussed. Chapter Five presents results obtained by analysing zeolite templated carbons. Also, the chemical and textural properties were discussed and related to the CO_2 uptake of the materials. Chapter Six presents the result obtained from surface modification of selected carbons. In this chapter, the influences of the acidic and basic surface functional groups on the materials CO_2 uptake levels were discussed. Finally, the conclusions and further work is presented in Chapter Seven.

CHAPTER TWO

2 Literature review

2.1 Introduction

Carbon capture and storage (CCS) is a broad term that encompasses a number of technologies that can be used to capture carbon dioxide from point sources, such as power plants, compress it, and transport it mainly by pipeline to suitable storage locations. Captured carbon dioxide may be stored in deep subsurface geological formations, in oceans, terrestrial ecosystems, and through mineral carbonation (WRI, 2012). This technology is a critical option in the portfolio of solutions available to combat climate change. It allows for significant reductions in CO_2 emissions from fossil-based systems, enabling a bridge to a sustainable energy future (Rackley, 2010; Sioshansi, 2010). Figure 2.1 presents a summary of CCS.

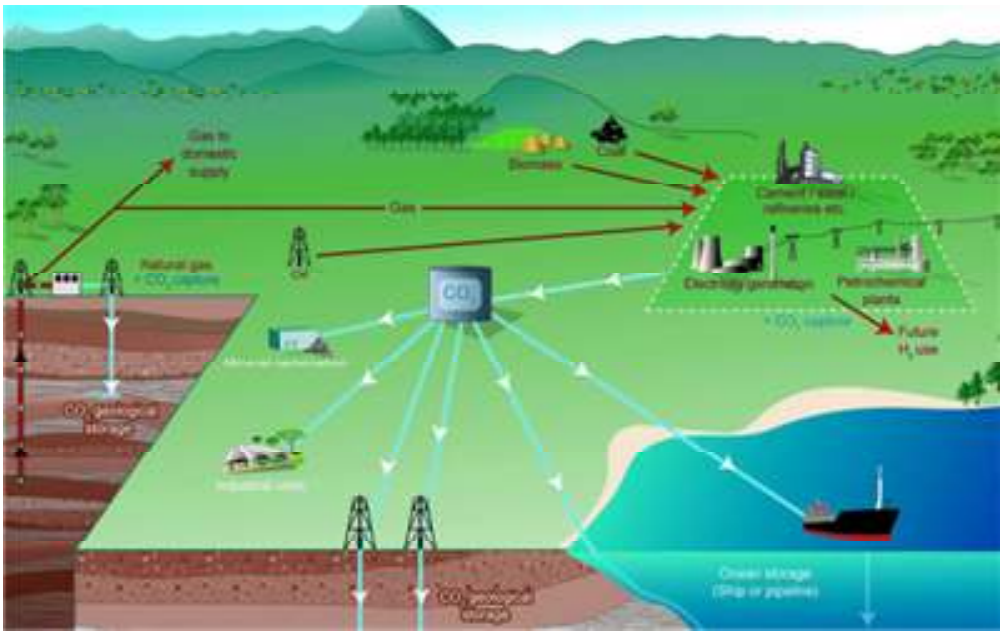

Figure 2.1. Typical CCS flowchart (IPCC, 2005).

There are currently three main approaches to capturing CO_2; post-combustion, pre-combustion, and oxy-fuel combustion. In post-combustion, the CO_2 is removed after direct combustion of the fossil fuel in air. This approach is usually applied to conventional power stations. The carbon dioxide is captured from exhaust gases. The idea of pre-combustion plant involves oxidizing the fuel in a gasifier before combustion. This process produces "syngas" which is made of carbon oxides and hydrogen. The resulting carbon emissions can be removed from the stream, while the hydrogen is burned as fuel to generate electricity. In Oxy-fuel combustion, the fuel is burned in pure oxygen instead of air. The flue gas is mostly CO_2 and water vapour. While the CO_2 is captured for storage, the water vapour is condensed through cooling (Gerard and Wilson, 2007). This chapter concentrates on technologies and systems for CO_2 capture, with emphasis on 2nd generation and novel 3rd generation technologies.

2.2 Systems for CO_2 capture from fossil fuels

Systems for CO_2 capture from fossil fuel combustion may be categorised into four distinct technologies; pre-combustion, post-combustion, oxyfuel combustion, and industrial process capture systems. The capture component of these systems uses either one or a combination of the following physical and chemical separation processes; absorption, adsorption, cryogenics and membranes. The choice of a suitable CO_2 capture technology depends on the characteristics (temperature, total pressure and partial pressure) of the gas stream from which CO_2 is to be separated (Table 2.1). This mainly depends on the power plant technology. The CO_2 content ranges from 3% to 15%, the lower end of this range (3-5%) is typical for gas-fired plants while the upper end (12-15%) for coal-fired plants (Rackley, 2010). A range of technologies are currently in place for the separation and capture of CO_2 from gas streams. Figure 2.2 shows the technology options for CO_2 capture.

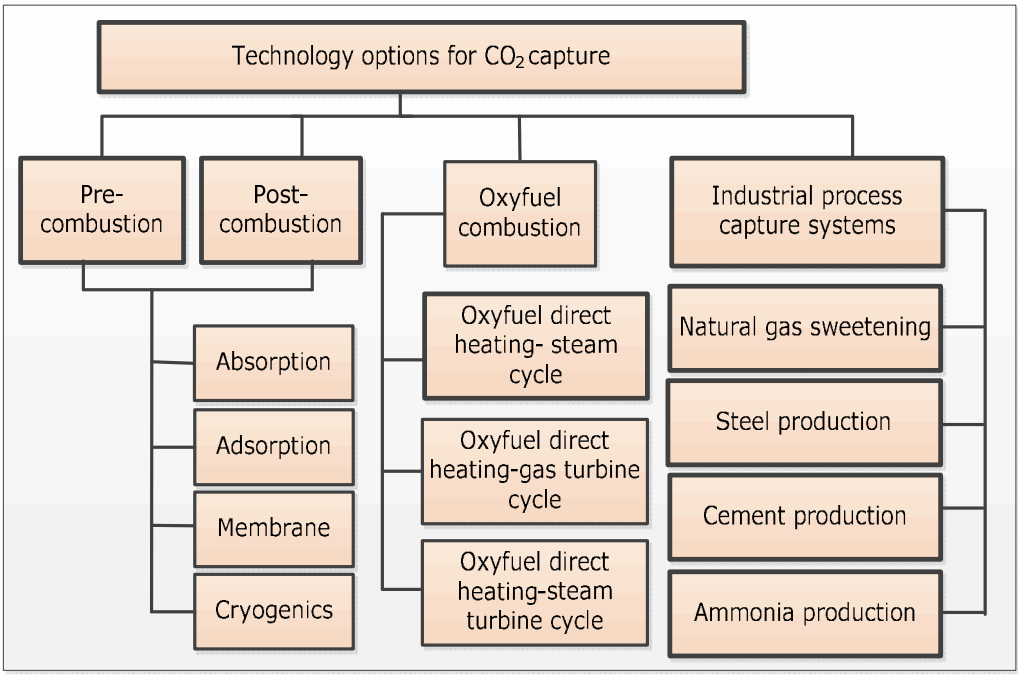

Figure 2.2. Technology options for CO_2 capture (Adapted from IPCC 2005).

The pre-combustion system combines the latest coal gasification technology with the highly efficient combined cycle power generation technology, that has been developed for natural gas combustion. The Integrated Gasification Combined Cycle (IGCC) is an example of system that uses this process. The syngas generated in the gasifier of IGCC is a gaseous mixture of CO and H_2 at high pressure (Rackley, 2010). Depending on the type of gasifier design, the temperature and pressure conditions vary from 800-1400 ^{o}C and 20-3400 kPa respectively (Gerard and Wilson, 2007). Typical commercial gasification process today operates in the range of 2500-8000 kPa depending on application (Higman, 2010). The syngas is passed through water-gas shift reaction (Equations 2.1 and 2.2). This reaction converts the CO into CO_2 which will be ready for capture.

$$Coal\ gasification \rightarrow CO + H_2 \ldots\ldots\ldots\ldots (2.1)$$

$$CO + H_2O_{(g)} \rightarrow CO_2 + H_2 \ldots\ldots\ldots\ldots\ldots\ldots 2.2)$$

It is easier to capture and separate CO_2 from the syngas because of the high concentration of CO_2 and the high pressure (approximately 7.3 kPa) of the syngas (Gerard and Wilson, 2007). This also makes it possible to use less energy to compress the CO_2 to desired pressure level for pipeline transportation. Table 2.1 shows the typical gas conditions for the pre-, and post-, and oxy fuel combustion carbon capture.

Table 2.1. Typical gas conditions.

	Pre-combustion capture (before water gas shift)[a]	Post combustion capture[b]	Oxy-fuel combustion capture[c]
Gas composition			
CO_2	35.5 %	15-16 %	87.95 mol%
H_2O	0.2 %	5-7 %	3.51 mol%
H_2	61.5 %	-	-
O_2	-	3-4 %	8.54 mol%
CO	1.1 %	20 ppm	-
N_2	0.25 %	70-75 %	-
SO_x	-	800 ppm	-
NO_x	-	500 ppm	-
H_2S	1.1 %	-	-
Conditions			
Temperature	40 ^oC	50-75 ^oC	247 ^oC
Pressure	50-60 bar	1 bar	17 bar

[a] (Rectisol, 2006): [b] (Granite and Pennline, 2012); [c] (Lui et al., 2012)

The pre-combustion capture system has a lower energy penalty compared to the other technology options (DECC, 2012b), hence, its applicability to my research work. It also has multi-product flexibility since the H_2 produced after CO_2 capture can be used in the gas turbine to generate power or other valuable uses.

Pre-combustion carbon capture technologies are extremely efficient compared to post-combustion flue gas capture due to increased concentration of CO_2. CO_2 emissions may be reduced by 90 to 95 percent in a pre-combustion system (MNA, 2012). The world's first pre-combustion CCS pilot plant (14 MWth) has been in operation since 2010 at ELGOGAS IGCC (335), in Spain (Haszeldine, 2009). An example of technology with pre-combustion carbon capture is the integrated gasification combined cycle (IGCC). IGCC technology has three basic components. In the gasification phase, heat, pressure, pure oxygen and water are used to break coal down into its component parts and convert it into a clean synthetic gas (syngas). The syngas is cleaned before it can be converted by methanation into substitute natural gas (SNG) which eventually fuels the power turbines. Remaining particulates are removed from the syngas in the particulate scrubber. Carbon monoxide is converted by the shift reaction into carbon dioxide (CO_2). The gasification process makes it possible to capture most of the mercury, sulphur and carbon dioxide (CO_2) in the syngas. The captured CO_2 will be transported via pipeline for use in enhanced oil recovery or storage in a saline geologic reservoir. The SNG, which is relatively high in energy content, powers a gas turbine and waste exhaust gas heat then powers a steam turbine. The higher energy content of the SNG (as compared with syngas) improves the efficiency of the power production. Because the SNG is a clean fuel, nitrogen oxide (NOx) also can be reduced considerably during and after combustion. The results are substantially lower emissions compared to conventional pulverized coal plants.

Oxy-fuel combustion involves the use of pure oxygen instead of air for the combustion process. It is easier to capture almost all the CO_2 using this method because only CO_2, water and traces of other compounds are formed as

flue gases. The principal attraction of oxy-combustion is that it avoids the need for a costly post-combustion CO2 capture system. Instead, however, it requires an air separation unit (ASU) to generate the relatively pure (95-99 percent) oxygen needed for combustion. Roughly three times more oxygen is needed for oxy-fuel systems than for an IGCC plant of comparable size, so the ASU adds significantly to the cost. Oxy-fuel combustion system has higher boiler efficiency and a much lower NO_x formation level (Gerard and Wilson, 2007). It has been reported by Figueroa et al., (2008) that this technology gives a nitrogen-free combustion which leads to reduction in equipment size, heat losses, and savings in the cost of flue gas treatment. This also opens the possibility for a zero-emission technology in coal power plants, since almost all the CO_2 from the plant can be captured. However, lack of fundamental knowledge for boiler design for pure oxygen combustion limits the application of this technology (Edward et al., 2007; Maroto-Valer, 2010). Also, large quantity of oxygen is required for a typical power plant, and as temperature may go out of control during combustion, large quantity of CO_2 is required for cooling. There are also concerns that oxy-fuel combustion systems may have higher CO emissions which may pose environmental problems (Edward et al., 2007). The oxy-fuel combustion system might be more expensive due to the cost involved in producing pure oxygen. Oxy-fuel combustion has been studied in laboratory and pilot plant facilities at scales of 30 MW_t (Edward et al, 2012). By 2020, the UK plans to demonstrate the first oxyfuel plant with a capacity of 100-500MW_e (Cameron et al., 2011).

Post-combustion capture technologies capture CO_2 after normal fuel combustion in air. This system leads to a flue gas with diluted stream of CO_2 mixed with a large amount of N_2 and small proportions of H_2O, O_2, and CO.

One of the most commonly used processes for flue gas removal is flue gas scrubbing using amine solvents (Maceiras et al., 2008).

In a modern coal-fired power plant, pulverized coal (PC) is mixed with air and burned in a furnace or boiler. The heat released by combustion generates steam, which drives a turbine-generator. The hot combustion gases exiting the boiler consist mainly of nitrogen (from air) plus smaller concentrations of water vapour and CO_2 formed from the hydrogen and carbon in the fuel. Additional products formed during combustion from impurities in coal include sulphur dioxide, nitrogen oxides and particulate matter (fly ash). These regulated air pollutants, as well as other trace species such as mercury, must be removed to meet applicable emission standards. In some cases, additional removal of pollutants (especially SO_2) is required to provide a sufficiently clean gas stream for subsequent CO_2 capture. With current technology, the most effective method of CO_2 capture from the flue gas of a PC plant is by chemical reaction with an organic solvent such as monoethanolamine (MEA), one of a family of amine compounds. In an absorber, the flue gas is "scrubbed" with an amine solution, typically capturing 85 to 90 percent of the CO_2. The CO_2-laden solvent is then pumped to a second vessel (regenerator or stripper), where heat is applied in the form of steam to release the CO_2. The resulting stream of concentrated CO_2 is then compressed and piped to a storage site, while the depleted solvent is recycled back to the absorber. There is still on-going research and development in this area. Some of the solvents required for its functionality are lost through physical losses, entrainment, vapourization, and chemical degradation during operation (Yokoyama, 2004; Yagi et al., 1992; Mandal et al., 2001). To date, post-combustion capture has been proven on

rigs at up to ~60 MW. The Ferrybridge pilot plant is an example of a project which captures 100 tonnes of CO_2 per day (DECC, 2012b).

Other industrial process streams exist which are sources of CO_2 emissions but which are not captured including cement and steel production, and processing of food and drinks during fermentation (Rackley, 2010; IPCC, 2005b). CO_2 can be captured from these streams by using the post-combustion, oxy-fuel combustion and/or pre-combustion techniques.

2.3 Cost reduction and alternative capture technologies

2.3.1 Cost reduction

All main capture technologies have four common components- development and capture costs, compression, balance-of-plant, and host plant compensation (IEA, 2006). Note that balance of plant refers to the remaining items not covered by other categories, and typically would include supporting facilities and peripherals such as water treatment, fuel handling, storage and treatment, controls and instrumentation, transformers, switchgear and electrical connections.

Compression cost is highest for post combustion, especially for gas, slightly less for oxy combustion and much lower for pre combustion. Pre combustion's lower requirement reflects the fact that gasification processes work at elevated pressures (DECC, 2010; ZEP, 2011). Host plant compensation is a product of the energy penalty (in percentage terms) and the specific capital expenditure (capex) of the host plant. Therefore, the host plant compensation is much less for gas post combustion, since the efficiency penalty and the capex costs are

low. The host compensation for post combustion coal is much higher, with pre combustion having a greater penalty given the initial high costs of host plant (despite a lower energy penalty) (DECC, 2012b). The key components for each capture option are presented in Table 2.2.

Table 2.2. Key components for each catpure option.

	Post combustion	Oxy combustion	Pre combustion
Pre-development costs	*	*	*
Absorber	*		
Stripper/regenerator	*		
Air separation		*	
Gas conditioning		*	
Water shift			*
Acid gas treatment			*
CO_2 compression	*	*	
Balance of plant	*	*	*
Host plant compensation	*	*	*

Source: Mott McDonald estimates

Given the early stage of CCS development, there are no commercial scale full chain projects operating. Therefore, there is great uncertainty in making cost projections. However, there is certainty regarding the host plant costs (for super critical coal and combine cycle gas turbine (CCGT), at least). Although, there are uncertainties about future capital costs as engineering, procurement and construction (EPC) markets have become commoditised (and subject to demand and supply pressures), and fuel prices are even more uncertain. Analysis by DECC, (2012c) suggests that post- and oxy- combustion coal are seen as the most expensive options with capture levelised costs of £41-62 MWh^{-1} in 2013 (Table 2.3), but technologies (especially oxy combustion) are projected to see deep reductions in absolute and relative terms. Post combustion gas, starting from a lower level (£29-42 MWh^{-1}) shows a less dramatic reduction, but still remains the lowest cost capture option. Pre-

combustion, which is expected to have a lower incremental cost in the near term than the other coal options (at £33-52 MWh^{-1}), is projected to see a more modest decline than the other options, albeit some improvement on its trend over the last two decades. Levelised cost of electricity from both coal and gas plant with CCS is projected to fall to £100 MWh^{-1} in the 2020s. The post- and oxy- combustion coal options are projected to see a £16-19 MWh^{-1} (30-48%) reduction in levelised costs between 2013 and 2040, versus £10-12 MWh^{-1} (27-43%) for gas and £4-9 MWh^{-1} (8-29%) for pre-combustion (DECC, 2012c) .

Table 2.3. Projected levelised generation costs of the carbon capture components in £/MWh (Edward et al., 2007).

	Levelised cost (£/MWh)				Period-on-period reduction (£/MWh)		
Low cost path:	2013	2020	2028	2040	2020	2028	2040
Post combustion coal	42.3	33.5	28.3	23.7	8.8	5.2	4.6
Post combustion gas	29.3	23.8	20.2	16.5	5.5	3.5	3.7
Oxy combustion coal	41.4	32.0	26.0	21.3	9.4	6.0	4.6
Pre combustion	32.9	28.3	25.2	23.6	4.6	3.2	1.6
High cost path:							
Post combustion coal	61.3	53.8	48.6	43.0	7.5	5.2	5.6
Post combustion gas	42.3	38.4	34.4	30.6	3.9	4.0	3.8
Oxy combustion coal	61.9	53.9	47.4	41.8	8.0	6.6	5.6
Pre combustion	51.7	49.6	48.2	47.9	2.1	1.4	0.4

*Levelised costs are for capture only including host plant compensation (i.e. incremental costs of capture on generation. Values were calculated using fixed fuel price

2.3.2 Alternative capture technologies

The selection of capture technology depends on the physical state, pressure, CO_2 partial pressure, and volume of gas to be separated (Thomas and Benson, 2005). At present, the most mature technologies to be used in CCS

demonstration plant are solvent based. Physical and chemical based solvents are currently the preferred technology for pre and post-combustion capture respectively. Solvent based technologies (pre and post-carbon combustion) and cryogenic separation (oxyfuel) are the most developed for CCS application and the closest to market and deployment. The energy penalties associated with these technologies has led to research and development of a range of alternative, or second and third generation CO_2 capture technologies (Figueroa et al., 2008). This drive for alternative technologies also stems from the need to reduce the costs associated with CCS as previously indicated in Section 2.3.1. Many of these technologies are currently at the laboratory/fundamental level of research in terms of materials and process development for CCS. Some of the alternative technologies are briefly discussed below.

2.3.2.1 Membranes for CO_2 Removal

Membranes are thin semipermeable barriers that selectively separate some compounds from others. This definition is necessarily broad because of the large variety of membrane materials separating an equally vast number of compounds in all phases. Applications include:

- Ceramic membranes for gas purification in the semiconductor industry
- Palladium-based metallic membranes for hydrogen extraction
- Silicon rubber membranes for organic vapour recovery from air
- Polyvinyl alcohol-based membranes for ethanol dehydration

Membrane gas separation shows different advantages over conventional processes and has been well described in Stern, (2002); Maier, (1998); and Koros, (2002). Although, membrane technology is widely used for gas separation, it is not yet applied on the scale of power plants (Basile and Julianelli, 2010). The only commercially viable membranes used for CO_2

removal are polymer based, for example, cellulose acetate, polyimides, polyamides, polysulfone, polycarbonates, and polyetherimide (Powell and Qiao, 2006). The most widely used and tested material is cellulose acetate, as used in UOP's membrane systems. Polyimide has some potential in certain CO_2 removal applications, but it has not received sufficient testing to be used in large applications. Cellulose acetate membranes were initially developed for reverse osmosis but are now the most rugged CO_2 removal membrane available (Dortmundt, and Doshi, 1999). More information on membrane and gas separation can be found in review papers; Noble and Stern, (1995) and Tabe-Mohammadi, (1999).

2.3.2.2 Ionic Liquids

Ionic liquids are broad category of salts, typically containing an organic cation and either an inorganic or organic anion. Ionic liquids are physical sorbents and little heat is required for regeneration (Miller, 2011). They can dissolve gaseous CO_2 and are stable at temperatures up to several hundred degrees centigrade (Plasynski, 2009). The stability offers the possibility of recovering CO_2 from flue gas without having to cool it first, resulting in substantially low regeneration energy (Rackley, 2010).

2.3.2.3 Sorption-Enhanced Water Gas Shift

Sorption-Enhanced Water Gas Shift (SEWGS) is a pre-combustion CO_2 capture process that removes both the CO_2 and CO which is from a syngas or coal derived gas at elevated pressure and temperatures of about 400 °C (Cobden et al., 2007) (Figure 2.3). It produces a hot stream of hydrogen and steam, which can be directly fed to a gas turbine, and a cooled stream of relatively pure CO_2, which can be compressed and transported to a subsurface injection location. The SEWGS process consumes steam, cooling water and electricity, but at a smaller amount than for conventional pre-combustion technologies.

As illustrated in Figure 2.3, at the adsorption stage, the CO_2 is adsorbed by the sorbent at high pressure. At the desorption stage, the system pressure is reduced as hot steam is passed through. This process removes the adsorbed CO_2 from the sorbent, leaving the sorbent ready for another adsorption process.

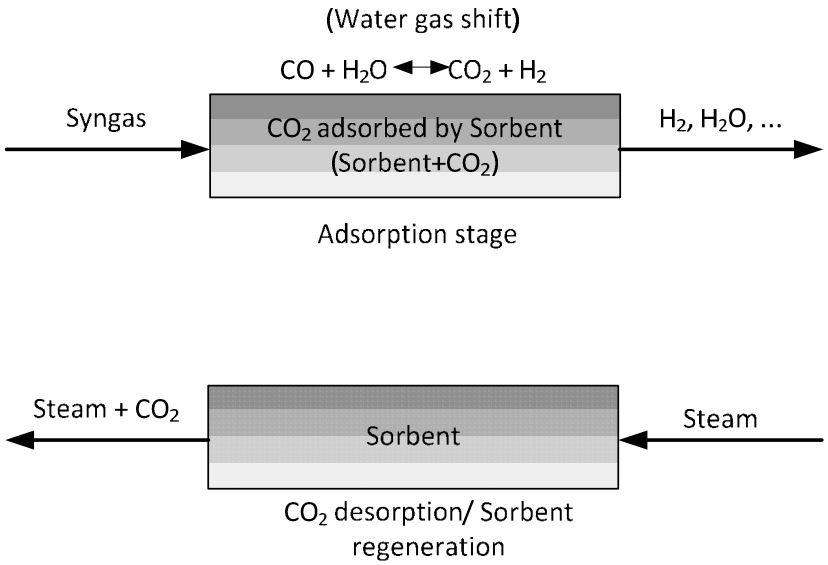

Figure 2.3. The SEWGS principle; reaction and adsorption at high pressure (upper) and desorption at low pressure (lower) (ERC, 2010).

SEWGS neither requires cooling of the syngas nor reheating of the hydrogen produced. It can replace the conventional CO_2 removal by low temperature water gas shift, cooling, condensing, washing, and reheating. Furthermore, the solid sorbent has important economic, safety and environmental advantages over liquid solvents or sorbents, as it is inexpensive, does not need to be replenished, can be used for extended periods, is non-hazardous and is not emitted directly or indirectly to the atmosphere (Van Selow et al., 1984).

2.3.2.4 Chemical-looping combustion

Chemical-looping combustion (CLC) is a combustion technology with inherent separation of the greenhouse gases including CO_2. The technique involves the use of a metal oxide as an oxygen carrier which transfers oxygen from the combustng air to the fuel. Hence, the direct contact between fuel and combusting air is avoided (Mattison et al., 2004; Mattison et al., 2006). Subsequently, the products from combustion, e.g. carbon dioxide and water, will be kept separate from the rest of the flue gases, e.g. nitrogen and any remaining oxygen. Two reactors in the form of interconnected fluidized beds are used in the process:

i) A fuel reactor where the metal oxide is reduced by reaction with the fuel,

$$M_yO_x:\ (2\mathrm{n}+\mathrm{m})M_yO_x+\ \mathrm{C}\mathrm{n}H_2\mathrm{m}\rightarrow\ (2\mathrm{n}+\mathrm{m})\mathrm{MyOx}-1\ +\ \mathrm{m}H_2\mathrm{O}+\ \mathrm{n}\mathrm{CO}_2\ \ldots\ldots\ldots(2.1)$$

and

ii) An air reactor where the reduced metal oxide from the fuel reactor is oxidized with air

$$\mathrm{M}_yO_x-1\ +\ \frac{1}{2}O_2\ \rightarrow\ \mathrm{M}_yO_x\ \ldots\ldots\ldots(2.2)$$

The outlet gas from the fuel reactor consists of CO_2 and H_2O, while the outlet gas stream from the air reactor contains only N_2 and some unused O_2. The net chemical reaction over the two reactors is the same as for normal combustion with the same amount of heat released, but with the important difference that CO_2 is inherently separated from nitrogen, and no extra energy is needed for this separation (Mohammad and Hugo, 2008). This is in contrast to known techniques for separating carbon dioxide from flue gas, where large

amounts of energy and expensive equipment are necessary (Mattisson and Lyngfelt, 2006).

2.4 CO_2 capture sorbent

A sorbent is a solid substance that adsorbs or absorbs another type of substance. The use of solid sorbents to capture CO_2 from flue gases has attracted significant attention in recent years (Liang, 2003; Wang et al., 2012; Choi et al., 2009). With rapid development in novel sorbent materials and innovative cyclic adsorption processes, sorption has become a key separation process in many process industry including chemical, petrochemical, environmental, pharmaceutical, and electronic (Deng, 2006; Yang et al., 2008). Commercial sorbents include: activated carbon, metal organic framework, zeolites, activated alumina, silica gels, and polymeric adsorbents. A range of CCS technologies which use this sorbents have been developed and improvements on existing technologies are currently in progress. However, CO_2 capture technologies need to operate with a minimum energy penalty on the host power plant, at reasonable capital and operating expenditure, have an acceptable plant footprint, and perform to achieve capture targets and produce CO_2 of high enough purity to meet the requirements and legislation for subsequent transport and storage (Oosterkamp and Ramsen, 2008). A range of sorbents have been developed that meet these specifications (Choi et al., 2009; Davidson, 2009). The use of solid adsorbents avoids the regeneration and handling of large volumes of liquids associated with absorption processes. Also, compared to aqueous amines, degradation in solid adsorbents is limited since mobility in solid systems is restricted.

Despite the reduced capital cost and power requirement for solid sorbents when compared to conventional monoethanolamine (MEA), there is the

problem of pressure drop and heat transfer (Yang et al., 2008; Olivares-Martín and Maroto-valer, 2012). Although commercial sorbents have been briefly discussed below, a review by Lui et al., (2012) and Samanta et al., (2012) provides further information on CO_2 capture sorbents. This review will focus more on the carbon based adsorbents as this is the main focus of this thesis.

The development of adsorbent with large selectivity, large adsorption capacity, fast adsorption kinetics, good mechanical strength and thermal stability, low cost and easily regenerable are key to desirable adsorbents for application in pre-combustion carbon capture (Wang et al., 2012b; Sayari et al., 2011, Choi et al.,. 2009). The synthesis process in this work has been designed in such a way as to facilitate the production of large internal pore volume and internal surface area, a controlled pore size distribution in the micropore range, and the use of low-cost materials. Also, controlled surface properties were achieved by adding selected functional group (amine and oxygen). Since physisorption is the mechanism of adsorption in pre-combustion carbon capture, weak interactions between adsorbate and adsorbent were desired. It is the aim of this research to synthesize adsorbents with up to 3 mmol g^{-1} adsorption capacity, as it has been stated by Gray et al., (2008) that adsorbents become competitive when they have uptake capacity greater than 3 mmol g^{-1}. This, according to Wang et al., (2012) will reduce the energy to 30 to 50% compared to MEA based process.

2.4.1 Metal Organic Frameworks (MOFs)

MOFs are new class of hybrid material built from metal ions with well-defined coordination geometry and organic bridging ligands. They are extended structures with carefully sized cavities that can adsorb CO_2. MOFs require low heat to recover adsorbed CO_2 and they have a high storage capability (Milward

and Yaghi, 2008). The overlap of the potential energy wells of the pore walls of MOFs enhances the adsorption capability of the material. Over 600 chemically and structurally diverse MOFs have been developed over the past several years, with MOF-77 showing one of the highest surface area and CO_2 uptake capacities (Willis 2010). A summary of CO_2 capacity of some MOFs at 25 ^{o}C and 16.7 kPa is presented in Table 2.4, while Figure 2.4 illustrates the structural and secondary building blocks of MOF-31-39. The amount of CO_2 adsorbed by the respective MOFs is highly dependent on the synthesis routes and the activation method used (Yazaydin et al., 2009). The CO_2 uptake values reported in Table 2.4 were presented in different units by the writers. In this table, these values have been converted to a common standard unit ($mmolg^{-1}$) for easy comparison. Also, the CO_2 pressure which alters flexible organic linkers in MOFs plays a vital role in determining the adsorption capacity of MOFs (Hong and Suh, 2012). Despite the fact that MOFs require low energy for regeneration, good thermal stability, tolerance to contaminants, attrition resistance, and low cost, additional work is needed to determine their stability over thousands of cycles and the effects of impurities at typical flue gas temperature and pressure.

Table 2.4. CO_2 uptake of some MOFs.

MOF	**CO_2 uptake (mmol g^{-1})**	**References**
Mg-MOF-74	6.5	Chae et al., (2004)
Co-MOF-74	3.9	Huang et al., (2003)
Zn-MOf-74	2.0	Rosi et al., (2005)
Pd (2-pymo)$_2$	1.0	Chen et al., (2006)
UMCM-150(N)$_2$	0.48	Loiseau et al., (2006)
MIL-47	0.30	Ferry et al., (2005)
ZIF-8	0.19	Ma et al., (2007)
IRMOF-3	0.19	Park et al., (2006)
MOF-177	0.16	Szeto et al., (2006)
IRMOF-1	0.15	Bourrelly et al., (2005)
UMCM-1	0.13	Lui et al., (2006)

Figure 2.4 Schematic illustration of secondary building units (SBUs) for MOF-31-39 including linkers and resulting topologies (Jaheon et al., 2001).

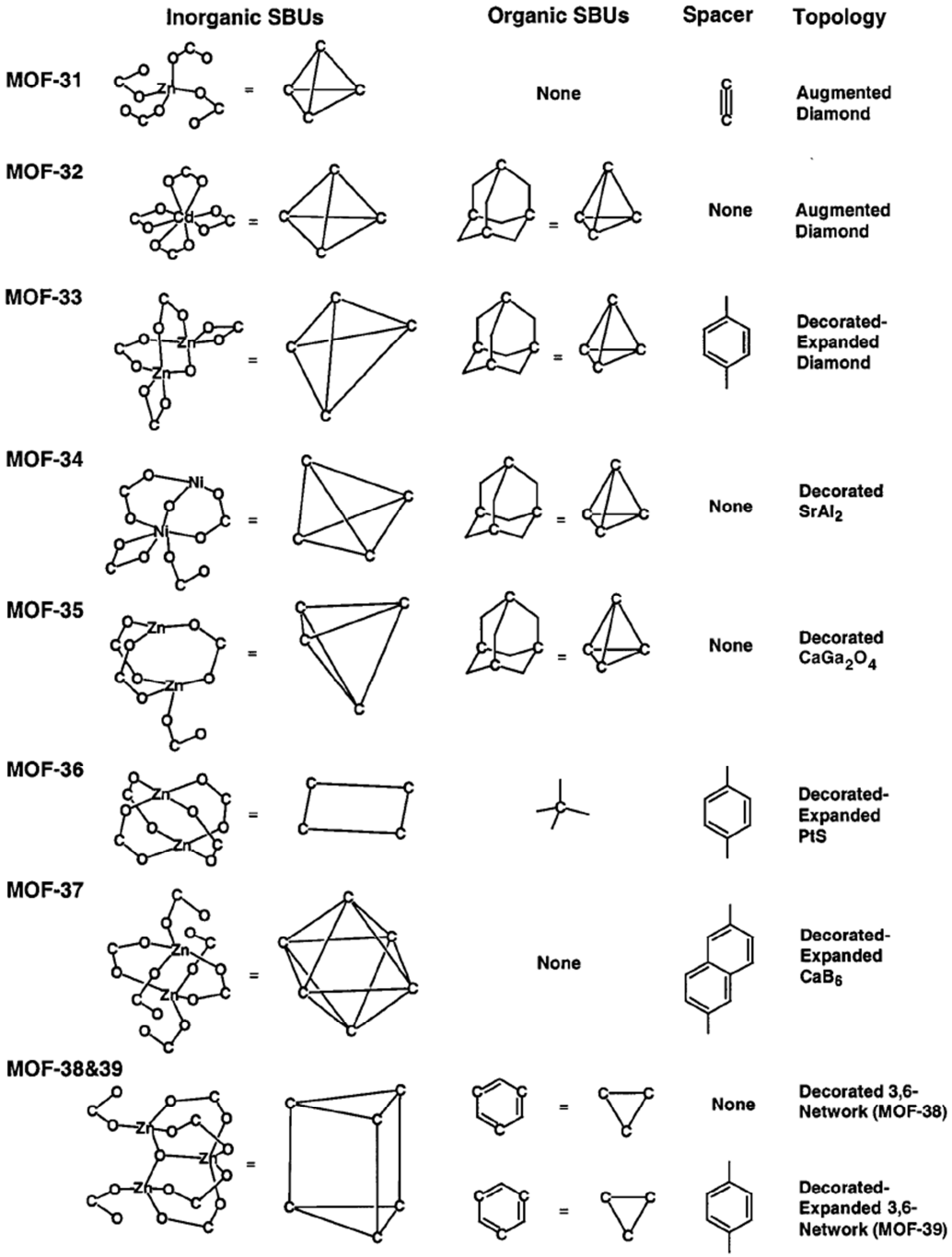

2.4.2 Zeolites

Zeolites are crystalline solids structures made of a network of silicon, aluminium and oxygen that form a framework with cavities and channels inside where cations, water and/or small molecules may reside. The chemical formula for zeolites can be represented as;

$$w\mathrm{Na_2O} \cdot x\mathrm{Al_2O_3} \cdot y\mathrm{SiO_2} \cdot z\mathrm{H_2O} \ldots\ldots\ldots (2.3)$$

Where, w is the cation type, x is amount of aluminium terahedra in moles, y is amount of silicon terahedra in moles and z is amount of water of crystallisation in moles. Zeolites are unique adsorbers owing to their special surface chemistries and crystalline pore structures. They have shown promising results from separation of CO_2 from PSA processes (Dong et al., 1990; Cheu et al., 1996). Structural illustration of the γ-type zeolites, β-type, and Mordenite is presented in Figures 4.1 (a, b and c) respectively.

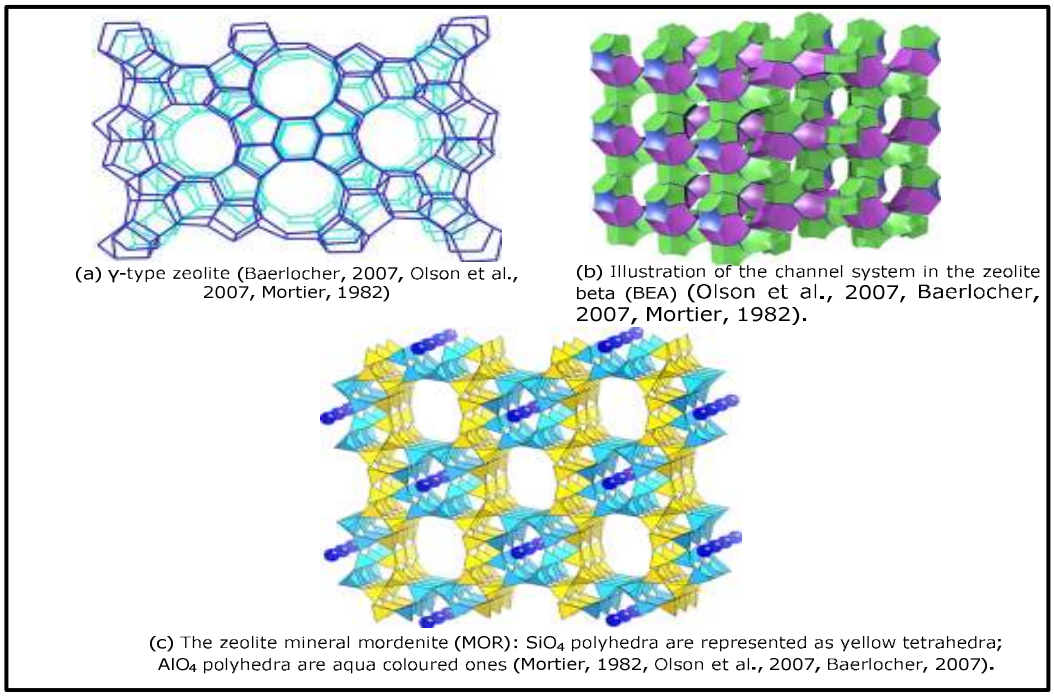

(a) γ-type zeolite (Baerlocher, 2007, Olson et al., 2007, Mortier, 1982)

(b) Illustration of the channel system in the zeolite beta (BEA) (Olson et al., 2007, Baerlocher, 2007, Mortier, 1982).

(c) The zeolite mineral mordenite (MOR): SiO_4 polyhedra are represented as yellow tetrahedra; AlO_4 polyhedra are aqua coloured ones (Mortier, 1982, Olson et al., 2007, Baerlocher, 2007).

Figure 4.1 Structural illustration of γ-type, β-type, and Mordenite zeolites

Zeolites are promising for carbon capture application in pre-combustion carbon, especially as their adsorption capacity is not affected by the presence of water vapour at ambient conditions (Siriwardane et al., 2012; Siriwardane et al., 2005). However, regeneration energy has always been of great concern (Cejka and Heyrovsky, 2005). By using zeolites as adsorbent, CO_2 uptake capacities of 2.5 to 3 mol kg^{-1} have been reported by Ranjani et al., (2003) at 25 ^{o}C and 17 to 20 bar. Adsorption capacity of 5.1 mol kg^{-1} has also been reported by Ranjani et al., (2001). These results suggest the usefulness of zeolites for carbon capture. However, drawbacks like high regeneration energy (Barrer, (1978), still need to be addressed if they are to be employed in pre-combustion carbon capture. Review articles on zeolites are available at Barrer, (1978), Auerbach et al., (2003), Gedeon et al., (2008) and Cejka et al., (2007a).

2.4.3 Activated alumina

Activated alumina is a porous form of aluminium oxide, prepared either directly from bauxite ($Al_2O_3 \cdot 3H_2O$) or from the monohydrate by dehydration and recrystallization at elevated temperature. Surface areas are in the range of 250-350 m^2g^{-1} depending on the activation temperature and the source of raw materials (Deng, 2006). Activated alumina demonstrates moderate adsorption affinity for CO_2, which makes it a suitable candidate for removing water and CO_2 from air in a PSA process (Deng, 2006). Apart from its use as a catalyst, the adsorption properties of activated alumina has been explored extensively in the purification of air (Jain and Tseng, 2000; Zou et al., 2001). The use of activated alumina for CO_2 adsorption using PSA technique have been found promising by Golden et al., (1998) and Gaffney et al., (1999).

Application to carbon capture was possible due to its resistance to steam and good mechanical and thermal stability properties, with high adsorption capacity (Zou et al., 2001).

2.4.4 Silica gel

Silica gel is a partially dehydrated form of polymeric colloidal silicic acid with formula $SiO_2 \cdot nH_2O$. The water of crystallisation is present in the form of a chemically bonded hydroxyl groups which amounts to about 5 wt%. Depending on the method of manufacture, silica gel has spherical particles of size 2-20 nm, which aggregates to form the sorbent with pore size 6-25 nm and 100-850 m^2g^{-1} surface area depending on gel density (Deng, 2006). However, its size depends on the size of the original micro particles used in its manufacture. Its surface consists of mainly S-OH and Si-O-Si polar groups which enables it to adsorb water, alcohols, phenols, amines etc. The properties of silica can be easily tailored by surface modification to prepare materials with desired properties and applications (Rinker et al., 2000) including CO_2 capture (Tao et al., 2010). As for a practical approach, polyethyleneimine (PEI) is used in production of modified silica material (Chibowski et al., 2009). Recently, synthesized silica-based materials containing amino groups have demonstrated high capacities for CO_2 (Gargiulo et al., 2007; Knowles et al., 2005a; Knowles et al., 2005b). A 2.5 wt% uptake value have been reported by Gregory et al., (2005) at 105 ^oC. An extensive review of material development and CO_2 capture is covered in Samanta et al., (2012).

Existing commercial sorbents like zeolites, activated alumina, and silica gels will continue to play important roles in adsorptive separation and purification for pre-combustion carbon capture, and other industrial processes in the near future. However, they cannot meet the needs of future technological

developments in the new energy economy and stringent environmental regulations (Samanta, 2012). MOFs have shown better promise regarding CO_2 capture compared to the other sorbents, perhaps because of their higher surface areas, stability, and the availability of metal cluster and polymer molecules which constitutes its structure (Rowsell and Yaghi, 2004). The developments of 2nd and 3rd generation technologies remains the key to promising CCS future, but systematic investigations are needed on both synthesis methods and adsorption characteristic studies. This is the main reason for undertaking this study.

2.5 Carbon materials

2.5.1 Activated carbons

Activated carbon is a microporous inert carbon with a large internal surface area (up to 1500 m^2g^{-1}). On this surface, organic molecules from liquids or gases can be adsorbed. Activated carbons are normally made by thermal decomposition of carbonaceous materials followed by activation with steam or carbon dioxide at elevated temperature (700-1100 ^oC) (Goyal, 2005). Carbons can also be activated chemically by using KOH. The structure developed is a function of the carbonisation and activation temperatures (Ruthven, 1984). The activation process involves essentially the removal of tarry carbonization products formed during pyrolysis, thereby opening the pores (Goyal, 2005; Ruthven, 1984).

The structure of activated carbon consists of elementary micro-crystallites of graphite stacked in random orientation (Figure 2.5). The spaces between the crystals form the micropores with pore size distribution typically trimodal.

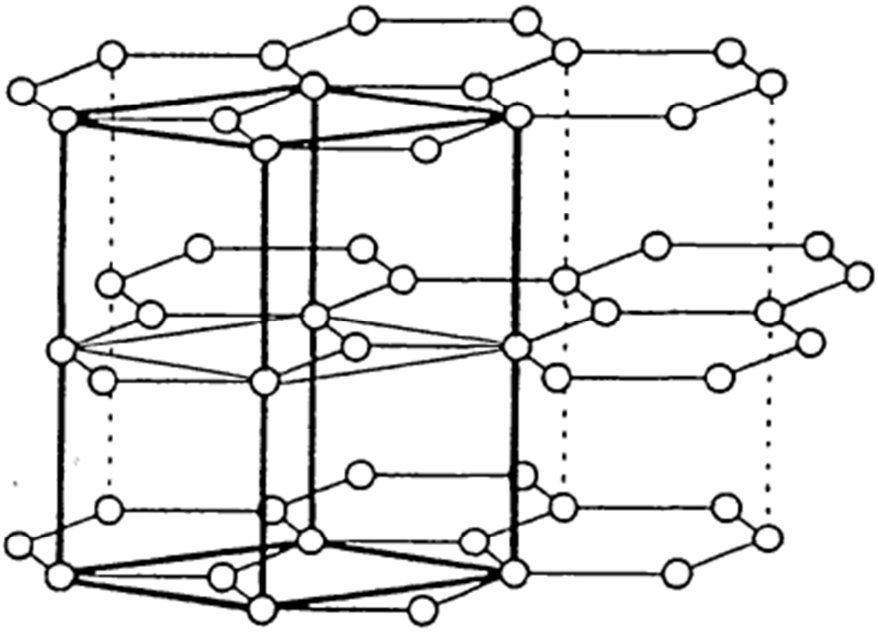

Figure 2.5 structural illustration of carbon showing a unit cell of graphite (Haris 1997)

The conditions of the initial pyrolysis and activation procedure determine the distribution and the total pore volume associated with each pore size. Activated carbons tend to be hydrophobic and organophilic because its surface is essentially nonpolar, or slightly polar as a result of surface oxidation (Patrick, 1995). The pores in activated carbon are divided into three groups; the micropores with diameter less than 2 nm, the mesopores with diameter between 2 and 50 nm, and the macroporores with diameter greater than 50 nm. A typical range of pore size distribution in materials is shown in

Table 2.5. Pore sizes in a carbon material (IUPAC, 2012).

	Micropores	Mesopores	Macropores
Diameter (Å)	<20	20-500	500
Pore volume (cm^3 g^{-1})	0.15-0.5	0.02-0.1	0.5-0.5
Surface area (M^2 g^{-1})	100-1000	10-100	0.5-2

(Particle density 0.6-0.9 g cm^{-3}; porosity 0.4-0.6)

The adsorption behaviour of activated carbon cannot be interpreted on the basis of the surface area and pore size distribution only. It has a pore structure which determines its adsorption capacity, a chemical structure which influences its interaction with polar and non-polar sorbates, active sites in the form of edges, and dislocations and discontinuities which determines its physisorption with other atoms (Patrick, 1995). This makes activated carbon an excellent and versatile adsorbent (Biniak et al., 1997). Activated carbons in its difference forms are in high demand for different applications including the removal of SO_x and NO_x, purification of helium, and hydrogen separation from syngas and hydrogenation processes etc. It also gains application in adsorptive removal of odour, colour, and taste, and other undesirable organic and inorganic pollutants in drinking water, and industrial applications; pharmaceutical, chemical, and food (Bansal and Goyal, 2005). The chemical nature of the surface area explains its ability to adsorb a wide range of organic compounds and metal ions, but limits its potential for chemo-selective processes (Ruthven, 1984).

Activated carbon comes in different physical forms; powdered, granulated, and the fibrous activated carbon. The powdered activated carbon (PAC) has finer particles and allows faster adsorption. However, they cause high pressure drop in fixed beds, which are difficult to regenerate (Knappe et al., 1998). The

granulated activated carbons (GAC) with 0.6-4.0 mm granules size are hard, abrasion resistance and relatively dense to withstand operating conditions (Aygun et al., 2003). The fibrous activated carbons (FAC) are more expensive than the others but have the capability to be moulded easily into the shape of adsorption systems, and produce low hydrodynamic resistance to flow. Other forms of activated carbons are; extruded activated carbon, beaded activated carbon, impregnated carbons and polymer coated carbons.

2.5.2 Carbon synthesis

Activated carbons can be made from any carbonaceous material. The base raw material and pre-treatment can affect many of the physical characteristics of carbon (Patrick, 1995). These different properties make some carbons better suited than others for specific applications. Carbons made from lignite tend to have a large pore diameter and that makes them better suited for the removal of large molecules from liquids. Carbons from bituminous coal have a broad range (fine to wide) of pore diameters. They are well suited for general de-chlorination and the removal of a wider variety of organic chemical contaminants from water, including the larger colour bodies. Review by Harris et al., (2009); Danafar et al., (2009); Bazargan et al., (2012); and Shaikjee et al., (2012) presents details on carbon synthesis from different materials.

However, activated carbons made for pre-combustion carbon capture must have a well-defined structure with suitable active sites, microporosity, and high internal surface area, and easily regenerable (Biniak et al., 1997; Jasen And Van Bekkum, 1994). Hence, carbon for this purpose must be made from base materials that can absolutely transfer their vital properties to the synthesized carbons (Kyotani, 2006; Kyotani et al, 2003; Kyotani, 2003).

Some physical properties can be important in determining which carbon is best suited for a specific application. For instance, the abrasion resistance of activated carbons can be important if the carbon is to be used in an application where frequent back-washing will be required (Mazzoni et al., 2011). This property is not necessary for materials in fixed bed systems, but may be important in a moving bed system.

The standard activation route for carbons has been discussed in Patrick, (1995). The synthesis route for carbons determines their textural properties which play a key role in its adsorption properties. Research breakthrough on the synthesis of microporous carbons have increased over the years due to increased application in areas such as adsorption of large molecules, catalysis (Fuertes, 2004), and superconductors (Fuertes et al., 2005). Highly structured microporous carbon materials are currently in high demand by the storage and electrode industries. Meso/microporous carbons have been employed for CO_2 capture (Macario et al., 2005; Garsuch et al., 2006; Fagueroa et al., 2008) over the years. They have also been used for separation of gases and liquids (Alvarez et al., 2007; Parmentier et al., 2009) in industry, methanol fuel cell application, as well as catalytic supports or for energy storage in double layer capacitors (Wang et al., 2010; Fracknowiak and Beguin, 2001). For pre-combustion carbon capture, solid adsorbents (eg. microporous carbons) have been seen as a potential option for gas separation in carbon capture, especially as mass transfer and easy accessibility to sites in structural micropores are important. Also, it is a technology to embrace if carbon capture is to be affordable, environmentally acceptable, and commercially viable by 2020 (Kwon et al., 2011).

The synthesis of ordered microporous carbon materials from inorganic template materials have been reported (Kyotani, 2003; Su et al., 2004; Peng-Xiang et al., 2005; Kyotani, 2006, Chen et al., 2007) using different template materials (Table 2.6). Also, different techniques (Fajula et al., 2003) have been applied in filling carbon into the nanochannels of zeolite; impregnation of the host material with organic compounds such as polyfurfuryl alcohol (Ma et al., 2002), generation of phenol formaldehyde resin inside the pore system of zeolite or the deposition of pyrolytic carbon into zeolite channels by propylene chemical vapour deposition (CVD) (Ma et al., 2002; Takashi, 2003; Peng-Xiang et al., 2005). Template carbonisation method consists of the carbonisation of an organic compound in nanospace of a template inorganic substance and liberation of the resulting carbon from the template. The concept of template carbonisation technique is shown in Figure 2.6.

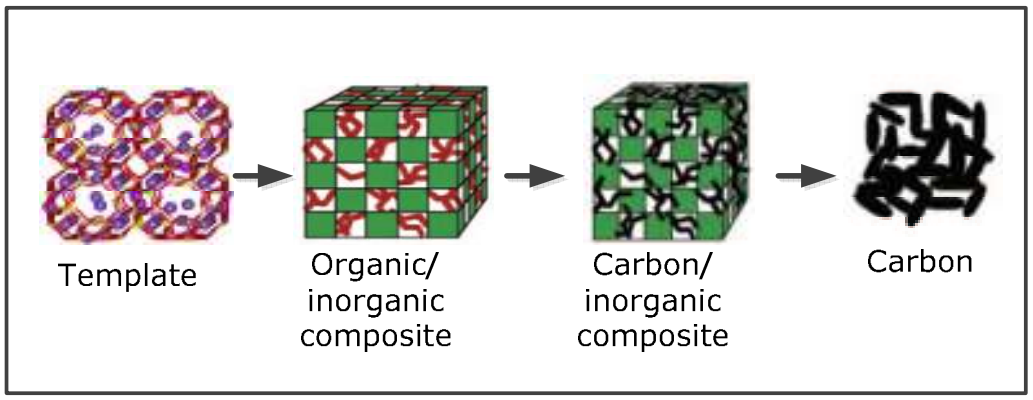

Figure 2.6. Concept of template carbonisation technique using inorganic porous template. The red and black parts correspond to carbon precursor and carbon respectively (Kyotani, 2006).

It has been reported by Kyotani, (2006) that synthesizing carbons at temperatures greater than 600 ^{o}C would result to carbon deposition on the external surface of the zeolite particles, which subsequently results in low

regularity of the resultant carbons. This effect was avoided by producing templated carbons at 600 ^{o}C. For this research work, templated carbons have been chosen as adsorbents rather than other forms of carbon because their base material is cheap and their properties can be altered by the synthesis process to obtain controlled pore structure which suits application for CO_2 capture.

Table 2.6. Summary of some carbon synthesis base materials and techniques.

Base material	**Technique**	**Surface area (m^2 g^{-1})**	**Micropore volume (cm^3 g^{-1})**	**References**
Zeolite	Templating	1150-3600	0.4-1.5	Ma et al., (2002)
Almond shell	Direct carbonisation	8-1090	0.06-0.18	Plaza et al., (2010a)
Wood	Direct carbonisation	43-1361	0.17-0.26	Plaza et al., (2010b)
Zeolites	Templating	180-2050	0.1-1.5	Kyotani et al., (2003)
Silica	Templating	520-1520	0.04-0.6	Armandi et al., (2008)
Phenolic resin	Direct carbonisation	691-1284	0.3-0.5	Tennison (1998)
Zeolite	Templating	1320-2260	0.54-1.11	Kyotani, (2003)
Zeolite	Templating	711-3683	0.33-1.6	Su et al., (2004)
Zeolite	Templating	1600-2400	0.66-1.24	Garsuch et al., (2005)
Zeolites	Templating	648-1722	0.33-0.60	Su et al., (2005)
Clay	Templating	330-490	0.08-0.15	Bendosz et al., (1994)
Silica	Templating	770-1480	0.06-0.1	Armandi et al., (2007)

Ma et al. (2002) have reported that two-step process of filling carbon into zeolite channels by impregnation of furfuryl alcohol, and CVD of propylene was indispensable for preparing carbon with high periodic ordering. Also, they

inferred that the key point for appearance of both good long-range periodicity and very high BET surface area with almost no mesoporosity in carbons is the application of low-temperature CVD. Kyotani et al., (2003) also attempted to synthesize porous carbon using other types of zeolites (zeolite β, ZSM-5, mordenite and zeolite L). Two methods were used in filling the nano-channels of the zeolites; CVD method using propylene and impregnation-CVD using zeolite/polyfurfuryl alcohol composite prepared in the same manner as Ma et al. (2002). Results showed that optimum carbon filling method for one zeolite was not the same for other zeolites. Also, the degree of the regularity of long-range ordering in the carbons strongly depends on the zeolite type.

Peng-Xiang et al., (2005) found that the use of CVD gas with a small molecular size and low CVD temperature (600 ^{o}C) is the key factor for obtaining ordered microporous carbon, when template technique was used to synthesize microporous carbon. Results showed that the micropore size of samples were small and more homogeneous. This was attributed to both the zeolite framework and unfilled space in the composite, which become carbon micropores when the carbon is liberated from the composite. Phenol-formaldehyde resins were used as precursor for the preparation of microporous carbon based materials (Martin et al., 2011b). The equilibrium CO_2 capture and performance of carbons under pre-combustion capture conditions is not limited to the surface of the material alone, but to both the micropore volume and the average micropore width (Martin et al., 2011a). It was demonstrated that the capacity of adsorbed CO_2 at atmospheric pressure correlates better with narrow microporosity. CO_2 uptake capacity greater than 10 wt% was achieved.

Zeolite dissolution in hydrofluoric acid (HF) is a vital process in the synthesis of carbons from zeolite templates. If the carbons developed by carbonisation of precursors within zeolite channels are not liberated, the whole essence of templated carbon generation will not be achieved. So, the importance of zeolite dissolution in HF is to liberate the templated carbons from the zeolite channels. HF has been chosen as the dissolution chemical for zeolites in this work because, it removes silicon, aluminium, magnesium and other components at rates proportional to their concentrations in the lattice (Kline and Fogler, 1981), unlike HCl which acts on silicates and preferentially removes aluminium, magnesium, and iron from silica lattice structure.

The zeolites used in the work have high silica-alumina proportion and this according to literature (Hartman and Fogler, 2005; Kline and Fogler, 1981) will affect their dissolution rate. The Si-to-Al framework ratio plays a universal role in dissolution mechanism, and doesn't depend on framework type. The mechanism by much zeolites dissolve in the presence of hydrofluoric acid had been studied by Kline and Fogler (1981). If there is insufficient HF to effectively dissolve all of the zeolite in the pore space, fines could be generated by cleavage of O-Si-O groups, which in turn leads to partially dissolved zeolite and tend to detach from the formation and block the pore. Zhuxian et al., (2006) has shown that complete zeolite removal from carbon/zeolite composite by HF is achieved when less than 3 wt% of residual weight is achieved after burn off operation in a thermogravimetric analyser.

Apart from inorganic templates, the use of biomass as carbon source has been reported to produce good porosity and high surface area carbons. One of such work has been reported by Zhang et al., (2008) to involve the use of cornstalk to produce high surface area and highly microporous carbon, after

carbonisation and KOH activation. Results showed that the pore size remained within the micropore range (1-2 μm), whereas, the BET surface area varied from 2140-3200 m^2 g^{-1} depending on the concentration of KOH used. Fierro et al., (2006) prepared activated carbon of Kraft lignin with ortho-phosphorus acid at various temperatures (400-650 ^oC), weight ratio of ortho-phosphorus acid to lignin (P/L = 0.7-1.75) and impregnation times (1-48 hours). Irrespective of carbonisation temperature, results showed essentially microporous carbons with 80% total micropore volume. Maximum surface area of 1305 m^2 g^{-1} and 0.67 cm^3 g^{-1} of pore volume were achieved at 600 ^oC. Pyrolysis of acid-impregnated lignin produced a reduced pore volume and BET surface area at temperatures higher than 600 ^oC. Finally, increased impregnation time lowered the surface area and pore volume, even at higher activation temperatures.

It is obvious from literature that the activated carbons produced from different precursors provided large spectrum of pore structures and surface chemistry (Kyotani, 2006; Ma et al., 2002). They have successfully been employed as adsorbents in many different gas separation and purification applications of practical importance including CO_2 capture. It is no wonder that molecular engineering of pore structure and surface chemistry of activated carbons have opened up new potential applications such as gas separation using nanoporous carbon membrane, gas drying, pollution abatement and natural gas storage (Figueroa, 2008). Although, other templating materials like silica exist, zeolites have been reported to completely transfer their physical properties to synthesized carbons, if synthesis steps are carefully followed (Kyotani, 2003). Zeolites have been chosen as the template material for this research work because of their high pore regularity, active sites, well defined pore size

distribution and relatively high surface area, and their ability to transfer these properties onto the synthesized carbons. Based on explicit literature cited in Ma et al., (2002), Barata-Rodrigues et al., (2002), and Kyotani (2006), the templating technique with carbonisation temperature not exceeding 700 ^{o}C, will produce carbons of desired characteristics for this research work.

2.5.3 Carbon post production treatments

Carbon based adsorbents often do not have suitable chemical nature or suitable porous structure. The main purpose of a modification operation is to develop the internal porous structure or chemical changes in a carbonaceous substance (Leboda, 1993). Carbon modification has been seen to improve material's surface chemistry and enhances adsorbates properties for applications (Li et al., 2002). The functionalisation of pore surfaces of microporous carbons alters surface properties such as acidity, or specific affinity (Pevida et al., 2008). This can be achieved by the formation of different types of surface groups. These groups include carbon-oxygen surface groups, formed by oxidation of the carbon surface with oxidizing gases or solutions (Plaza et al., 2010); carbon-hydrogen groups obtained by treatment with hydrogen gas at elevated temperatures (Balooch and Olander, 1975); carbon-nitrogen surface groups obtained by treatment with ammonia (Pevida et al., 2008); carbon-sulphur surface groups obtained by treatment with elementary sulphur, carbon disulphide, H_2S, SO_2, and carbon-halogen surface groups formed by treatment with halogen in gaseous or solution phase (Moreno-Castilla et al., 1985; Lopez-Gonzalez et al., 1982; Blayden and Patrick, 1967). Figure 2.7 shows functional groups attachment to carbon surfaces after modification.

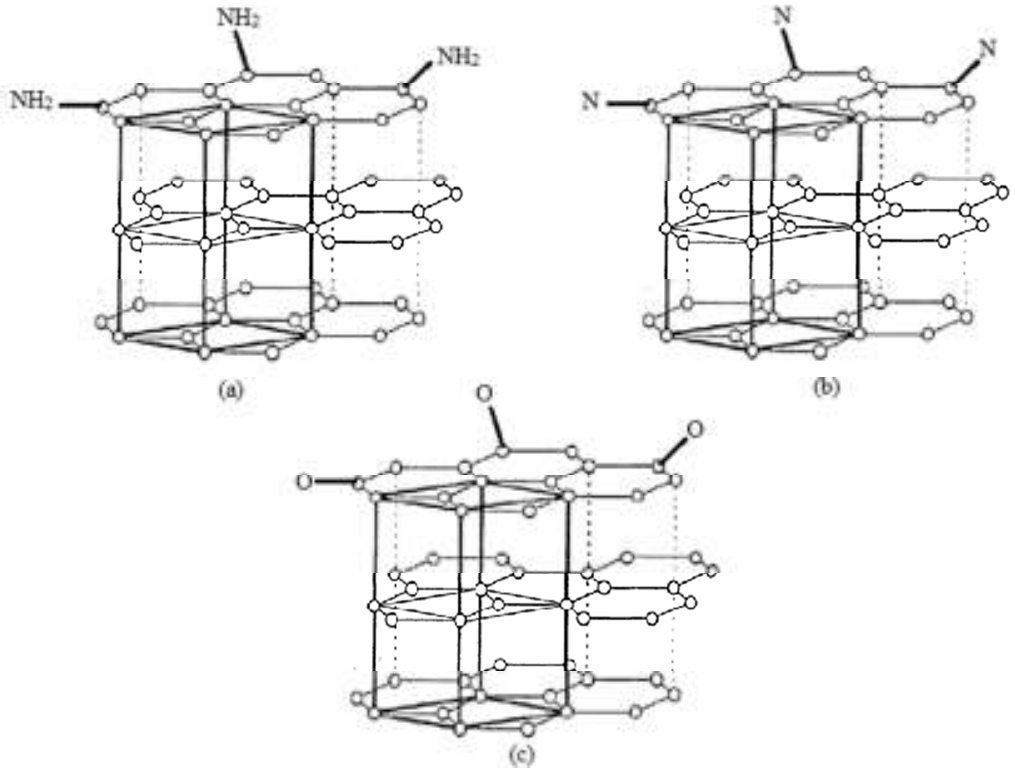

Figure 2.7 illustration of surface modification by attachment of functional groups on carbon surface; (a) amine functional group, (b) nitrogen functional group, (c) oxygen functional group

Edges or corners in carbons constitute the main adsorbing surface. When these surface groups are bonded or retained at the edges or corners of the aromatic sheets, they are expected to modify the adsorption characteristics and adsorption behaviour of these carbons (Rai and Singh, 1971; Plaza et al., 2010). Degassing and impregnating carbon surfaces with metals are other methods of modifying carbon surfaces (Hutton et al., 1993). Activated carbon impregnated with metal and their oxides dispersed as small particles, are widely used in several gas-phase reactions, both in the industry and for human protection against hazardous gases and vapour (Hutton et al., 1993).

Impregnation modifies the gasification characteristics and alters the porous structure of carbon products.

Chemical modification of carbons has been studied using different modification methods (Table 2.7). Also, the effects of surface modification on carbons and activated carbons have been reported to increase adsorption capacity (Shan et al., 2008), and cause changes in surface chemistry and porosity of carbons (Seredych et al., 2009). Previous work by Pevida et al., (2008), Arenillas et al., (2005), Pevida et al. (2008b) and Plaza et al., (2009) have shown that activated carbons with basic surface functional groups are good CO_2 absorbers. The findings from the aforementioned literature influenced the choice of surface modification method undertaken in this study. It is desired to produce a modified carbon with increased adsorption capacity, increased surface chemistry, with little or no change in carbon porosity. Hence, the chemical modification undertaken for this study was based on the procedure reported in Kaneko et al., (1989) and Tsumokawa and Yoshikawa, (1996). These procedures are explained in Chapter Three.

Table 2.7 Chemical modification in carbons

Material	Modification method	Surface Area (m^2g^{-1})	Micropore volume (m^3g^{-1})	Mesopore volume (m^3g^{-1})	Source
Coal-based activated carbon	Oxidation	658-960	-	-	Chingombe et al., (2005)
Carbon whiskers	Oxidation	16-608	0.01-0.48	-	Masafumi et al., (1994)
Activated carbon	Oxidation	300-1600	0.06-0.71	0.1-0.3	Lyubchik et al., (2002)
Activated carbon	Amination & Ammoxidation	932-1092	-	-	Jasen and Van Bekkum, (1994)
Carbon black	Oxidation	8-1000	-	-	Papirer et al., (1996)
Carbon nanotube	Organic ydrazines	-	-	-	Yokoi et al., (2005)
Carbon nanotube	Oxidation	-	-	-	Kyotani et al., (2001)
Granular activated carbon	Oxidation	431-648	-	-	Chen et al., (2003)
Carbon nanotube	Cellulose acetate	-	-	-	Ke, (2009)
Activated carbon	Oxygen plasma treatment	917-1050	0.37-0.43	0.71-0.85	Garcia et al., (1998)
Activated carbon	Microwave treatment	219-1341	0.09-0.62	-	Nabais et al., (2004)
Carbon nano fibre	CVD and heat treatment	19-300	0.01-0.17	0.03-0.35	Lee et al., (2007)
Carbon black	Oxygen plasma	-	-	-	Takada et al., (1996)
Carbon nanotube	Ethylene Glycol Plasma	-	-	-	Avila-Orta et al., (2009)
Activated carbon	Oxidation and ammonia treatment	1071-1178	0.44-0.48	-	Biniak et al., (1997)
Activated carbon	Metal oxides	256-1084	0.13-0.44	0.03-0.50	Figueiredo and Ferraz, (1982)
Carbon black	Oxidation	47-64	-	-	Horita et al., (1996)
Activated carbon	microwave radiation	-	-	-	Lui et al., (2010)

2.6 CO_2 cyclic processes

CO_2 cyclic processes are techniques used to regenerate CO_2 from sorbent materials during adsorption operations. Three highly established processes are used in the process industrial; temperature swing adsorption (TSA), pressure swing adsorption (PSA), and vacuum swing adsorption (VSA). These are briefly discussed below.

2.6.1 Temperature swing adsorption

Regeneration of adsorbent in TSA process is achieved by temperature increase. This process is used for the removal of volatile organic components (VOCs) from air (Tlili et al., 2009). A typical TSA operation consists of a two or three-step processes (Ko et al., 2002). Clausse et al., (2004) studied the adsorption of gas mixtures in TSA adsorbers under various heat removal conditions. For any given partial pressure of the adsorbate in the gas phase (or concentration in the liquid phase), an increase in temperature leads to a decrease in the quantity adsorbed. TSA process generally enable desorption of any components provided that the temperature is high enough. In administering TSA, it is important to ensure that the regeneration temperature does not cause degradation of the adsorbents.

A change in temperature alone is not used in commercial processes, because there is no mechanism for removing the adsorbate from the adsorption unit once desorption has occurred. Passage of a hot purge gas or steam through the bed to sweep out the desorbed components is always used, in conjunction with the increase in temperature (Haring, 2007). TSA processes are used exclusively for treating feeds with low concentrations of adsorbates. TSA is not very favourable due to the high vapour consumption needed for heating the column. Moreover, the thermal inertia of the solid would lead to long heating

and cooling times, which means that the time needed for regeneration is much longer than the adsorption step (Bonjour et al., 2005; Pirngruber et al., 2009).

Since one of the aims of this work is to reduce the energy penalty associated with pre-combustion carbon capture, TSA becomes an inappropriate cyclic process to employ in this work, especially as gas feed from coal gasification are at low temperature and high pressure.

Pressure swing adsorption

Pressure swing adsorption (PSA) is a well known method for gas mixture separation. As reported in patents (Leitgeb, 1988, Knaebel, 1991, Yee et al., 1995), there exist three major phases of PSA. At the firtst phase, the components of the gas feed is selectively adsorbed under pressure to obtain a gaseous stream with reduced adsorbable components. At the second phase, the adsorber is subjected to a multistage expansion to desorb the previously adsorbed components. Finally, the pressure is increased to the adsorption pressure and the cycle is reapeated. To enhance a complete regeneration of adsorbents, a purge gas is usually passed at the lowest possible pressure through the adsorber to flush out desorbed proportions from the the adsorber and to lower the partial pressure of the components to be desorbed.

Because of its lower energy and cost penalty, PSA can be applied industrially in gas drying, solvent vapour recovery, fractionation of air, production of hydrogen from steam methane reformer (SMR) and petroleum refinery of gases, separation of carbon dioxide and methane from landfill gas, carbon monoxide-hydrogen separation, normal isoparaffin separation, alcohol dehydration, and separation of CO_2 from syngas (Schell, 2009). A simplified dynamic model for a PSA air separation process is developed based on linearized mass transfer rate expressions and binary Langmuir equilibrium

(Hassan et al., 1986). Water shift gas (WSG) product streams (H_2 and CO_2) are often delivered at approximately 2 MPa and 850-950 ^oC, recovering over 90% of the hydrogen stream with >99.99% purity (Reynolds et al., 2005). A 99.8-99% CO_2 recovery have been reported by Schell et al., (2009) using PSA. Application of PSA process have been reported to remove CO_2 from gas streams using activated carbons (Kikkinides et al., 1993; Chue et al., 1995).

Anshul et al., (2010) have showed in their work that PSA/VSA is a promisiing technology for pre-combustion capture systems having achieved CO_2 recovery of 98%, and minimal power consumption with 98% purity. Although the development of practical processes of gas separation by PSA has been extremely successful over the years (Ranjani et al., 2003). Ritter and Ebner, (2007) provide a comprehensive review on the use of adsorption technologies for CO_2 removal in gasification. It is clear that PSA cycles will not only recover H_2 at high purity, but simultaneously recover highly pure CO_2 stream in gasification, ready for transportation and storage (Ritter and Ebner, 2007). This makes PSA a desired process/technology for application in pre-combustion carbon capture.

Vacuum swing adsorption

Vacuum swing adsorption (VSA) is a modification of the PSA process, and was developed to improve regeneration efficiency with lower power consumption and easier operating procedure (Ruthven, 1984; Plaza et al., 2007; Soonchul et al., 2011). In this process, a partial vacuum is applied to the sorbent bed during the desorption stage. VSA cycle is similar to PSA, except for the absence of the pressurisation step, which makes it simpler and more cost effective. It differs from PSA by the use of low absolute pressures and it is completely dependent on the nature of the gas component and its affinity to

the sorbents (Soonchul et al., 2002). More than 90% CO_2 with 95% purity have been reported by Xiao et al., (2009) using a VSA process.

The regeneration technique used for pre-combustion carbon capture must be one with reduced energy penalty, and compression costs. Considering these facts, the TSA is ruled out as an option for physisorption. The PSA and VSA remain candidates for pre-combustion carbon capture. However, the PSA would be adopted as the technique for CO_2 regeneration for this work because, CO_2 uptake will be measured at high pressure. Since CO_2 is at high partial pressure during coal gasification (Clayton et al., 2002), it would be appropriate to utilise this high partial pressure and save energy and cost that would have been needed for pressurisation and compression.

2.7 Summary

Thus far, different base materials and methods have been used to produce activated carbons for experimental purposes. Most research on templated carbon has focused on characterisation of these materials without further effort on application to carbon capture. This may be due to the nature of the various preparation methods used, which allowed only small quantities of carbons to be produced. Even when uptake capacities are measured, they are obtained at ambient temperature and pressure. This leaves the question of application of templated carbons to carbon capture, and the determination of uptake capacities of these materials at high pressure conditions.

CHAPTER THREE

3 Methods and Experimental

3.1 Introduction

This chapter introduces the fundamental techniques used in obtaining results presented in this thesis. It starts with the description of the working principles of the analytical equipment, followed by the experimental procedure used to analyse materials. Also, the design and construction of a chemical vapour deposition (CVD) rig has been reported here. Figure 3.1 presents a flowchart of method and experimental analysis undertaken in this research work.

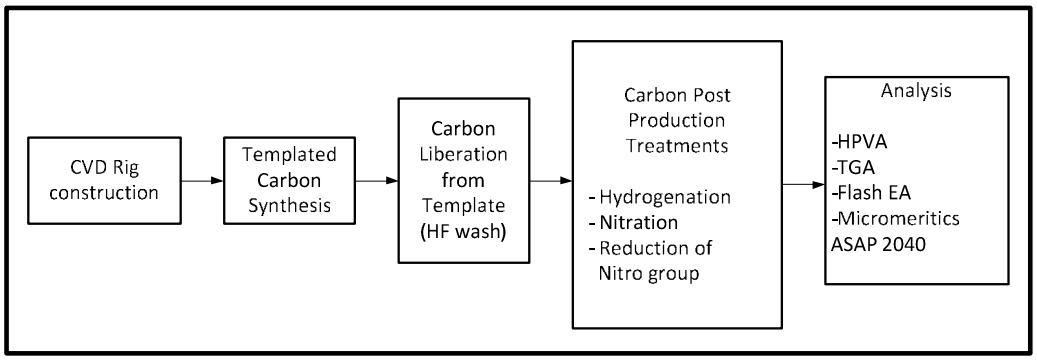

Figure 3.1. Experimental method flowchart.

3.2 Construction of the vertical furnace & reactor for chemical vapour deposition (CVD)

A vertical furnace and chemical vapour deposition (CVD) rig was used for carbonisation of zeolite/furfuryl alcohol (FA) composite (Figure 3.2). A vertical furnace orientation was selected as it will allow better mixing to promote uniform carbonisation of the carbon/zeolite composite in the quartz tube, as compared to the horizontal tube which may only allow surface carbonisation of zeolite/FA composite. A quartz tube (38 mm I.D with sinter located at the middle) was used as the reactor as it could withstand temperatures reaching 1200 ^{o}C. The sinter serves a base for the materials during the entire carbonisation operation. The quartz tube setup was designed such that two silicon rubber stoppers were placed at the top and bottom to prevent air from getting into the tube during carbonisation operation. Nitrogen gas supplied at 142.5 mL min^{-1} was passed from the bottom of the tube to create an inert condition in the tube and to prevent oxidation reaction from occurring in the tube. The system was purged for 30 minutes before the start of the experiment. Acetylene gas required for the CVD operation was also piped into the apparatus at a flow rate of 7.5 mL min^{-1}, and controlled by a flow meter. The design of the CVD rig is shown in Figure 3.2. Acetylene was chosen as the CVD gas as it possesses smaller molecular size in comparison with the inner diameter of the zeolite channels (Kyotani, 2006). This allows for easy acetylene diffusion in the channels whilst avoiding pyrolytic decomposition on the external surface of the zeolite.

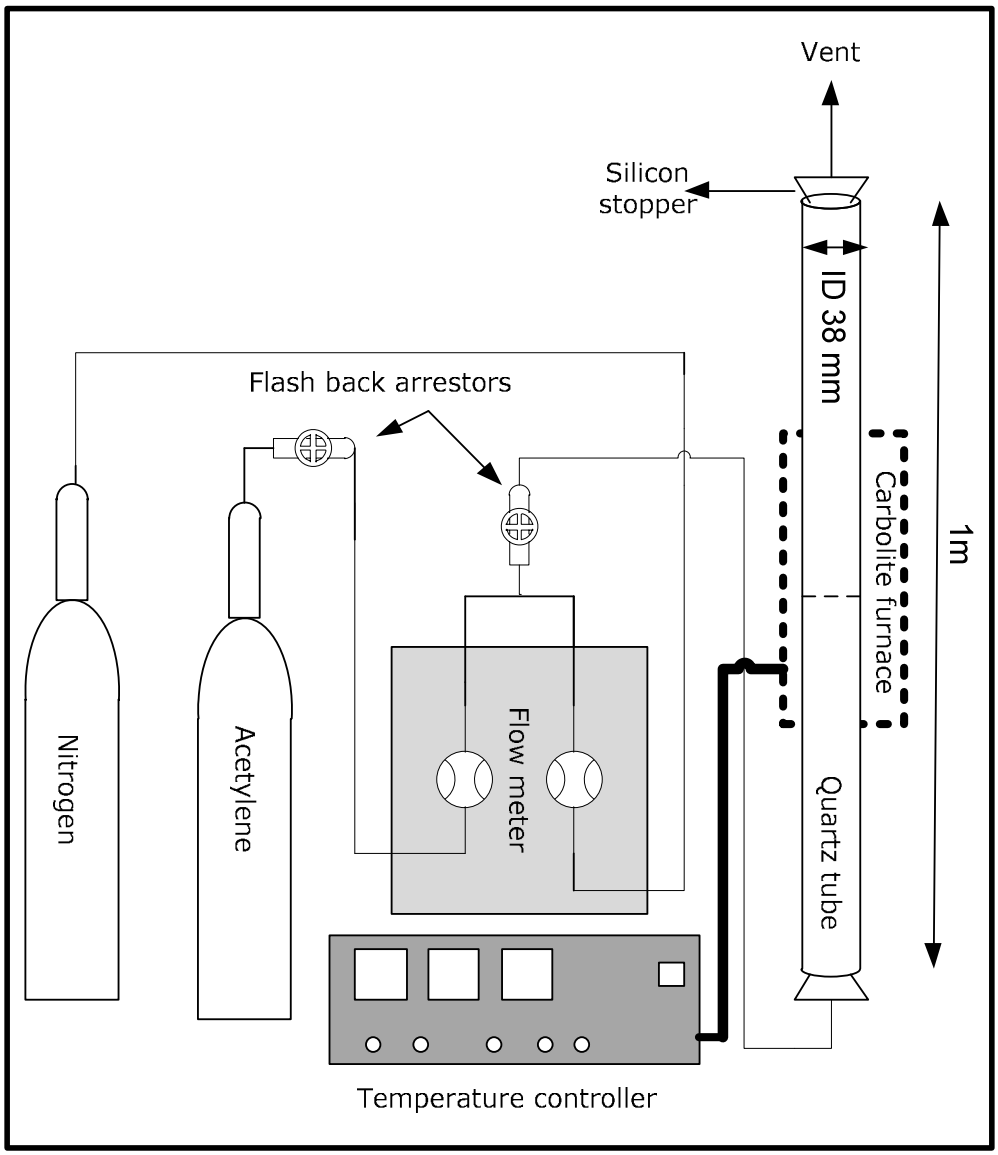

Figure 3.2. Schematic of vertical furnace/CVD rig.

Acetylene is a flammable gas with a flash point at 17 ^{o}C. This makes it highly flammable at very low temperature. For this reason, two separate flash back arrestors have been used in the design of the rig. The first arrestor was used at the acetylene cylinder head while the second arrestor was used at the junction where the nitrogen and acetylene gas supply meet. This is to further arrest any acetylene from flowing into the furnace and prevent an explosion

should the first arrestor fail. Cold air supply was piped to the top and bottom ends of the quartz tube to provide cooling to prevent the silicone stoppers from burning and deteriorating. A vent was included in the design to pass off all volatiles resulting from the combustion to prevent contact and inhalation by the operator and those in the vicinity of work.

The acetylene gas cylinder can supply acetylene at a maximum pressure of 200 bar, however, the regulator has been set to release acetylene at a maximum of 1.2 bar of pressure to avoid overpressure within the delivery pipes. For safety reason, all experiment was performed within the temperature range of the furnace (1200 ^{o}C), and the Proportional Integral Derivative (PID) control system of the furnace was programmed to operate the furnace at a maximum of 700 ^{o}C

3.1 Furnace calibration

In order for accurate temperature measurements to be taken, strict control must be maintained throughout the temperature programs of the furnace. The PID control system of the furnace must be understood and optimised for constant temperature program to be maintained.

In order to achieve the PID values of the temperature controller accurately, an iterative process of each parameter was undertaken until a plot (Figure 3.3) which is close to the ideal was obtained. The PID values for this were DAC = 1.0, cycle time = 17 seconds, proportional band = 225 ^{o}C, derivative time is 1.0 second, and the integral time = 5 minutes.

From Figure 3.3, it is clear that the temperature-time profile for the controller is approximately the same as the profile required. Point B shows a steady ramp rate which is the same as required. The initial overshoot (point A) was

as a result of control warm up characteristics of the temperature controller, while the overshoot recorded at the 'soak' stage (point C) was due to temperature overshoot from the temperature controller. However, this overshoot was automatically corrected as the 'soak' time increased (point D) (Speyer, 1994; Smith 2009).

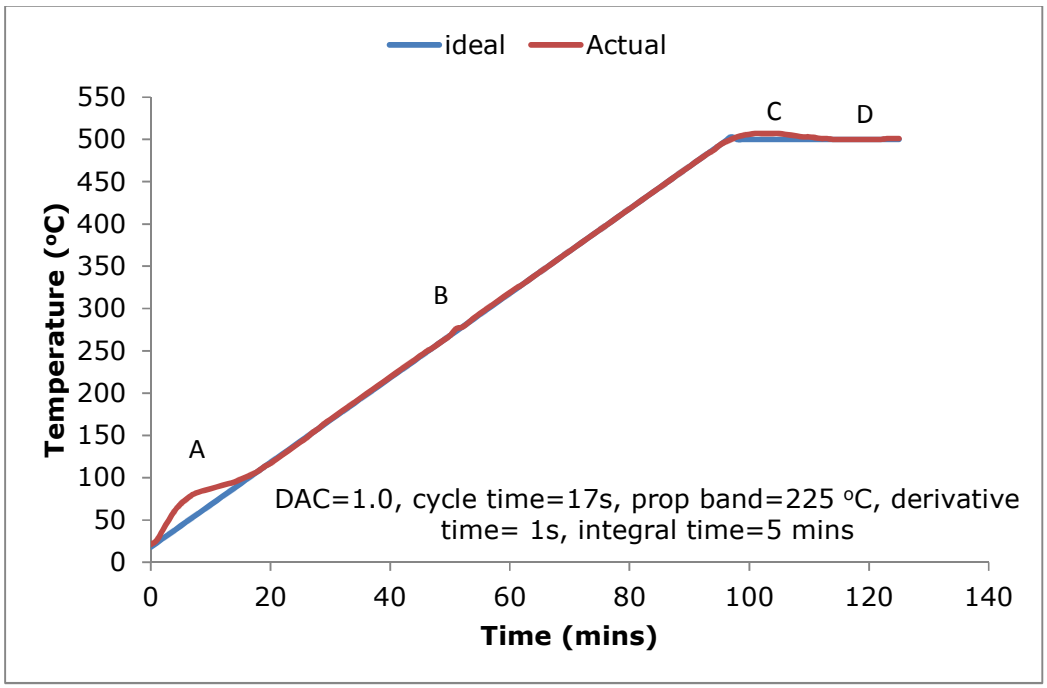

Figure 3.3. Accurate temperature control profile.

A = initial overshoot from temperature controller; B = actual heating rate proportional to ideal heating rate; C = overshoot from temperature controller due to overheating; D = overshoot corrected with increased soak time

3.2 Experimental procedure for templated carbon preparation

The zeolites used in this study were obtained from Tosoh Corporation Europe. Three different zeolites; γ-type zeolite (HSZ 320 NAA), Mordenite (HSZ 690 HOA), and β-type zeolite (HSZ 930 HOA) have been used as templates for this work. The method employed for this synthesis is based on the methods specified in Peng-Xiang et al., (2005), and the carbon synthesis operations are discussed below.

Two synthesis routes were explored for the production of templated carbon in this study (Figure 3.4). The first route was the direct carbonisation of acetylene into zeolites channels, and the second route was the introduction of a precursor-furfuryl alcohol (FA) into the zeolites channels (Figure 3.5) before acetylene carbonisation. In both cases temperature of 600 or 700 ^{o}C was used for CVD. A list of all the materials and synthesis conditions in this study is presented in Table 3.1, and full details for the synthesis conditions is provided in Section 3.2.1 to 3.3.3. Sample codes have been used for easy identification of materials, for example, γ-AC6-5% represents a templated carbon synthesized from γ-type zeolite, and carbonised at 600 ^{o}C with 5% acetylene in N_2. While γ-PFA-AC6-5% represents the same materials as γ-AC6-5% but with the addition of FA precursor.

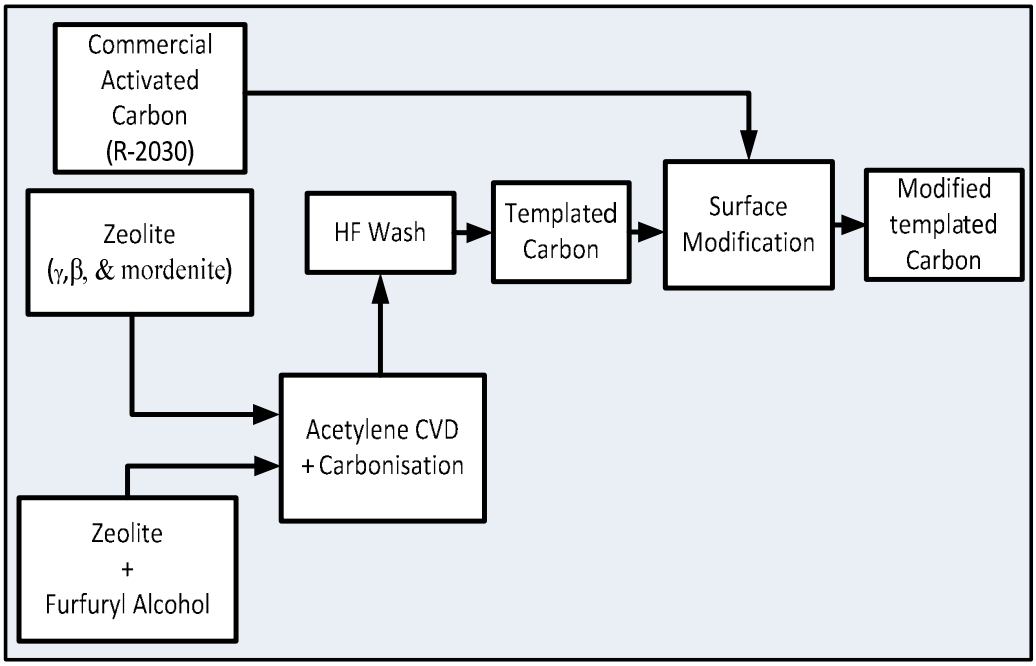

Figure 3.4. Flowchart of carbon synthesis route for this study.

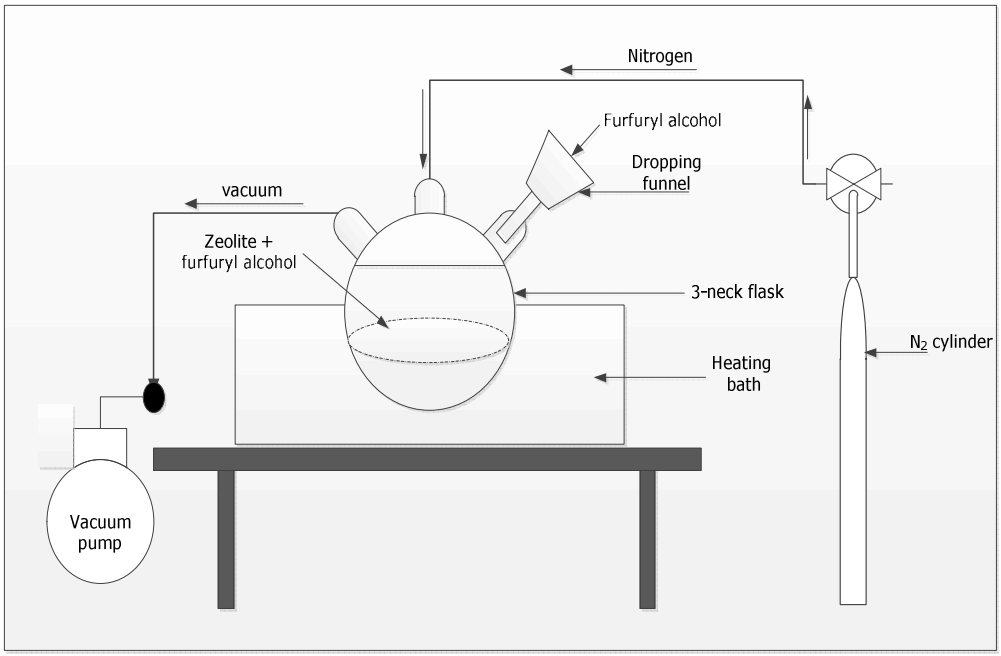

Figure 3.5. Setup for synthesis of templated carbons.

Table 3.1. Carbon synthesis matrix.

Parent zeolite	Sample name	CVD temperature (°C)	Precursor (PFA) addition	PFA carbonisation temperature (°C)	Secondary activation temperature (°C)	Hold time (Hour)	Acetylene loading (mL min^{-1})
HSZ 320 NAA	γ-AC6-2%	600	-	-	-	-	2
	γ-AC6-5%	600	-	-	-	-	5
	γ-AC7-2%	700	-	-	-	-	2
	γ-AC7-5%	700	-	-	-	-	5
	γ-PFA-AC6-2%	600	✓	600	-	4	2
	γ-PFA-AC6-5%	600	✓	600	-	4	5
	γ-PFA-AC6+AC7-5%	600&700	✓	600&700	700	4	5
	γ-PFA-AC6+AC7-2%	600&700	✓	600&700	700	4	2
	γ-PFA-AC7-5%	700	✓	700	-	4	5
HSZ 930 NHA	β-AC6-2%	600	-	-	-	-	2
	β-AC6-5%	600	-	-	-	-	5
	β-AC7-2%	700	-	-	-	-	2
	β-AC7-5%	700	-	-	-	-	5
	β-PFA-AC6-5%	600	✓	600	-	4	5
	β-PFA-AC6+AC7-5%	600&700	✓	600&700	700	4	5
	β-PFA-AC7-5%	700	✓	600	-	4	5
HSZ 690 HOA	M-AC6-2%	600	-	-	-	-	2
	M-AC6-5%	600	-	-	-	-	5
	M-AC7-2%	700	-	-	-	-	2
	M-AC7-5%	700	-	-	-	-	5
	M-PFA-AC7-5%	700	✓	700	-	4	5

CVD= Chemical vapour deposition; PFA= Polyfurfuryl alcohol; HSZ 320 NAA= γ-type zeolite; HSZ 930 NHA= β-type zeolite; HSZ 690 HOA= Mordenite zeolite

3.2.1 Experimental procedure for zeolite carbonisation

The zeolites were initially dried at 105 ^{o}C for six hours before acetylene carbonisation. About 5 g of zeolites were placed into a quartz tube and mounted on the CVD rig (Figure 3.2) through which nitrogen gas was passed for approximately 30 minutes to remove any residual oxygen. After this, the zeolites were heated to 600 ^{o}C or 700 ^{o}C as required in the vertical quartz reactor at the rate of 5 ^{o}C min^{-1} under N_2 flow for two hours, after which acetylene (7.5 mL min^{-1}) was fed into the reactor for four hours. The reaction of acetylene onto the zeolite resulted in pyrolytic carbon deposition in the zeolite pore structure. The resulting zeolite/carbon composite was cooled to room temperature under N_2 atmosphere. Acetylene was chosen as the chemical vapour deposition gas throughout the carbon preparation process in this work. This is because acetylene consists of small size molecules that can easily enter the zeolite channels during carbonisation (Kyotani, 2006). Temperature profile for the CVD operation is presented in Figure 3.6.

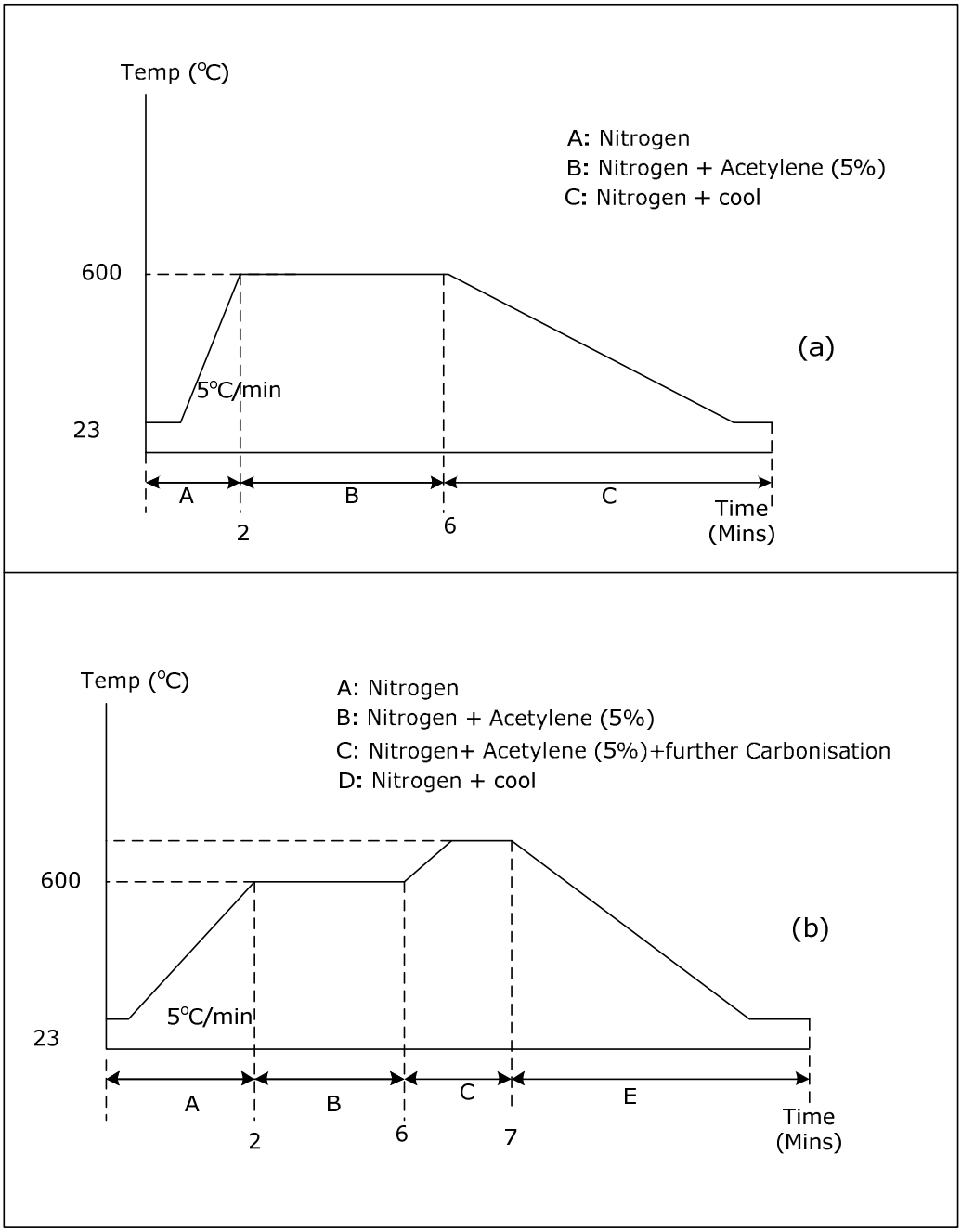

Figure 3.6. Temperature profile of CVD: (a) CVD at 600 °C, (b) CVD at 700 °C.

3.2.2 Polymerisation of furfuryl alcohol onto zeolite channels

The zeolite was initially dried in a flask and kept at 150 ^{o}C under vacuum (200 mbar) for 6 hours to dry. Liquid furfuryl alcohol (FA) (4 mL g^{-1} of zeolite) was introduced into the flask under reduced pressure at room temperature. The system's pressure was increased to atmospheric pressure by introducing N_2, and subsequently stirred at room temperature for 8 hours. The polymerisation of FA in zeolite channels was carried out by heating the resultant mixture at 80 ^{o}C for 24 hours, then at 150 ^{o}C for 8 hours in a flow of N_2. The resulting mixture was centrifuged and filtered, followed by washing with mesitylene to remove any unreacted FA from the zeolite. The resulting polyfurfuryl alcohol (PFA)/zeolite composite was carbonised as described in Section 3.2.1.

3.2.3 Hydrofluoric acid (HF) wash and drying Process

It was necessary to determine the appropriate volume of HF to use for complete removal of zeolite from one gram of carbon. Zhuxian et al. (2006) have reported that complete zeolite removal from carbon/zeolite composite is achieved when a residual mass of zeolite of less than 3 wt% is achieved after burn off operation in a thermogravimetric analyser. To confirm this on studied samples, one gram of carbon/zeolite composite was placed in 100 mL and 30 mL of HF respectively for wash at room temperature for 6 hours. The aim of using two different quantities of HF is to ascertain the least possible amount of HF required to achieve complete zeolite dissolution. Results from TGA analyses (Table 3.2) showed that residual mass was less than 3 wt% of the total sample weight after sample burn off at 800 ^{o}C, signifying total dissolution of the zeolite template in the carbon. Based on these results, 30 mL HF solution was adopted for HF wash throughout this work.

Table 3.2. TGA results from burn off operation of zeolite/carbon composite.

HF volume used (mL)	Moisture (wt.%)	Volatile (wt.%)	Fixed carbon (wt.%)	Residual weight wt%)
30	23.93	5.46	69.89	0.72
100	2.38	9.99	86.40	1.23

30 mL of 47 wt% HF solution was used per gram of carbon/zeolite or PFA/zeolite composite. The carbonised material was slowly added to the HF solution in a teflon beaker while a magnetic stirrer was stirring. The magnetic stirrer was allowed to stir at 300-400 rpm for 6 hours. The resulting mixture was poured into a teflon centrifuge tube, and separated at 4000 rpm for 5 minutes in a centrifuge (Rotofix 32A Zentrifugen) to recover the carbon from the HF solution. The mixture was filtered and washed with deionized water and dried using a vacuum filtration system. Teflon beakers were used throughout this process to avoid HF attack on the washing apparatus. It should be noted that all HF washing processes was done in a designated laboratory fume hood at room temperature.

3.3 Surface modification of carbons

3.3.1 Hydrogenation of templated carbons

Hydrogenation of synthesized templated carbons is the first stage in preparing the carbon surfaces for modification. Hydrogen bonds are easily formed on the polycondensed aromatic rings of carbons and serve as reactive sites for amines. Hydrogenation of carbon can be achieved by heating with hydrogen under pressure and at elevated temperatures. Yield decreases with increasing temperature. Hydrogenation can be controlled by adjusting the hydrogen pressure and reaction temperatures (Taylor, 1999). This hydrogenation

process is easy to apply, and the absence of air in the reaction process reduces susceptibility towards oxidation. The hydrogenation step employed in this research work was achieved by adopting the method of Kaneko et al., (1989). Figure 3.7 shows an illustration of the modification steps undertaken.

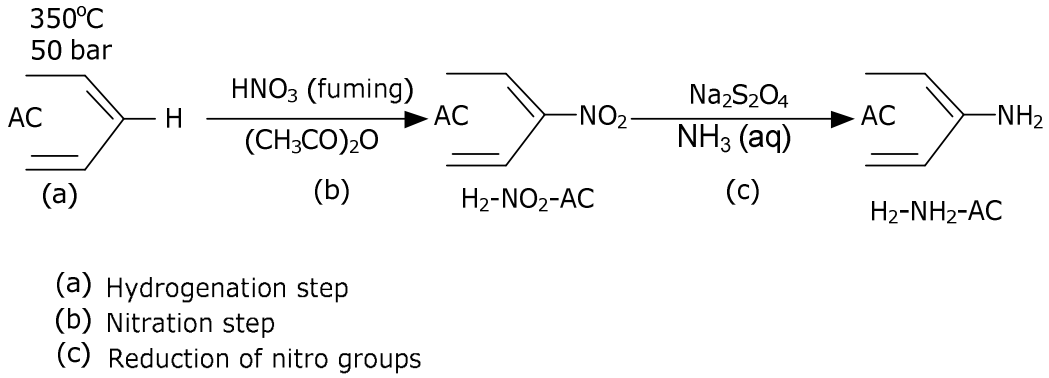

(a) Hydrogenation step
(b) Nitration step
(c) Reduction of nitro groups

Figure 3.7. Modification steps for activated carbons under study.

Hydrogenation was carried out in a fixed bed hydropyrolysis (HyPy) apparatus (Figure 3.8). The apparatus and procedure have been described elsewhere (Meredith et al., 2004; Love et al., 1995). Briefly, the carbon samples were placed in a reaction tube and heated using resistive heating from 50 ^{o}C to 350 ^{o}C at the rate of 10 ^{o}C min^{-1} under hydrogen gas at 4 and 5 MPa of pressure for 20 minutes. The hydrogen sweep was at a flow rate of 5L min^{-1} measured at ambient temperature and pressure. After this, the materials were cooled to room temperature under hydrogen and at atmospheric pressure. The temperature-time profile for hydrogenation of synthesized carbons is presented in Figure 3.9.

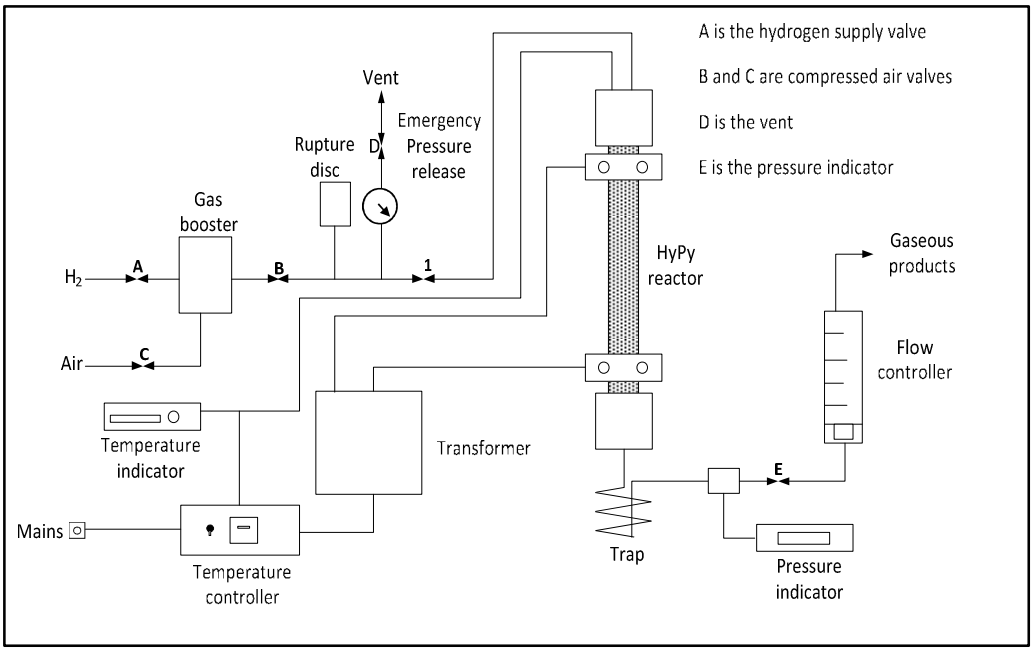

Figure 3.8. A schematic of the Hydropyrolysis apparatus.

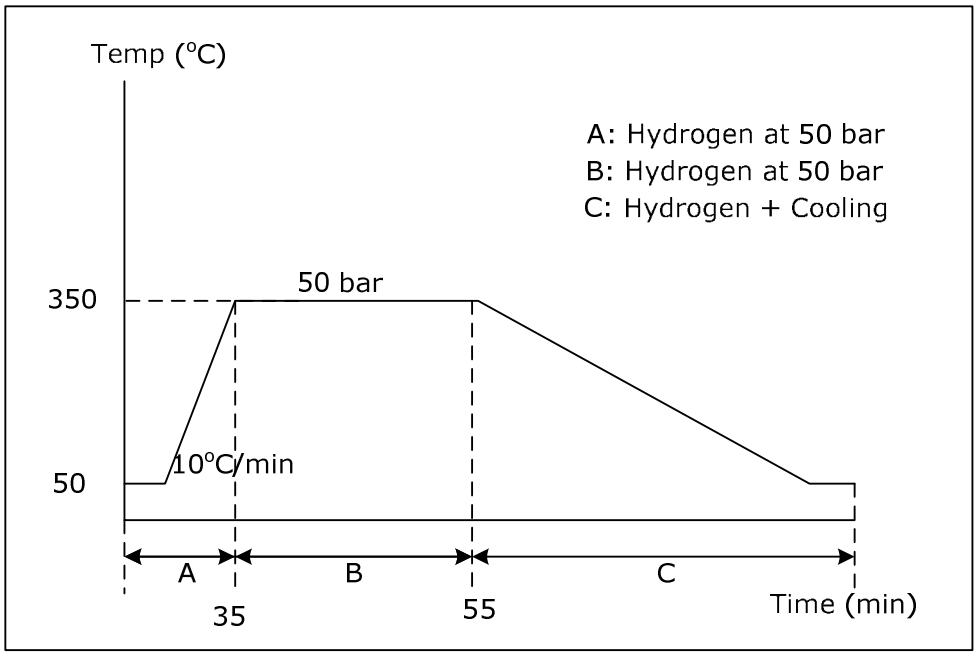

Figure 3.9. Temperature profile for hydrogenation of synthesised carbons.

3.3.2 Nitration of templated carbon

Nitration and reduction of nitro group in the carbons was carried out using the method of Yoshikawa and Tsumokawa, (1996). The introduction of amino groups onto the carbon was achieved by the addition of nitrate groups onto the surface of the carbon followed by their reduction. For nitration of polycondensed aromatic rings of carbons, 120 mL of acetic anhydride was poured into a three-necked flask, and 3 g of carbon was added. 30 mL of fuming nitric acid was added (drop wise) to the whole suspension (Figure 3.10). The mixture was stirred with a magnetic stirrer at temperature below 5 ^{o}C for 5 hours, and then at room temperature for another 5 hours. After the reaction, the content of the flask was poured into a beaker containing 1L of ice-cold water. The supernatant solution was removed by decantation and the carbon material precipitated was washed with distilled water until the filtrate was neutral. It was then dried under vacuum (150 mbar) for 24 hours.

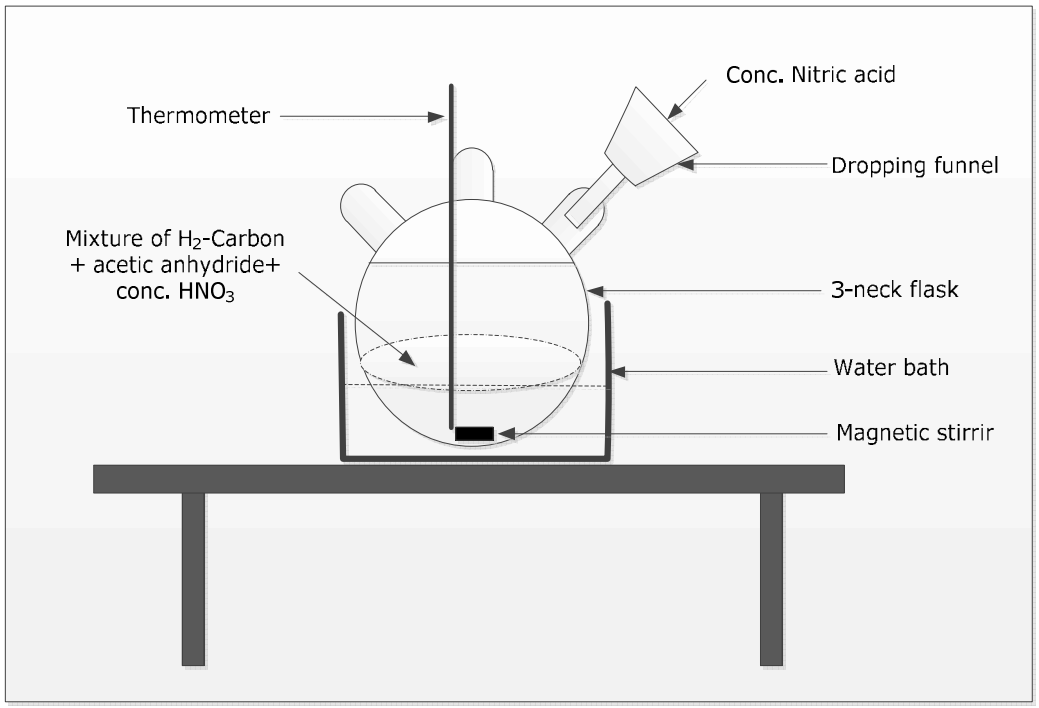

Figure 3.10. Setup for the nitration of synthesized carbons.

3.3.3 Reduction of the Nitro Groups on the Carbon

Reduction of the nitro groups on the carbon was carried out by adding 50 mL of distilled water and 80 mL of 15% sodium hydrosulfite aqueous solution into a 200 mL flask containing 12 mL of 30% ammonia water. The mixture was stirred with a magnetic stirrer at room temperature for 24 hours in nitrogen atmosphere. After the reaction, the carbons was filtered and washed with distilled water until the filtrate was neutral. The resulting amine modified carbon was vacuum dried (150 mbar) at 110 ^{o}C.

3.4 Oxidation of phenolic resin activated carbons

This section of work was conducted by Plaza et al., (2012). Oxidised carbons were produced by modifying a spherical phenolic-resin-derived activated carbon supplied by MAST Carbon Ltd. (Kozynchenko and Tennison, 2001), from now on referred as M. This was used as the base material for which different oxidation treatments were compared.

A first series of oxidised carbons were prepared by stirring 1 g of carbon in 10 mL of a saturated solution of ammonium persulfate in sulphuric acid (1 M) at room temperature for different periods of time: 1, 3 and 24 hours (Moreno-Castilla et al., 1997). The samples will be referred as MAP-1, MAP-3 and MAP-24, respectively. The excess solution was removed by repeated washing of the treated carbon with water purified by reverse osmosis (Milli-RO), until the washings presented neutral pH. Finally the samples were dried overnight in a vacuum oven at 100 ^{o}C and 150 mbar.

A series of nitric acid oxidised carbons were prepared by placing 1 g of carbon in a round bottom flask with 10 mL nitric acid (1 M and 16 M). The contents

were stirred at 90 ^{o}C for different periods of time: 1, 3 and 24 hours. All the samples were thoroughly washed with purified water until the washings were no longer acidic. Finally, the samples were dried overnight in a vacuum oven at 100 ^{o}C and 150 mbar. The carbons produced by this treatment will be referred as MNA1-1, MNA1-24, MNA16-1 and MNA16-3. It is expected that the extent of oxidation will increase at the higher concentration of nitric acid. It has been previously reported that temperatures in the range of 80-100 ^{o}C are required to provide an adequate rate of oxidation (Golden and Sircar, 1990).

A gas phase oxidised carbon was prepared by heating 1 g of carbon in a horizontal furnace under a flow rate of 100 mL min^{-1} of nitrogen, until the desired temperature (420 ^{o}C) was reached. Following, a flow rate of 10 mL min^{-1} of dry compressed air was added to the nitrogen stream, and the sample was held at this temperature for additional 3 hours, before being cooled to room temperature under nitrogen. The carbon obtained was denoted as MAM. The temperature of 420 ^{o}C was selected because it has been reported to be the optimum temperature for the formation of surface oxides (Donnet, 1968; King, 1937). The extent of the oxygen incorporation through the different oxidation treatments was determined by the ultimate analysis of the samples.

3.5 Pore Structure Characterisation of the Carbons

Micromeritics ASAP system

The micromeritics ASAP system uses the gas sorption technique to generate high-quality data for applications that require high performance/high sample throughput. Standard features include six independently operated analysis ports, and a programmable, and fully automated sample preparation module with twelve independently operated ports. Both mesoporous and microporous samples may be characterized using the conveniently built-in t-plot reports.
The Micromeritics ASAP uses the "Physi ViewCalc "(an Excel spreadsheet tool) to calculate BET surface area, Langmuir surface area, t-plot micropore volume, and t-plot external surface area.

The pore structure characterization of the carbon materials was carried out using a Micromeritics ASAP 2420 (Micromeritics Norcross, GA, USA) with N_2 adsorption isotherm measured at -196 ^{o}C. The basics of the analytical technique are simple; a sample contained in an evacuated sample tube is cooled (typically) to cryogenic temperature. Then, it is exposed to analysis gas at a series of precisely controlled pressures. With each incremental pressure, the number of gas molecules adsorbed on the surface increases. The pressure at which adsorption equilibrium occurs is measured and the universal gas law is applied to determine the quantity of gas adsorbed. As adsorption proceeds, the thickness of the adsorbed film increases. Any micropores in the surface are quickly filled, then the free surface becomes completely covered, and finally larger pores are filled. The process may continue to the point of bulk condensation of the analysis gas. Then, the desorption process may begin in

which pressure systematically is reduced resulting in liberation of the adsorbed molecules. As with the adsorption process, the changing quantity of gas on the solid surface is quantified. These two sets of data describe the adsorption and desorption isotherms. Analysis of the isotherms yields information about the surface characteristics of the material.

3.5.1 Experimental procedure

About 200 mg of sample was weighed and placed in the sample tube to degas under vacuum at 300 ^{o}C for 24 hours prior to adsorption measurements. The sample is then exposed to nitrogen gas at a series of precisely controlled pressures. With each incremental pressure, the number of nitrogen molecules adsorbed on the surface increases. The pressure at which adsorption equilibrium occurs is measured and the universal gas law is applied to determine the quantity of gas adsorbed. The apparent surface areas (S_{BET}) were calculated from the physical adsorption of N_2 using the Brunauer, Emmett and Teller (BET) method (see Section 3.7.2). The adsorption data were measured at -196 ^{o}C in the relative pressure range (P/P_0) of 0.01 to 0.10 nm in order to give positive BET constants. Total pore volume was calculated as the amount of nitrogen adsorbed at P/P_0 = 0.99, and the pore volumes in the pores ranging from 19 to 50.1 nm were evaluated by the BJH method (Barrett, 1951) and recorded as mesopore volume. The micropore volumes were calculated by the Dubinin-Radushkevich (DR) method (Gil and Grange, 1996; Rand, 1976), assuming an affinity coefficient of 0.33 (see Section 3.7.3). The pore size distribution was calculated using the Non Local Density Functional Theory (NLDFT) method (Neikmark, 1995) from the adsorption data between 0.00 to 0.90 P/P_0 assuming slit pore geometry.

3.6 Adsorption isotherm

The adsorption isotherm is widely employed for representing the equilibrium states of an adsorption system. This is because it gives useful information regarding the adsorbate, adsorbent and the adsorption process. Adsorption isotherm also helps to determine the surface area of the adsorbent, the volume of the pores, and their size distribution, heat of adsorption, and the relative absorbability of a gas or a vapour on a given adsorbent. Data for isotherms analysis is gathered from gravimetric or volumetric studies, in which the change in mass with changing pressure is recorded at a constant temperature. The pores of the adsorbate are emptied under vacuum, and then a stream of the adsorbate (either gas or vapour) is exposed to the material to give the isotherm. The change in mass corresponds to the amount of gas or vapour adsorbed by the material. A plot of amount adsorbed in mmol g^{-1} against relative pressure (P/P^0) gives the adsorption isotherm. The saturation vapour pressure is the pressure at which the vapour is in equilibrium with its non-vapour phase, which is specific at a given temperature. Gas/vapour condensation usually occurs at $p/p^0 = 1$. For volumetric data, when the sample reaches equilibrium with the adsorbate gas, the final equilibrium pressure is recorded, and used to calculate the quantity of gas adsorbed by the sample. A plot of the equilibrium volume adsorbed against the equilibrium pressure gives the adsorption isotherm.

3.6.1 Classification of isotherms

Six possible isotherm shapes can be obtained from isotherm data and are classified according to Brunauer, Deming, Deming and Teller (BDDT) classification. These isotherm types are shown in Figure 3.11.

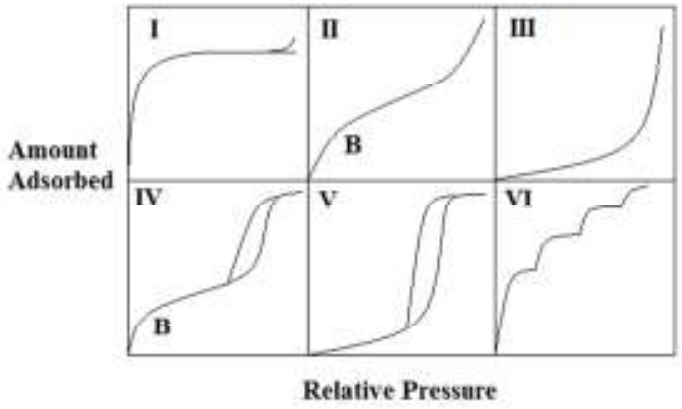

Figure 3.11. BDDT classification of isotherms (Goyal and Bansal, 2005).

Type I isotherm

This isotherm is concave to the relative pressure axis. As the majority of micropore filling occurs at relative pressure of less than 0.1, the steep uptake at the start of this isotherm is indicative of an adsorbent with a microporous structure. Materials which show this type of isotherm include zeolites, activated carbons and metal organic frameworks.

Type II isotherm

This isotherm shape is obtained when gases are adsorbed onto non-porous solids. Monolayer coverage occurs, followed by multilayer coverage at the start of the linear section of the isotherm marked Point B on Figure 3.11. Nitrogen adsorption on non-porous or macroporous powders such as carbons or oxides often gives this type of isotherm.

Type III isotherm

This isotherm can be exhibited by non-porous and microporous solids. It often results when there are weak interactions between adsorbate and adsorbent, leading to a convex shape isotherm. The uptake increases at higher relative

pressure after a molecule of adsorbate has been adsorbed. Adsorption of water on activated carbons exhibits this type of isotherm.

Type IV isotherm

This isotherm follows the same shape as the Type II isotherm, with the first section being attributed to the same monolayer – multilayer formation. This isotherm contains a "hysteresis" loop (see Section 3.6.2), and takes place in the mesoporosity of a material. Hysteresis is often associated with capillary condensation.

Type V isotherm

This isotherm has the same shape as a Type III isotherm, but displaying a "hysteresis" loop.

Type VI isotherm

This stepped isotherm was first introduced as a theoretical isotherm, and indicates an adsorption on homogenous, non-porous surfaces. The steps shown on the isotherm indicates the presence of multilayer.

3.6.2 Adsorption hysteresis

Hysteresis loops generally occur in the multilayer region of adsorption isotherms, as shown in isotherm types IV and V above. Hysteresis loops are associated with the filling and emptying of mesopores. In carbon based materials the hysteresis is based on pore filling (capillary condensation).

3.7 Methods for interpreting the adsorption isotherms

Isotherm models are used to interpret the adsorption isotherms. There are four isotherm models which can be used for analysis: Langmuir, Brunauer – Emmett - Teller (BET), Dubinin Radushkevich method (DR), Temkin adsorption isotherm and Freundlich models. These models make use of the isotherm data to produce a linear plot for analysis. The Langmuir, the Freundlich, and the Temkin are very important for chemisorption. Although, the Langmuir and the Freundlich isotherms are equally important for physisorption, the BET equation and the Dubinin equations are more important for analysis of the physical adsorption of gases and vapour on porous carbon (Goyal and Bansal, 2005). As such, only the BET, Langmuir and Dubinin isotherm models have been discussed in this work.

3.7.1 Langmuir Model

The Langmuir isotherm equation is the first theoretically developed adsorption isotherm equation. Subsequent equations were either based on this equation or its concepts (Ruthven, 1984; Goyal and Bansal, 2005). The Langmuir model is based on three major assumptions:

- The surface of the adsorbent contains adsorption sites which are all energetically homogenous.
- Only one molecule may be adsorbed onto one site, and coverage stops at monolayer capacity.
- The adsorbed molecules have no interaction with other adsorbed molecules.

In the Langmuir model, at equilibrium the rate of adsorption is equal to the rate of desorption. The Langmuir equation can be written as

$$\frac{n}{n_m} = \frac{bp}{1+bp} \ldots\ldots\ldots (3.1)$$

Where n is the number of moles adsorbed per gram of the adsorbent and n_m is the monolayer capacity in moles, p represents the pressure of the system, b the Langmuir constant.

The Langmuir equation is applicable to Type I isotherms. When originally applied, the amount adsorbed at the plateau of the isotherm was thought to be the value of monolayer coverage. This has since been amended as the plateau was reported to be associated with the completion of pore filling rather than monolayer coverage (Rouquerol et al., 1999).

3.7.2 Brunauer – Emmett – Teller (B.E.T) model

Type II and Type IV isotherms are often classified as B.E.T isotherms. In the 1930's Brunauer and Emmer worked on the adsorption of nitrogen onto a synthetic iron ammonia catalyst (Rouquerol et al., 1999; McMillan and Teller, 1950). This led to the discovery of the sigmoidal shaped Type II isotherm, and multilayer formation. They discovered that the change from monolayer capacity to multilayer capacity occurred at Point B (see Figure 3.11), the start of the linear section of the isotherm (Rouquerol et al., 1999). The equation they derived built on the Langmuir model to take into account multilayer adsorption. The assumptions used in deriving this model were the same as Langmuir, with the following additions:

- Unrestricted multilayer formation may take place. The first layer of adsorbed molecules acts as a base for the adsorption of the second layer of molecules, which in turn acts as a base for the adsorption of

the third layer, and so on, so that the concept of localization is maintained in all layers.

- Only the uppermost layers of molecules in the multilayer system are in dynamic equilibrium with the vapour.
- The forces of interaction between the adsorbed molecules are neglected, so at equilibrium, the rate of condensation on the bare surface is equal to the rate of evaporation from the first layer.

The summation of the amount adsorbed in all the layers yields the BET equation (3.2$\frac{P}{n(P_0-P)} = \frac{1}{n_m C} + \frac{(C-1)}{n_m C}\left(\frac{P}{P_0}\right) \ldots\ldots\ldots (3.2)$. From this, the BET surface area of the adsorbent may be calculated using equation (3.3).

$$\frac{P}{n(P_0 - P)} = \frac{1}{n_m C} + \frac{(C-1)}{n_m C}\left(\frac{P}{P_0}\right) \ldots\ldots\ldots (3.2)$$

$$C \approx e^{-\left(\Delta H^0{}_{AD} + \Delta H^0{}_{VAP}\right)/RT} \quad \ldots\ldots\ldots (3.3)$$

Where C is the BET parameter, R is the universal constant, $\Delta H^0{}_{AD}$ is the values of enthalpy of adsorption, T is the temperature, and $\Delta H^0{}_{VAP}$ is the values of enthalpy of vapourization.

The BET equation is very useful for explaining adsorption data on nonporous and macroporous surfaces. It is the most widely used adsorption isotherm model for surface area studies (Blackman, 2005) with nitrogen being the standard adsorptive at -196 ^{o}C (Brunauer et al., 1940). The equation sometimes loses its applicability on microporous adsorbents. Some authors are of the view that the BET concept loses it meaning because the adsorption takes place through volume filling of micropores (Goyal and Bansal, 2005). In the relative pressure range of 0.05 to 0.35, the BET adsorption isotherm is

most frequently linear. At lower relative pressures, equation (3.2) is not usually valid because the influence of surface heterogeneity becomes significant. It also losses its validity at higher relative pressures due to the occurrence of adsorption by capillary condensation and physical adsorption.

3.7.3 Dubinin-Radushkevich (DR)

Dubinin proposed a new theory of pore filling, rather than the adsorption via layers as proposed by Langmuir and Brunauer. Dubinin proposed the theory of the volume filling of micropores, where adsorption occurs through the filling of micropores from the smallest to the largest pores (Dubinin, 1989; Dubinin, 1974; Dubinin, 1980; Dubinin, 1981). The Dubinin-Radushkevich method allows the calculation of micropore volume from the low pressure regions of the DR plot. The DR plot is based on a Gaussian distribution of energy within the micropores, which is related to the pore size, due to the potential energy of pore walls increasing with increasing pore wall proximity. The DR plot is obtained by analysing isotherms of CO_2 adsorption at 0 ^{o}C.

The general form of the DR equation is:

$$\ln W = \ln K - D\left(\ln\frac{p^0}{p}\right)^2 \text{.... ... .(3.4)}$$

Where $D = \frac{W_0}{\beta^2}(RT)^2$ = a measure of the pore size distribution of the adsorbent, W_0 is the micropore volume, W = amount adsorbed at pressure p; K = total amount adsorbed; p = pressure; p^0 = saturation vapour pressure, a constant characterising the pore-size distribution, β is a constant called the affinity coefficient for a given pair of vapour, and its value is independent of the temperature and the nature of the porosity of the given adsorbent (active

carbon). β is thus a measure of the absorbility of a given vapour used on a given carbon with respect to the vapour selected as standard.

A plot of $\ln W$ against $\left(\ln \frac{p^0}{p}\right)^2$ is a straight line with slope D and intercept W_0. The steeper the gradient of the line, the wider the distribution of micropore sizes. The intercept W_0 gives the micropore volume. Any deviations from a linear plot can be explained by the presence of larger porosity, or the filling of larger pores, such as mesopores. This plot makes it possible to calculate the micropore volume from the low-pressure part of the isotherm and offers the possibility of using different adsorbates as molecular probes.

3.7.4 Density functional theory (DFT)/ non-linear density functional theory (NLDFT)

DFT/NLDFT describes the gas adsorption process at the fluid-solid interface. It provides a method by which the total experimental isotherm can be utilized to determine both microporosity and mesoporosity as a continuous distribution of pore volume with respect to pore size. Conventional data reduction methods apply to particular regions of the isotherm, and require transitions to other methods when moving between these regions. DFT/NLDFT provides a continuous distribution, with smooth transition between regions and all data are used. In DFT, variational method is used to minimise the free energy functional, and this makes it easy to determine the density profile. For systems whose fluids are simple and near-spherical molecules, the accuracy of the DFT model isotherm obtained competes with those from molecular simulation. However, the computational time needed by DFT is typically about one percent of the time needed to complete a simulation for the same system (Schuth et al., 2002). Although, DFT is difficult to apply for more realistic

disordered pore structures, it has computational advantage over molecular simulation for simple fluids and pore shapes like slits, spheres, or cylinders.

3.8 Flash elemental analyser

Elemental Analysis (EA) is a process that analyses the elemental (H, C, N, O) composition of a chemical compound. It examines the weight percent of each element in the compound to determine the compound's composition. The elemental analysis of this research work was conducted using the Flash Elemental Analyser (Flash EA 1112 series) with MAS 200 R autosampler, controlled by Eager Xperience, and manufactured by Thermo Electro Corporation.

Experimental procedure

About 3 mg of sample is wrapped inside a tin capsule and introduced into the combustion reactor via the MAS 200 Autosampler together with a proper amount of oxygen. After combustion, the reaction gas products are carried by a helium flow to a layer filled with copper. It is then swept through a GC column that provides the separation of the combustion gases and finally detected by a thermal conductivity detector.

Samples were prepared and analysed in triplicate to check reproducibility of results. Total run time is less than 8 minutes. A complete CHNO report is automatically generated by the Eager 300 dedicated software and displayed at the end of the analytical cycle.

Hydrogen correction was carried out by using data obtained from the proximate analysis of the samples. The method parameters are as detailed below:

Temperatures: Furnace 900 ^{o}C, Oven 65 ^{o}C

Gases: Helium 250 kPa, Oxygen 300 kPa

Carrier 140 mL min^{-1}, Reference 100 mL min^{-1}, Oxygen 250 mL min^{-1}

Timing: Sampling delay 12 seconds, Oxygen injection end 8 seconds

Separation: Multi-separation column PTFE, 2m x 5mm

Detection: Thermal conductivity detector.

3.9 Thermogravimetric analyser

Thermogravimetric Analyzer (TGA) Q-500 manufactured by TA Instruments (**Error! Reference source not found.**) was used for the proximate analysis, thermal stability, and CO_2 uptake capacity of adsorbents at ambient pressure. The TA Q500 TGA is equipped with a Hi-ResTM option to complement the standard mode for conducting TGA experiments. The TGA measures the weight change in a material, either as a function of increasing temperature, or isothermally as a function of time, in a controlled atmosphere. The TGA Q-500 operates in the temperature range from ambient to 1000 ^{o}C, and has an isothermal temperature accuracy of ±1 ^{o}C and isothermal temperature precision of ±0.1 ^{o}C. It has a weighing capacity of 1.0g, a sensitivity of 0.1 µg and a precision of ±0.01 %.

3.9.1 TGA experimental procedures

Proximate analysis

Proximate analysis was conducted on materials to determine the amount of moisture, volatiles, fixed carbon and ash present in it. To determine this, about 10 mg of sample was placed in a platinum specimen pan and heated to 110 ^{o}C at the rate of 20 ^{o}C min^{-1} under nitrogen atmosphere. It was held isothermal for 15 minutes to remove moisture from the samples. The system's temperature was raised to 900 ^{o}C at the rate of 10 ^{o}C min^{-1}, and left isothermal for 20 minutes. The gas was automatically changed to air at the

end of the 20 minutes. The system was left isothermal for another 20 minutes for complete sample burn out to occur. After this, the system was then cooled to 100 ^{o}C at the rate of 50 ^{o}C min^{-1}. The proximate results (moisture, volatiles, fixed carbons, and ash contents) were obtained by calculating the corresponding weight changes between each successive isothermal condition at the end of the experiment.

CO_2 uptake tests

The sample was dried as specified above. After this, the sample was cooled to 25 ^{o}C at the rate of 15 ^{o}C min^{-1}, and allowed to equilibrate. Gas was automatically changed to CO_2 and the system was left isothermal for another 30 minutes for CO_2 uptake to occur. Adsorption tests for selected adsorbents were also performed at 40, 60, and 80 ^{o}C to compare uptake at the different temperatures. Results obtained were automatically logged by the computer, and from these, the CO_2 uptake capacity was calculated.

Temperature programmed desorption (TPD)

Samples were dried as described above, and CO_2 uptake undertaken as specified above. After adsorption had taken place, the system's temperature was ramped to 250 ^{o}C at the rate of 5 ^{o}C min^{-1}, still under CO_2 atmosphere. After this, the system was cooled to 50 ^{o}C at a ramp rate of 50 ^{o}C min^{-1}. Results obtained (weight increase or decrease) were logged automatically by the computer.

3.10 Adsorption kinetic models

It is important to understand the rate or kinetics of adsorption which can be very useful for adsorber design and operation. To describe the adsorption processes of adsorbents in this research quantitatively, and identify the adsorption mechanism, the pseudo-first order and pseudo-second order

adsorption kinetic models have been used. It is a common approach to fit experimental data with a series of popular models and find the most suitable one which provides the best fit. Ho and McKay, (1999) and Khezami et al., (2005) have used this models to study the adsorption kinetics of Congo red and chromium (VI) respectively on activated carbon. Reviews on models for adsorption kinetics are available elsewhere (Ho, 2004; Ho, 2006; Plazinski et al., 2009).

3.10.1 Pseudo-first-order

Lagergren's first order equation (Yuh-Shan, 2004) is the earliest model to describe the kinetic of an adsorption process based on adsorption capacity. It is summarized as follows:

$$\frac{dq_t}{dt} = k_1(q_e - q_t) \dots\dots\dots (3.11)$$

where q_e and q_t (mmol g^{-1}) are the adsorption capacities at equilibrium and time t (s), respectively. Furthermore, k_1 (s^{-1}) is the rate constant of pseudo-first-order adsorption. After integration with its initial condition of $q_t = 0$ at $t = 0$, the integrated form of Equation (3.11) becomes:

$$\ln\left(\frac{q_e}{q_e - q_t}\right) = k_1 t \dots\dots\dots.. (3.12)$$

which can be rearranged to

$$q_t = q_e(1 - e^{-k_1 t}) \dots\dots\dots\dots (3.13)$$

3.10.2 Pseudo-second-order

The pseudo-second-order adsorption kinetic model is expressed as (Ho and McKay, (1999):

$$\frac{dq_t}{dt} = k_2(q_e - q_t)^2 \dots\dots\dots (3.14)$$

where q_e and q_t (mmol g^{-1}) have the same definitions as that in the pseudo-first-order model. In addition, k_2 (mmol g^{-1} s^{-1}) is the rate constant of pseudo-second-order adsorption. With its initial condition of $q_t = 0$ at $t = 0$, the integrated form of Equation (3.14) becomes:

$$\frac{1}{q_e - q_t} = \frac{1}{q_e} + k_2 t \ldots\ldots\ldots (3.15)$$

which can be rearranged to

$$q_t = \frac{t}{\frac{1}{k_2 q^2{}_e} + \frac{t}{q_e}} \ldots\ldots\ldots (3.16)$$

3.10.3 Correlation coefficients and error function

The conformity between the experimental data and the model simulated values were expressed by the square of the adjusted correlation coefficients R^2, (Equation 3.17) and error function Err, (Equation 3.18).

$$R^2 = 1 - \left(\frac{\sum_{i=1}^{m}\left(q_{i,exp} - q_{i,sim}\right)^2}{\sum_{i=1}^{m}\left(q_{i,exp} - \overline{q_{exp}}\right)^2}\right).\left(\frac{m-1}{m-p}\right) \ldots\ldots\ldots\ldots (3.17)$$

$$Err = \sqrt{\left(\frac{1}{m-p}\right).\sum_{i=1}^{n}\left(q_{i,exp} - q_{i,sim}\right)^2} \ldots\ldots\ldots (3.18)$$

where $q_{i,exp}$ is the experimental data of CO_2 adsorbed, $q_{i,sim}$ is the value simulated by the models, $\overline{q_{exp}}$ is the average of experimental data. Furthermore, m is the number of experimental data, and p is the number of parameters of the model. High R^2 value, close to 1, and low error function indicate that the model can successfully describe the kinetics of the adsorption process.

3.11 Error analysis

It is crucial to understand that all measurements of physical quantities are subject to error or uncertainties. In order to draw valid conclusions, the error must be indicated and dealt with properly. As such, all the measurements undertaken in this research was repeated at least five times to ascertain reproducibility and to calculate the error associated with each measurement.

Standard error was used in calculating the errors associated with the measurements in this thesis. Standard error is given as

$$\frac{s}{\sqrt{n}} \text{ ..... } (3.19)$$

Where s is sample standard deviation given as

$$\sigma = \sqrt{\frac{\sum_x^n (x - \bar{x})^2}{n - 1}} \text{ ... ... } (3.20)$$

and *n* is the size (number of the observations) of the sample.

3.12 The high pressure volumetric analyser (HPVA)

The High Pressure Volumetric Analyser (HPVA) from Particulate Systems was used for volumetric analysis in this thesis. It is designed to obtain high-pressure adsorption isotherms using gases such as hydrogen, methane, and carbon dioxide employing the static volumetric method. The volumetric technique consists of introducing (dosing) a known amount of gas (adsorbate) into the chamber containing the sample to be analysed. When the sample reaches equilibrium with the adsorbate gas, the final equilibrium pressure is recorded. This process is repeated at given pressure intervals until the

maximum pre-selected pressure is reached. Each of the resulting equilibrium points (volume adsorbed and equilibrium pressure) is then plotted to provide an isotherm. Also, these data are then used to calculate the quantity of gas adsorbed by the sample. The amount of gas adsorbed by the sample is calculated by referencing the "REFPROP" included in the system's software (calculations in the REFPROP is based on formulae presented in Section 3.12.3.

Excellent reproducibility and accuracy are obtained by using separate transducers for dosing the sample and for monitoring the pressure in the sample chamber.

The adsorption equilibrium state was considered to occur when the respective temperature and pressure of the cells were constant. During the adsorption, the adsorption cell is enclosed in a water bath and the temperature maintained constant within 0.01 ^{o}C by the refrigerating circulator (Julabo FC31 circulating water bath).

The pre-measurement procedures for the HPVA are presented in the following subsections.

3.12.1 Free space analysis

The HPVA system is designed such that it performs free space analysis (FSA) each time a fresh analysis is done. FSA on the HPVA was achieved using helium gas. Helium is dosed into the cell containing the sample. At equilibrium manifold temperature and pressure, the free space around the sample are measured and recorded. Using the ideal gas equation, the free space is calculated. At the end of any analysis, the HPVA system accounts for the free space while calculating the volume of CO_2 adsorbed by materials.

3.12.2 Pre-measurement procedure

3.12.2.1 Blank analysis

Blank analysis was conducted using CO_2 gas. An empty sample cell was inserted in the water bath and firmly fastened to the analysis arm of the HPVA. A known volume of water was poured into the water bath to keep the sample cell at room temperature. Before dosing the system with CO_2, the manifold pressure and temperature are automatically recorded. As CO_2 is dosed into the sample cell, the equilibrium pressure and temperature reading at the manifold are also automatically recorded. The ideal gas equation (Gi-moon et al., 2005) is employed to automatically calculate the blank volume. The equipment was allowed to run at 25 and 40 ^{o}C so as to get the blank volumes for both temperatures. All operations were automatic. Results obtained (blank volume) from this analysis were used to compute accurate CO_2 adsorption measurements. This was achieved by manually subtracting the blank volume from the volume of CO_2 measured by the system at the end of each experiment.

3.12.2.2 Sample loading

About 1-2 g of sample is placed in a thoroughly cleaned steel sample cell. A gasket made of stainless steel is placed on the cell top to prevent materials from being sucked into the HPVA system. The sample cell is then attached to the degas/analysis port of the HPVA as the case may be.

3.12.2.3 Degas procedure

After sample loading operation, the sample cell was inserted into a furnace and attached to the degas limb of the HPVA. The furnace was set to heat up to 120 ^{o}C. The equipment was left to run overnight for complete degas. Complete degas is obtained when the vacuum gauge reads below 12 milli Torr.

3.12.2.4 Analysis procedure

The apparatus was maintained at vacuum following the degas process. The cell containing the degased sample was then attached to the analysis port of the HPVA. The temperature controlled water bath was placed in position and cold water was emptied into it until the cell was completely immersed in the water. The circulating water bath was operated at 25 ^{o}C or 40 ^{o}C depending on desired operating temperature, to ensure uniform temperature within the sample cell throughout the experiment.

As the experiment starts, the system automatically records the equilibrium temperature, pressure and other parameters relating to the experiment. The experiment was left to run until all data resulting from the analysis is collated by the computer. The total time taken to analyse a particular sample depends on the sample's porosity.

3.12.3 The HPVA experimental procedure

The HPVA Series 100 (HPVA-100) analysers capable of achieving pressures up to 100 bar was used for this study. Diagram of the HPVA and its associated equipment is presented in Appendix 5. It has pressure reading accuracy of ±0.04% full scale with a stability of ±0.1%. The operating procedure to determine an adsorption isotherm is to admit CO_2 into the system's manifold, to measure its equilibrium temperature and pressure. CO_2 adsorption capacity is measured by expanding the CO_2 into the adsorption cell, and finally, record the equilibrium temperature and pressure.

Before all operations, the adsorbent was degassed to eliminate trace impurities. After degas operation, pure CO_2 gas was introduced into the loading cell, and its pressure and temperature were automatically measured when the cell stabilized. Then the valve between the loading and sample cells was opened, allowing the gas to contact the adsorbent. The pressure and

temperature were measured after equilibrium was achieved, and the number of moles of CO_2 remaining in the two cells was calculated by the computer. Calculations were made to correct for compressibility of CO_2 in the system. The HPVA system references a "REFPROP" at every step of the analysis to obtain and correct for CO_2 compressibility. The compressibility factors found in REFPROP were based on the mixture of the gas at each step and the temperature/pressure data. The following calculations were used to calculate the volume of CO_2 dosed in the system and the volume adsorbed after analysis.

Calculations for volume dosed:

$$VolA = \left[\left(\frac{(P_mA - P_m0)(manifold\ volume)}{(83.14472)(T_mA + 273.15)(compresibility\ factor\ ZA)}\right)(22414)\right] \dots\dots\dots (3.21)$$

$$VolB = \left[\left(\frac{(P_mB - P_m0)(manifold\ volume)}{(83.14472)(T_mB + 273.15)(compresibility\ factor\ ZB)}\right)(22414)\right] \dots\dots\dots (3.22)$$

$$Volume\ dosed\ = VolA - VolB = Total\ Volume\ dosed \dots\dots\dots (3.23)$$

Calculations for volume adsorbed:

$$V_sNAds = \left[\left(\frac{(analysis\ free\ space)(P_s - P_s0)}{(83.14472)(T_{ms} + 273.15)(compresibility\ factorZS)}\right)(22414)\right] \dots\dots\dots (3.24)$$

$$V_{xl}NAds =$$

$$\left[\left(\frac{(P_s - P_s0)(ambient\ free\ space - 7 - analysis\ free\ space)}{(83.14472)(ambient\ temperature + 273.15)(compresibility\ factor\ Zxl)}\right)(22414)\right] \dots\dots\dots (3.25)$$

$$V_{xu}NAds = \left[\left(\frac{(P_s - P_s0)(7)}{(83.14472)(T_mB + 273.15)(Zxu)}\right)(22414)\right] \ldots\ldots\ldots \quad (3.26)$$

$$VOl\ NAds = V_{xl}\ NAds + V_{xu}\ NAds + V_s\ NAds \ldots\ldots\ldots (3.27)$$

$$Vol\ Ads\ = Total\ volume\ dosed - Vol\ NAds \ldots\ldots\ldots (3.28)$$

$$Vol\ Ads\ g^{-1} = \frac{Vol\ Ads}{sample\ weight} \ldots\ldots\ldots (3.29)$$

$$wt\% = \left(\frac{(Vol\ Ads\ g^{-1})(4401)(100)}{22414}\right) \ldots\ldots\ldots (3.30)$$

$$Vol\ Ads = wt\% - Vol\ NAds \ldots\ldots\ldots (3.31)$$

Explanation to the different abbreviations used in Equations 3.21-3.30 are presented in Table 3.3.

Table 3.3. abbreviations and interpretation of symbols used in Equations 3.21-3.30.

P_m	Manifold target pressure for dosing (bar)
P_mA	Pressure of manifold before dosing (bar)
T_mA	Temperature of manifold before dosing (°C)
ZA	Compressibility of Adsorbate at P_mA and T_mA
Vol A	Volume of adsorbate in manifold before dosing (cm^3)
P_mB	Pressure of manifold after dosing (bar)
T_mB	Temperature of manifold after dosing (°C)
ZB	Compressibility of adsorbate at P_mB and T_mB
Vol B	Volume of adsorbate in manifold after dosing (cm^3)
Vol Dosed	Volume of adsorbate dosed to sample this step (cm^3)
Total Dosed	Total volume of adsorbate dosed to sample (cm^3)
Ps	Pressure of sample after dosing (bar)
Ts	Temperature of sample after dosing (°C)
ZS	Compressibility of adsorbate at Ps and Ts
Vs NAds	Volume of adsorbate in sample cylinder after dosing
Zxl	Compressibility of adsorbate at Ps and T_mA
Vxl	Volume of adsorbate in lower stem after dosing (cm^3)
Zxu	Compressibility of adsorbate at Ps and T_mB
Vxu	Volume of adsorbate in upper stem after dosing (cm^3)
Vol NAds	Total volume of adsorbate below valve 1 after dosing (cm^3)
Vol Ads	Volume adsorbed by sample (cm^3)
Vol Ads/g	Volume adsorbed by sample/sample mass (cm^3)
wt%	Percentage of sample weight that is adsorbate (wt%)
Comp Fact ZA	is based on P_mA and T_mA
Comp Fact ZB	is based on P_mB and T_mB
Comp Fact ZS	is based on Ps and Ts
Comp Fact ZXL	is based on Ps and ambient temperature
Comp Fact ZXU	is based on Ps and T_mB
Critical pressure	73.80 (bar)
Critical temperature	304.10 (K)

Ambient free Space	15.983039
Analysis free Space	1.000000
Manifold volume	24.422899 (cm^3)
Experiment temperature	25 ^oC
Ambient temperature	25 ^oC
T_m0	35.159917 ^oC
T_s0	24.8325253 ^oC
P_m0	0.0009202 bar
P_s0	0.00022444 bar

CHAPTER FOUR

4 Phenolic Resin Activated Carbons for CO_2 Capture in Gasification

4.0 Introduction

In this chapter, the characterisation and CO_2 capture capacity of phenolic resin derived activated carbons produced by MAST Carbon Ltd. UK have been reported. The aim of this chapter is to evaluate the CO_2 uptake capability of the materials at atmospheric and high pressure conditions, up to 4.0 MPa. The effect of textural characteristic on CO_2 adsorption will be discussed, and the adsorbent with the highest CO_2 uptake will be identified. Full synthesis information can be found in patent (Kozynchenko et al., 2001). However, sample codes have been used for easy identification. Codes E1, TE3, and TE9 indicate the level of pore formers; 11, 16, and 20 represent the level of hexamine cross linking agent used, and 22C, 38C, 49C, 00C, 40C, and 30C represent the level of activation in carbon dioxide. For example, E1/11-22C represent a phenolic resin activated carbon with E1 pore former, 11 hexamine cross linking agent and 22% burn-off degree. For simplicity, abbreviations have been used to represent the different materials as seen in Table 4.1

4.1 Elemental analysis and pore structure characterisation of carbons

The textural properties of the carbons are presented in Table 4.1, while the chemical properties are shown in Table 4.2. Surface area of the materials was observed to be greater than 1000 $m^2\ g^{-1}$. The N_2 adsorption isotherms of MC1, MC2, and MC3 which are presented in Figure 4.1 and that of MC11 presented in Figure 4.4 are Type I according to the BDDT classification (Goyal, 2005), showing that they are mainly microporous materials. However, the MC4, MC5 and MC6 (Figure 4.2) and MC10 (Figure 4.4) show a Type IV adsorption isotherm and a hysteresis loop at relative pressures above 0.7, which is in agreement with a well-developed mesoporosity also assessed by non-linear density functional theory (NLDFT) analysis. The rise in the adsorption isotherms of MC7, MC8, and MC9 (Figure 4.3) at high partial pressures (above 0.9) indicates the presence of porosity in the macropore range. Practically, no mesoporosity has been developed in these samples. The shape of the adsorption isotherms at low partial pressures also indicates the presence of micropores. Amount of nitrogen adsorbed can be seen to be function of the material's surface area and total pore volume. The maximum nitrogen adsorption volume of each carbon correlates to the total pore volume present in the material. This is observed in the different carbons as shown in Table 4.1 and Figure 4.1, Figure 4.2, Figure 4.3, and Figure 4.4. MC6 having highest total pore volume (1.21 cm^3g^{-1}) showed the highest nitrogen adsorption volume of about 730 cm^3g^{-1}. Similarly, increasing carbon surface area translated to increased nitrogen adsorption on the carbons. MC6 has the highest surface area and recorded the highest nitrogen adsorption value.

Table 4.1 pore structutre properties of activated phenolic resin carbons measured at -196 ^{o}C.

Sample name	N_2 adsorption @ -196 ^{o}C							
	Abbreviation	S_{BET} ($m^2\ g^{-1}$)	W_o ($cm^3\ g^{-1}$)	V_{Meso} ($cm^3 g^{-1}$)	V_p ($cm^3\ g^{-1}$)	W_o/V_p	V_{meso}/V_p	ρ_{He} ($g\ cm^{-3}$)
E1/11-22C	MC1	851	0.35	0.01	0.35	0.98	0.04	2.01
E1/11-38C	MC2	1247	0.33	0.03	0.54	0.61	0.05	2.09
E1/11-49C	MC3	1440	0.33	0.04	0.63	0.52	0.12	2.10
TE3/20-00C	MC4	730	0.29	0.24	0.61	0.47	0.39	1.85
TE3/20-22C	MC5	1112	0.35	0.31	0.82	0.43	0.37	2.07
TE3/20-40C	MC6	1722	0.33	0.38	1.21	0.27	0.79	2.14
TE9/16-00C	MC7	640	0.28	0.09	0.48	0.58	0.18	1.93
TE9/16-20C	MC8	1055	0.35	0.11	0.71	0.50	0.15	2.13
TE9/16-30C	MC9	1377	0.32	0.28	0.96	0.34	0.29	2.16
NH_3 Treated beads	MC10	1276	0.56	0.46	1.02	0.55	0.45	2.11
Monolith	MC11	1395	0.58	0.01	0.58	1.00	0.02	2.13

S_{BET}: surface area, W_o: micropore volume, V_P: total pore volume, V_{meso}: mesopore volume, ρ_{He}: helium density.

See Section 3.7 for information on how these parameters are calculated

Table 4.2 Ultimate analysis of the phenolic resin activated carbons.

Sample	N (wt.%)	C (wt.%)	H (wt.%)	O* (wt.%)
MC1	0.24	89	1.00	5.02
MC2	0.29	88	0.45	6.92
MC3	0.60	89	0.61	6.50
MC4	0.75	88	0.89	7.11
MC5	0.40	87	0.49	8.42
MC6	0.36	89	0.22	7.95
MC7	0.21	88	0.51	7.32
MC8	0.17	90	0.24	3.86
MC9	0.18	91	0.20	4.92
MC10	0.23	92	0.42	7.04
MC11	0.81	92	0.15	5.76

*calculated by difference; dry ash free basis

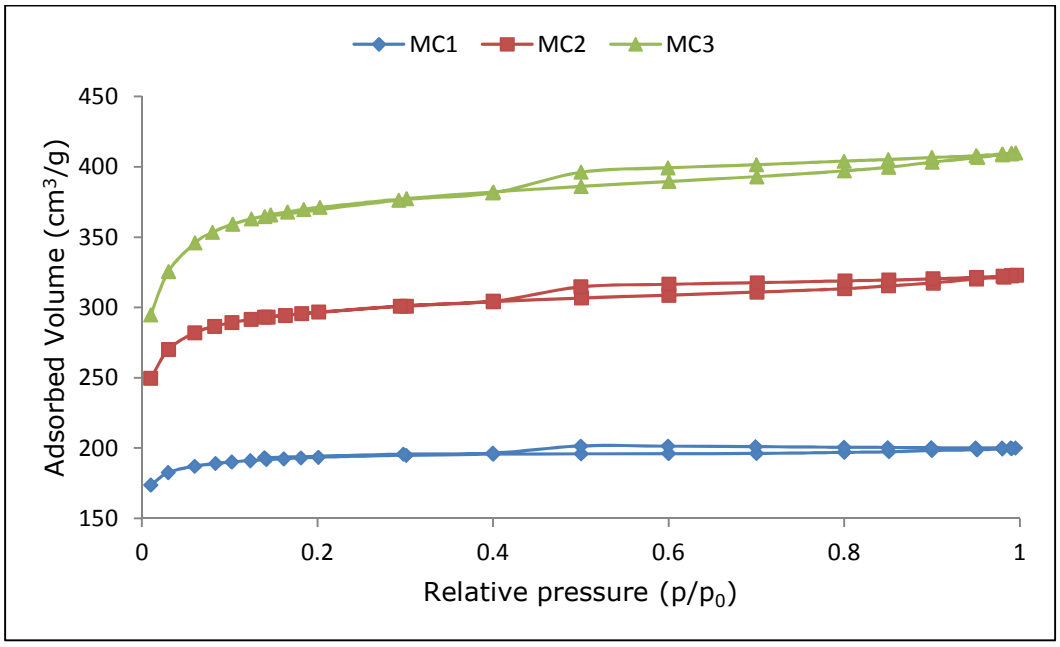

Figure 4.1. N_2 Adsorption isotherm For MC1, MC2 and MC3 measured at -196 ^{o}C.

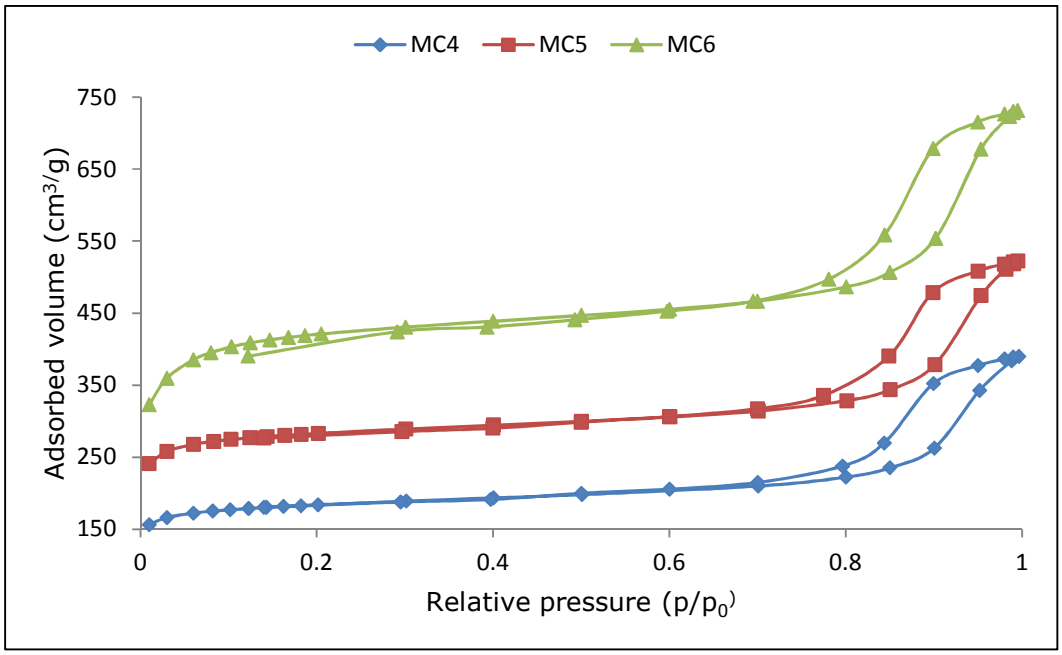

Figure 4.2. N_2 Adsorption isotherm for MC4, MC5 and MC6 measured at -196 ^{o}C.

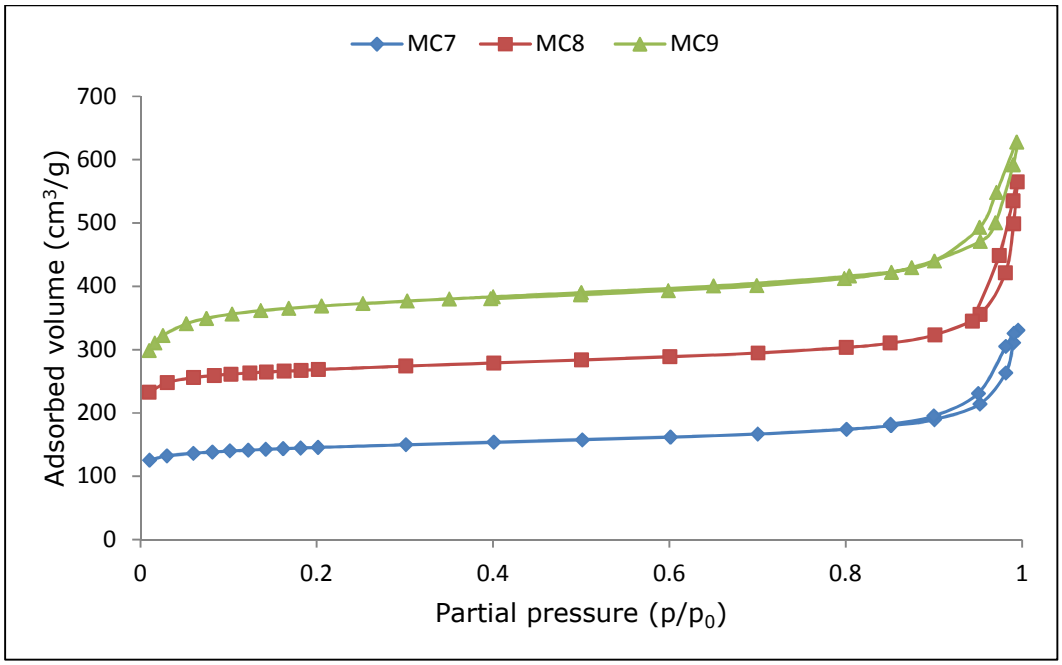

Figure 4.3. N_2 adsorption isotherms for MC7, MC8 and MC9 measured at -196 ^{o}C.

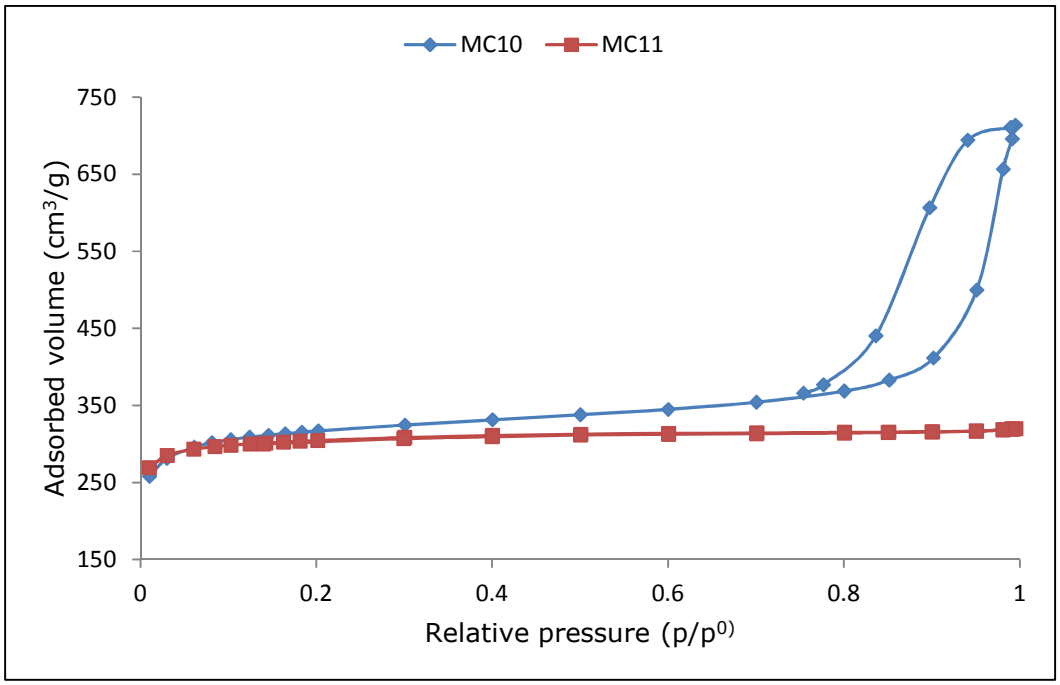

Figure 4.4. N_2 adsorption isotherms for MC10 and MC11 measured at -196 °C.

4.2 CO_2 Uptake Capacity at atmospheric pressure

The CO_2 uptake performance of the adsorbents was evaluated using a Q500 TGA. This was conducted by measuring the mass uptake of the samples when exposed to 100% pure CO_2 (Section 3.9.1). All the samples under study had their highest CO_2 adsorption capacities at room temperature, with the increase in temperature leading to reduction in CO_2 adsorption capacity, the typical performance for a physisorbent. For example, CO_2 uptake of MC1 reduced from 2.85 mmol g^{-1} to 0.52 mmol g^{-1} when the temperature was increased from 25 to 50 °C. This is as expected due to the exothermic character of physisorption, which is the only mechanism available for CO_2 capture on activated carbons (Drage et al., 2009; Martin et al., 2010). Among the

adsorbents, MC11 had the highest CO_2 uptake of ca. 3.3 mmol g^{-1} while MC4 had the lowest CO_2 adsorption capacity of approximately 2.4 mmol g^{-1} (Table 4.3). Higher than that (2.1 mmolg^{-1}) reported in Gil et al., (2012).

Table 4.3. CO_2 uptake capacities of phenolic resin carbons at 25 ^{o}C, atmospheric pressure and 100% CO_2 concentration.

Sample name	CO_2 uptake (mmol g^{-1})
MC1	2.8 ± 0.02
MC2	2.9 ± 0.06
MC3	2.8 ± 0.12
MC4	2.4 ± 0.05
MC5	2.8 ± 0.11
MC6	2.7 ± 0.20
MC7	2.4 ± 0.10
MC8	2.9 ± 0.10
MC9	2.8 ± 0.11
MC10	2.7 ± 0.03
MC11	3.3 ± 0.60

Samples were run at least three times to demonstrate that results obtained from the TGA were reproducible, and the errors are shown in Figure 4.5. MC2, MC7 and MC10 showed little or no deviation from their mean adsorption values, while the minimum deviation for MC6 is 0.0004 mmol g^{-1}. Hence, an indication that all the adsorbents tested except the MC14 would give similar results under the same experimental conditions when required. Also, as the errors are so small, there is confidence in performance comparison of the different materials. The MC11 sample showed a slight difference in its performance with 0.72 mmol g^{-1} deviation from its mean adsorption value. This was further investigated by analysing five different sections of the sample

taken from different areas of MC11. Results showed that the amount of CO_2 adsorbed differ from one section to the other (Figure 4.5). This indicates that MC11 possesses non-uniform surface properties as a result of the synthesis process.

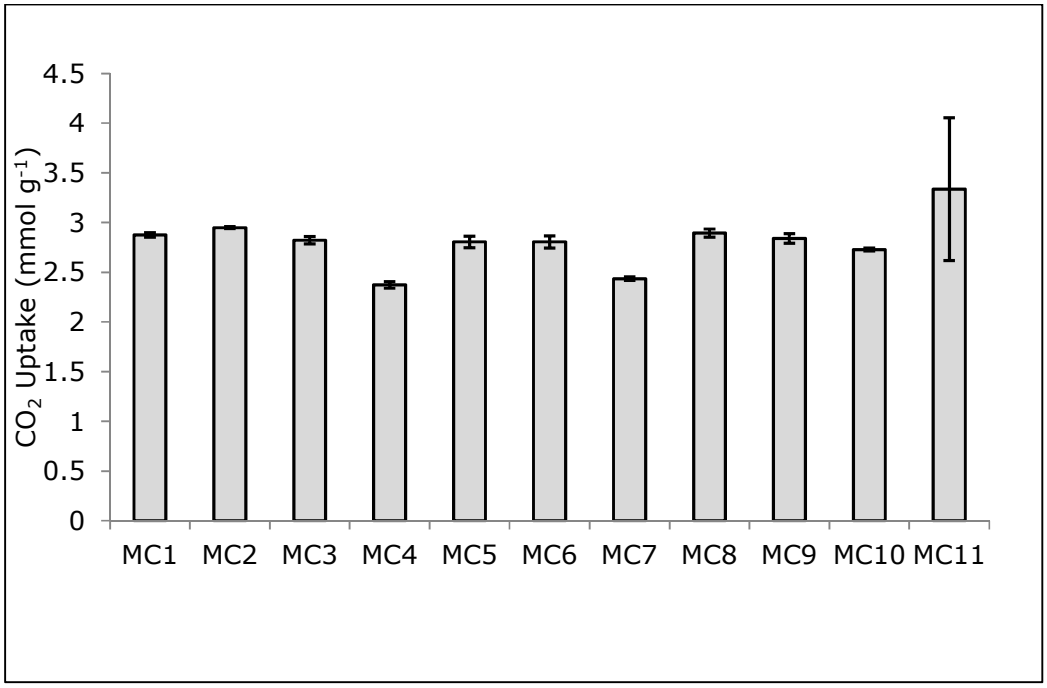

Figure 4.5. CO_2 adsorption capacity of the phenolic resin carbons at 25 ^{o}C and atmospheric pressure. Error bars are calculated from multiple analysis of the materials.

Table 4.4. Five different runs for MC11 showing different CO_2 uptake at 25^{o}C.

Sample name	CO_2 uptake (mmol g^{-1})
1	3.3
2	2.2
3	3.2
4	2.8
5	2.1

4.2.1 Effect of total pore volume, surface area and micropore volume on CO_2 adsorption

The pore volume and the surface area of an adsorbent may give an indication of the suitability of the material for CO_2 capture. Since the molecular size of CO_2 is 0.209 nm (Cazorla-Amoros and Linares-Solano, 1996a), only pores which are less than 1.0 nm have been reported to be effective for CO_2 capture at atmospheric pressure (Cazorla-Amoros and Linares-Solano, 1996b). As shown in Table 4.3, the CO_2 adsorption capacities range from 2.4 to 3.3 mmol g^{-1} for surface area ranging from 640 to 1734 m^2g^{-1}. The high micropore volume of the adsorbents may have contributed to the adsorption capacity, in that, the more microporous a material is, the more likely its voids are filled by CO_2 (Martin et al., 2010; An et al., 2009; Drage et al., 2009; Guang-Ping et al., 2010; Martin et al., 2011a) (Figure 4.7). The trend of CO_2 adsorption capacity increases with increasing surface area and micropore volume (Figure 4.6 and Figure 4.7). The total pore volume of the samples did not play a major role in the adsorption (Figure 4.8). This is expected as only the presence of micropores in carbons has been attributed to be the adsorption points for CO_2 (Martin et al., 2010). Also, no positive trend was observed for the plot between CO_2 uptake capacity and total pore volume (Figure 4.8).

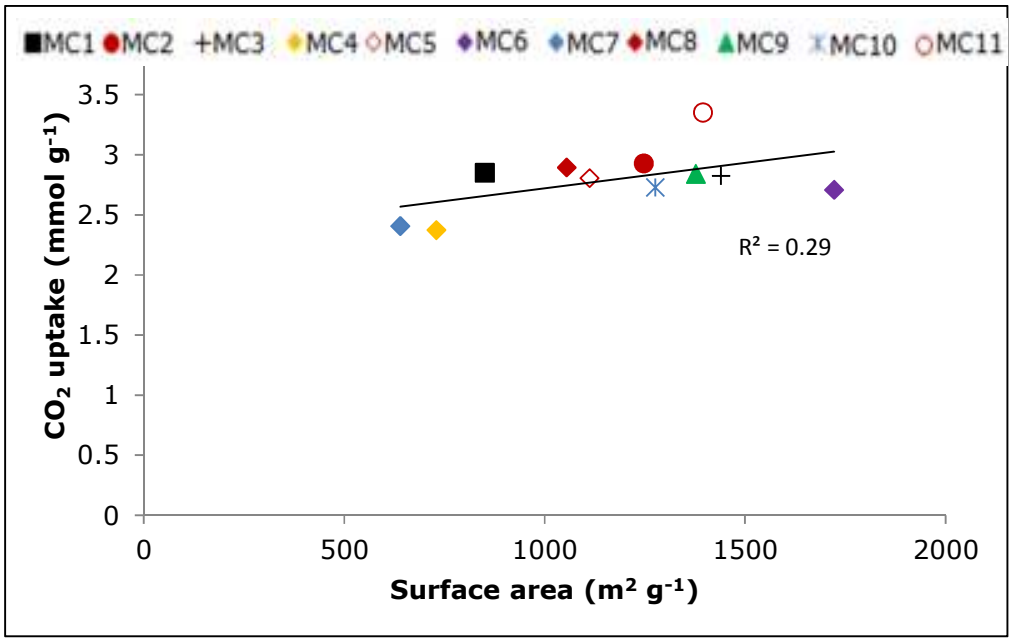

Figure 4.6. CO_2 adsorption capacity in relation to BET surface area at ambient temperature and pressure.

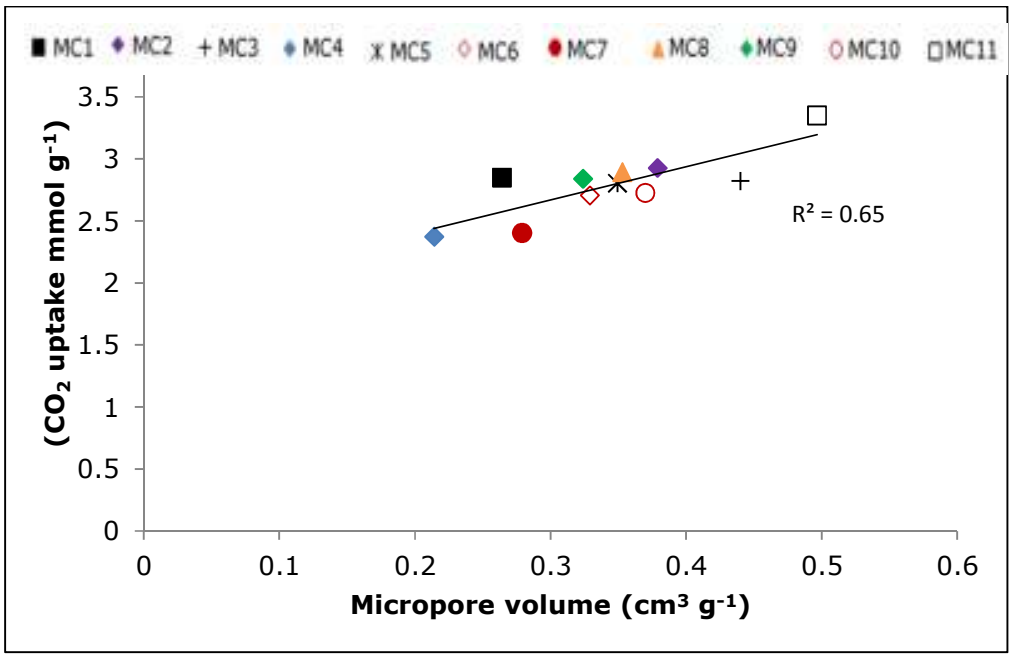

Figure 4.7. CO_2 adsorption capacity in relation to micropore volume at ambient temperature and pressure.

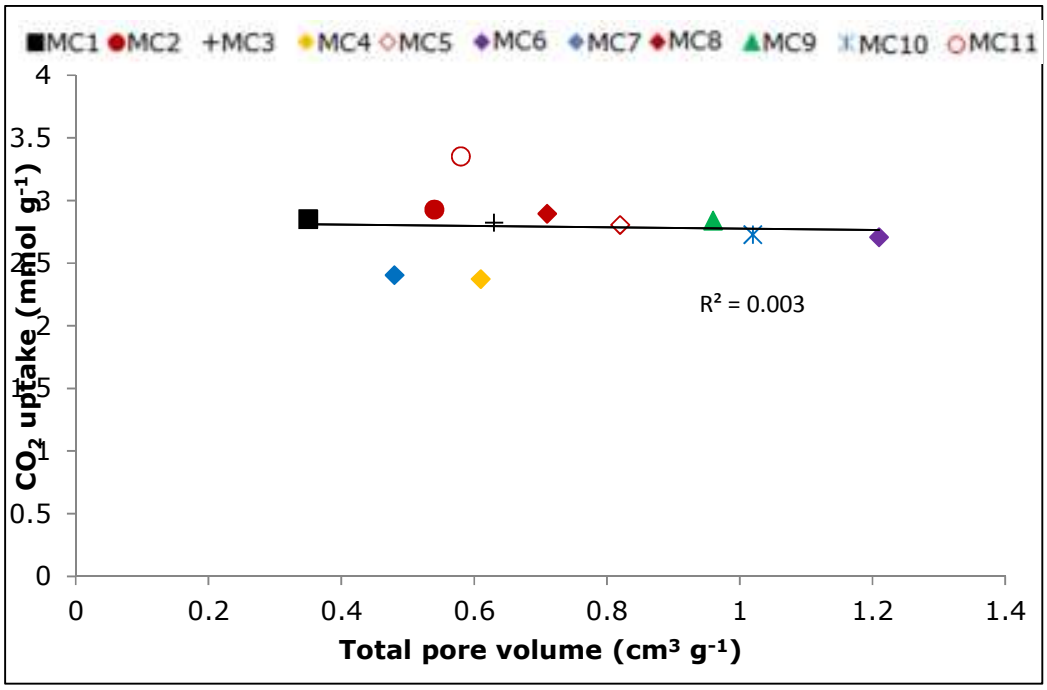

Figure 4.8. CO_2 adsorption capacity in relation to total pore volume at ambient temperature and pressure.

4.2.2 CO_2 Adsorption and temperature

It is obvious from Figure 4.9 and Figure 4.10 that the amount of CO_2 adsorbed by individual adsorbent material depends on the temperature as expected. As indicated in Figure 4.9, the highest adsorption occurred at room temperature. At higher temperatures, the adsorption capabilities of the carbons reduce progressively. These results give an indication that higher temperatures are not necessary for effective adsorption capabilities of the samples, although higher temperatures give a route for regeneration of adsorbents when TSA cycles is employed. This finding is in agreement with results obtained by Drage et al., (2009) when they developed activated carbon adsorbents for pre-combustion CO_2 capture.

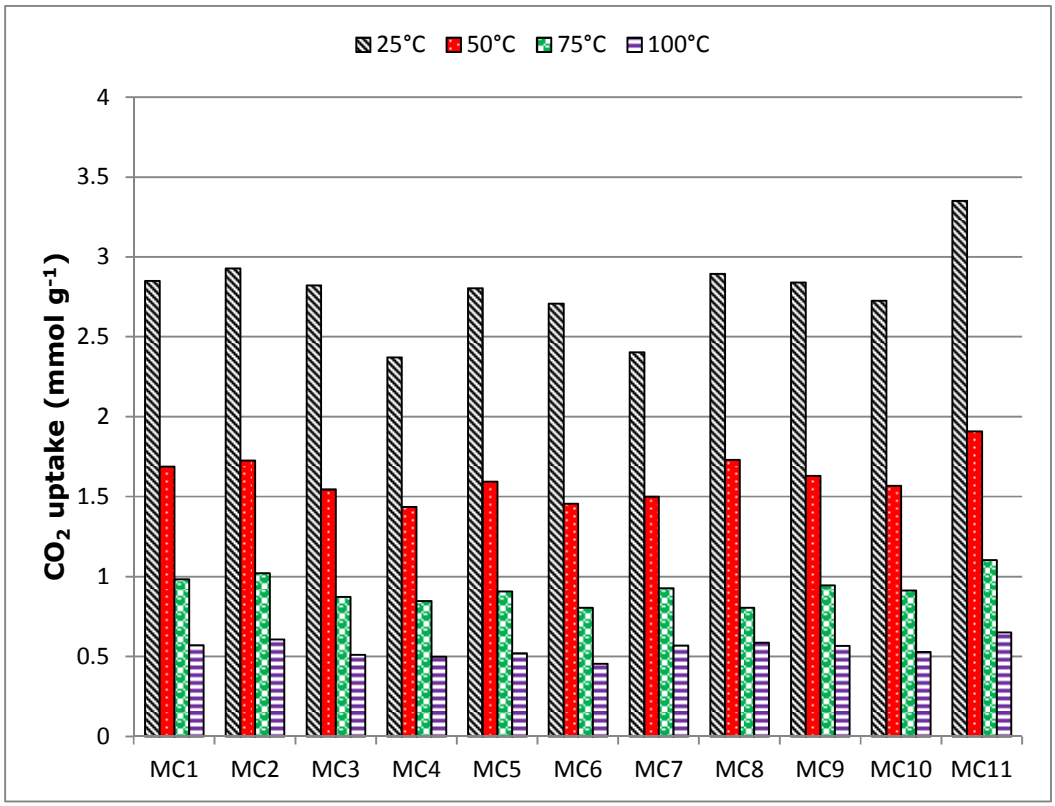

Figure 4.9. CO_2 adsorption at 25, 50, 75, and 100 ^{o}C determined by TG analysis.

Although, individual adsorbent has different maximum adsorption capacities at 25 ^{o}C, their trends are similar. Figure 4.10 shows the TPD profile of the adsorbents. It could be inferred that the adsorbents have similar surface chemistry, retaining less CO_2 capacity at elevated temperature compared to other adsorbents. The CO_2 interactions with the adsorbents surfaces are identical. Rates of CO_2 adsorption decrease uniformly as the temperature increased (Figure 4.10). For example, between 25 ^{o}C and about 30 ^{o}C, there was sharp drop in CO_2 adsorption of approximately 0.3 mmol g^{-1} $^{o}C^{-1}$, whereas, between about 36 and 40 ^{o}C, they showed approximately 0.2 mmol g^{-1} $^{o}C^{-1}$ decrease in adsorption. All samples showed a steady 0.1 mmol g^{-1} $^{o}C^{-1}$ reduction above 140 ^{o}C. Trend of adsorption may be attributed to the large

surface area of the samples and their possession of micropores volumes. As the temperature of the system is increased, the amount of CO_2 adsorbed decreases steadily and tend to zero at 200 ^oC.

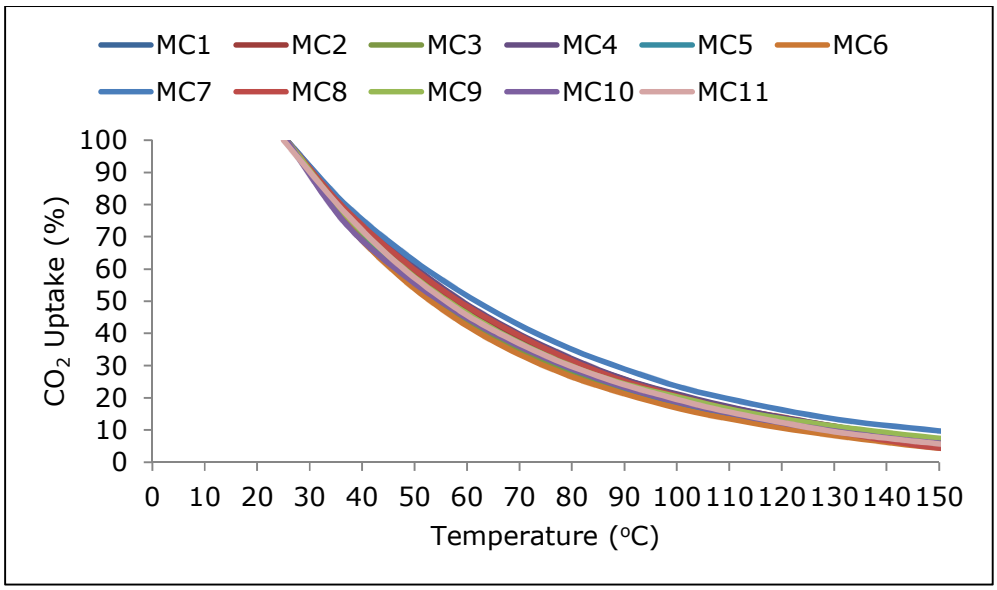

Figure 4.10. Non-isothermal CO_2 capture tests: heating rate of 0.25 $^oC\ min^{-1}$ in 98 mL min^{-1} of CO_2 flow.

4.3 CO_2 uptake at high pressure

This section presents the results of CO_2 uptake measurements at high pressure conditions using HPVA (Section 3.12). Uptake performance has also been related to their textural properties. A range of adsorbents; MC1, MC3, MC4, MC5, and MC11 were selected for this measurements. These adsorbents were selected based on their textural properties and CO_2 uptake performance to cover the range of material studied under ambient pressure conditions.

Total pore volume played a key role in the CO_2 uptake capacity measurements at high pressure. As pressure is increased, the CO_2 uptake capacity of adsorbents increases (Garcia et al., 2011). Unlike observation recorded at

ambient pressure measurements where CO_2 uptake was observed to be due to the contributions from only the micropore and surface area of the adsorbent, CO_2 uptake at high pressure have been observed to be solely due to contribution of the total pore volume(Figure 4.11), and is independent of the micropore size (Martin et al., 2011). Adsorption trends shown in Figure 4.12 and Figure 4.13 suggest that increase in surface area and micropore volume does not affect the amount of CO_2 adsorbed by the adsorbents under high pressure measurement condition. MC4 showed the highest CO_2 uptake capacity at 4.1 MPa. This is about 5 times higher than the amount measured at ambient pressures (Figure 4.14). All other adsorbents except MC1 and MC11 also showed about 5 times more CO_2 uptake capacity at higher pressures than that recorded at high pressures. While the uptake capacity of MC1 doubled at ambient pressure, that of MC11 was tripled in comparison with performance at ambient pressure.

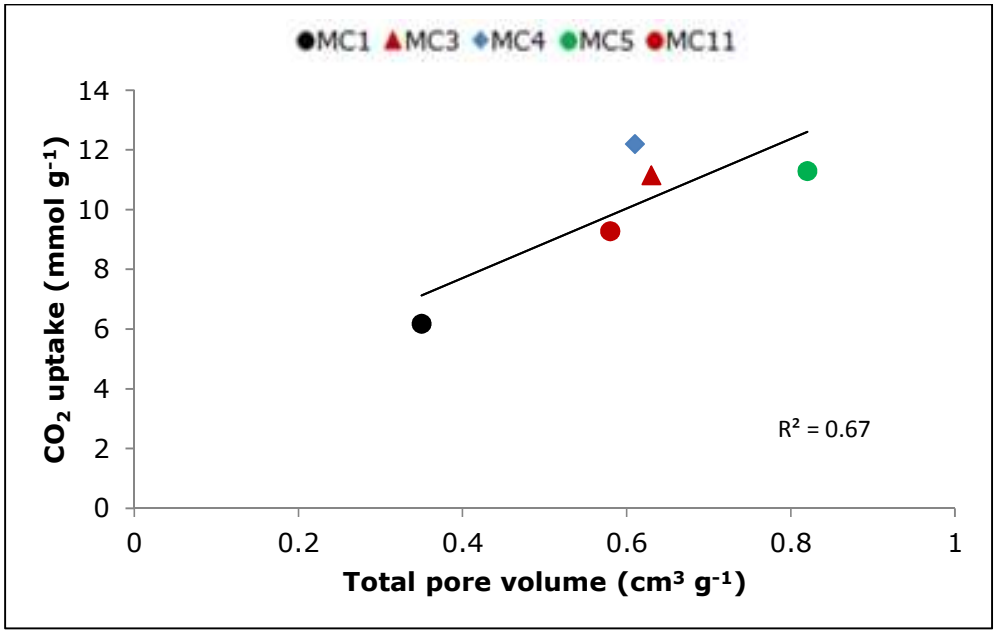

Figure 4.11. Correlation of CO_2 uptake capacity and total pore volume measured at 25 ^{o}C and 4.1MPa.

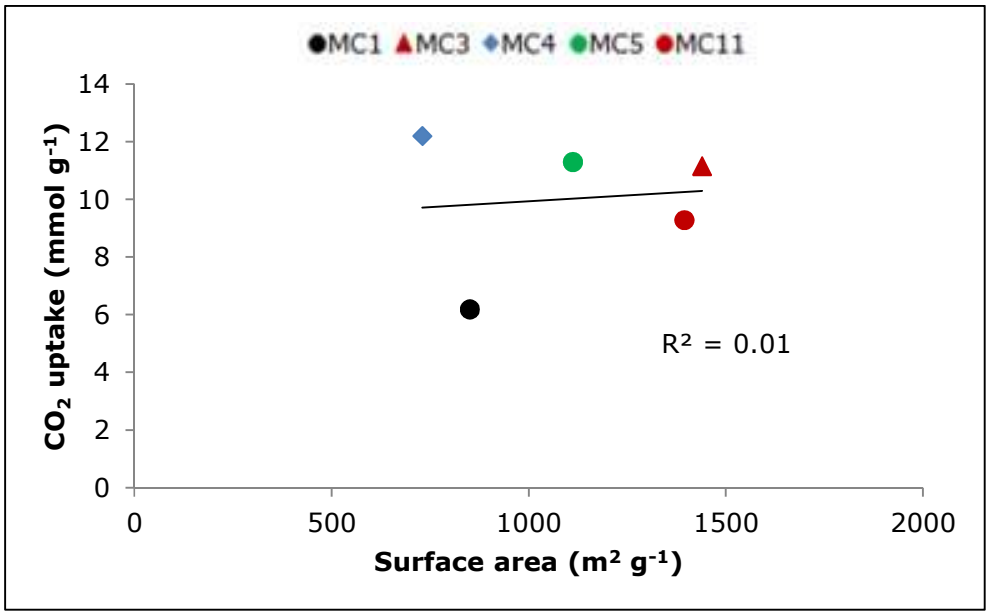

Figure 4.12. Correlation of CO_2 uptake capacity and surface area measured at 25 °C and 4.1MPa.

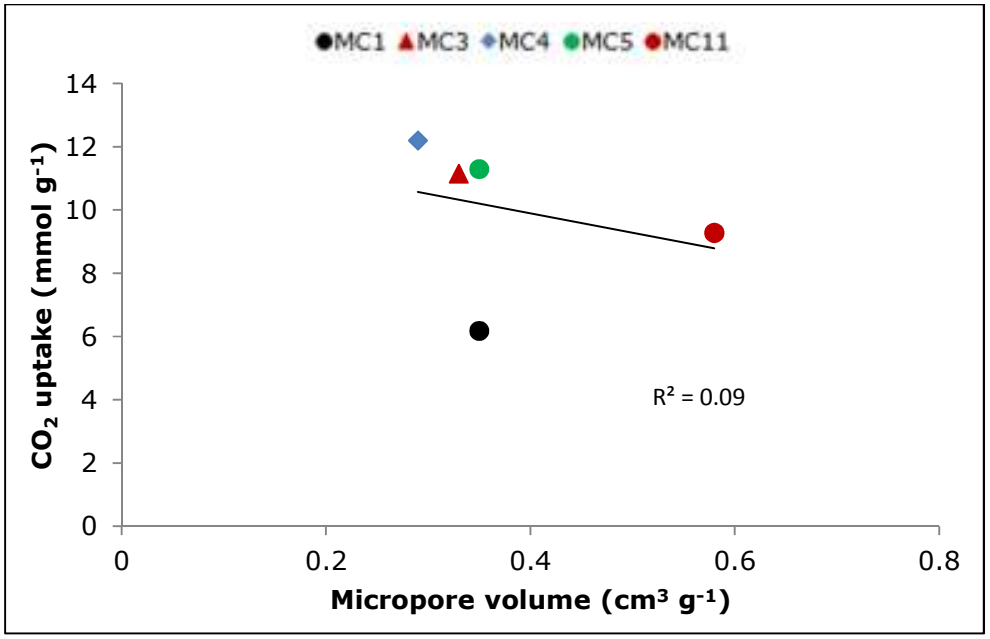

Figure 4.13. Correlation of CO_2 uptake capacity and micropore volume measured at 25 °C and 4.1MPa.

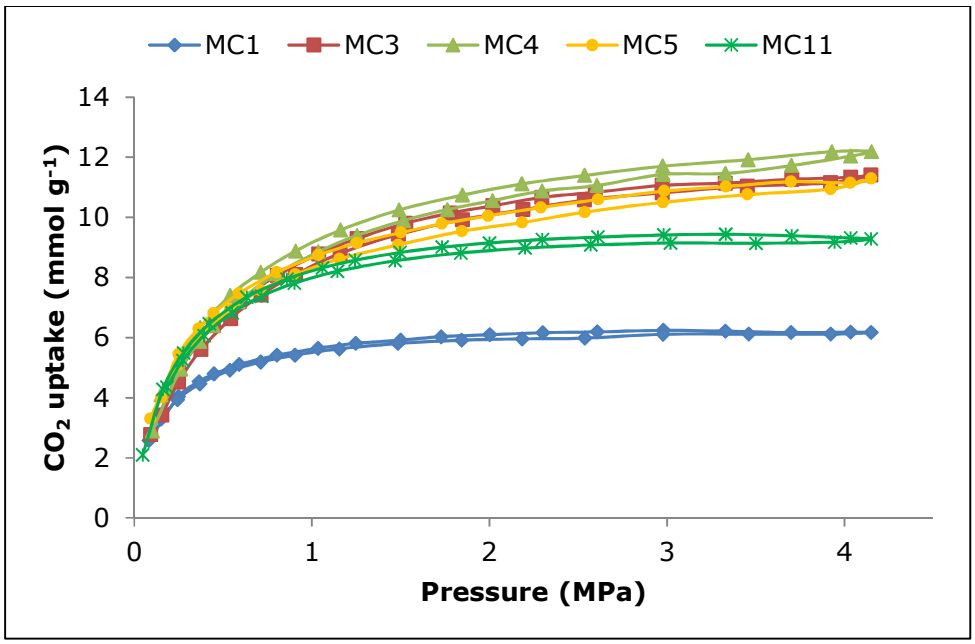

Figure 4.14. CO_2 adsorption isotherm measured at 25 ^oC and 4.1 MPa.

4.4 Summary

The CO_2 uptake capacities of phenolic resin activated carbons have been evaluated at ambient and high pressure conditions. The micropore volume and surface area of adsorbents have been found to be responsible for amount of CO_2 adsorbed at ambient pressures. However, at higher pressures, CO_2 uptake capacity depends on the total pore volume and not on the size of the micropore. MC11 was seen to possess the highest CO_2 uptake of 3.3 mmol g^{-1} at ambient conditions while, MC4 possessed the highest CO_2 uptake (approximately 12.2 mmol g^{-1}) at higher pressures. Increased temperature was observed to reduce the CO_2 capacity of the adsorbents.

CHAPTER FIVE

5 Zeolite templated carbons

5.1 Introduction

In this chapter, a range of templated carbons have been synthesized using zeolites as template, acetylene chemical vapour deposition (CVD), with and without furfuryl alcohol as precursor. The principal aim of the materials development is to produce high pore volume and area surface adsorbents for CO_2 capture at high pressure and application in gasification. (See literature review in Section 2.5.2 for background on templates and Section 3.2 on carbon synthesis). This chapter reports the evaluation of CO_2 uptake on templated carbons at ambient and high pressure conditions. The performance of the materials will be related to the syntheses variables, for example parameters like acetylene loading, presence of precursor and carbonisation temperatures. This study is unique in that it reports for the first time on the CO_2 uptake of zeolite β templated carbons.

5.2 Pore structure properties of the zeolite template

Three zeolite types, β, γ and mordenite, with significantly different textural properties (Table 5.1) were used to investigate how their textural properties influence the structure of the templated carbons produced. Surface areas of the zeolites are reported and were found to differ significantly between the three types (Table 5.2). The γ-type and the mordenite zeolites give a Type I adsorption isotherm (Figure 5.1) according to the BDDT classification (Goyal

and Bansal, 2005) indicating that majority of the pores are in the micropore range. Practically, no mesoporosity is present in these materials as indicated in the shape of the adsorption isotherms at low partial pressures. However, the β-type zeolite showed a type IV adsorption isotherm and a hysteresis loop at relative pressures above 0.4, which is in agreement with a well-developed mesoporosity assessed by NLDFT theory (Neimark, 1995). The unusual hysteresis loop observed between 0.6 and 0.8 relative pressures may be resulting from structural or channel defects in the β-type zeolite.

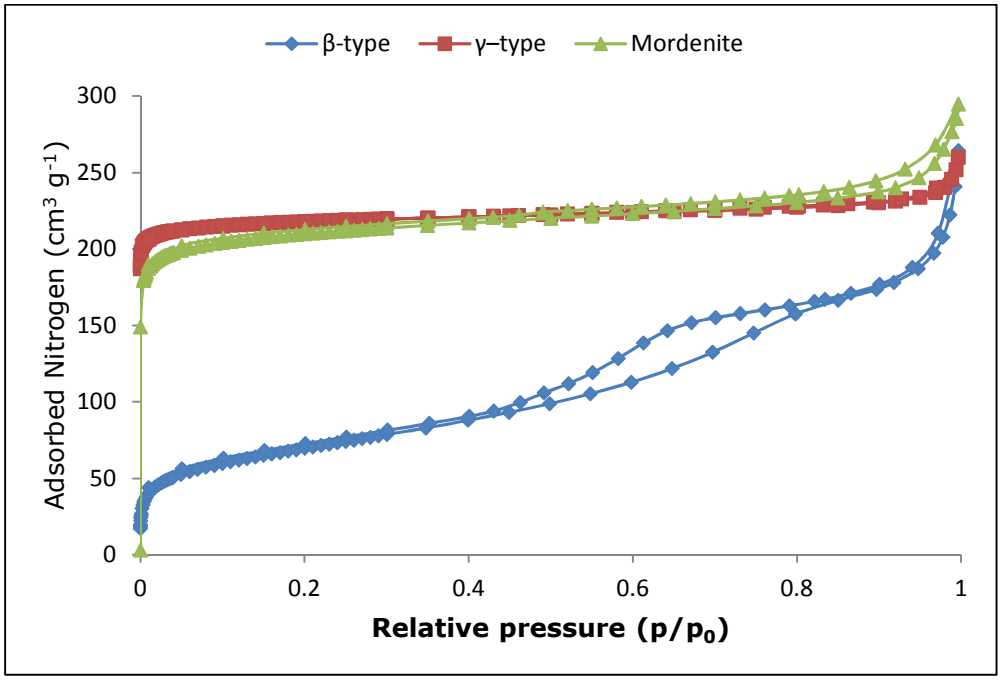

Figure 5.1. Nitrogen adsorption isotherms for mordenite, β-type and γ-type zeolites measured at -196 °C.

Table 5.1. Properties zeolites used for this study.

Zeolite type	γ-type zeolite	β- type zeolite	mordenite
Cation type	Na	NH_4	H
SiO_2/Al_2O_3 (mol mol^{-1})	5.5	27	200
Na_2O (wt%)	12.5	<0.05	<0.05
Crystal size (μm)	0.2-0.4	0.02-0.04	0.1x0.5
Mean particle size (μm)	7-10	3-6	5-7

Table 5.2 Porosity characterisation of zeolites used for this study.

Sample name	N_2 adsorption @ -196 °C							
	S_{BET} (m^2 g^{-1})	E_0 ($kJmol^{-1}$)	W_o (cm^3 g^{-1})	V_p (cm^3g^{-1})	V_{meso} (cm^3 g^{-1})	V_{meso}/W_o	W_o/V_p	ρ_{He} (g cm^{-3})
γ-type zeolite	897	41.91	0.33	0.36	0.04	0.12	0.92	2.16
β- type zeolite	252	19.23	0.06	0.22	0.22	3.67	0.27	2.04
mordenite	836	29.09	0.32	0.33	0.09	0.28	0.97	2.25

S_{BET}: surface area, E_0: characteristic energy, W_o: micropore volume, V_P: total pore volume, V_{meso}: mesopore volume, ρ_{He}: helium density

5.3 Effects of template and different synthetic conditions on the textural properties of adsorbents

The textural characteristics of the templated adsorbents were observed to be controlled by the textural properties of the zeolite as well as the synthesis conditions. Textural and chemical properties of the synthesized carbons are presented in Table 5.3 and Table 5.4, with nitrogen adsorption isotherms of synthesized adsorbents presented in Figure 5.2, Figure 5.3 and Figure 5.4. The textural properties of the zeolite templates are seen to control the textural properties of the carbons (Figure 5.2, Figure 5.3, Figure 5.4, and Table 5.3). A wide range of BET surface areas and micropore volume (W_o) were determined to be dependent on the different synthesis conditions (Table 5.3). There is a clear trend of the β-type zeolite producing consistently high surface area carbons (1343 to 1841 $m^2 g^{-1}$), whilst those from the γ-type are more variable (404 to 2404 $m^2 g^{-1}$) and on the whole lower.

Table 5.3 Porosity characterisation of the templated carbons

	N_2 adsorption @ -196 °C							
Sample name	S_{BET} (m^2 g^{-1})	E_0 ($kJmol^{-1}$)	W_o (cm^3 g^{-1})	V_p (cm^3g^{-1})	V_{meso} (cm^3 g^{-1})	V_{meso}/ W_o	W_o /Vp	ρ_{He} (g cm^{-3})
γ-AC6-2%	587	13.96	0.25	0.39	0.17	0.68	0.64	1.82
γ-AC6-5%	671	18.14	0.25	0.49	0.15	0.21	1.66	2.49
γ-AC7-2%	1207	14.62	0.50	0.74	0.19	0.38	0.75	1.89
γ-AC7-5%	1128	15.85	0.45	0.59	0.20	0.41	0.83	1.91
γ-PFA-AC6-2%	604	12.91	0.25	0.52	0.22	0.88	0.56	1.83
γ-PFA-AC6-5%	746	13.99	0.32	0.56	0.22	0.69	0.70	2.32
γ-PFA-AC6+AC7-5%	1099	14.04	0.46	0.77	0.27	0.59	0.69	1.76
γ-PFA-AC6+AC7-2%	404	13.84	0.17	0.33	0.14	0.82	0.52	2.25
γ-PFA-AC7-5%	2404	13.84	1.00	1.44	0.38	0.38	0.94	2.26
β-AC6-2%	1839	20.78	0.75	1.03	0.25	0.31	1.02	1.68
β-AC6-5%	1839	21.98	0.74	1.02	0.21	0.29	1.12	2.06
β-AC7-2%	1591	21.65	0.64	1.76	0.32	0.34	0.84	1.65
β-AC7-5%	1384	22.65	0.56	0.74	0.15	0.31	0.87	2.51
β-PFA-AC6-5%	1841	22.76	0.75	1.02	0.25	0.33	0.94	1.53
β-PFA-AC6+AC7-5%	1645	23.54	0.65	0.89	0.20	0.31	0.89	2.39
β-PFA-AC7-5%	1343	22.65	0.53	0.74	0.17	0.32	0.83	2.58
M-AC6-2%	147	18.91	0.06	0. 14	0.10	1.00	0.50	1.84
M-AC6-5%	66	15.84	0.02	0.11	0.06	3.00	0.40	1.91
M-AC7-2%	223	15.50	0.09	0.21	0.10	1.11	0.75	1.88
M-AC7-5%	262	12.04	0.06	0.45	0.33	5.50	0.32	1.73
M-PFA-AC7-5%	480	13.40	0.11	0.92	0.67	7.29	0.23	2.00

S_{BET}: surface area, E_0: characteristic energy, W_o: micropore volume, V_P: total pore volume, V_{meso}: mesopore volume, ρ_{He}: helium density

Table 5.4 Results of ultimate analysis of templated carbons calculated by dry ash free basis

Samples	*Carbon yield (%)	C (Wt.%)	H (Wt.%)	N (Wt.%)	O (Wt.%)
γ-AC6-2%	28	92.7	2.4	0.1	4.7
γ-AC6-5%	25	93.1	2.4	0.1	4.4
γ-AC7-2%	29	91.5	2.4	0.1	6.0
γ-AC7-5%	29	91.9	2.3	0.1	3.7
γ-PFA-AC6-2%	29	93.7	2.6	0.1	3.6
γ-PFA-AC6-5%	30	95.6	2.4	0.1	1.9
γ-PFA-AC6+AC7-5%	30	94.8	2.3	0.1	2.8
γ-PFA-AC6+AC7-2%[+]	44	75.6	2.0	0.1	22.0
γ-PFA-AC7-5%	30	93.4	1.9	0.2	4.5
β-AC6-2%	56	90.9	2.1	0.2	6.8
β-AC6-5%	59	89.2	2.0	0.2	8.6
β-AC7-2%	59	92.3	1.6	0.1	6.0
β-AC7-5%	57	94.8	1.6	0.1	3.5
β-PFA-AC6-5%	62	93.2	2.0	0.3	4.5
β-PFA-AC6+AC7-5%	60	93.7	1.7	0.3	4.3
β-PFA-AC7-5%	62	93.7	1.4	0.3	4.6
M-AC6-2%	13	91.4	2.5	0.3	5.8
M-AC6-5%	13	91.9	2.6	0.3	5.2
M-AC7-2%	13	93.9	2.1	0.2	3.8
M-AC7-5%	16	90.8	1.9	0.2	7.1
M-PFA-AC7-5%	25	91.0	1.4	0.2	7.4

[+] Increased oxygen content may be due to incomplete zeolite removal or incomplete carbonisation of zeolite

The surface area (S_{BET}) and micropore volumes (W_o) of the γ-type templated carbons show similar results to similar templated carbons reported by Su et al., (2004), Sevilla and Fuertes, (2012), Ma et al., (2002), and Barata-Rodrigues et al., (2003). Surface area is lowest for the mordenite template carbons (66-480 $m^2 g^{-1}$). Pore size distribution is also influenced by the zeolite template and can been seen from differences in the nitrogen adsorption isotherms (Figure 5.2, Figure 5.3, and Figure 5.4). A Type I isotherm is observed for carbons derived from γ-type and β-type zeolites, with some

hysteresis noted for some carbons, especially those derived from the γ-type zeolite suggesting the presence of some mesoporosity (Figure 5.3). NDFT analysis indicates that predominantly the pores of the γ-type templated adsorbents are distributed in the 2 and 5 nm range (Figure 5.6). This finding is in agreement with carbons from templated ammonium form of zeolite (Su et al., 2004) where similar S_{BET} and W_o have been reported for γ-type templated carbons carbonised at 600 and 700 °C. The β-type zeolite derived activated carbons are predominantly microporous with a high characteristic energy (E_0) above 20 kJ mol^{-1} (Table 5.3), and majority of their pores predicted to be below 2 nm by the NDFT analysis (Figure 5.5). Carbons derived from mordenite have significantly lower surface area and are characterised by a type IV nitrogen adsorption isotherm, the broad hysteresis (Figure 5.4) indicating the presence of mesoporosity, with a wide pore distribution in the 2 and 5 nm range and above.

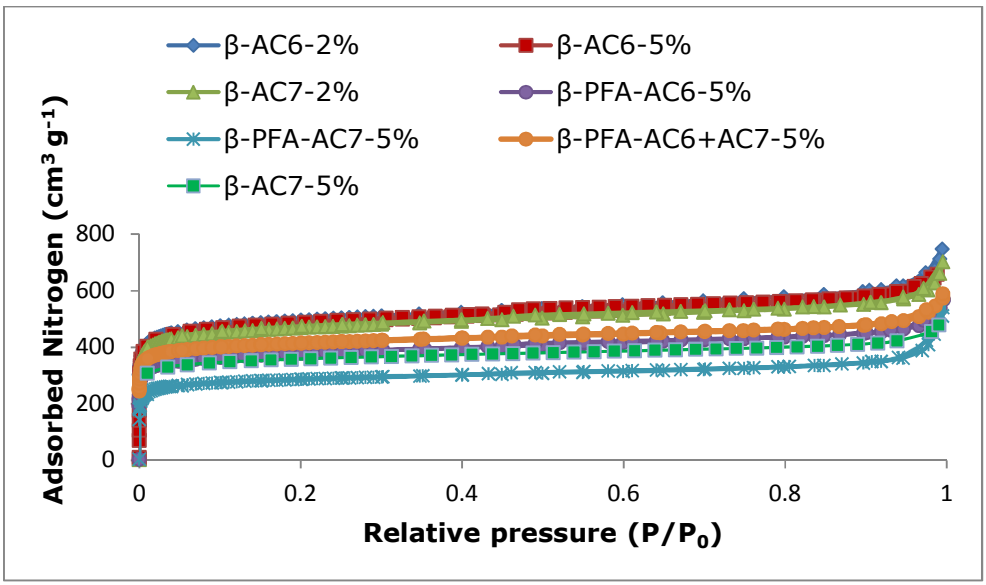

Figure 5.2. Nitrogen adsorption isotherms for β-type zeolite templated carbons measured at -196 °C.

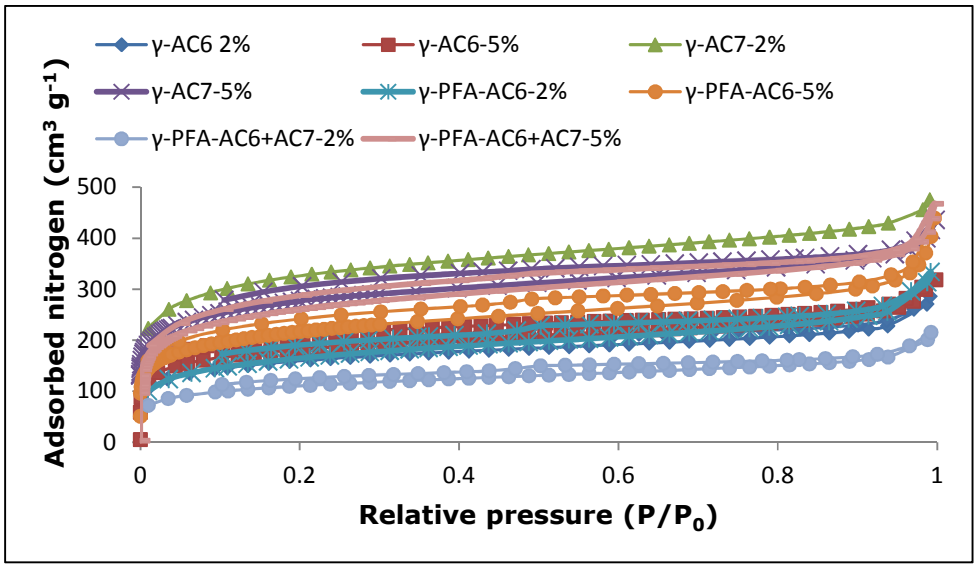

Figure 5.3. Nitrogen adsorption isotherms for γ-type zeolite templated carbons measured at -196 °C.

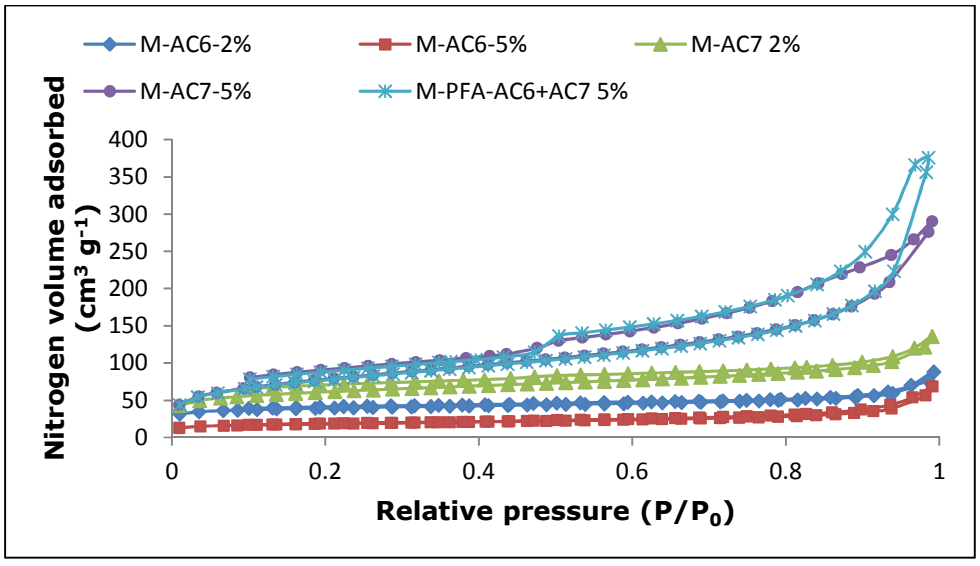

Figure 5.4. Nitrogen adsorption isotherms for mordenite templated carbons measured at -196 °C.

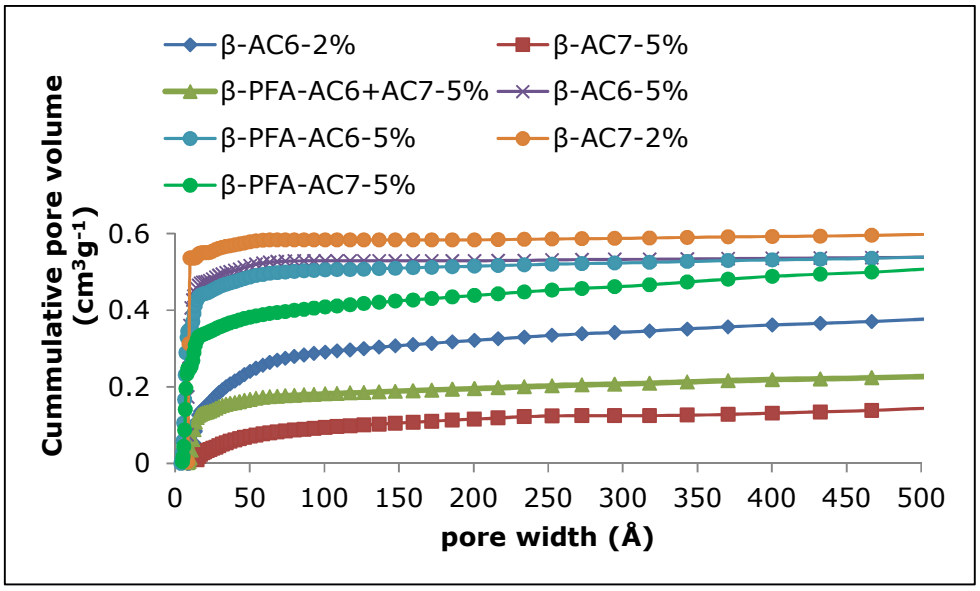

Figure 5.5. NLDFT pore size distribution for zeolite β templated carbons measured at -196 °C.

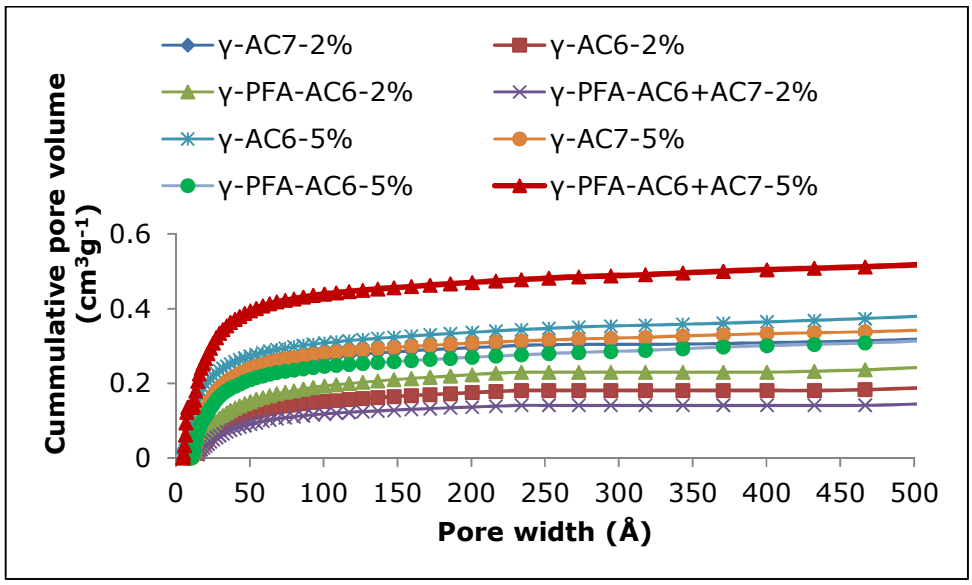

Figure 5.6. NLDFT pore size distribution for zeolite γ templated carbons measured at -196 °C.

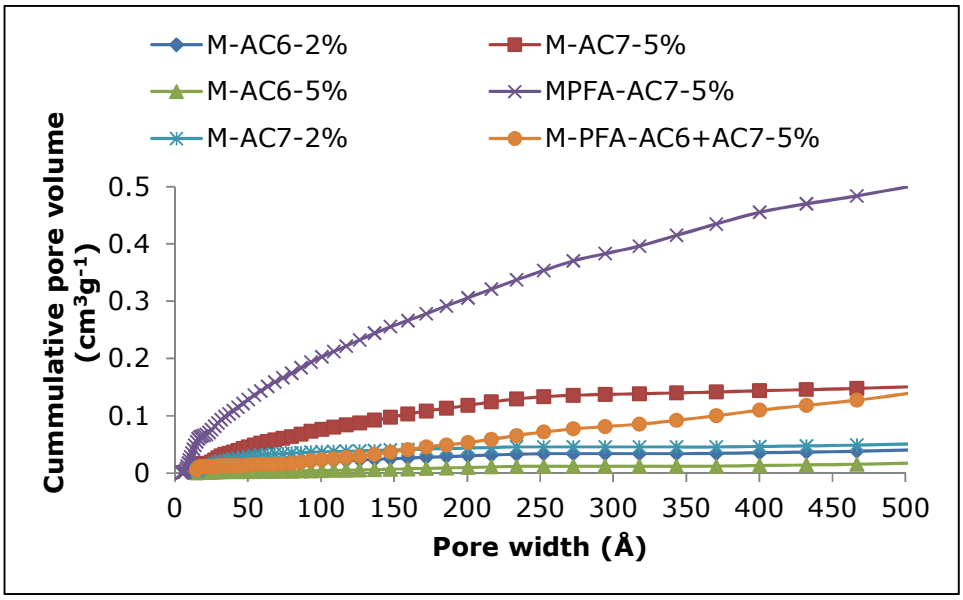

Figure 5.7. NLDFT pore size distribution for mordenite templated carbons measured at -196 °C.

The zeolite templates also influenced the yield of carbons from the different synthetic routes (Table 5.4). Whilst variable, higher carbon yields were obtained from the γ-type (30-45%) and β-type (50-60%) zeolites compared to the mordenite template (15-25%). The low carbon yield from the mordenite template is attributed to the textural properties of the template which determines if a stable three dimensional carbon material can be formed. It has been previously reported that the presence of unfilled channels in the carbon/zeolite composite can lead to a collapse of regular network structure, when the composite is subjected to HF acid wash (Kyotani, 2006; Su et al., 2004), which through SEM and XRD analysis tests has determined the carbon yields to be dependent on the interconnectivity of the zeolite pore structure (Kyotani, 2003). β-type zeolites are reported (Kyotani, 2003) to have two types of channels of different sizes, with the larger channels intercrossing in two dimensions allowing the resultant carbons to retain this two or three-dimensional regularity and a stable structure. The β–type derived carbon has

more carbon yield than the γ–type derived carbon because in the former, the whole three-dimensional regularity may have been preserved, while the latter kept only the two-dimensional regularity of the structure. The mordenite on the other hand showed smaller carbon yield and may be due to partly filled channels resulting from very narrow channels. This one-dimensional structure possesses three channels, of which only the largest channel could be partially filled while the other two remained difficult to fill as a result of very narrow channel size. This has impacted negatively on carbon formation during carbonisation.

The addition and polymerisation of polyfurfuryl alcohol into the zeolite template prior to CVD has previously been reported to increase the S_{BET} of synthesized zeolite templated carbons (Ma et al., 2002; Barata-Rodrigues et al., 2002). The influence of furfuryl alcohol (FA) addition in this study was determined to depend on the zeolite template. A systematic increase in the BET surface area for the γ-type templated carbons was observed, being most pronounced for γ-PFA-AC7-5% and was double that of γ-AC7-5% (Table 5.3). Total pore volume and mesopore volumes increased for the γ-type templated carbons whilst the increase in micropore volume (W_0) was modest except for γ-PFA-AC7-5% for which the value doubled from 0.45 $cm^3\ g^{-1}$ to 1.00 $cm^3\ g^{-1}$. The PFA synthesis route also increased the surface area and pore volume (W_o, V_p, V_{meso}) of the mordenite produced carbon, and significantly increased the carbon yield (Table 5.4). On the contrary, the PFA synthetic route resulted in no significant change in the surface area or the total-, micro- and mesopore volumes for the β-type zeolite templated carbons (Table 5.3). These results indicate that the addition of PFA results in greater textural development in carbon materials synthesized from predominantly microporous zeolite

templates (γ and mordenite), whilst being of no benefit when used for the predominantly mesoporous β–type zeolites. This finding is in contrast with previous findings (Barata-Rodrigues et al., 2002; Kyotani, 2003) which reported that mesopores provide spaces for FA infiltration which increases the surface area, micro-and mesopore volumes of the material available for carbonisation.

In agreement with previous work (Su, 2004; Ma et al., 2002; Kyotani, 2003; Kyotani, 2006), increasing activation temperature from 600 to 700 ^{o}C results in the development of carbons with increased S_{BET} for the mordenite and γ-type templated carbons. In the case of the γ-type templated carbons, the increase in activation temperature doubled the S_{BET} and micropore volume in all cases. Whereas about 18% increase in S_{BET} was recorded for the mordenite templated carbons under the same condition. This finding is in agreement with report by Su et al., (2004) when they synthesized and characterised microporous carbons using templated ammonium-form zeolite γ. The influence of activation temperature is observed to be dependent on the template type, with an increase in activation temperature reducing the S_{BET} for the β-type templated carbons. The effects of the acetylene loading on the templated carbons differ from one template to the other. While it has little or no effect on the S_{BET} of β-type templated carbons, approximately 14% increase in S_{BET} was recorded for the γ-type templated carbons. For example, the γ-AC6-2% with 2% acetylene has S_{BET} of 587 $m^2 g^{-1}$. This value increased to 671 $m^2 g^{-1}$ when the acetylene loading was increased to 5%. For the mordenite templated carbons acetylene loading positively influenced carbon synthesized at 700 ^{o}C than those obtained at 600 ^{o}C. Results from ultimate analysis (Table 5.4) for the adsorbents showed that the acetylene loading used had little or no effect

on the carbon yields of some of the templated carbons (Table 5.4). This effect has also been reported by Barata-Rodrigues et al., (2003) when they used propylene CVD as carbon precursor. It was found that propylene CVD did not significantly alter the amount of carbon in a β-type templated carbon, and was suggested to be a consequence of completely filled or blocked pores resulting from FA polymerisation.

5.4 CO_2 capacity measurements at atmospheric pressure

Figure 5.8 and Figure 5.9 show the dependence of adsorption capacity of studied adsorbents on the S_{BET} and micropore volume respectively at 25 ^{o}C. A good correlation was seen to exist between the CO_2 uptake and surface area (Figure 5.8), and micropore volume (Figure 5.9). This explains the dependence of CO_2 uptake capacity of these adsorbents on surface area and micropore volume at atmospheric pressures. In terms of the CO_2 adsorption capacity, the templated carbons can be arranged in the following order modenite < γ-type < β-type templated carbons. It has been suggested by Patrick (1995) that the distribution of micropore size, as opposed to total pore volume, is key factor in gas adsorption at ambient temperature. The adsorbents with the largest volume of narrow micropore (β-type templated carbons) exhibited the highest CO_2 uptake. This further emphasises the importance of size of micropore volume in determining the CO_2 uptake of the adsorbents (Martin et al., 2011a). In order to find out if the total CO_2 uptake came from contributions of the micropores or mesopores, a plot of CO_2 uptake against the ratio of micropore and total pore volume (W_o/V_p) and mesopore and total pore volume (V_{meso}/V_p) was considered. Results showed that more of the CO_2 uptake was as a result of contributions from micropore rather than the

mesopores, especially for the β–type and γ–type templated carbons. Figure 5.10 reveals a more linear trend as compared to Figure 5.11.

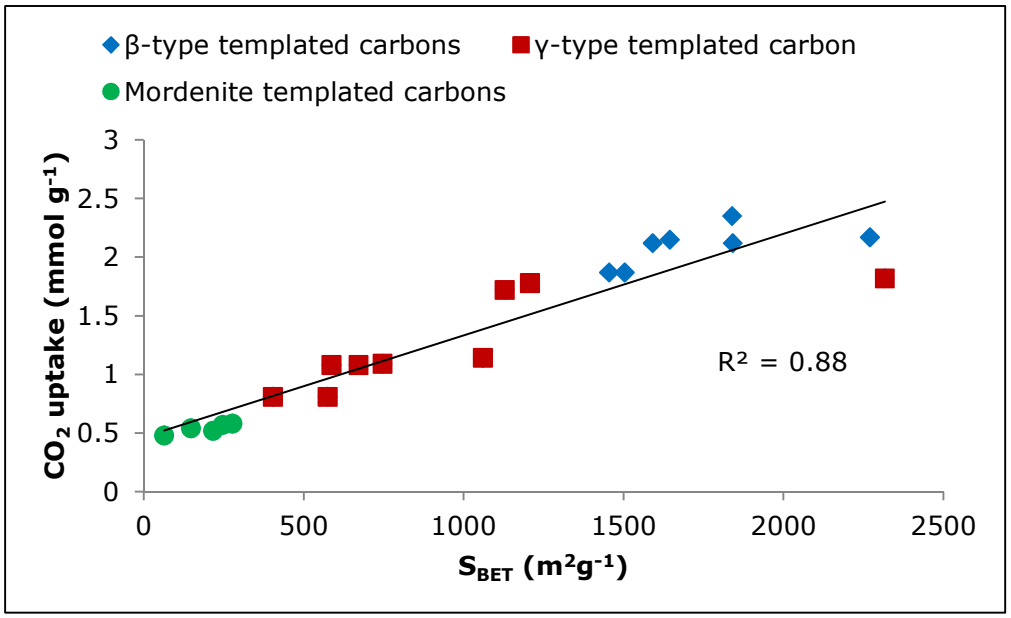

Figure 5.8. Effect of S_{BET} on CO_2 uptake of studied adsorbents at 25 °C

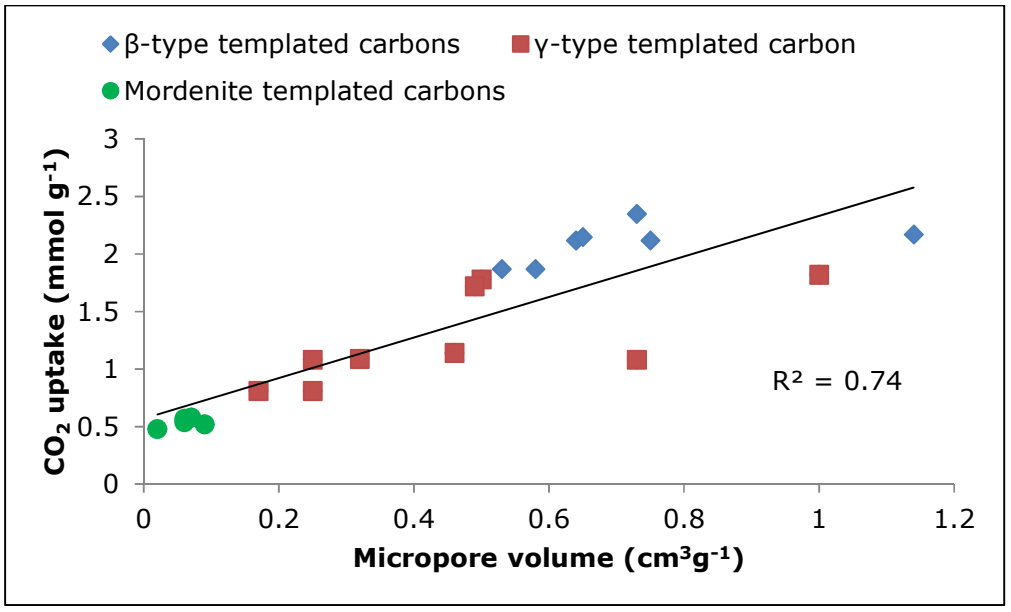

Figure 5.9 Effect of micropore volume on CO_2 uptake of studied adsorbents at 25 °C.

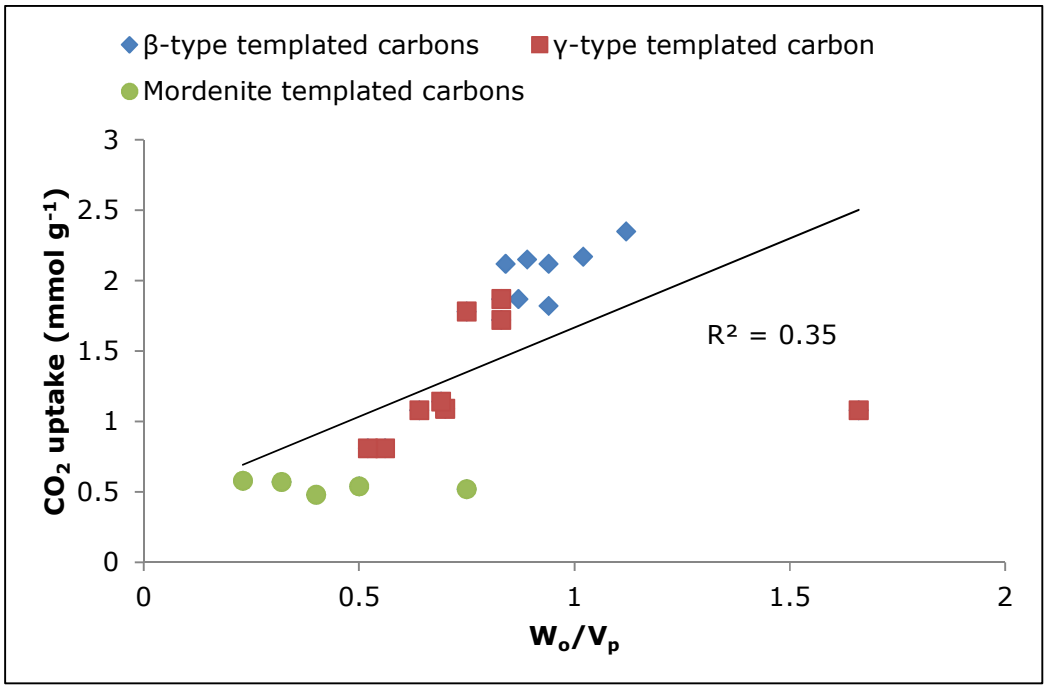

Figure 5.10 Contribution of micropores to CO_2 uptake

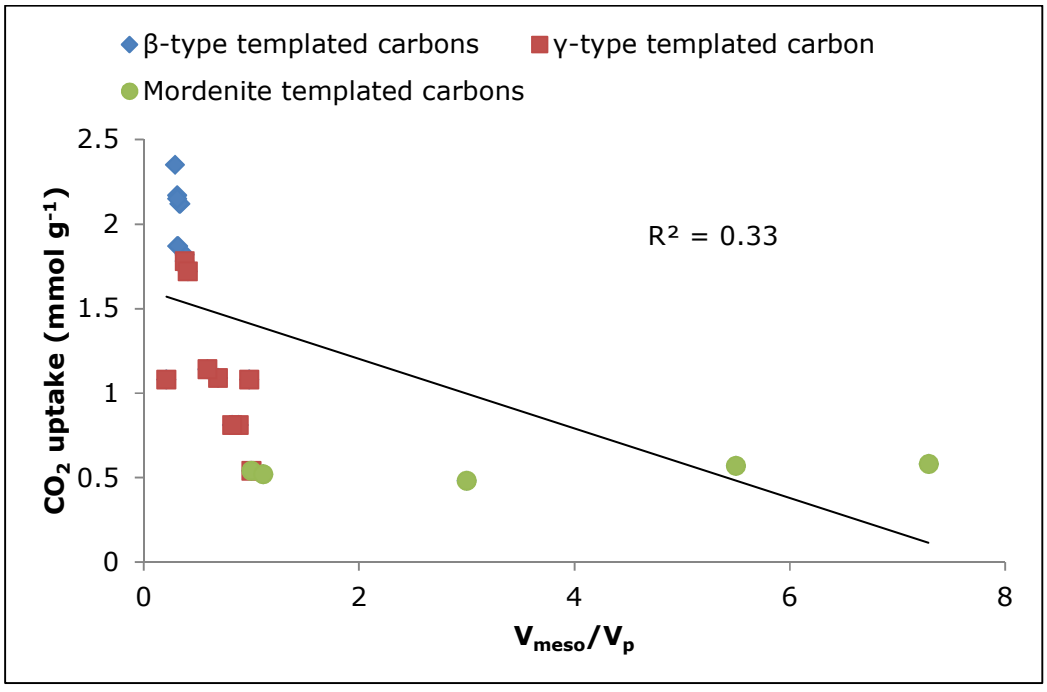

Figure 5.11 Contribution of mesopores to CO_2 uptake

All the β-type templated carbons possess higher CO_2 adsorption capacity at 25 ^oC compared to the other templated materials in this study, with β-AC6-5% showing a 2.35 mmol g^{-1} CO_2 uptake. Although, different synthesis methods were used for the production of carbons, this result has been found to be higher than the CO_2 adsorption capacities reported in Plaza et al., (2010) and Prespiorski et al., (2002) when they studied CO_2 uptake on ammoxidised carbons and phenolic resin based carbons. But lower than those reported for the phenolic resin carbons in Chapter 4 (see Table 4.3).

For the γ-type templated carbons, the CO_2 uptakes range from approximately 0.8 to 1.8 $mmolg^{-1}$, depending on the synthesis technique used (as shown in Table 5.5). The highest CO_2 uptake in this series was observed in γ-PFA-AC7-5% with micropore volume and S_{BET} of 1.0 cm^3 g^{-1} and 2404 m^2 g^{-1} respectively. The mordenite templated carbons exhibited an exceptionally low CO_2 adsorption, just slightly above 0.5 $mmolg^{-1}$ compared to the other adsorbents under investigation.

Table 5.5. CO_2 Uptake of adsorbents measure at ambient pressure conditions.

Sample name	*Carbon yield (%)	15% CO_2 uptake (mmol g^{-1})	100% CO_2 uptake (mmol g^{-1})	Ratio (%)	CO_2 uptake (mmol cm^{-3})
γ-AC6-2%	28	0.38	1.08	35	1.97
γ-AC6-5%	25	0.33	1.08	31	2.69
γ-AC7-2%	29	0.49	1.78	28	3.36
γ-AC7-5%	29	0.48	1.72	28	3.29
γ-PFA-AC6-2%	29	0.25	0.81	31	1.48
γ-PFA-AC6-5%	30	0.34	1.09	31	2.53
γ-PFA-AC6+AC7-5%	30	0.36	1.14	32	2.01
γ -PFA-AC6+AC7-2%	44	0.21	0.81	26	1.82
γ-PFA-AC7-5%	30	0.46	1.82	25	4.11
β-AC6-2%	56	0.32	2.17	15	3.65
β-AC6-5%	59	0.47	2.35	20	4.84
β-AC7-2%	59	0.44	2.12	21	3.50
β-AC7-5%	57	0.44	1.87	24	4.69
β-PFA-AC6-5%	62	0.45	2.12	21	3.24
β-PFA-AC6+AC7-5%	60	0.48	2.15	22	5.14
β-PFA-AC7-5%	62	0.38	1.87	20	4.83
M-AC6-2%	13	0.17	0.54	32	0.99
M-AC6-5%	13	0.17	0.48	35	0.92
M-AC7-2%	13	0.24	0.52	46	0.98
M-AC7-5%	16	0.22	0.57	39	1.09
M-PFA-AC7-5%	25	0.19	0.58	33	1.16

*Carbon yields after HF wash; Ratio was calculated as the ratio of 15% CO_2 uptake to 100% CO_2 uptake.

These results will obviously be linked to the adsorbents possessing very narrow micropore volume and S_{BET} of between 0.02 and 0.11 $cm^3\,g^{-1}$ and 66 to 480 $m^2\,g^{-1}$ respectively. The least squares regression for all the plots on CO_2 adsorption in relation to S_{BET} (Figure 5.8) and micropore volume (Figure 5.9) gave a value that is approximately equal to 0.8. This indicates a correlation in the adsorption figures recorded for these materials.

Also, errors (Figure 5.12) associated with uptake capacity have shown that the β-AC6-5% templated carbons showed the lowest followed by the γ-PFA-AC7-5% templated carbon and M-PFA-AC7-5% carbon.

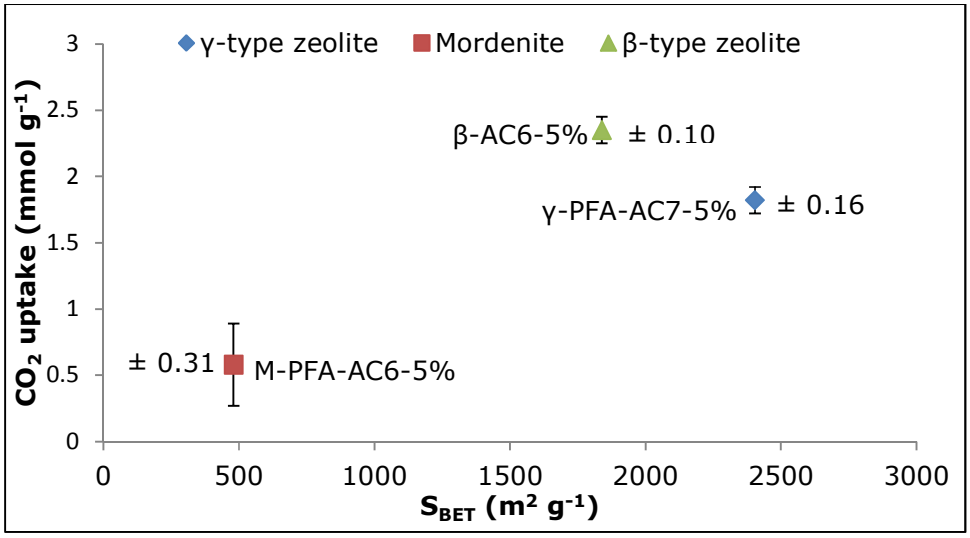

Figure 5.12. Errors associated with CO_2 uptake of the different adsorbents at 25 ^{o}C.

When the CO_2 uptake was calculated as a function of the measured particle density (amount of CO_2 adsorbed per unit volume of adsorbent) (Table 5.5), it was observed that denser adsorbents adsorbed more CO_2 on volumetric basis. Adsorbents with higher densities tend to have higher CO_2 uptake capacities per volume than their less dense counterpart. For example, the γ-AC6-2% and the γ-AC6-5% have an uptake value of 1.08 mmol g^{-1} each. When particle densities were considered, the latter recorded approximately 39% increase in CO_2 uptake capacity compared the former. Under this consideration, the β-PFA-AC6+AC7-5% has the highest CO_2 uptake capacity of 5.14 mmol cm^{-3} followed by β-AC6-5% and β-PFA-AC7-5% having capacities of 4.84 mmol cm^{-3} and 4.83 mmol cm^{-3} respectively. This result was expected as it has been observed (see Section 5.3 and Table 5.5) that the β-type templated carbons

consist mainly of micropores while the γ-type and mordenite templated carbons consists mainly mesopores. So, the more mesoporous a carbon is, the less it weighs, and the lower its density. This also suggests that mesopores are not active to CO_2. The volumetric capacities are an important consideration for application of these materials. As reported by Drage et al., (2009), the volumetric capacity of the materials will have a significant impact on the size of plant and can be as important as the overall mass based capacity performance.

The partial pressure of a gas is the pressure a gas in a mixture would exert if it were the only gas present in a volume under consideration. If CO_2 gas is put in a cylinder containing another gas like nitrogen, it would experience a reduced partial pressure due to the presence of the other gas. Gas streams in post-combustion contain NO_x, SO_x, CO_2, and other trace gases, each having a partial pressure. As the number of gases increase in a system, the partial pressure of each gas reduces. In order to find out the effect of CO_2 partial pressure on adsorbents, a test was carried out to evaluate the performance of these adsorbents in a binary mixture of nitrogen and CO_2 in a ratio that simulates that of a flue gas stream from post-combustion. Results of 15% CO_2 in nitrogen are also presented in Table 5.5. The CO_2 uptake recorded was lower than that obtained at 100% CO_2 stream. This is expected as partial pressure of CO_2 reduced in this mixture. However, about 20-35% adsorption was recorded in comparison to that adsorbed by these materials using 100% CO_2 stream. This result suggests the application of these adsorbents in post-combustion carbon capture where there is reduced CO_2 partial pressure.

CO_2 uptake analysis was also performed at 40, 60 and 80 ^oC for selected adsorbents; and Results obtained are presented in Table 5.6. As expected, the

CO_2 uptake reduces as temperature increased from 25 ^oC to 80 ^oC, because the materials are physisorbent (Drage et al., 2009). The highest CO_2 uptake was recorded at 25 ^oC. This was expected as physisorption is the only mechanism for CO_2 capture at room temperature (Zhang et al., 2010).

Table 5.6. CO_2 uptake for selected templated carbons at 25, 40, 60 and 80 ^oC measured at atmospheric pressure.

Samples	25 ^oC (mmol g^{-1})	40 ^oC (mmol g^{-1})	60 ^oC (mmol g^{-1})	80 ^oC (mmol g^{-1})
γ-AC6-2%	1.12	0.68	0.41	0.25
γ-AC6-5%	1.08	0.66	0.41	0.26
γ-AC7-5%	1.72	1.10	0.67	0.41
γ-PFA-AC6-2%	0.81	0.51	0.30	0.17
γ-PFA-AC7-5%	1.14	0.98	0.70	0.45
β-AC6-5%	2.35	1.36	0.81	0.51
β-AC7-5%	1.87	1.22	0.72	0.46
β-AC6-2%	2.17	1.47	0.85	0.48
β-PFA-AC7-5%	1.87	1.13	0.65	0.39
β-PFA-AC6-5%	2.12	1.34	0.81	0.49
β-PFA-AC6+AC7-5%	2.15	1.28	0.74	0.44

CO_2 uptake values reported in this study are higher than those for similar microporous carbons reported elsewhere (Huang et al., 2003; Guang-Ping et al., 2010; Martin et al., 2010; Chunzhi et al., 2010; Przepiorski et al., 2002) (.

Table 5.7). The maximum adsorption recorded by Przepiórski et al., (2002) was 87.8mg g^{-1} Ξ 1.99 mmol g^{-1}, Plaza et al., (2010) also recorded a 1.5 and 2.1 mmol g^{-1} uptake for two different amminated samples at 25 ^oC while Chunzhi et al., (2010) and Guoying et al. (2010) reported a 1.92 mmol g^{-1} and 1.4 mmol g^{-1} uptake at the same temperature respectively. Lastly, Huang et

al., (2003) reported a 2-3 wt% (0.5-0.7 mmol g^{-1}) adsorption for similar material in their work. Even the mordenite template carbons with the lowest CO_2 uptake of 0.48 mmol g^{-1} recorded a better uptake compared to 0.43 mmol g^{-1} CO_2 adsorption recorded by Huang et al., (2003).

Table 5.7. Comparison of CO_2 uptake capacities at ambient conditions between this study and literatures.

Material type	Maximum CO_2 uptake (mmol g^{-1})	Reference
Templated carbons	2.35	This study
Phenolic resin carbon	1.99	Przepiórski et al., (2002)
Activated carbons	1.5 and 2.1	Martin et al., (2010)
Activated carbons	1.92	Chunzhi et al., (2010)
Carbon monolith	1.4	Guang-Ping et al., (2010)
Activated carbons	0.5-0.7	Yang et al., (2011)
Activated carbon	2.21	Plaza et al., (2009)
Activated carbon	2.1*	Gil et al., (2012)
Phenolic-formaldehyde activated carbon	6.5	Martin et al., (2012)

*uptake measured at 35 ^{o}C

5.5 Adsorption kinetic studies

The kinetics of CO_2 adsorption on γ-AC6-5% templated carbon was studied by isothermal adsorption at different temperatures (25, 40, 60, and 80 °C), using the pseudo first order and pseudo second order models. The isothermal graphs are presented in Figure 5.13 to Figure 5.16, and the estimated parameters values and corresponding correlation coefficients are presented in Table 5.8.

The pseudo first order model provides the best fit to isothermal CO_2 adsorption data at the temperatures studied. The first order nature of this reaction has been attributed to mode of transport of the reacting species on the surface of the carbon. In this case, the carbon is viewed as a flat surface with specific sites, at which adsorbed molecules (CO_2) are located. These sites are assumed to have energy depth which is larger than the energy of the CO_2 molecules. The CO_2 molecules at each site must attain enough energy to move from one site to the next vacant site for adsorption to take place (Duong, 2008). Hence, in first order reaction kinetics, the rate of CO_2 diffusion into the carbon surface is faster than the chemical reaction on the carbon surface. Similar results have been reported by Zhang et al., (2010a) when they studied the adsorption kinetics of CO_2 on Zeolite 13X and activated carbon. The γ-AC6-5% adsorbent showed a curve which fits better to the pseudo first order model than the pseudo second order model. This finding is further supported by the R^2 values and error function obtained for the pseudo first and second order models. It was observed that the R^2 for the pseudo first is in the order of 0.99, with corresponding error function in the range of 1.6-3.3 (Table 5.8). Since the correlation coefficient is greater than 0.99, it indicates the applicability of this kinetic model and the first order nature of the adsorption process of CO_2 on the templated carbons (Hameed et al., 2007). Activation energy of -3.5224 kJ mol^{-1} was calculated for this material. This may suggest the possible application of this material for pre-combustion carbons capture where maximum CO_2 uptake occurs at room temperature.

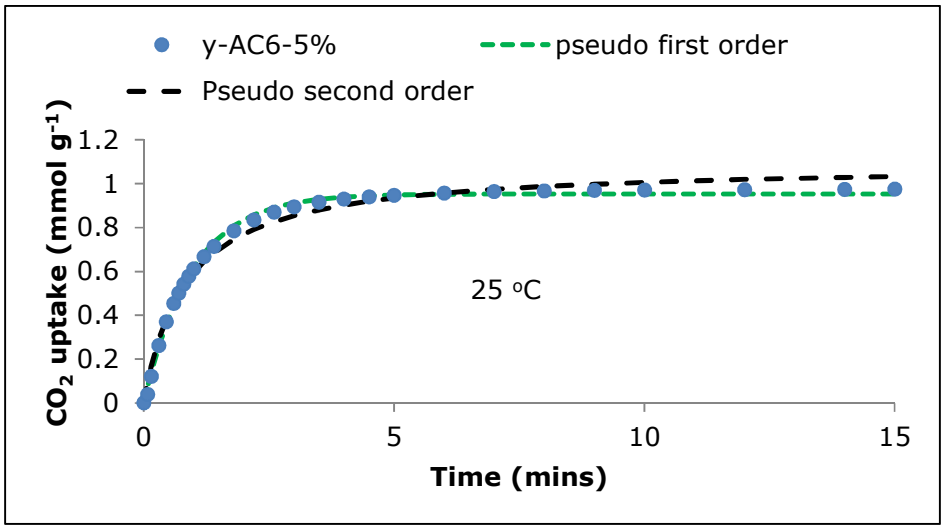

Figure 5.13. CO_2 adsorption on γ-AC6-5% at 25 °C. The experimental data was fitted by the pseudo-first order and pseudo-second order models.

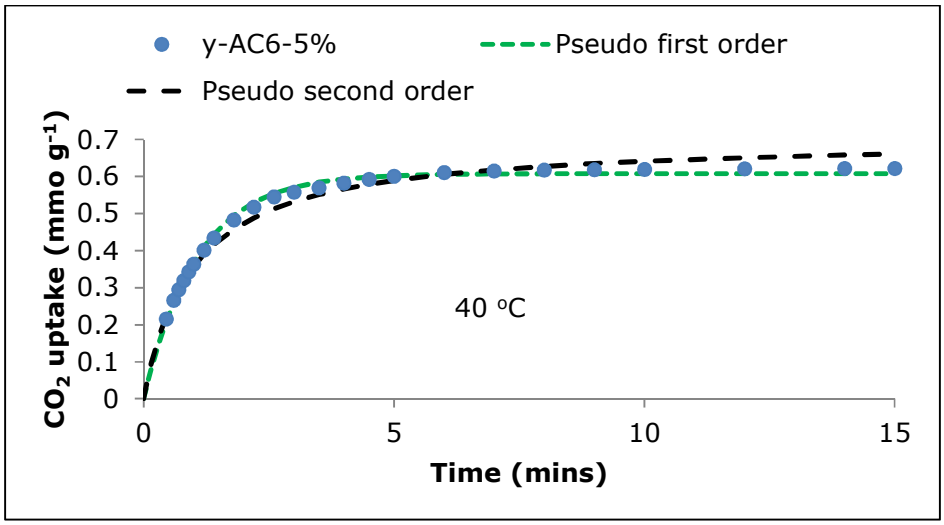

Figure 5.14. CO_2 adsorption on γ-AC6-5% at 40 °C. The experimental data was fitted by the pseudo-first order and pseudo-second order models.

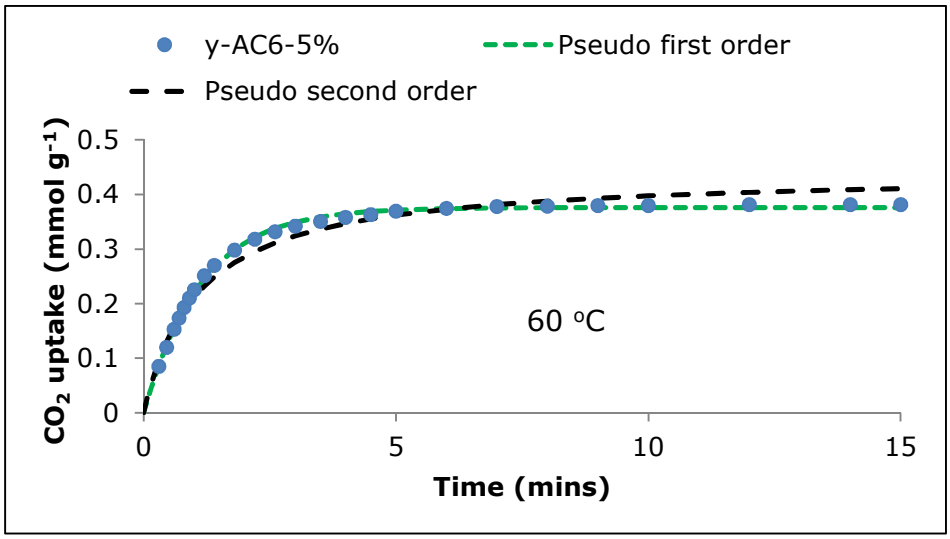

Figure 5.15. CO_2 adsorption on γ-AC6-5% at 60 °C. The experimental data was fitted by the pseudo-first order and pseudo-second order models.

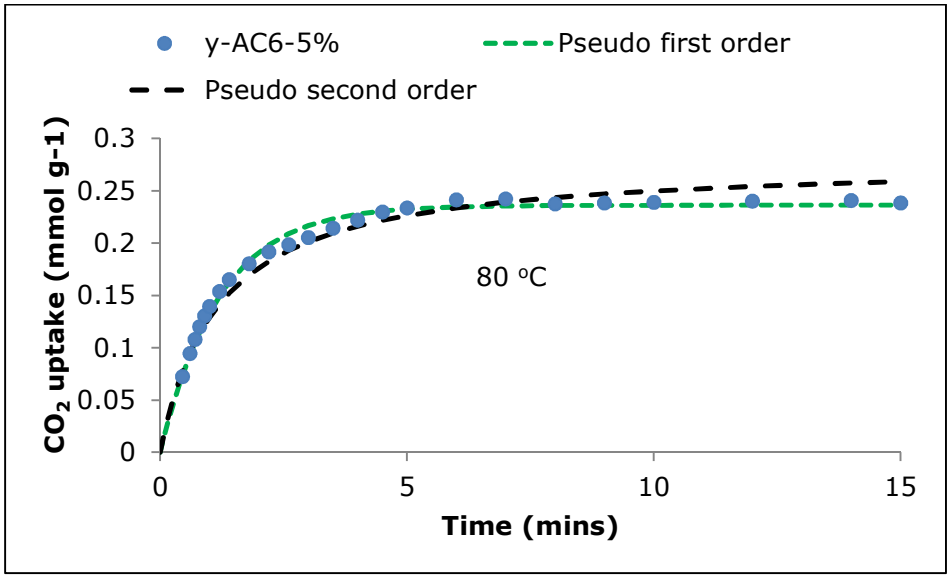

Figure 5.16. CO_2 adsorption on γ-AC6-5% at 80 °C. The experimental data was fitted by the pseudo-first order and pseudo-second order models.

Table 5.8. Kinetic model parameters for the CO_2 adsorption on templated carbon (γ-AC6-5%)) at different temperatures.

T		25 °C	40 °C	60 °C	80 °C
$q_{e,exp}$		1.08	0.66	0.41	0.26
Pseudo-first order	q_e	0.98	0.92	0.38	0.24
	k_1	1.046	0.935	0.881	0.831
	R^2	0.9955	0.9959	0.9969	0.9918
	Err	1.9	2.0	1.6	3.3
Pseudo-second order	q_e	0.92	0.62	0.38	0.24
	k_2	1.101	1.469	2.112	3.090
	R^2	0.9797	0.9772	0.9709	0.9742
	Err	4.1	4.0	5.9	6.3

(T: °C; $q_{e,exp}$: mmol g^{-1}; q_e: mmol g^{-1}; k_1: s^{-1}; k_2: mmol g^{-1} s^{-1}; k_a: s^{-1}; a: mmol g^{-1} s^{-1}, a: g $mmol^{-1}$)

5.6 High pressure CO_2 adsorption

This section presents results from high pressure analysis of the templated carbon on the HPVA. The high pressure CO_2 uptake capacities of the materials with relation to textural properties are discussed. Data reported here are for selected adsorbents; γ-AC7-5%, β-AC6-5%, β-AC7-2%, β-PFA-AC6+AC7-5%, γ-PFA-AC7-5%, β-AC6-2%, β-PFA-AC6-5%, and β-PFA-AC7-5%. These selections were made such that a wide range of adsorbents representing the different synthesis parameters (see Section 3.2 on carbon synthesis) and textural properties are represented (Table 5.3).

Results have shown that, at high pressure, surface area and micropore volume may not have played a role in the adsorption capacity of adsorbents (Figure 5.18 and Figure 5.17 respectively), the total pore volume was seen to play a more significant role at this condition (Figure 5.19). This conclusion was drawn based in the R^2 value for the respective adsorption capacity tests reported in Figure 5.17, Figure 5.18, and Figure 5.19. Similar trend have been reported

for the phenolic resin activated carbons in Chapter 4 (Section 4.3). However, a better adsorption trend was recorded for the templated carbon than the phenolic resin activated carbons (comparing Figure 4.7, Figure 4.6, and Figure 4.8 with Figure 5.17, Figure 5.18, and Figure 5.19 respectively). This further explains the dependence of adsorption capacity on total pore volume rather than micropore size at high pressure (Martin et al., 2011).

The volumetric adsorption isotherm of CO_2 on the templated carbons at 25 and 40 ^{o}C are shown in Figure 5.20 and Figure 5.21 respectively. The isotherms presented in this section are similar to those reported by Jeng et al., (2010) at similar temperatures and pressures, where CO_2 isotherms were found to be Type I according to BDDT classification. No hysteresis has been found as operating conditions are not beyond the vapour pressure of CO_2. CO_2 uptake increased rapidly as pressure increased to 3.5 MPa, and gradually after this point. This phenomenon may indicate the reversibility of the adsorption process, and also suggests a stronger interaction between the CO_2 molecules and the active sites in the activated carbons at these pressures (Gensterblum et al., 2009). The isotherms generated in this study are in total agreement with those reported by Dreisbach et al., (1999) as Type I isotherms were observed by them at high pressures. Also, adsorption rates are high at lower pressures than at higher pressures. The γ–type adsorbents have lower adsorption rates at low pressures than the β–type carbons. The β-AC7-2% showed the highest CO_2 uptake capacity at 25 and 40 ^{o}C and 4.1 MPa (Figure 5.20 and Figure 5.21). There was at least 52% more CO_2 uptake in this material compared to the other adsorbents at 25 ^{o}C. This exceptional uptake behaviour may be attributed to the high total pore volume (1.76 cm^3 g^{-1}) (see Table 5.3) of this adsorbent which played a significant role in its adsorption

capacity at high pressure. Guillot et al., (1999) and Shuji et al., (2005) have reported in their work that CO_2 adsorption on the walls of the larger micropores (secondary micropore filling) contributes to the overall uptake capacity of activated carbons. This may also suggests the reason for the improved individual CO_2 uptake values recorded on the materials at high pressures. It must be pointed out at this point that this material has an exceptionally high total pore volume in comparison to the other materials developed. Given that there is little data at this point to fully confirm this trend, more data would be required before fully attributing performance at this level to total pore volume.

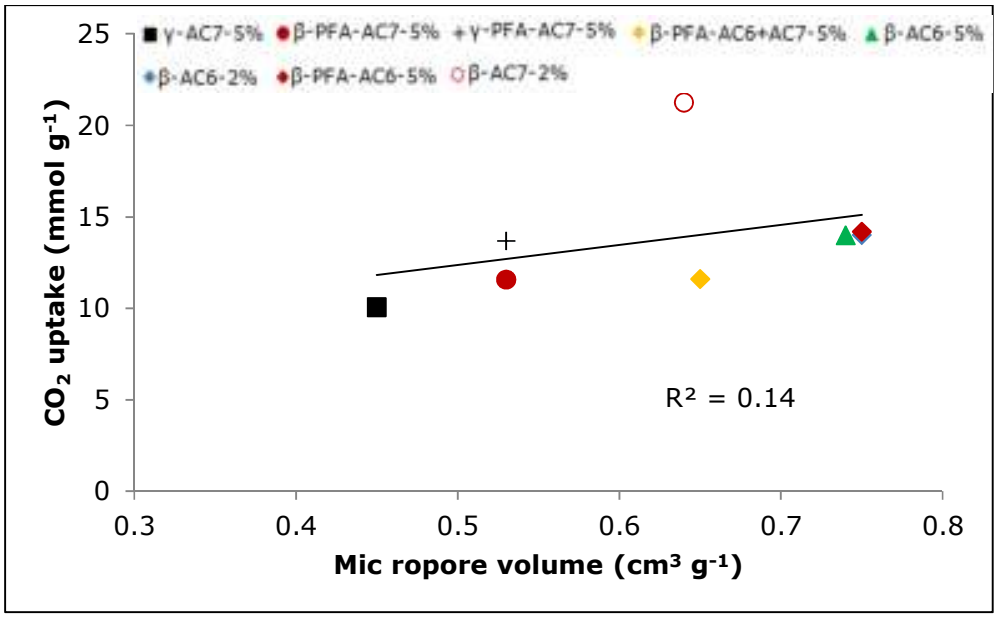

Figure 5.17. Effect of micropore volume on CO_2 uptake capacity of carbons at 4.1 MPa.

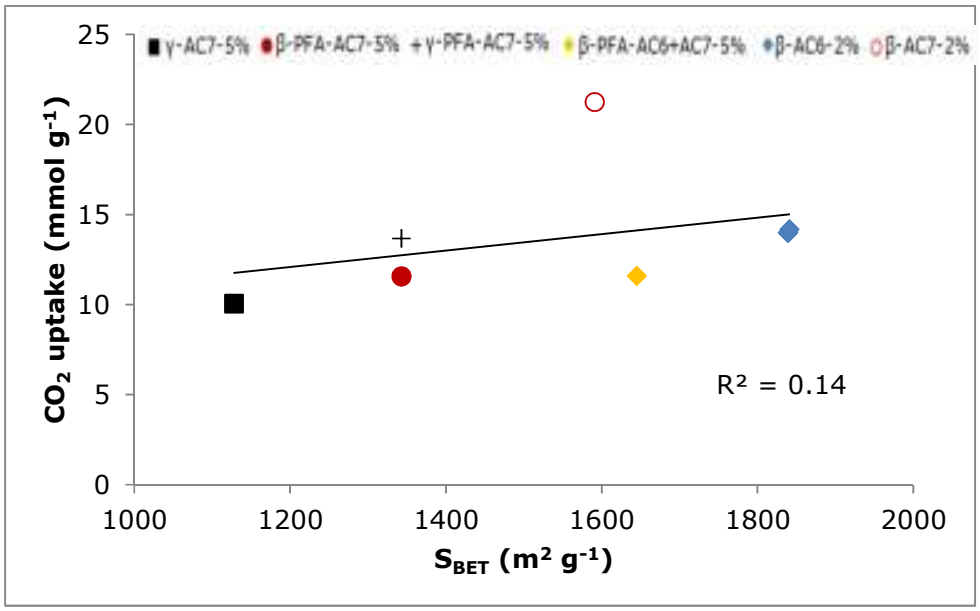

Figure 5.18. Effect of surface area on CO_2 uptake capacity of studied adsorbents at 4.1 MPa.

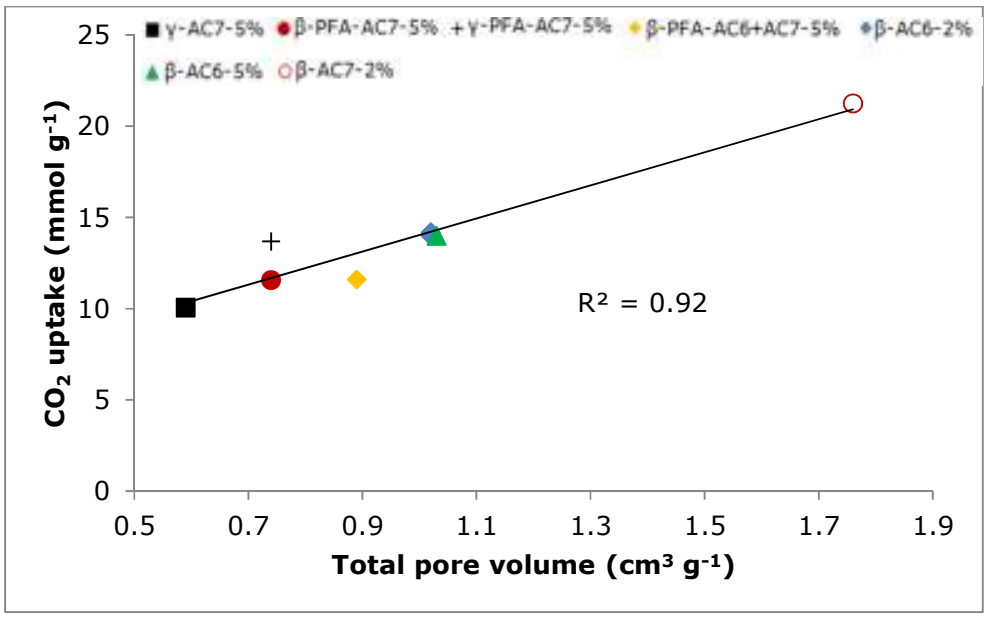

Figure 5.19. Effect of total pore volume on CO_2 uptake capacity of studied adsorbents at 4.1 MPa.

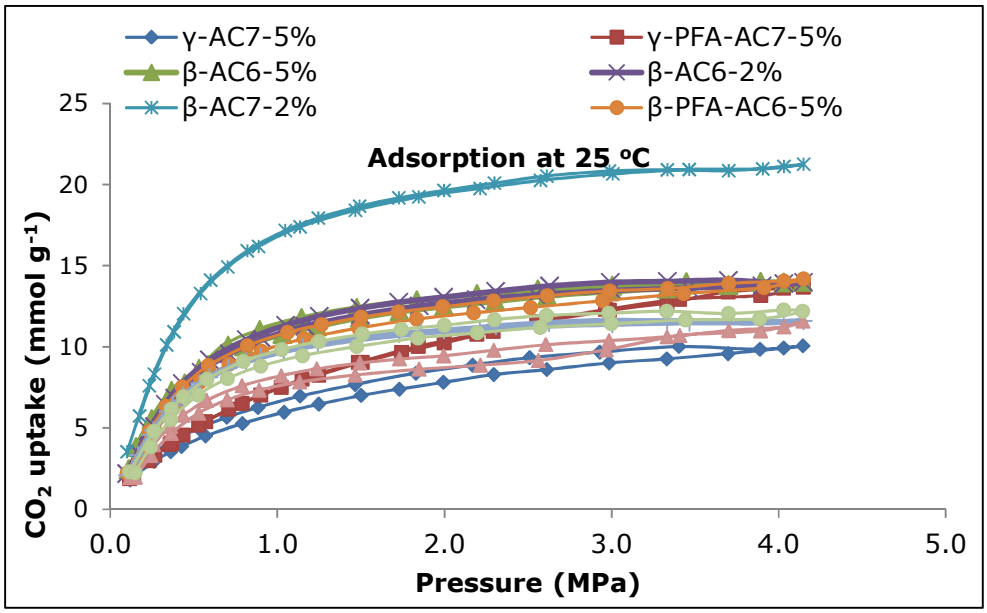

Figure 5.20. CO_2 adsorption isotherms measured at 25 °C.

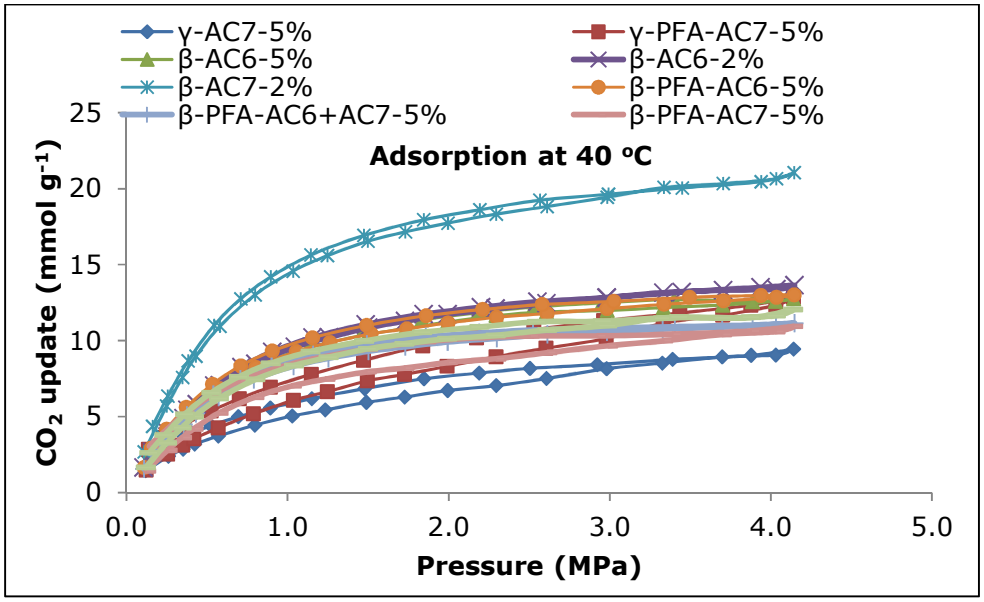

Figure 5.21. CO_2 adsorption isotherms at 40 °C.

Pressure swing adsorption (PSA) can be simulated by examining the adsorption/desorption isotherms (Figure 5.22; see Appendix 1 and 2 for more results) at atmospheric and higher pressures. The desorption isotherm

obtained after pressure was reduced to about 0.1 MPa for all the templated carbons show approximately 98% of CO_2 removed from the materials at 25 and 40 ^{o}C. Although, the desorption curve did not totally coincide with adsorption curve at lower pressures (see Figure 5.22 and Appendix 1). This suggests the need for extra energy to totally desorb CO_2 from the adsorbents (Weihong, 2009). This has led to the proposal of the use of combined temperature and pressure swing adsorption cycles for regeneration operation.

The highest uptake capacities reported for the templated carbons are more than double the amount reported in Heins et al., (1990) and Dreisbach et al., (1999) under similar experimental conditions and techniques for activated carbons. It is also higher than the 9.8 mmol g^{-1} reported in Martin et al., (2012) when they studied the CO_2 uptake on phenol-aldehyde resin based activated carbons at 3 MPa, and the 10.7 mmol g^{-1} reported by Drage et al., (2009) when they studied CO_2 uptake on activated carbons at 3 MPa.

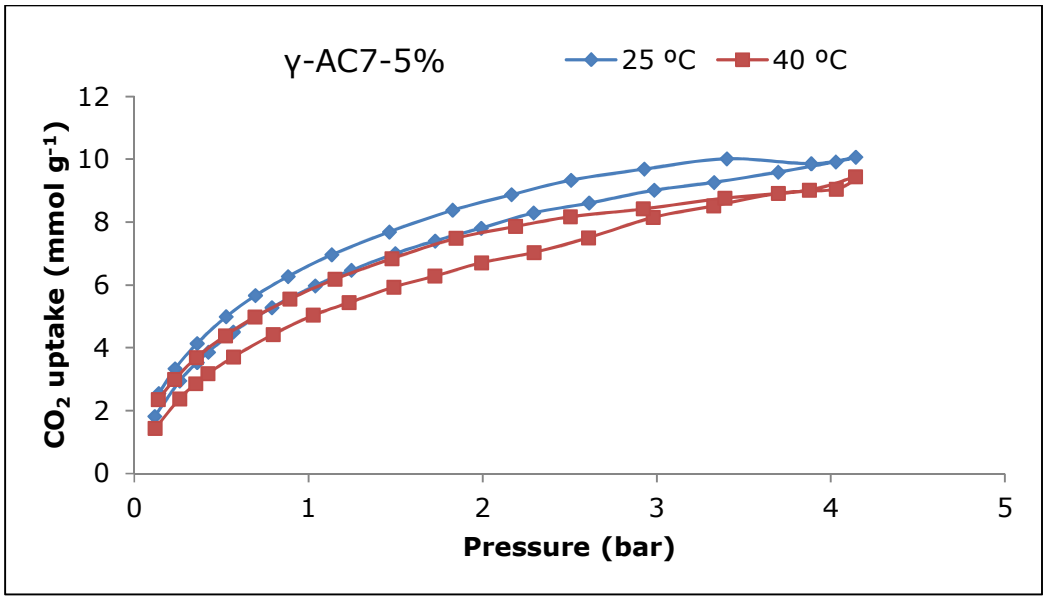

Figure 5.22. CO_2 uptake of γ-AC7-AC-5% at 25 and 40 ^{o}C at high pressure.

Increased CO_2 uptake recorded here when compared to those obtained for the same materials at atmospheric pressure (see Section 5.4) may be attributed to three things; the presence of very narrow micropores, absolute pore filling or the filling of supermicropores in the adsorbents (Alcaniz-Monge et al., 1995), and the overcoming of the repulsive force (activated diffusion) between pores surfaces and the CO_2 molecules within the micropores as a result of high pressure CO_2 application (Krkljuš, 2011).

Also as explained in Section 5.4 at ambient pressure, high density adsorbents seem to have higher CO_2 uptake (mmol cm^{-3}) records. Some materials will have a higher volumetric capacity than others, even though their mass uptake might be the same or less. Similar observations were made at high pressure test conditions too. Take the β–AC6-2% and β–AC6-5% for example (Figure 5.23), at 4.1 MPa, they have almost identical mass uptake, yet the volumetric capacity for β–AC6-5% is far higher than that of β–AC6-2%. The β–AC7-2% has the highest CO_2 uptake capacity on mass basis (21 $mmolg^{-1}$) as well as on volumetric basis (35 $mmolcm^{-3}$) (Figure 5.23). The denser an adsorbent is, the higher its volumetric CO_2 uptake capacity. Also, approximately 31 mmol cm^{-3} of CO_2 (Figure 5.23) was captured by the β-PFA-AC7-5% adsorbent at 4.1 MPa compared to 4.83 mmol cm^{-3} recorded at atmospheric pressure. This is expected as this adsorbent is mainly microporous, and purely microporous material tends to have higher densities (Patrick, 1995).

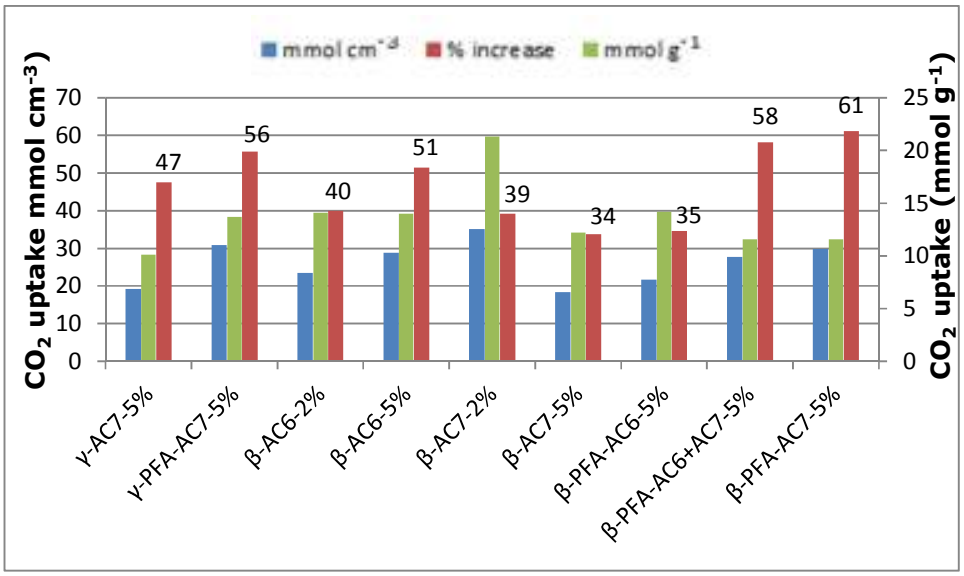

Figure 5.23. Adsorption comparison at 25 °C between mmol g^{-1} and mmol cm^{-3} at 4.1 bar.

5.7 Summary

A range of microporous carbon has been synthesized and tested for CO_2 uptake performance at ambient and higher pressures. The properties of the carbons produced and performance of the adsorbents on CO_2 uptake depends highly on the carbon synthesis technique employed. The adsorbents can be arranged in the following order based on CO_2 uptake performance at ambient conditions; <modenite templated carbons < γ-type templated carbons < β-type templated carbons. Results have shown that the addition of PFA results in greater textural development in carbon materials synthesized from predominantly microporous zeolite templates (γ-type and mordenite), whilst being of no benefit when used for the predominantly mesoporous carbon. As observed in this study, no single synthesis parameter can be attributed to the textural characteristics obtained in the studied materials. To synthesize an adsorbent with characteristics of interest, a combination of the different

synthesis parameters may be used. The β-type zeolite derived carbon generated a range of activated carbons with higher S_{BET} and micropore volumes than those derived from γ-type zeolite and mordenite. Increase in activation temperature and addition of furfuryl alcohol enhanced the S_{BET} of most of the materials under study. Maximum S_{BET} of 2404 m^2g^{-1} and 1.0 cm^3 g^{-1} of micropore volume were recorded. Up to 2.35 mmol g^{-1} of CO_2 adsorption capacities was recorded at 25 ^oC, and this performance have been observed to depend highly on the textural properties of these adsorbents, more especially, their microporosity. There has been a correlation between the CO_2 uptake level and increasing microporosity and material's surface area.

Results on high pressure CO_2 uptake capacities have shown that textural properties of adsorbents play a key role in their uptake capacities. While surface area and micropore volume are key to high CO_2 uptake capacities at atmospheric pressure, total pore volume was seen to influence the uptake capacities of adsorbents at higher pressure more than micropore and surfaces area. A maximum of approximately 21.3 mmol g^{-1} of CO_2 uptake capacity have been reported for the β–AC7-2% in this chapter. This value is seven times higher than the 3 mmol g^{-1} target predicted for minimising energy penalty associated with power generation, for adsorbents application in post-combustion CCS (Drage et al., 2012; Wang et al., 2012).

CHAPTER SIX

6 Influence of carbon surface modification

6.1 Introduction

In this chapter, two different surface modification routes; ammonia and oxidation treatments have been explored to modify a commercial activated carbon (R-2030), zeolite templated carbons and phenolic resin activated carbons. Ammonia treatment was used for the R-2030 activated carbon and the zeolite templated carbons, while the oxidation treatment was used for the phenolic resin activated carbon. The ammonia and oxidation treatment processes added amine functional groups and oxygen functional groups respectively to the carbon surfaces. Full details of the modification process for the amine treatment and oxidation treatment can be found in Sections 3.3 and 3.4 respectively of Chapter three.

This chapter is divided into three sections. The first section discusses the results obtained for the amine modified commercial activated carbon. The second section discusses the results obtained for the oxidized phenolic resin activated carbon, and the third section presents the results of the amine modified templated carbons at ambient and high pressure conditions.

6.2 Amine modified commercial activated carbon

The unmodified commercial activated carbon, from now on referred to as CL has 800 $m^2\ g^{-1}$ surface area and particle sizes greater than 2.36 mm (Table 6.1). H_2-NH_2-CL_{40} and H_2-NH_2-CL_{50} annotations have been used to represent the amine modified carbons. The H_2-NH_2CL_{50} represents an amine modified carbon which was hydrogenated at 5 MPa, while H_2-NH_2-CL_{40} represents carbon that was hydrogenated at 4 MPa of pressure (see Section 3.3).

The N_2 adsorption isotherms for CL, H_2-NH_2-CL_{40} and H_2-NH_2-CL_{50} presented in Figure 6.1 are Type I according to the BDDT classification (Goyal and Bansal, 2005) showing they are mainly microporous materials. NDFT analysis (Figure 6.2) indicates that the pores of the unmodified and modified adsorbents are predominantly distributed in the 0 and 2 nm range.

Table 6.1. Textural properties of amine modified activated carbon measured at -196 ^oC.

Sample name	Total pore volume ($cm^3\ g^{-1}$)	Micropore volume ($cm^3\ g^{-1}$)	Micropore area ($m^2\ g^{-1}$)	$S_{(BET)}$ ($m^2\ g^{-1}$) Error ± 1.5
CL	0.50	0.33	694	704
H_2-NH_2CL_{40}	0.34	0.27	595	607
H_2-NH_2CL_{50}	0.32	0.30	652	668

This implies that the modification has little or no effect on the textural properties of the modified activated carbon. Although the amount of nitrogen adsorbed were slightly affected. This is expected as the amine molecules occupy some spaces in the pore structure of the material after modification.

The textural properties of the amine modified carbon are presented in Table 6.1. The textural properties of the modified carbon were only slightly altered by the introduction of amine. Results show there was only 6 and 16% reduction in surface area of H_2-NH_2-CL_{50} and H_2-NH_2-CL_{40} respectively, and 9% and 18% reduction in micropore volume respectively compared to the unmodified CL carbon. This further explains the isotherm obtained for these adsorbent as seen in Figure 6.1. Also, ultimate analysis results showed that the total elemental carbon remained high for the modified carbons (

Table 6.2). Also, the amount of elemental nitrogen (Nitrogen loading) tripled for the amine modified carbons compared to the original CL carbon, indicating a success in surface modification. The reduction in the nitrogen loading seen in

Table 6.2 may be due to reduced active sites resulting from higher pressure. The micropore volume was observed to remain unchanged while the total pore volume decreased after modification. This suggests that the amine modification took place in the meso and larger pores of the carbons.

Table 6.2. Ultimate analysis for the R2030 and amine modified adsorbents

Sample name	C (wt.%)	H (wt.%)	N (wt.%)	O (wt.%)
CL	96.99	0.18	0.41	2.42
H_2-NH_2CL_{40}	95.23	0.03	1.43	3.32
H_2-NH_2CL_{50}	93.21	0.24	1.29	5.26

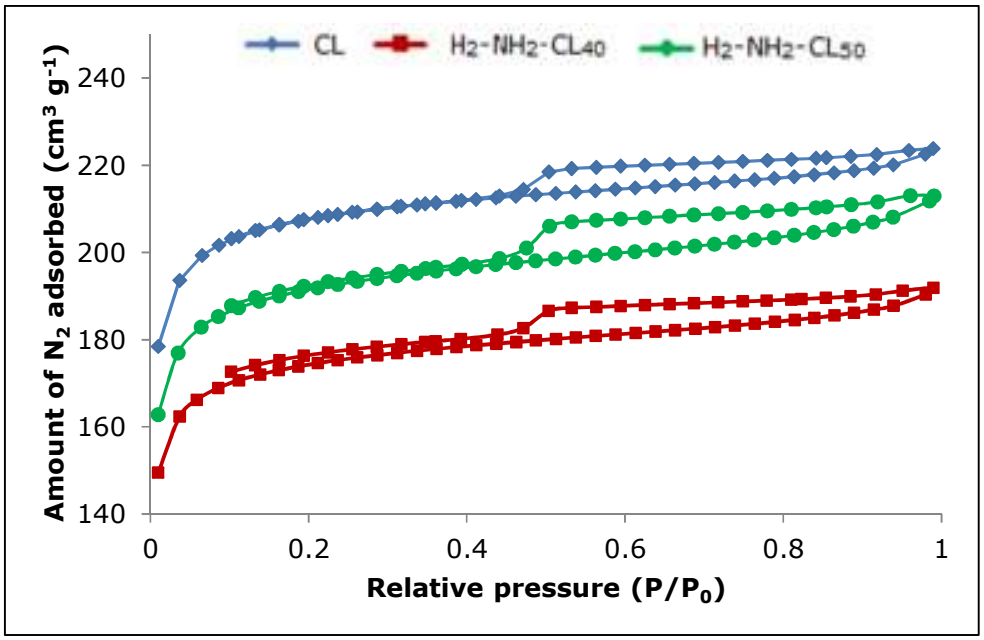

Figure 6.1. Nitrogen adsorption isotherm of unmodified and modified commercial activated carbon measured at -196 °C.

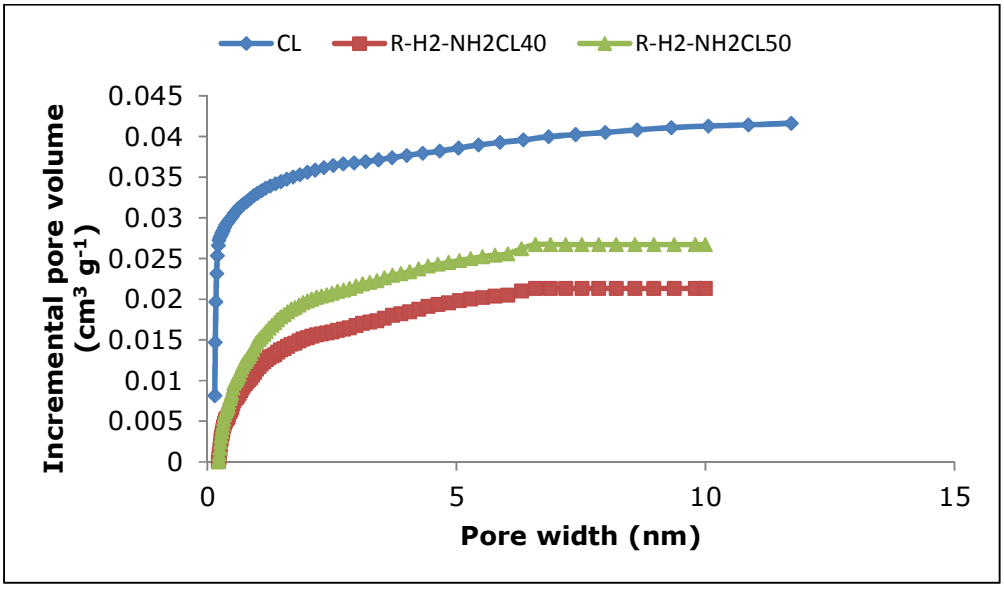

Figure 6.2. NLDFT pore size distribution for unmodified and modified commercial activated carbon measured at -196 °C.

6.2.1 CO_2 uptake measurements of commercial activated carbon

CO_2 uptake measurements show that the modified adsorbents have higher uptake capacities than the unmodified adsorbent at 25 ^oC Table 6.3. The unmodified commercial activated carbon showed a 2.4 mmol g^{-1} of CO_2 uptake capacity, while the modified ones showed approximately 2.5 and 2.7 mmol g^{-1} of CO_2 uptake capacities, with maximum standard deviation of 0.04 after six adsorption tests compared to the unmodified one (CL). At ambient temperature and pressure test conditions, total pore volume, surface area and micropore volume was observed not to play a major role in the uptake performance of these adsorbents. Although just few points have been represented here, adsorption trends were seen to decrease as the micropore volume, surface area, and total pore volume increased respectively (Figure 6.3, Figure 6.4, and Figure 6.5 respectively). This shows opposite trend to those observed for the templated carbons (see Figure 5.8 and Figure 5.9 in Section 5.4 for comparison), and suggest that the effect of the textural properties have been to some respect over ridden by the chemical modification. More data point would have provided a better correlation, but this was not taken due to time constraint.

In nitrogen atmosphere, the TPD profile shows that CO_2 desorbed exponentially with increasing temperature (Figure 6.6), while a non-isothermal CO_2 capture test (Figure 6.7) shows the inverse proportional relationship of CO_2 adsorption to temperatures. In both profiles, the desorption rates were slower for the amine modified carbons. This signifies a stronger adsorption sites and increased CO_2 affinity on the amine modified carbon. This also shows a significant success in surface modification of the materials.

Table 6.3. CO_2 uptake capacities of CL and amine modified commercial activated carbons at ambient pressure.

Sample name	CO_2 uptake @ 25 °C (mmog-1)	15% CO_2 ($mmolg^{-1}$)	Ratio (%)
CL	2.42 ±0.01	0.88	23
H_2-NH_2CL_{40}	2.53 ±0.04	1.03	23
H_2-NH_2CL_{50}	2.65 ±0.03	1.01	23

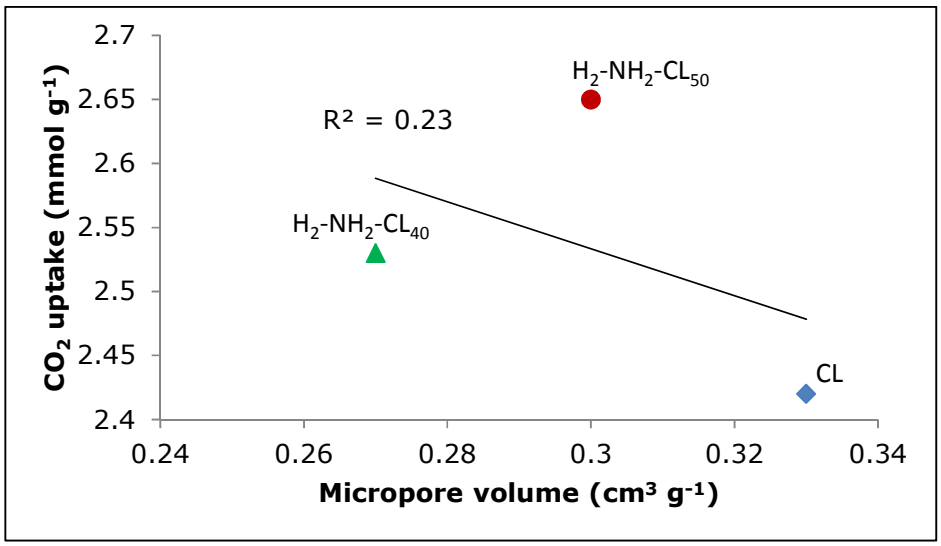

Figure 6.3. CO_2 uptake trend for commercial active carbon and modified carbon with respect to micropore volume measured at ambient temperature and pressure.

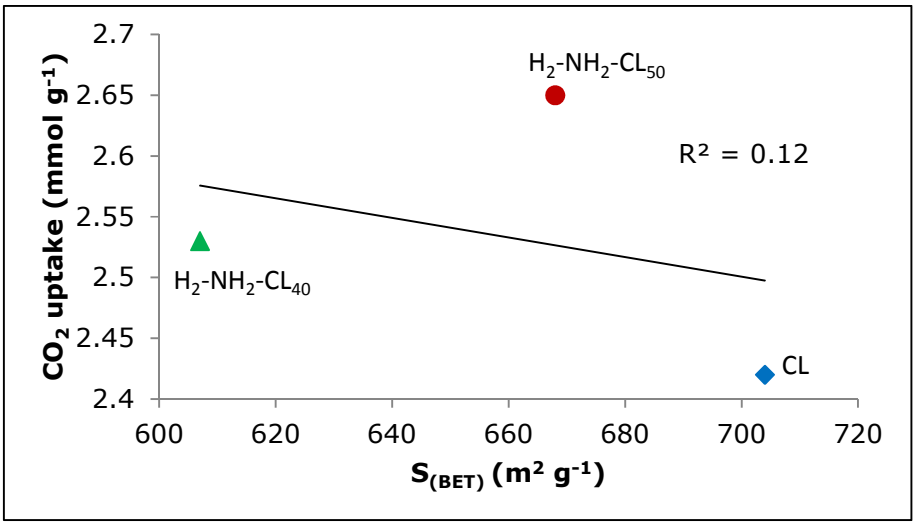

Figure 6.4. CO_2 uptake trend for commercial active carbon and modified carbon with respect to surface area measured at ambient temperature and pressure.

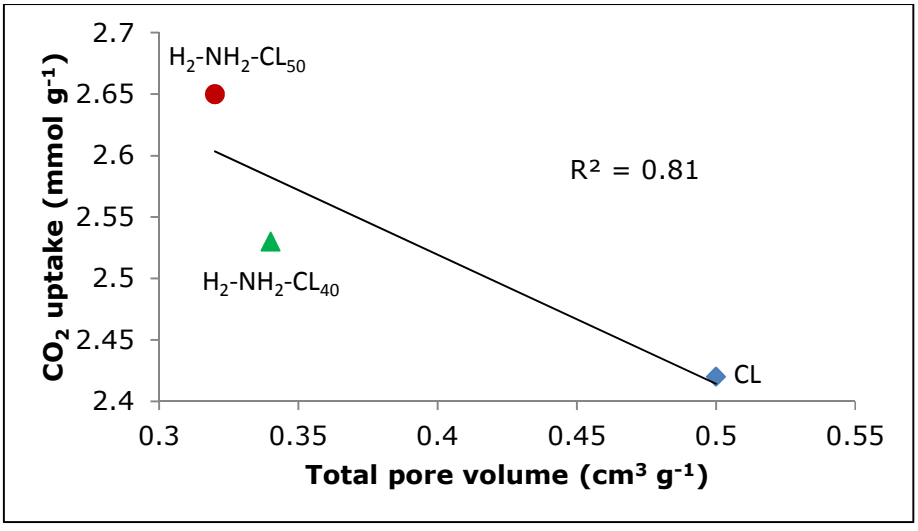

Figure 6.5. CO_2 uptake trend for commercial active carbon and modified carbon with respect to total pore volume measured at ambient temperature and pressure.

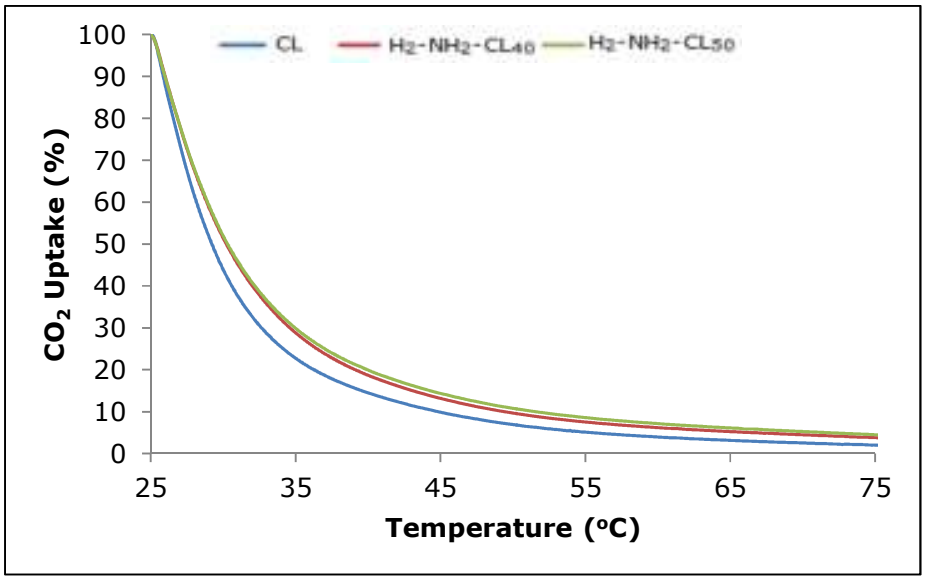

Figure 6.6. Temperature programmed desorption for CL, H_2-NH_2CL_{40}, and H_2-NH_2CL_{50}: heating rate of at 5 °C min^{-1} in 98 cm^3 min^{-1} of N_2 flow at ambient pressure.

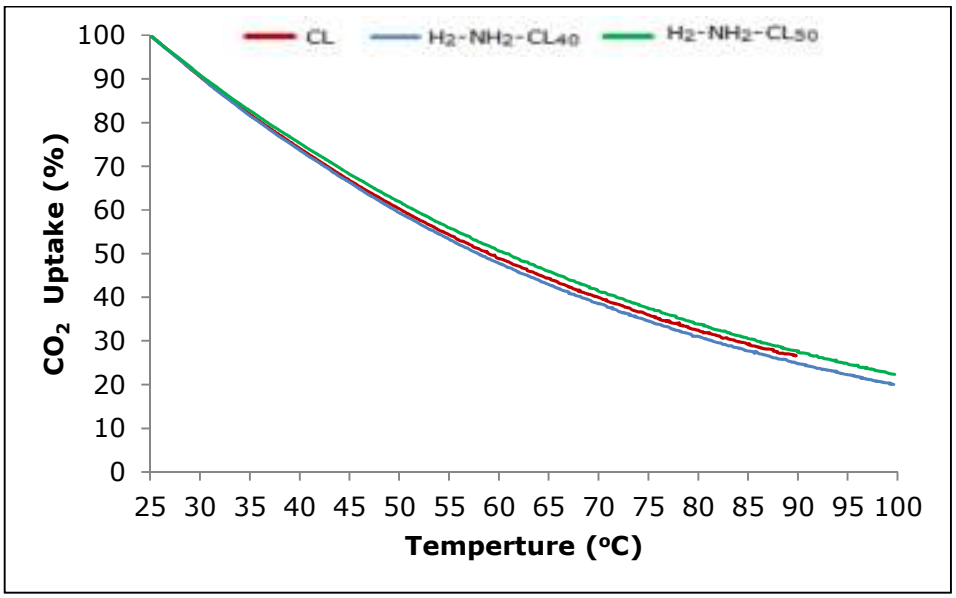

Figure 6.7. Non-isothermal CO_2 capture tests: heating rate of 0.25 °C min^{-1} in 98 mL min^{-1} of CO_2 flow at ambient pressure.

CO_2 uptakes recorded at high pressures (Figure 6.8) were more than those recorded at ambient pressure for the unmodified and amine modified commercial activated carbons. Approximately 6.6, 5.2, and 6.5 mmol g^{-1} of CO_2 uptake capacities were recorded for CL, H_2-NH_2CL_{40}, and H_2-NH_2CL_{50} respectively at 4.1 MPa (

Table 6.4). Despite amine modification, the H_2-NH_2CL_{50} has approximately the same adsorption capacity with CL at 4.1 MPa, while the H_2-NH_2CL_{40} showed lower CO_2 capacity. This suggests that surface chemistry may not necessarily increase adsorption capacity for this carbon at high pressure, but may increase material's surface affinity to CO_2. CO_2 uptake trend for the adsorbents were seen to increase with increasing micropore volume (Figure 6.9) and surface area (Figure 6.10). Whereas no CO_2 uptake trend was observed for these materials with respect to the total pore volume (Figure 6.11).

Table 6.4. CO_2 uptake capacities of CL and amine modified commercial activated carbons at higher pressures up to 4.1 MPa.

Sample name	CO_2 uptake @ ambient condition (mmol g^{-1})	CO_2 uptake @ 4.1 MPa and 25 ^oC (mmol g^{-1})
CL	2.42 ±0.01	6.58 ±0.01
H_2-NH_2CL_{40}	2.52 ±0.04	5.15 ±0.05
H_2-NH_2CL_{50}	2.65 ±0.03	6.54±0.03

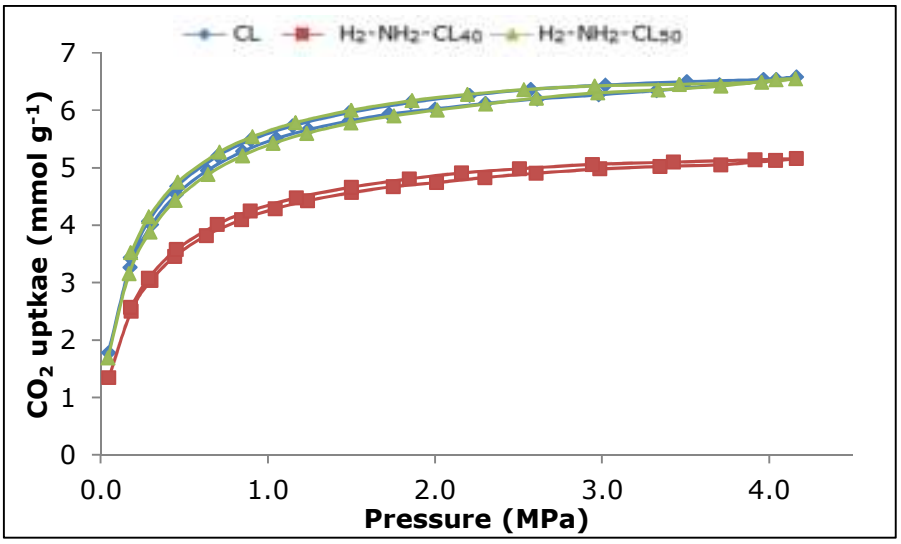

Figure 6.8. CO_2 Adsorption isotherm for unmodified and amine modified commercial activated carbon at 25 oC and pressures up to 4.1 MPa.

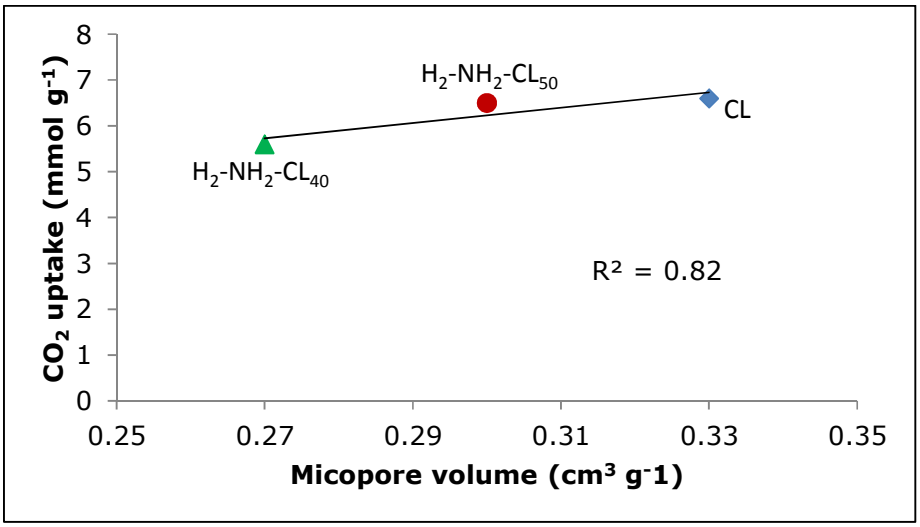

Figure 6.9. CO_2 uptake trend for commercial active carbon with respect to micropore volume measured at 25 ^{o}C and 4.1 MPa.

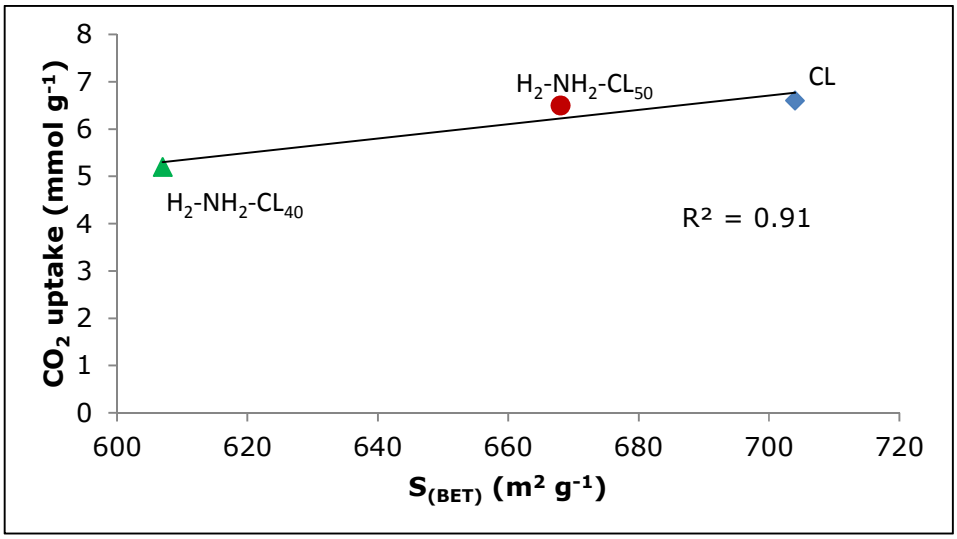

Figure 6.10. CO_2 uptake trend for commercial active carbon with respect to surface area measured at 25 °C and 4.1 MPa.

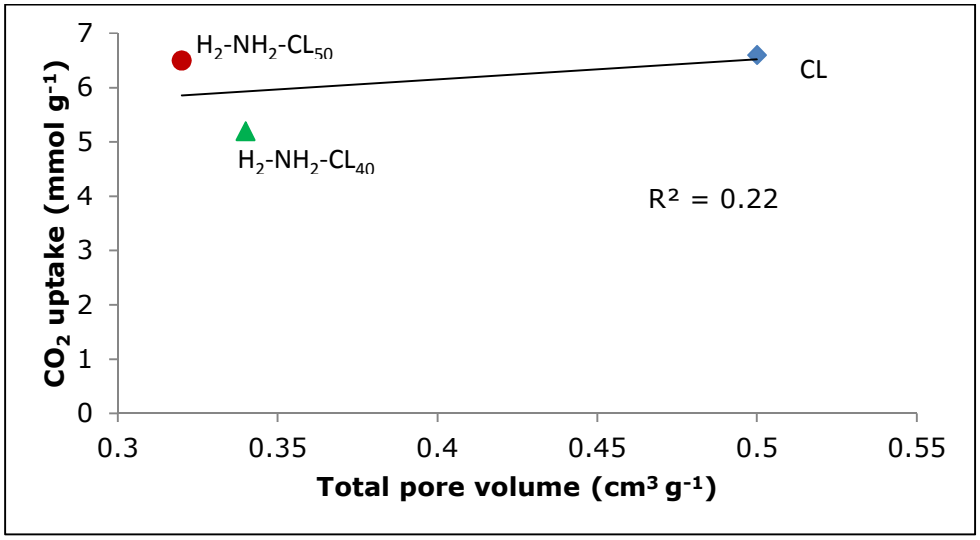

Figure 6.11. CO_2 uptake trend for commercial active carbon with respect to total pore volume measured at 25 °C and 4.1 MPa.

6.3 Oxidized phenolic resin activated carbon

This section presents the results obtained from oxidation of phenolic resin activated carbon. Oxygen surface functionalities were introduced onto the surface of phenolic resin activated carbon, with the aim of studying their influence over the CO_2 capture performance of the oxidised materials at ambient and high pressure conditions. Three different techniques were used to introduce these oxygen functionalities; oxidizing with 1M $(NH_4)_2SO_4$ at room temperature, oxidation with 1 and 16 M nitric acid, and gas phase oxidation by heating the carbons in air at 420 ^oC. Full details of modification process can be obtained in Section 3.4. For simplicity and easy material identification, M has been used to represent the unmodified phenolic resin carbons. MAP-1, MAP-3, and MAP-24 are carbons oxidized by 1 M saturated solution of ammonium persulfate in sulphuric acid for 1, 3 and 24 hours respectively. MNA1-1, MNA1-24, MNA16-1 and MNA16-3 are phenolic resin carbons oxidized by 1M and 16M nitric acid for 1, 24 and 3 hours respectively. Finally, the gas phase oxidised carbon has been represented as MAM.

It is important to state that the CO_2 uptake results at ambient conditions presented in this section was obtained from Plaza et al., (2012) (presently under review for publication).

6.3.1 Chemical and textural properties of Oxidized phenolic resin carbon

Table 6.5 summarises the textural parameters of the studied samples after 5 tests and illustrates the effect of the oxidation techniques on the textural properties compared to the original carbon, M. Except for the gas phase oxidation treatment, which showed an increase in surface area after

modification, the liquid phase oxidation treatments (MAP and MNA) recorded a decrease in surface area after modification in comparison with the original adsorbent M. This reduction can be attributed to a partial collapse of pore walls caused by the oxidation reaction and the surface tension of the oxidising solution (Matsumura, 1975). Results in Table 6.5 also showed that the microporosity was not significantly altered by the oxidation treatments (as seen in the micropore volume, W_o which is around 0.3 cm^3 g^{-1} for all the adsorbents). The moderate textural development is due to the partial gasification of the carbon with air. Therefore, the reduction in the total pore volume must come from the loss of wide microporosity.

The chemical properties of the materials showed a significant increase in the amount of oxygen on the modified materials as compared to the unmodified adsorbent (Table 6.6). The MAP and MNA samples showed between 79-88% and 82-91% increase in oxygen respectively, while the MAM showed 74% increase compared to the base material. This significant increase indicates a successful addition of oxygen functionalities to the adsorbents surfaces.

Table 6.5. Textural properties of oxidized phenolic carbons.

	N_2 adsorption measured at -196 °C			
Sample	S_{BET} ($m^2\ g^{-1}$)	W_o ($cm^3\ g^{-1}$)	V_P ($cm^3\ g^{-1}$)	ρ_{He} ($g\ cm^{-3}$)
M	1180	0.30	0.51	1.99
MAP-1	928	0.31	0.39	1.99
MAP-3	929	0.29	0.42	1.93
MAP-24	887	0.31	0.38	1.96
MNA1-1	894	0.31	0.38	1.99
MNA1-24	917	0.29	0.39	1.96
MNA16-1	941	0.31	0.41	1.96
MNA16-3	962	0.30	0.41	1.96
MAM	1196	0.31	0.53	2.02

S_{BET}: surface area; W_0: micropore volume; V_p: total pore volume; ρ_{He}: density

Table 6.6. Ultimate analysis calculated by dry ash free basis.

Sample	C (wt.%)	H (wt.%)	N (wt.%)	S (wt.%)	O (wt.%)
M	97.78	0.46	0.28	0.07	1.41
MAP-1	91.32	1.18	0.31	0.20	6.99
MAP-3	89.85	1.26	0.30	0.17	8.42
MAP-24	86.54	1.41	0.28	0.25	11.52
MNA1-1	90.21	1.06	0.77	0.15	7.81
MNA1-24	86.49	1.22	0.77	0.15	11.37
MNA16-1	82.69	1.75	0.77	0.23	14.56
MNA16-3	80.63	2.37	0.77	0.33	15.90
MAM	92.62	1.31	0.49	0.15	5.43

6.3.2 CO_2 uptake measurements at ambient pressure: influence of textural properties and surface chemistry

The results of the isothermal CO_2 adsorption tests carried out at 25 ^oC are summarised in Table 6.7. All oxidised samples present higher CO_2 adsorption capacity than the starting material, M. The liquid phase oxidized materials (in particular, MAP-3) recorded the highest CO_2 uptake capacity (2.9 mmol g^{-1}). The gas phase oxidized material showed only a slight increase in CO_2 uptake capacity (only 4% increase) compared to the starting material. The presence of stronger adsorbate-adsorbent interactions between the introduced oxygen surface groups and the CO_2 molecule enhanced CO_2 uptake. Based on the adsorption capacities recorded, it could be inferred that the adsorbate-adsorbent interactions is stronger for the liquid phase oxidized materials than the gas phase oxidized adsorbent. Although textural properties affect the CO_2 uptake performance of the adsorbents, higher texture development does not necessarily translate to higher adsorption capacity: the maximum CO_2 uptakes were obtained for the liquid phase oxidised samples. Thus it seems that surface chemistry is playing an important role in the adsorption of CO_2. Similar results were observed for the amine modified phenolic resin activated carbons in Section 6.2.1.

Table 6.7. CO_2 uptake of oxidized phenolic resin carbons at ambient conditions.

Sample	CO_2 uptake (mmol g^{-1})
M	2.2 ± 0.2
MAP-1	2.4 ± 0.2
MAP-3	2.9 ± 0.1
MAP-24	2.8 ± 0.1
MNA1-1	2.5 ± 0.1
MNA1-24	2.6 ± 0.2
MNA16-1	2.6 ± 0.2
MNA16-3	2.6 ± 0.2
MAM	2.3 ± 0.1

The CO_2 capture capacities reported in these materials are higher than the capacity of commercial activated carbons (between 1.6 and 2.1 mmol CO_2 g^{-1}) evaluated under similar conditions and reported by Plaza et al., (2007). Results obtained here are still higher than that (up to 2.2 mmol g^{-1}) reported by Pevida et al., (2008b) when they examined nitrogen enriched carbons under the same conditions. It is also higher than the 2.65 mmol g^{-1} CO_2 uptake capacities reported for the amine modified commercial activated carbon in Section 6.2. Likewise, urea-formaldehyde and phenolic resin-derived carbons have been reported to present capacities between 1.8 and 2.5 mmol CO_2 g^{-1} at 25 ^{o}C (Drage et al., 2007; Martin et al., 2010).

The amount of CO_2 adsorbed decreased gradually with increasing temperature during the non-isothermal capture tests (Figure 6.12), as expected for a predominantly physical adsorption process. The values fell from 2-3 mmol CO_2 g^{-1} at 25 ^{o}C, to approximately 0.5 mmol CO_2 g^{-1} at 110 ^{o}C. In the studied temperature range, all the oxidized adsorbents have higher CO_2 adsorption capacity than M, especially those prepared by oxidation in liquid phase. These results suggest again that the presence of the surface functional groups has a

beneficial effect on CO_2 adsorption. The effect of micropore volume, surface area and total pore volume at ambient temperature and pressure is presented in Figure 6.13, Figure 6.14, and Figure 6.15 respectively. No positive adsorption trend has been found for the CO_2 uptake capacities of the adsorbents with respect to micropore volume (Figure 6.13), surface area (Figure 6.14), and total pore volume (Figure 6.15).

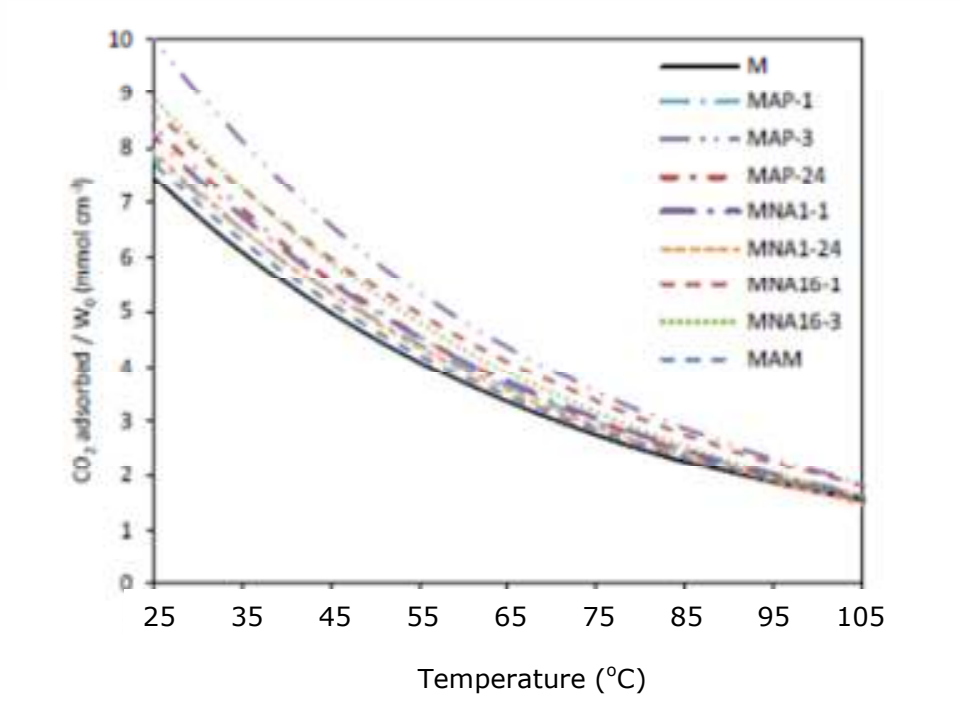

Figure 6.12. Non-isothermal CO_2 capture tests: heating rate of 0.25 $^0C\ min^{-1}$ in 98 mL min^{-1} of CO_2 flow.

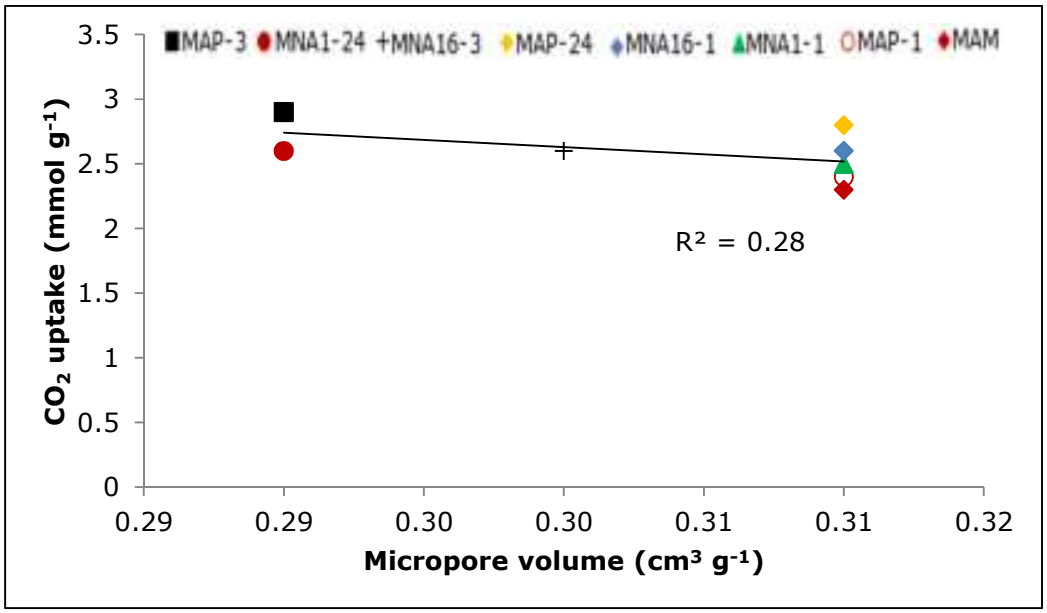

Figure 6.13. CO_2 uptake trend for oxidized carbon with respect to micropore volume measured at ambient temperature and pressure.

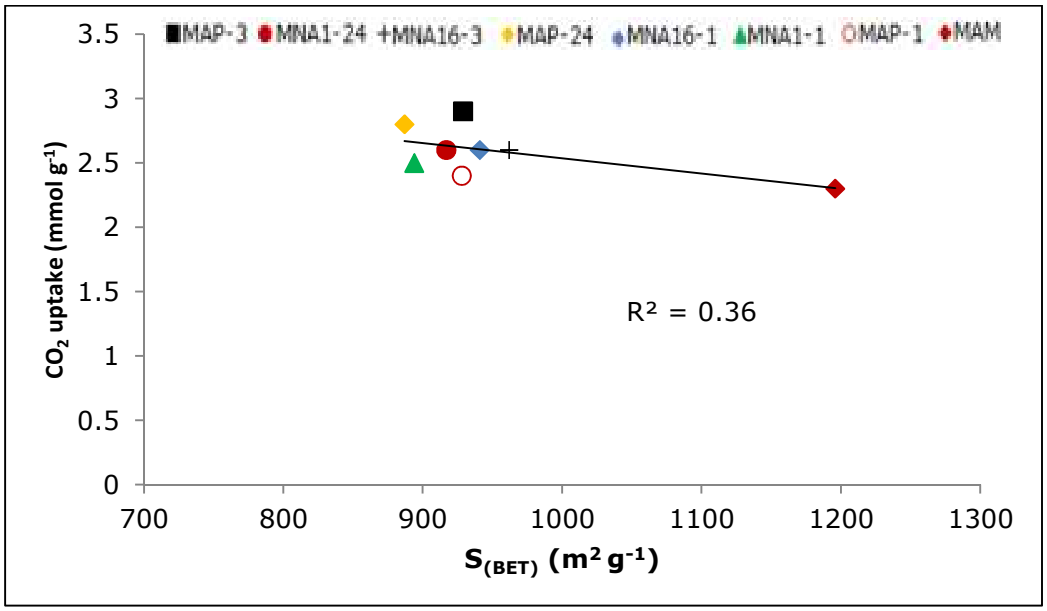

Figure 6.14. CO_2 uptake trend for oxidized carbon with respect to surface area measured at ambient temperature and pressure.

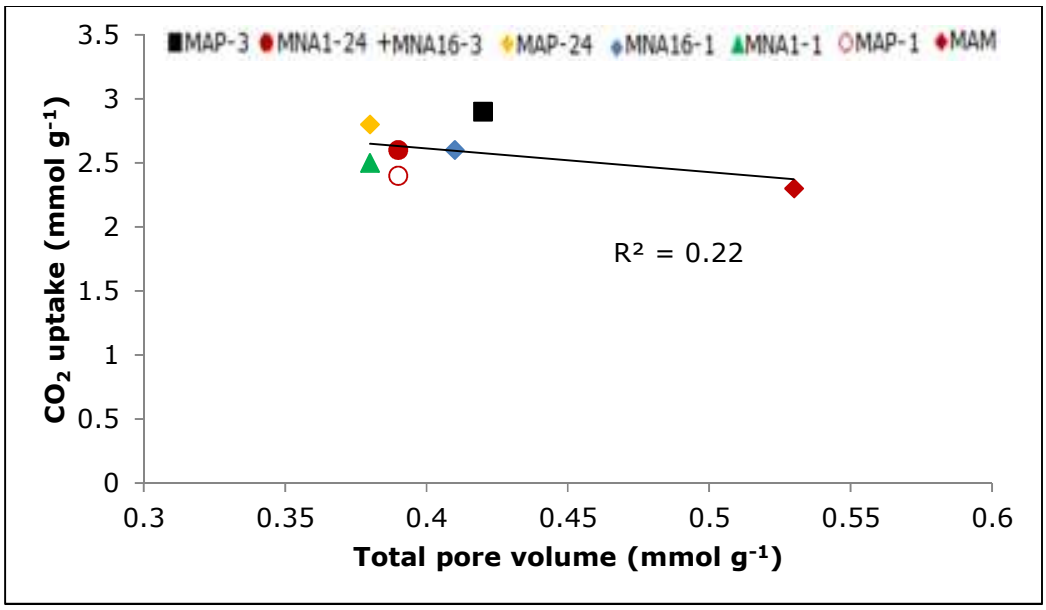

Figure 6.15. CO_2 uptake trend for oxidized carbon with respect to total pore volume measured at ambient temperature and pressure.

6.3.3 High pressure CO_2 uptake measurements on oxidized carbons

The results of high pressure CO_2 uptake performance at 25 and 40 ^oC are presented in Table 6.8. CO_2 uptake at high pressure and 25 ^oC was found to be at least 3 times higher than that recorded at 25 ^oC and atmospheric pressure. The extent of oxidation does not seem to affect the CO_2 uptake capacity for the MAP-1, MAP-13, and MAP-24 carbons. Increased temperature was observed to result in a decrease in the maximum CO_2 uptake range of approximately 8 to 10 mmol g^{-1} at 25 ^oC to approximately 8-9 mmol g^{-1} at 40 ^oC. The liquid phase oxidized carbons produced the highest range of CO_2 uptake capacities at both 25 and 40 ^oC compared to the gas phase oxidized carbon. The MNA16-1 carbon presented the highest CO_2 uptake for these oxidized carbons at both temperatures. Approximately 10.6 and 10.3 mmol g^{-1}

of CO_2 uptake was recorded at 25 and 40 ^oC respectively. While for the MAM carbon, there was approximately no change in the uptake levels at both temperatures, suggesting that gas phase oxidation has little or no effect on the CO_2 uptake of the carbons at high pressure.

Individually, the oxidized adsorbents have higher CO_2 uptake capacities at high pressure compared to that recorded at ambient pressures (see Section 6.3.2), increasing micropore volume, surface area, and total pore volume have shown no positive adsorption trends compared to that observed at ambient pressures.

Table 6.8. CO_2 uptake measurements for the oxidized carbons at 4.1 MPa.

Sample	4.1 MPa	
	25 ^oC (mmol g^{-1})	40 ^oC (mmol g^{-1})
MAP-1	8.38	8.20
MAP-3	10.02	9.26
MAP-24	8.65	7.57
MNA1-1	8.36	7.96
MNA1-24	9.97	9.03
MNA16-1	10.60	10.25
MNA16-3	8.65	8.15
MAM	8.00	7.56

The high pressure CO_2 adsorption isotherms for the oxidized carbons at 25 and 40 ^oC are presented in Figure 6.16 and Figure 6.17. Isotherms for individual adsorbents are presented in Appendix 6. The isotherms are steeper at lower pressures indicating a faster CO_2 uptake. These isotherms are in good agreement with those obtained from literature (Dreisbach et al., 1999). This is expected because the pores are devoid of CO_2 at the start of the adsorption tests, and active sites are free of the adsorbate molecules. As the test

progressed, the adsorbents become saturated with CO_2, and the rate of adsorption decreases. The desorption curves show that not all the adsorbed CO_2 were released during the desorption stage, suggesting the need for heat application for total adsorbate desorption to occur (Siriwardane et al., 2003).

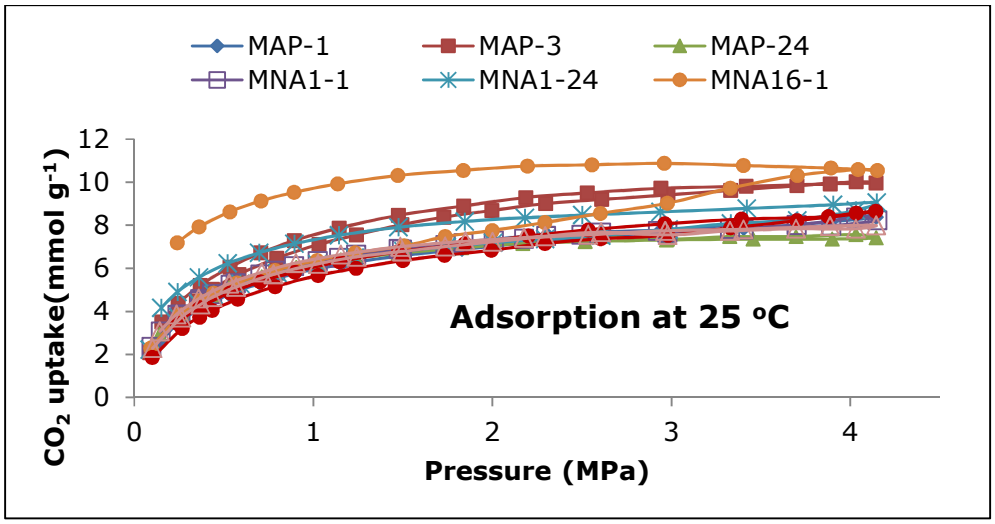

Figure 6.16. CO_2 adsorption/desorption isotherms for oxidized carbons at 25 °C and pressures up to 4.1 MPa.

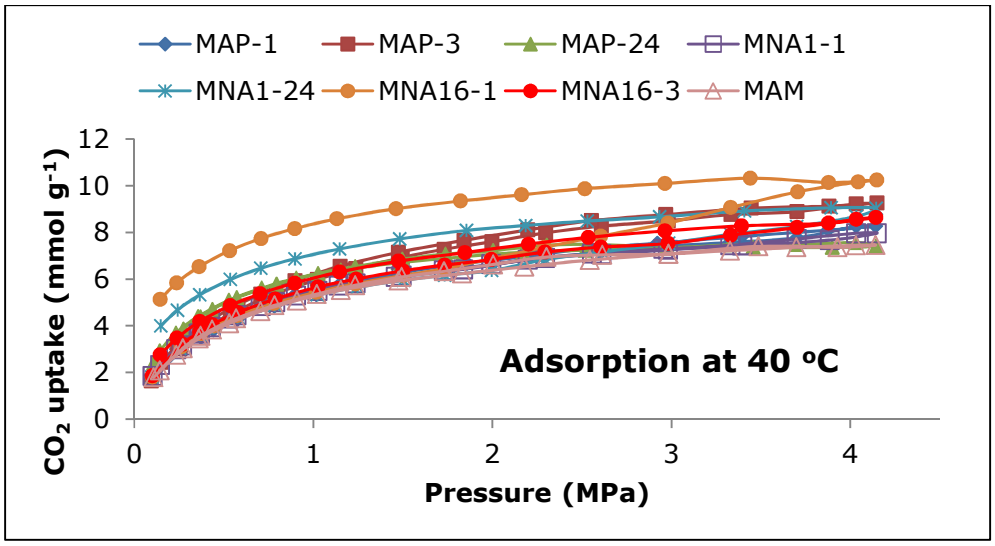

Figure 6.17. CO_2 adsorption/desorption isotherms for oxidized carbons at 40 °C and pressures up to 4.1 MPa.

This same adsorption trend has been observed during the high pressure CO_2 adsorption/desorption process of the zeolite templated carbons reported in Section 6.4. Apart from the MNA1-1 isotherm (Figure 6.18), all other isotherms (see appendix 2) show a desorption curve which lie just above the adsorption curve for both 25 and 40 ^{o}C test conditions. Although, the magnitudes of deviation from the adsorption curves differ from adsorbents to adsorbents, the MNA16-1 exhibited the widest gap. This phenomenon may suggest the swelling of the adsorbents during the adsorption stage, or trapping of CO_2 within the pores of the adsorbents during desorption operation. This observation has been reported to occur in polymer of intrinsic microporosity (PIM) by Budd et al., (2005) and Mckeown et al., (2006).

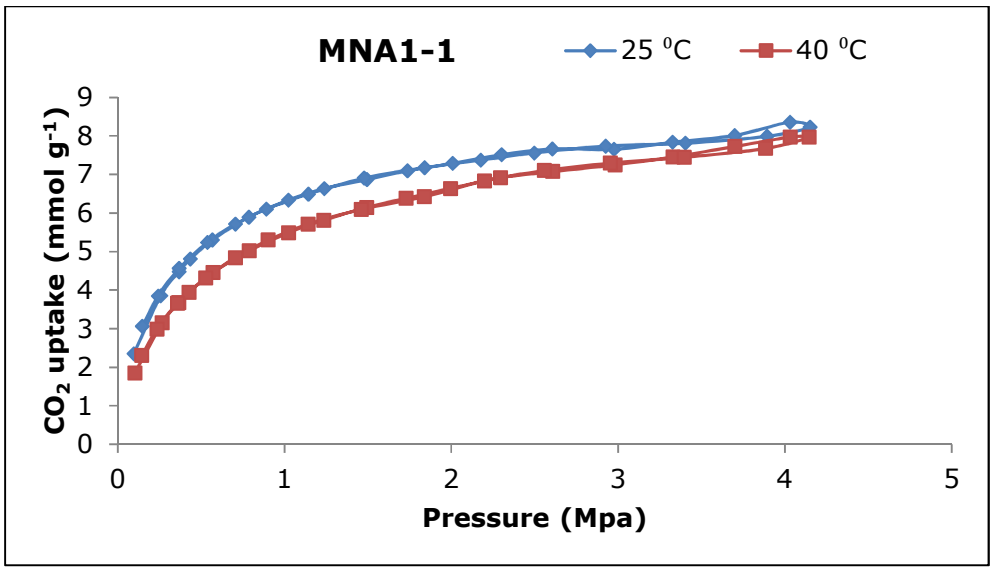

Figure 6.18. Adsorption isotherms for MNA1-1 carbons at 25 and 40 ^{o}C and pressures up to 4.1 MPa.

On the other hand, this may also suggest the effectiveness of the modification operation on the adsorbents, as same phenomenon have been observed for the amine modified templated carbons reported in Section 6.4.

All the isotherms presented in Figure 6.16 and Figure 6.17 have shown broader and flatter maximum compared to those observed in Figure 5.20 and Figure 5.21 for the unmodified templated carbons, indicating that pores are saturated more quickly in the modified materials. This observation has been reported by Weihong et al., (2004) to be consistent with narrow pore distributions.

All the oxidized adsorbents have CO_2 uptake capacities higher than those reported by Hines et al., (1990) and Dreisbach et al., (1999) at similar experimental conditions. The current report by Martin et al., (2012) on CO_2 uptake on phenol-aldehyde resin based activated carbons at pressures up to 3 MPa show CO_2 uptake capacities of approximatley 9.8, 8.4, and 7.3 $mmolg^{-1}$ at 25, 45, and 65 ^{o}C respectively. These values are also lower than the maximum uptake values reported in this study.

The adsorption trends for micropore volume, surface area and total pore volume at ambient temperature and higher pressure is presented in Figure 6.19, Figure 6.20, and Figure 6.21 respectively. Just as experienced at ambient temperature and pressure, no positive trend has been found for the CO_2 uptake capacities of the adsorbents with respect to micropore volume (Figure 6.19), surface area (Figure 6.20), total pore volume (Figure 6.21), and oxygen content of the adsorbent (Figure 6.22).

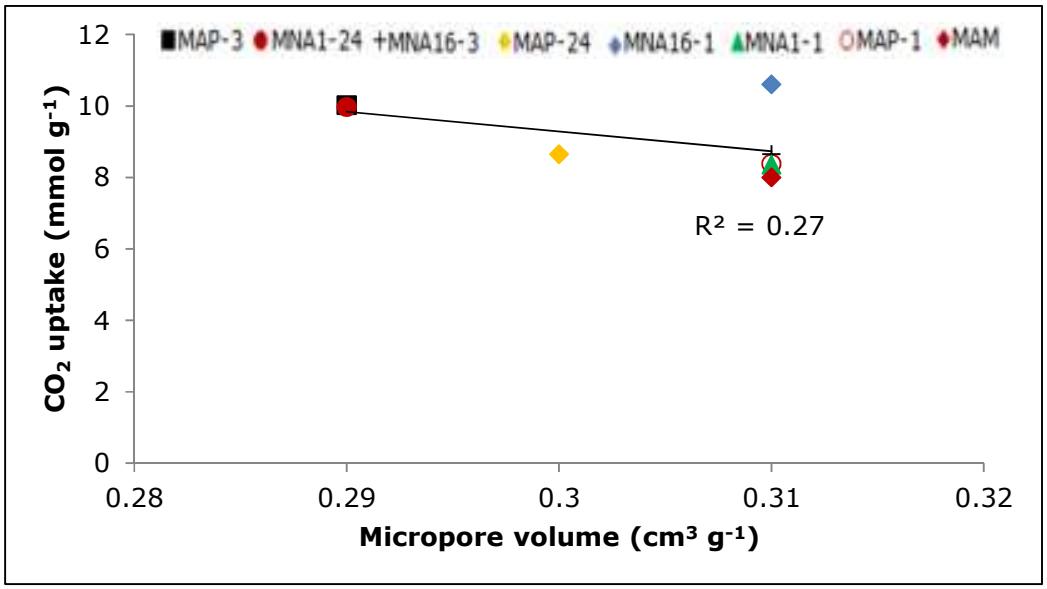

Figure 6.19. CO_2 uptake trend for oxidized carbons with respect to micropore volume measured at 25 °C and 4.1 MPa.

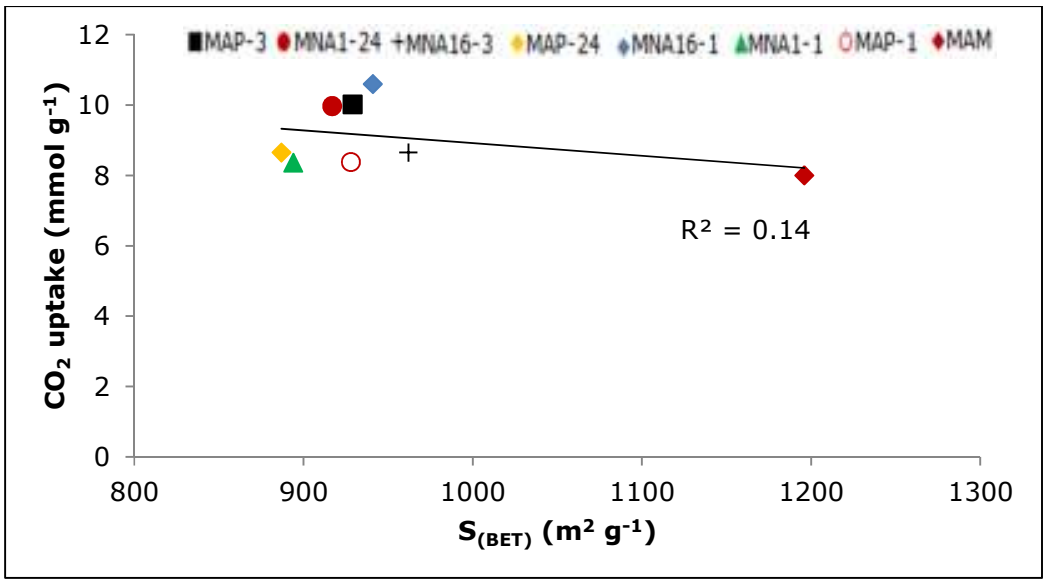

Figure 6.20. CO_2 uptake trend for oxidized carbon with respect to surface area measured at 25 °C and 4.1 MPa.

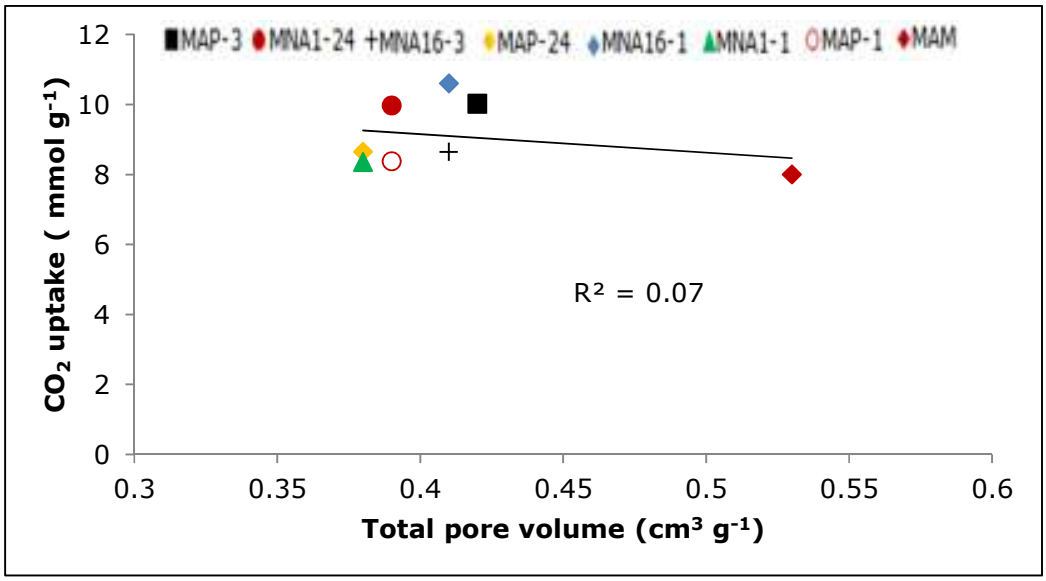

Figure 6.21. CO_2 uptake trend for oxidized carbon with respect to total pore volume measured at 25 and 4.1 MPa.

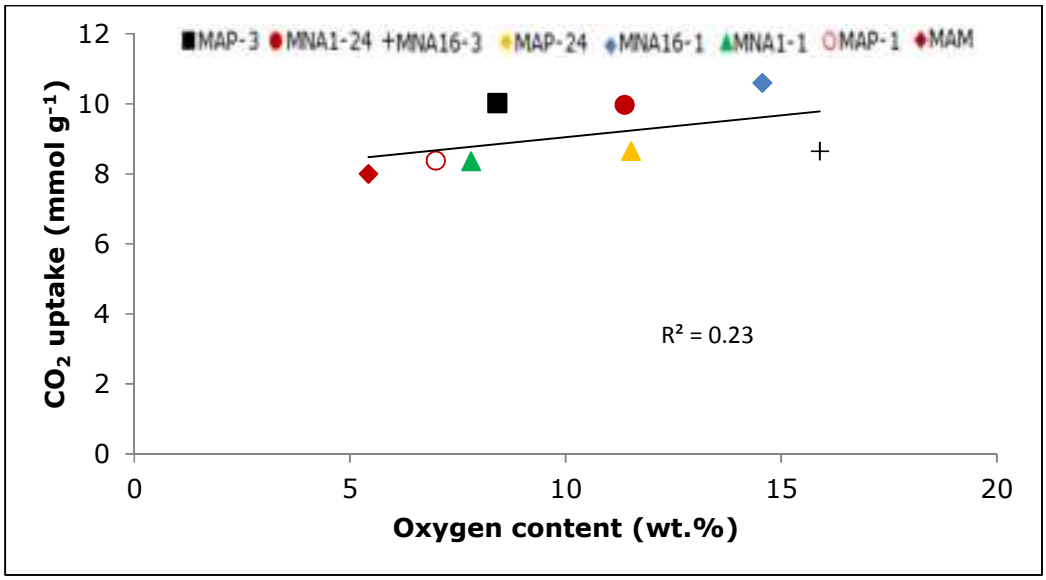

Figure 6.22. CO_2 uptake trend for oxidized carbon with respect to oxygen content of the adsorbent at 25 ^{o}C and 4.1 MPa.

6.4 Amine modified templated carbons

This section presents the results obtained from modifying the surface properties of templated carbons with amines. The amine surface functionalities were introduced onto the surface of the templated carbon, with the aim of studying the influence of surface chemistry on CO_2 capture performance of the materials at ambient and high pressure conditions. The surface modification was carried out by nitration and reduction of nitro groups from the carbons surface using Yoshikawa and Tsumokawa, (1996) method. Full detail of the modification process is presented in Section 3.3.

6.4.1 Textural properties

Just as observed for the unmodified templated carbon (see Figure 5.2 and Figure 5.3), a Type I isotherm was observed for amine modified β-type (Figure 6.23) γ-type (Figure 6.24) and templated carabons, with some hysteresis noted for the γ-type carbons suggesting the presence of some mesoporosity. These observations are further illustrated by the presentation of the pore size distribution profiles in Figure 6.25 and Figure 6.26. The high characteristic energy (Table 6.9) observed in the modified β-type adsorbents as compared to the γ-type modified carbons also give a good indication of the presence of micropores. However, the amount of nitrogen adsorbed by the modified β–type and γ–type carbons were reduced by 44-45% and 73-75% respectively compared with their unmodified carbons. This observation is expected because the modifying species is expected to occupy some spaces in the voids of the adsorbents after modification, reducing the total pore volumes available for nitrogen adsorption.

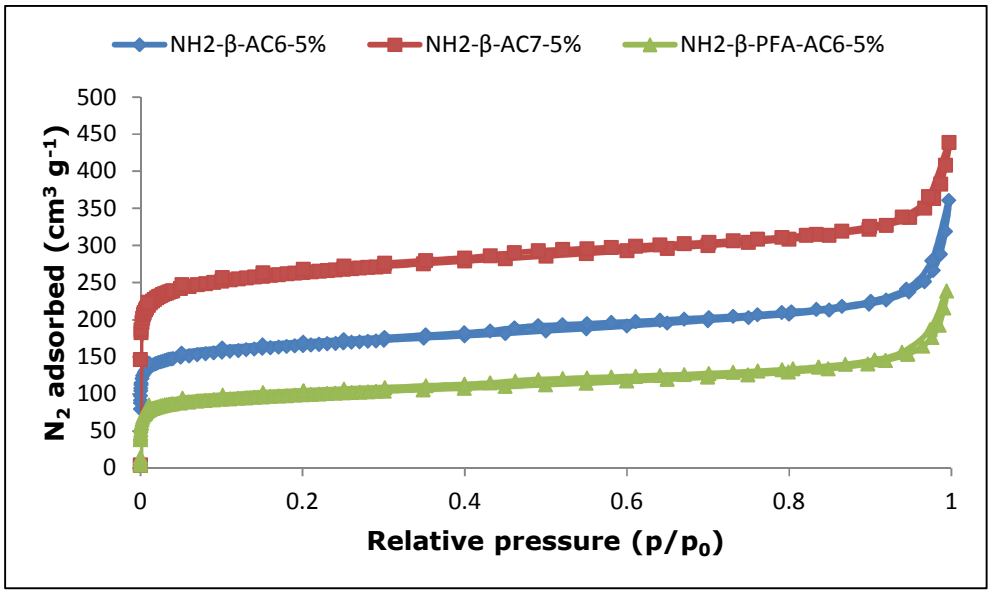

Figure 6.23. Adsorption/desorption profile for amine modified β-type carbons measured at -196 °C.

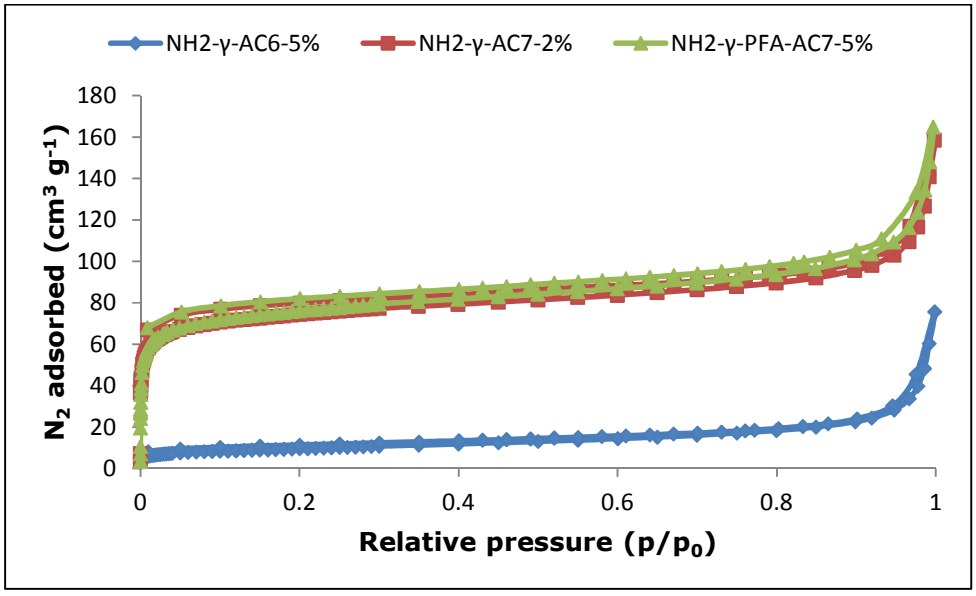

Figure 6.24. Adsorption/desorption profile for amine modified γ-type carbons measured at 196 °C.

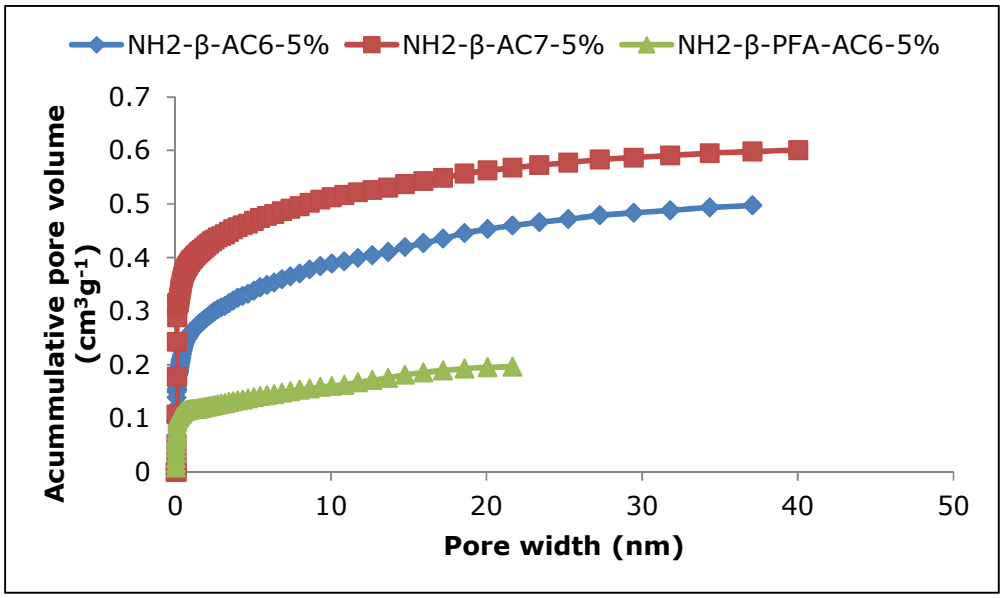

Figure 6.25. Pore distribution profile for amine modified β–type carbons measured at -196 °C.

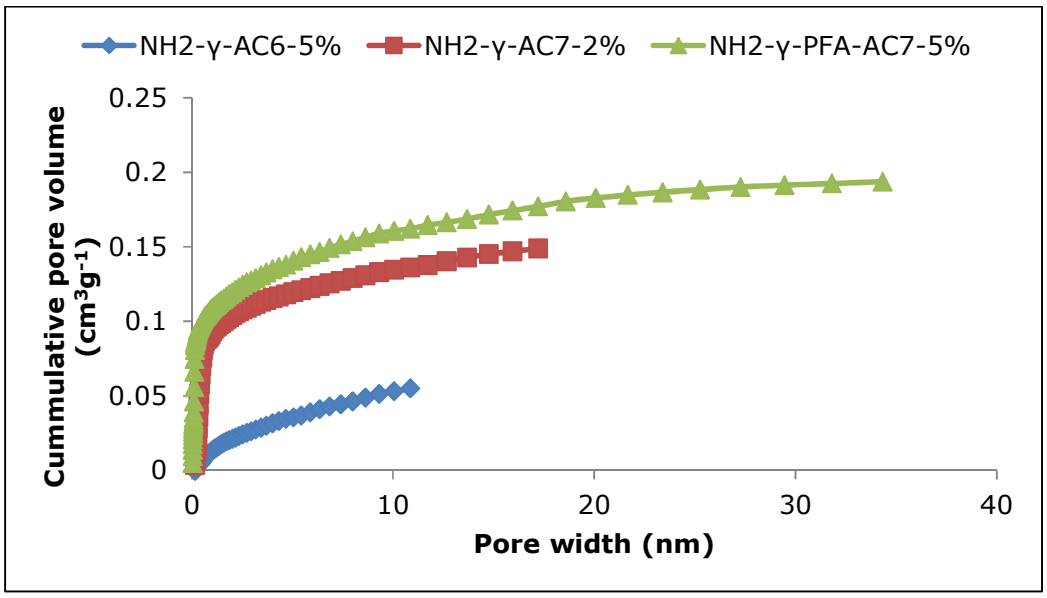

Figure 6.26. Pore distribution profile for amine modified γ-type carbons measured at -196 °C.

Success of surface modification of the studied adsorbent was observed in the increased nitrogen loading (Table 6.10) recorded after ultimate analysis as compared to the unmodified carbons (Table 5.4). At least approximately 300% increase in nitrogen loading have been recorded, with maximum loading (5.39 ≡ 500% increase) observed for the NH_2-γ-AC7-2% adsorbent. The modification of these materials has been observed to adversely affect the surface areas of the materials. The surface area of the adsorbents were reduced after modification when compared to the unmodified carbons. 26-80% and 76-95% reduction in surface area were recorded for the β–type and γ–type templated carbon respectively when compared to their unmodified counterpart (Table 5.3). The micropore volumes and the total pore volumes were also reduced after modification. Total pore and micropore volumes reduced by at least 19 and 3% respectively for the β–type modified carbon, while they reduce by at least 66% for the γ–type modified carbon compared to their unmodified counterpart reported in Table 5.3. Similar effect has been reported by Chen et al., (2003) and Garcia et al., (1998) when they modified active carbons using nitric acid and oxygen plasma respectively.

Thermal stability curves (Figure 6.27) derived from TG shows NH_2-β -AC7-5% as more thermally stable with a marginal mass loss of 26 wt.%. NH_2-β-AC6-5% and NH_2-γ-PFA-AC7-5% show similar mass losses, around 30 wt.%. NH_2-β-PFA-AC6-5% starts decomposing at a lower temperature (around 200 ^oC) and suggests the decomposition of weakly bound amines on the surfaces of the adsorbent (Plaza et al., 2010).

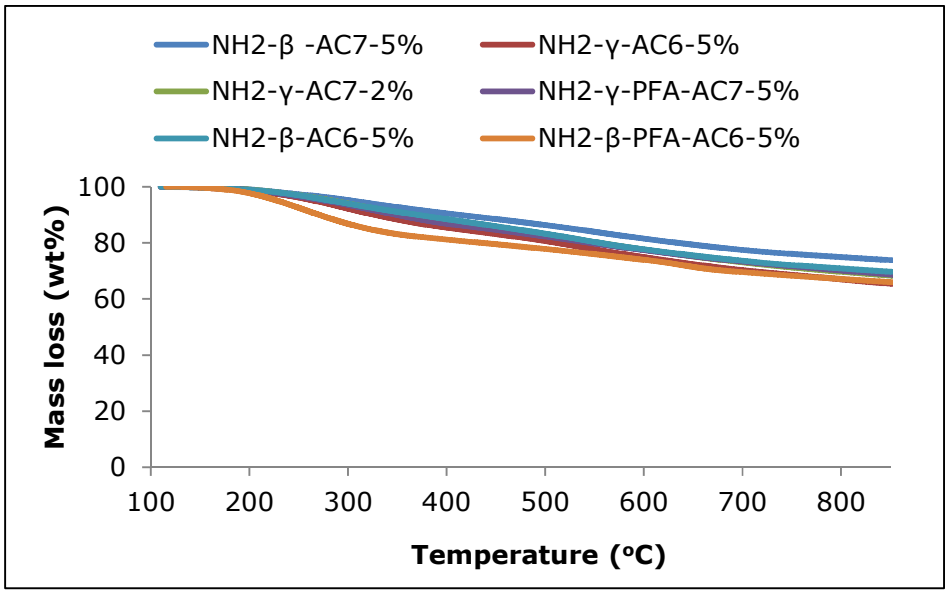

Figure 6.27. Thermal stability profile of amine modified adsorbents; heating rate 10 °C min^{-1} in nitrogen; 50 °C min^{-1} in air.

Table 6.9. Textural properties of amine modified carbons.

Amine modified carbons	S_{BET} ($m^2\ g^{-1}$)	E_0 ($kJmol^{-1}$)	W_o ($cm^3\ g^{-1}$)	V_p ($cm^3 g^{-1}$)	V_{meso} ($cm^3\ g^{-1}$)	$V_{meso}/\ W_o$	$W_o\ /V_p$	ρ_{He} ($g\ cm^{-3}$)
NH_2-β-AC6-5%	630	27.62	0.24	0.50	0.16	0.67	0.48	1.76
NH_2-β-AC7-5%	1021	24.61	0.39	0.60	0.68	1.74	0.65	1.84
NH_2-β-PFA-AC6-5%	374	20.90	0.14	0.20	0.15	1.07	0.70	1.71
NH_2-γ-AC7-2%	287	18.66	0.11	0.22	0.08	0.73	0.50	1.79
NH_2-γ-PFA-AC7-5%	290	16.94	0.11	0.19	0.10	0.91	0.58	1.82
NH_2-γ-AC6-5%	34	18.28	0.01	0.11	0.06	6.00	0.09	1.93

S_{BET}: surface area, E_0: characteristic energy, W_o: micropore volume, V_P: total pore volume, V_{meso}: mesopore volume, ρ_{He}: helium density

Table 6.10. Ultimate analysis of amine modified adsorbents (dry ash free).

Amine modified carbons	C (wt.%)	H (wt.%)	N (wt.%)	O (wt.%)	N/C
NH_2-β-AC6-5%	87.35	1.15	2.98	8.51	0.04
NH_2-β -AC7-5%	91.63	0.69	3.86	3.82	0.04
NH_2-β-PFA-AC6-5%	91.18	1.75	3.03	4.03	0.04
NH_2-γ-AC7-2%	89.67	0.36	5.39	4.58	0.07
NH_2-γ-PFA-AC7-5%	90.27	0.09	5.31	4.34	0.07
NH_2-γ-AC6-5%	86.95	1.49	2.89	8.67	0.04

6.4.2 CO_2 uptake of amine modified templated carbons at ambient pressure

The amine modified templated carbons showed reduced CO_2 uptake at 25 ^oC compared to the unmodified samples (see Section 5.4 in Chapter 5). This reduction may be due to CO_2 transport restrictions by narrow pores of the materials, resulting from amine loading (Plaza et al., 2007). Although, the ratio of 15% CO_2 to 100% CO_2 (which simulates the binary mixture of gas in exhaust of power plant) on the amine modified materials (Table 6.11) was observed to be higher than those reported for the unmodified carbons (Table 5.5). Higher ratio may be attributed to the presence of narrower porosity and nitrogen heteroatoms on the carbon matrix, which may have increased the delocalised π electrons in the system of the carbons (Plaza et al., 2011). Standard deviations of recorded CO_2 uptake data for the modified adsorbents indicate reproducibility of adsorption results (Table 6.11).

The adsorbents density played an important role in the amount of CO_2 adsorbed (Table 6.9 and Figure 6.28). This test was carried out to evaluate the performance of these adsorbents in a binary mixture containing nitrogen and CO_2 in a ratio that simulates that of a flue gas stream. The CO_2 uptake recorded was lower for 15% CO_2 stream than that obtained for 100% CO_2 stream. However, about 21-71% more CO_2 uptake was recorded in comparison to unmodified adsorbents at similar conditions (reported in Section 5.4 on Chapter 5). This suggests the applicability of these modified adsorbents in post-combustion carbon capture where CO_2 partial pressures are low. This also suggests that the amine modification enhanced the CO_2 selectivity of the materials (Pevida et al., 2008; Plaza et al., 2007; Plaza et al., 2010).

Table 6.11. CO_2 uptake of amine modified adsorbents at 25 °C.

Amine modified carbons	15% CO_2 uptake (mmol g^{-1})	100% CO_2 uptake (mmol g^{-1})	Ratio (%)	CO_2 uptake (mmol cm^{-3})	100% CO_2 uptake of unmodified carbons (mmol g^{-1})
NH_2-β-AC6-5%	0.82±0.02	1.76±0.06	47±1.5	3.10	2.35
NH_2-β-AC7-5%	0.62±0.12	2.93±0.09	21±7.8	5.39	1.87
NH_2-β-PFA-AC6-5%	0.58±0.04	0.93±0.04	62±4.5	1.59	2.12
NH_2-γ-AC7-2%	0.88±0.06	1.72±0.06	51±2.6	3.08	1.78
NH_2-γ-PFA-AC7-5%	0.58±0.04	1.73±0.01	46±4.1	3.15	1.82
NH_2-γ-AC6-5%	0.66±0.03	0.92±0.05	72±0.9	1.78	1.08

It is presumed that highly microporous materials may record higher densities. This is so because predominantly mesoporous adsorbents constitute larger voids in the material which consequently results to lower material density. 5.39 mmol cm^{-3} CO_2 uptake capacities were recorded for NH_2-β-AC7-5% when material density was considered. This high density effect was observed in all the modified carbons (Figure 6.28). No CO_2 uptake trends were observed for the modified adsorbents with respect to micropore volume (Figure 6.29), surface area (Figure 6.30), and total pore volume (Figure 6.31) as seen by the R^2 values, suggesting the textural properties did not have any impact these modified adsorbents at ambient pressure.

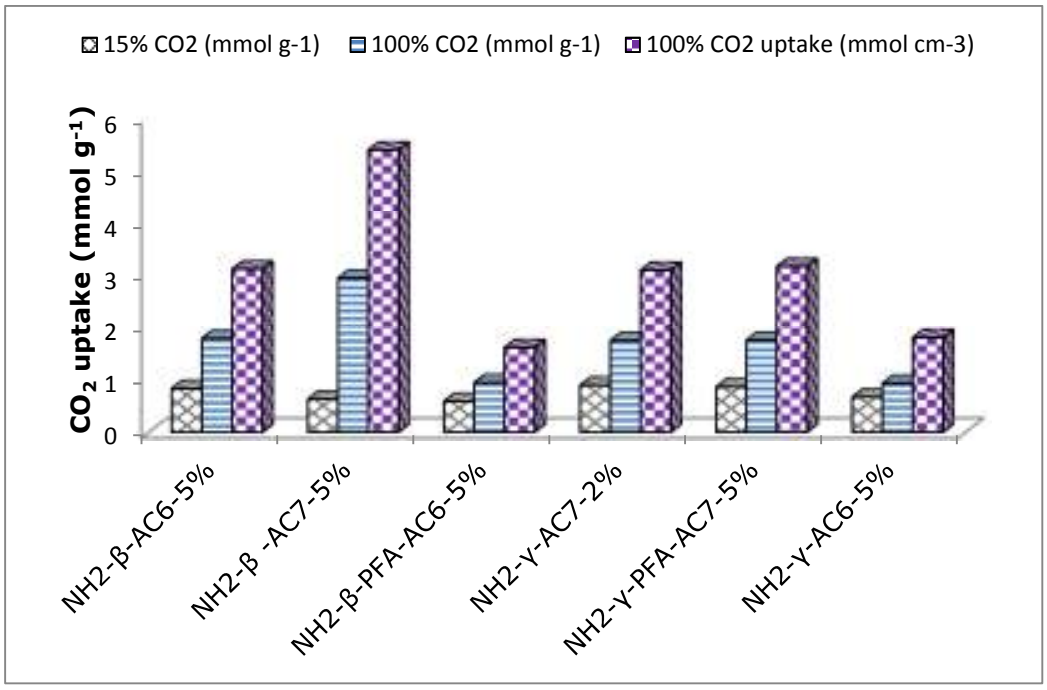

Figure 6.28. CO_2 uptake of amine modified templated carbons measured at ambient pressure conditions.

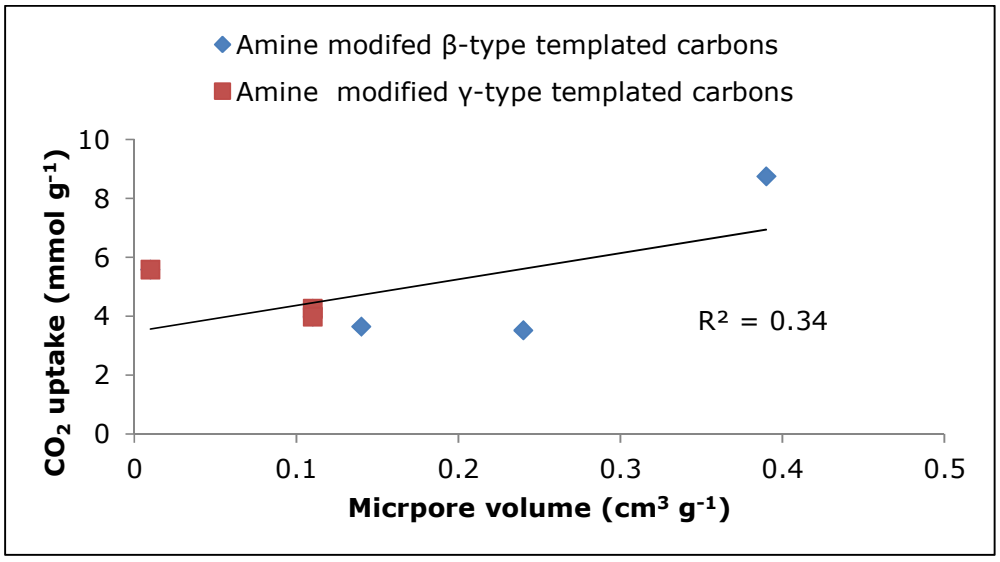

Figure 6.29. CO_2 uptake trend for amine modified templated carbons with respect to micropore volume measured at ambient pressure conditions.

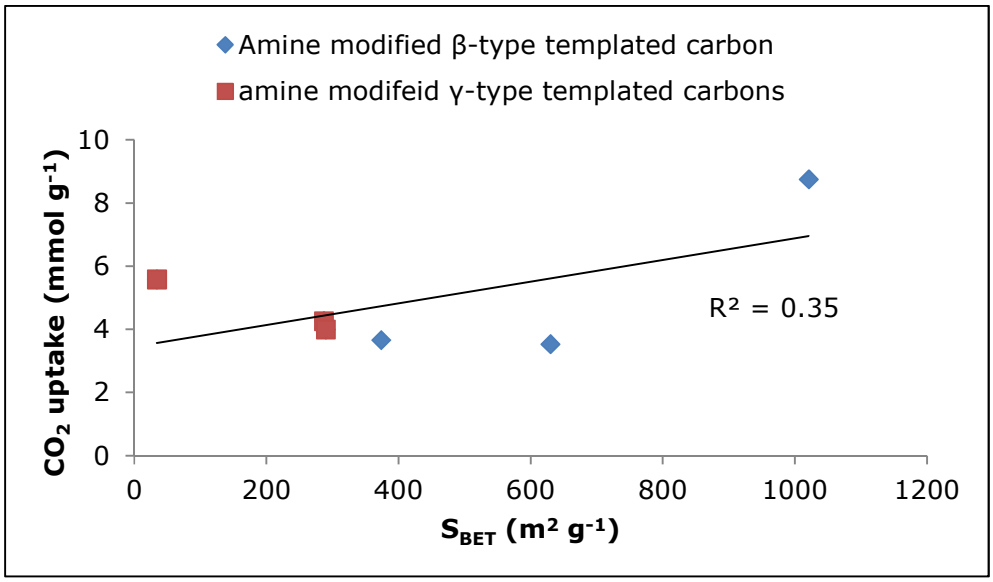

Figure 6.30. CO_2 uptake trend for amine modified templated carbons with respect to surface area measured at ambient pressure conditions.

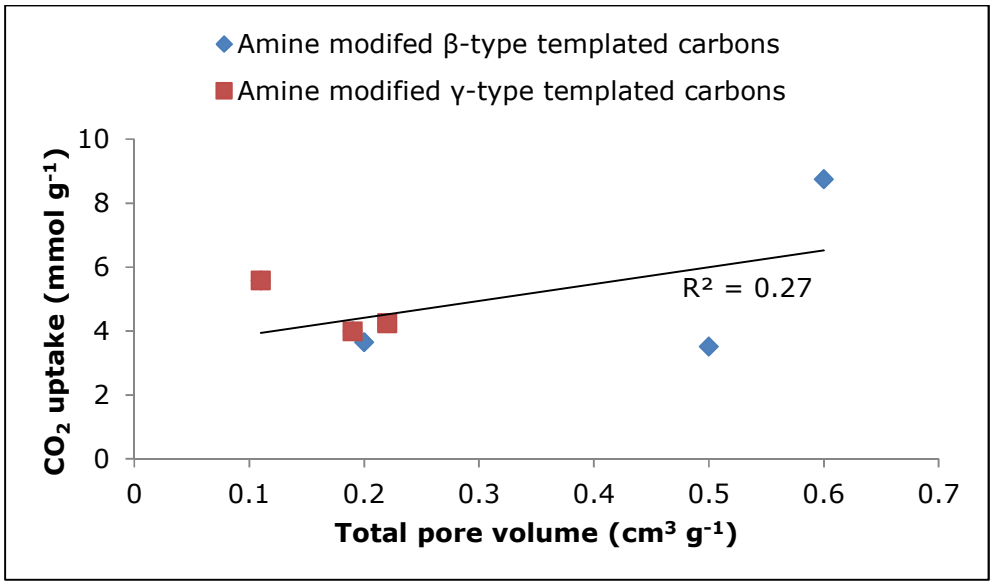

Figure 6.31. CO_2 uptake trend for amine modified templated carbons with respect to total pore volume measured at ambient pressure conditions.

The TPD profiles (Figure 6.32 and Figure 6.33) show the behaviour of the amine modified materials (saturated with CO_2) at higher temperatures compared to the unmodified materials. It could be observed that while the unmodified adsorbents lost approximately 90% of their captured CO_2 at about 40 ^oC, the modified adsorbents retained substantial amount of the adsorbate at this temperature. The NH_2-β-AC7-5%, NH_2-β-AC6-5% and NH_2-β-PFA-AC6-5% retained 18, 30, and 48% of CO_2 respectively while NH_2-γ-AC7-2%, NH_2-γ-AC6-5% and NH_2-γ-PFA-AC7-5% retained 36, 49, and 87% of adsorbed CO_2 respectively. However, the difference in capture capacities of the modified adsorbents decreased as the temperature increased, with NH_2-γ-PFA-AC7-5% and NH_2-β-PFA-AC6-5% losing their abiliity to adsorb CO_2 at 150 and 115 ^oC respectively.

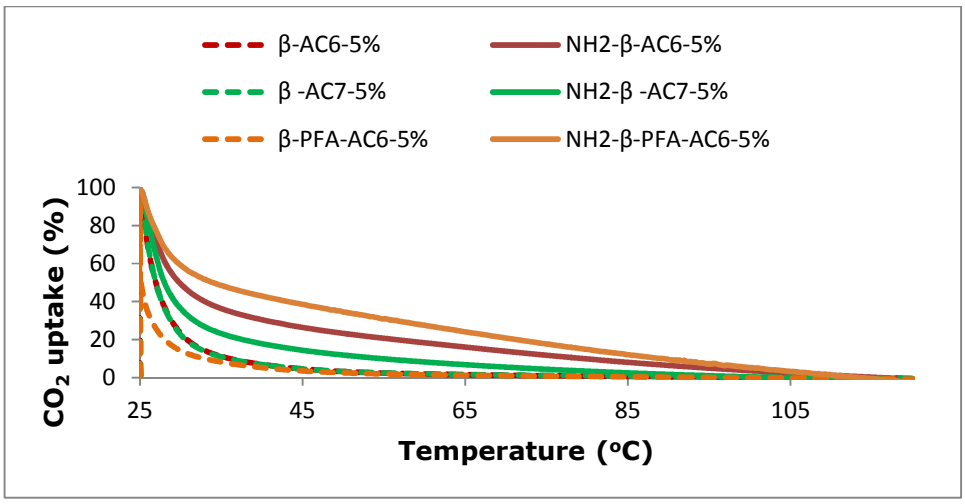

Figure 6.32. TPD profile for amine modified β-type adsorbents during heating in 98 mL min^{-1} of N_2 flow at a heating rate of 5 ^oC min^{-1} up to 105 ^oC.

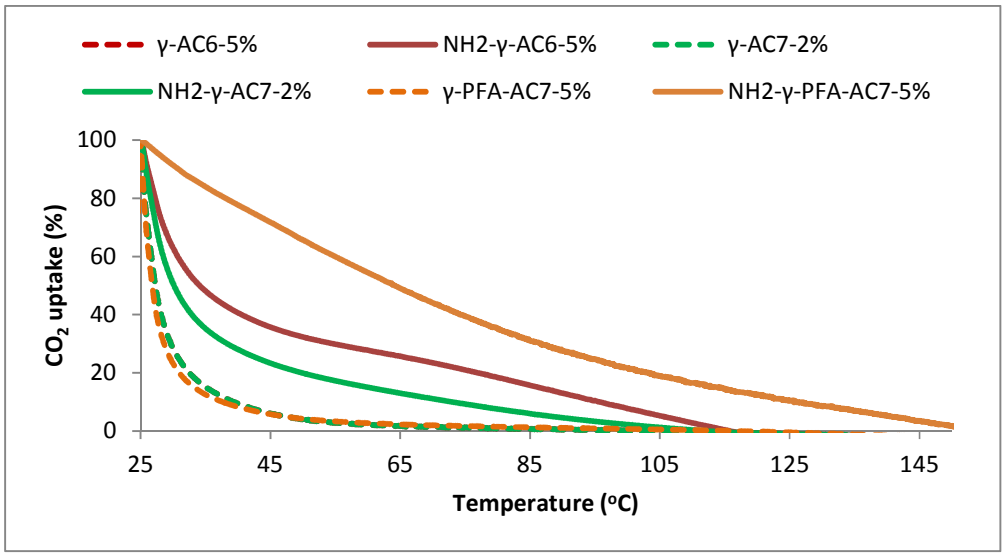

Figure 6.33. TPD profile for amine modified γ-type adsorbents during heating in 98 mL min^{-1} of N_2 flow at a heating rate of 5 °C min^{-1} up to 105 °C.

Although the maximum CO_2 uptake recorded for the amine modified materials is lower than those of the parent adsorbent (see Table 5.5). Increased CO_2 ratio (Table 6.11), CO_2 affinity (Figure 6.32 and Figure 6.33), and better thermal stability (Figure 6.27) has been achieved on the amine modified adsorbents. Higher selectivity observed for this amine modified adsorbents at low pressure may be attributed to their narrower porosity and favourable surface chemistry (Plaza et al., 2011) compared to their unmodified counterpart. Although a study on the total amount of basic sites on these materials was not undertaken, it has been reported by Zhang et al., (2011) that the amount of CO_2 adsorbed by a modified sample corresponds to the amount of basic sites on the samples. The highest uptake capacities reported here for modified adsorbents are higher than values reported for nitrogen functionalised carbons; 99 mg g^{-1} Ξ 2.25 mmol g^{-1} (Zhao et al., 2010), 2.18

mmol g^{-1} (Pevida, 2008b), and 59 mg g^{-1} Ξ 1.34 mmol g^{-1} reported by Chen et al., (2007) when they worked on CO_2 capture on nitrogen-rich carbons using a BEL adsorption instrument at 25 ^oC and atmospheric pressure. Also, the capture capacity reported in this study is 16 times higher than that reported by Gray et al., (2004) (174.5 μmol g^{-1} Ξ 0.175 mmol g^{-1}) when they studied CO_2 capture of amine-enriched fly ash carbon sorbents at 25 ^oC using a combination of diffuse reflectance infrared transform spectroscopy (DRIFTS) temperature programmed desorption and mass spectroscopy. The maximum uptake capacity reported in this work is also higher than the 65.7 mg g^{-1} Ξ 1.49 mmol g^{-1} reported by Maroto-Valer et al., (2005) for amine modified anthracite.

6.4.3 Adsorption kinetic studies

The kinetics of CO_2 adsorption on amine modified templated carbon (NH_2-γ-AC6-5%) was studied by isothermal adsorption at different temperatures (25, 40, 60, and 80 °C), using the pseudo first order and pseudo second order models. The isothermal graphs are presented in Figure 6.34 to Figure 6.37, and the estimated parameter values and corresponding correlation coefficients are presented in Table 6.12. The selected models have been thought to be associated with the surface-reaction kinetic step as controlling the sorption rate, which is more likely to be true for CO_2 adsorption on amine modified materials. The observed rate of chemical reactions is, generally speaking, the rate of the slowest or "rate determining" step. In diffusion controlled reactions the formation of products from the activated complex (product species) is much faster than the diffusion of reactants and thus the rate is governed by collision frequency (Atkins, 1998). Unlike the adsorption kinetic fit obtained

for the unmodified templated carbon (γ-AC6-5%) (See Figure 5.13 to Figure 5.16 in Section 5.5), where pseudo first order was observed to provide the best kinetic fit, the pseudo second order model have been found to provide the best fit to isothermal CO_2 adsorption data at 25, 40 and 60 ^oC for the NH_2-γ-AC6-5% adsorbent. At 80 ^oC, the pseudo first order model fits better for this material. Diffusion-controlled reactions have been observed to take place in the modified carbons. In second order reaction kinetics, the rate of CO_2 diffusion into the carbon surface is slower than the chemical reaction on the carbon surface. This diffusion limitation may be explained by the presence of modifying species (amines) at the active sites in the carbon.

The pseudo second order model have been reported to be useful in obtaining the best adsorption kinetic fit for commercial grade activated carbon during the removal of Congo red from aqueous solution (Mall et al., 2005). The high value of the adsorption kinetic constants indicates that the adsorbed CO_2 remains stable on the adsorbent (Ozkaya, 2006). This finding is further supported by the R^2 values and error function obtained for the Pseudo second order model. It was observed that the R^2 for the pseudo second order model ranges from 0.9972-0.9987, with corresponding error function in the range of 1-4.8 (Table 6.12). Since the correlation coefficient is greater than 0.99, it indicates the applicability of this kinetic model and the second order nature of the adsorption process of CO_2 on the modified templated carbons (Hameed et al., 2007). The activation energy for this amine modified adsorbent was observed to be -9.0894 kJ $mole^{-1}$, this is less than that obtained for the unmodified sample (see Table 5.8).

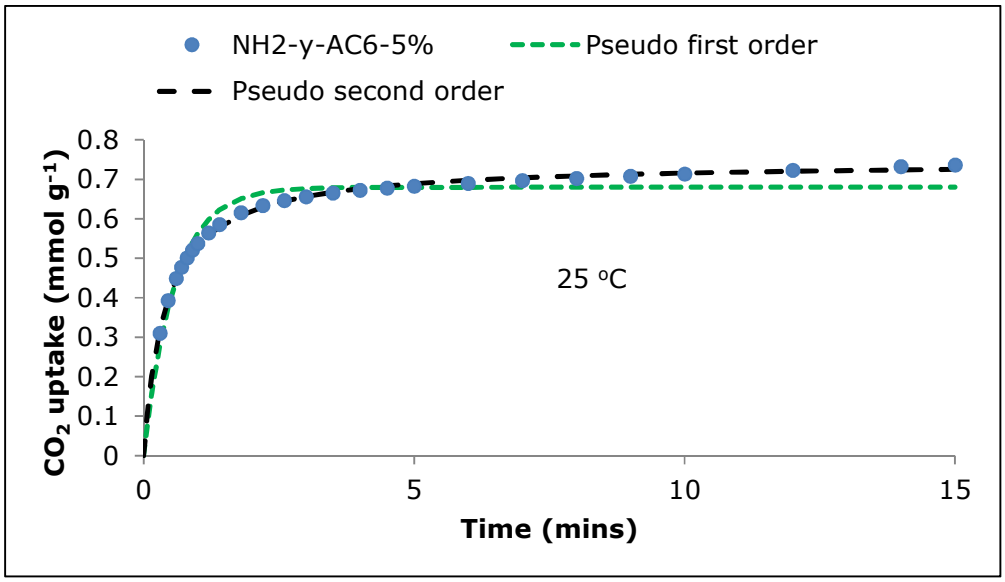

Figure 6.34. CO_2 adsorption on NH_2-γ-AC6-5% at 25 °C. The experimental data was fitted by the pseudo-first order and pseudo-second order models.

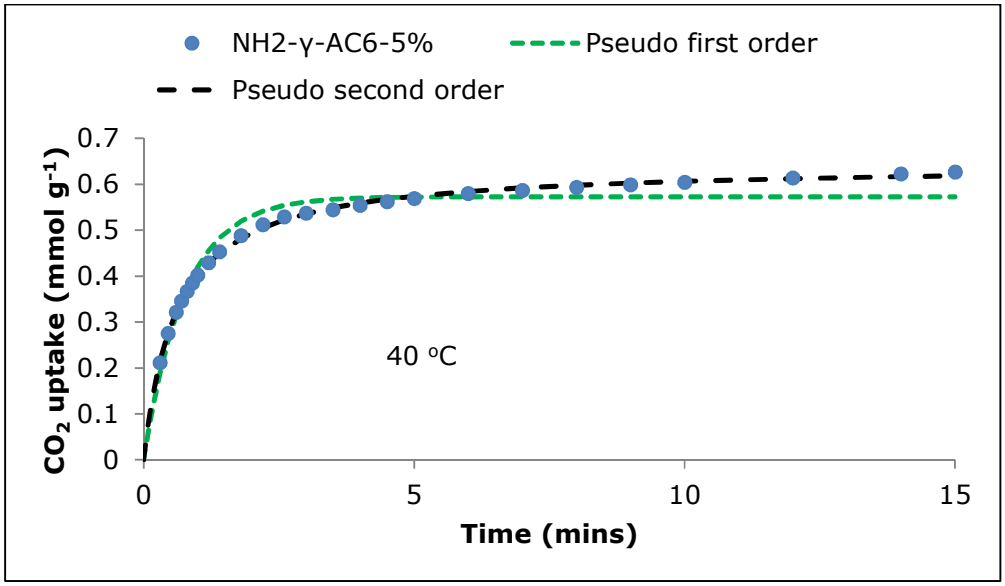

Figure 6.35. CO_2 adsorption on NH_2-γ-AC6-5% at 40 °C. The experimental data was fitted by the pseudo-first order and pseudo-second order models.

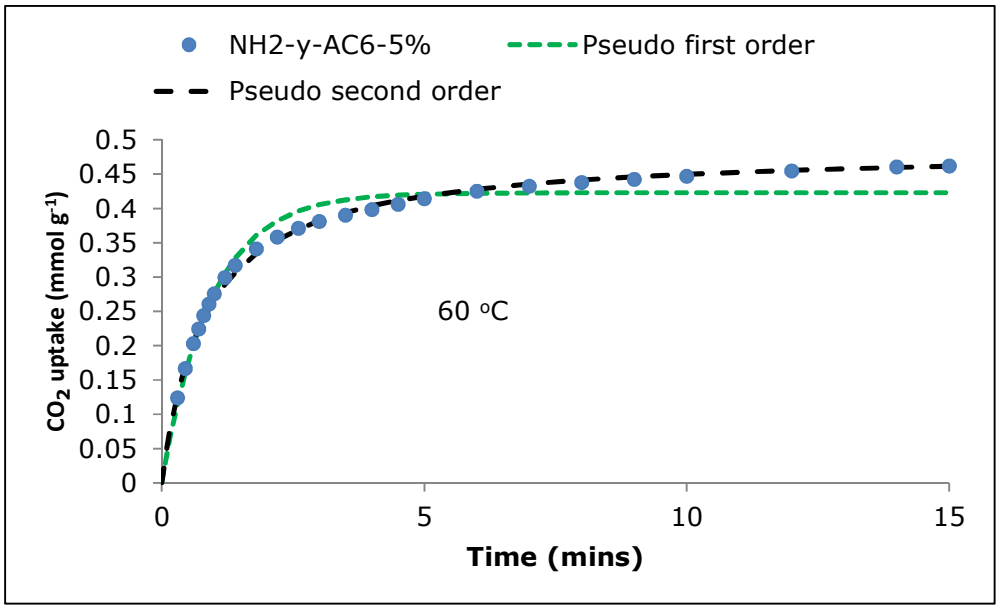

Figure 6.36. CO_2 adsorption on NH_2-γ-AC6-5% at 60 °C. The experimental data was fitted by the pseudo-first order and pseudo-second order models.

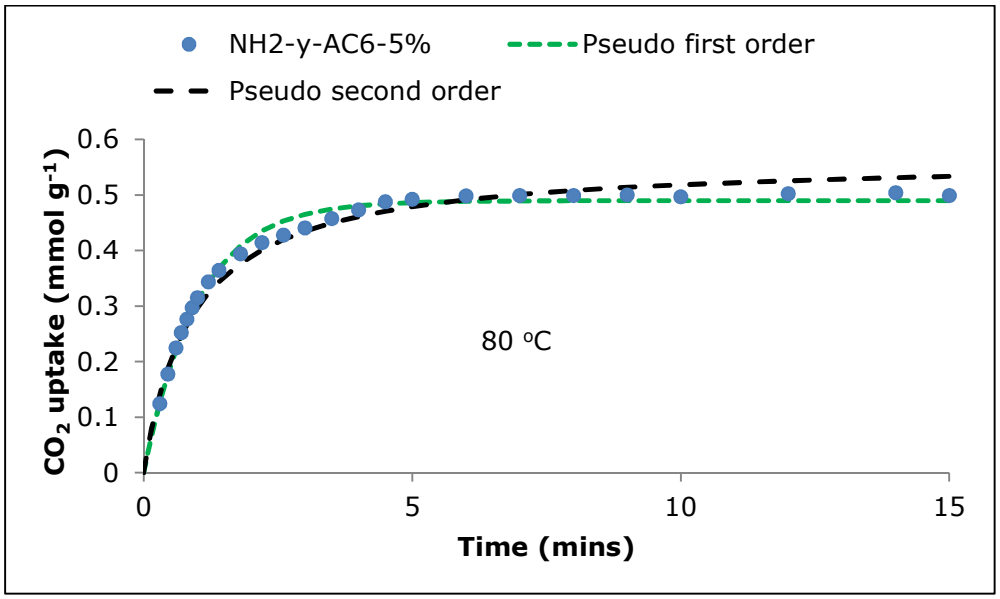

Figure 6.37. CO_2 adsorption on NH_2-γ-AC6-5% at 80 °C. The experimental data was fitted by the pseudo-first order and pseudo-second order models.

Table 6.12. Kinetic model parameters for the CO_2 adsorption on templated carbon (NH_2-γ-AC6-5%)) at different temperatures.

T		25 °C	40 °C	60 °C	80 °C
$q_{e,exp}$		0.92	0.67	0.48	0.32
Pseudo-first order	q_e	0.74	0.63	0.46	0.50
	k_1	1.763	1.323	1.065	0.997
	R^2	0.9385	0.9511	0.9631	0.9895
	Err	4.7	5.8	4.8	2.8
Pseudo-second order	q_e	0.74	0.63	0.46	0.50
	k_2	3.343	2.586	2.438	1.958
	R^2	0.9974	0.9987	0.9972	0.9800
	Err	1.0	0.8	2.0	4.8

(*T*: °C; $q_{e,exp}$: mmol g^{-1}; q_e: mmol g^{-1}; k_1: s^{-1}; k_2: mmol g^{-1} s^{-1}; k_a: s^{-1}; *a*: mmol g^{-1} s^{-1}, *a*: g $mmol^{-1}$)

6.4.4 High pressure CO_2 uptake measurements on amine modified templated carbons

The adsorption isotherms of the modified carbons showed no alteration after surface properties modification, this is in agreement with Guillot and Steockli (2003) when they proposed the use of reference isotherm for high pressure CO_2 adsorption in carbons at 0 °C. A type I isotherm was obtained for the amine modified templated carbons at ambient temperature and high pressure measurements (Figure 6.38). However, the shape of the isotherm obtained at high pressure was greatly influenced by surface modification compared to that obtained at low pressure CO_2 measurements (see Figure 5.20).

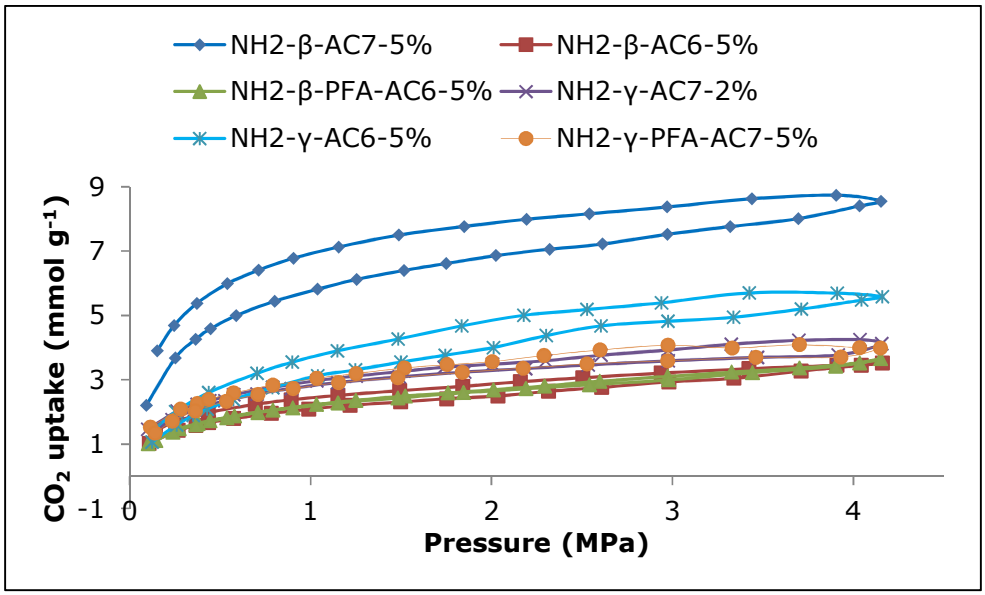

Figure 6.38. adsorption isotherm of amine modified templated carbons measured ambient temperature and 4.1 MPa.

Apart from the NH_2-β-PFA-AC6-5% and NH_2-β-AC6-5%, the remaining amine modified templated carbons showed a gap between the adsorption and desorption curves. This suggests that the NH_2-β-AC7-5%, NH_2-γ-PFA-AC7-5%, NH_2-γ-AC7-2% and NH_2-γ-AC6-5% may have experienced pore swelling during the adsorption stage. Same observation has been reported for the oxidized phenolic resin adsorbents in Section 6.3.3. The NH_2-β-AC7-5% sample showed the highest CO_2 uptake at 4.1 MPa, followed by the NH_2-γ-AC6-5% adsorbent. These high uptake measurements recorded for these two materials may be linked to the swelling of the pores due to high pressure. The CO_2 uptake capacities for the unmodified templated carbons reported for these carbons at ambient pressure were seen to be higher than those reported for them at higher pressures, except for the NH_2-β-AC7-5%. At least 65% uptake difference was observed between the adsorbents at ambient and high pressure

conditions. The great difference in uptake levels between the unmodified templated carbons (see Figure 5.20 in Chapter 5) and their modified counterparts reported in this section (Figure 6.38) may suggest the presence of partially or totally blocked micropores resulting from the modifying chemicals.

Just as reported for the amine modified commercial templated carbons, and the oxidized phenolic resin carbons, no CO_2 adsorption trend was observed with respect to micropore volume (Figure 6.39), surface area (Figure 6.40) and total pore volume (Figure 6.41) for the amine modified templated carbons at high pressure (as seen in the R^2 values for the respective plots). Overall, this suggests that CO_2 uptake at high pressure may not depend totally on micropore volume, surface area, or total pore volume, but on the material type.

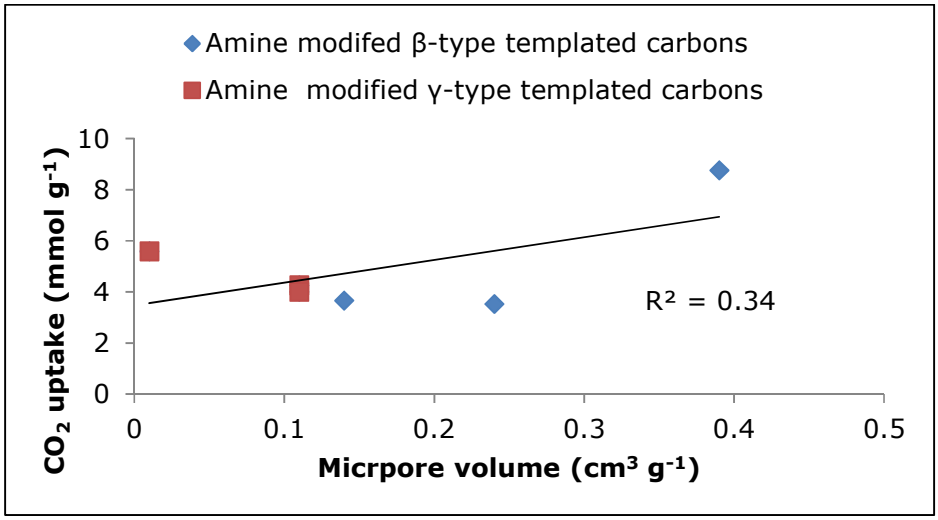

Figure 6.39. Correlation of equilibrium CO_2 uptakes at 4.1MPa with micropore volume for selected amine modified templated carbons.

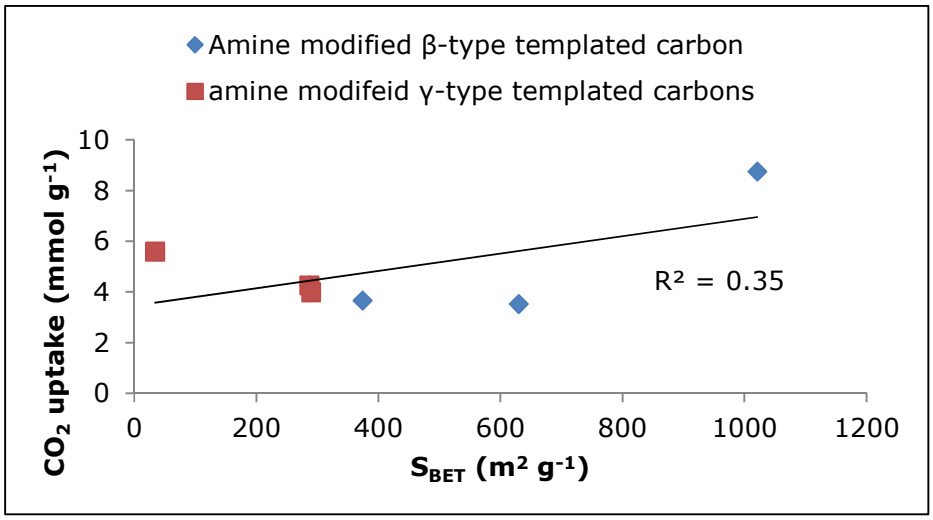

Figure 6.40. Correlation of equilibrium CO_2 uptakes at 4.1MPa with surface area for selected amine modified templated carbons.

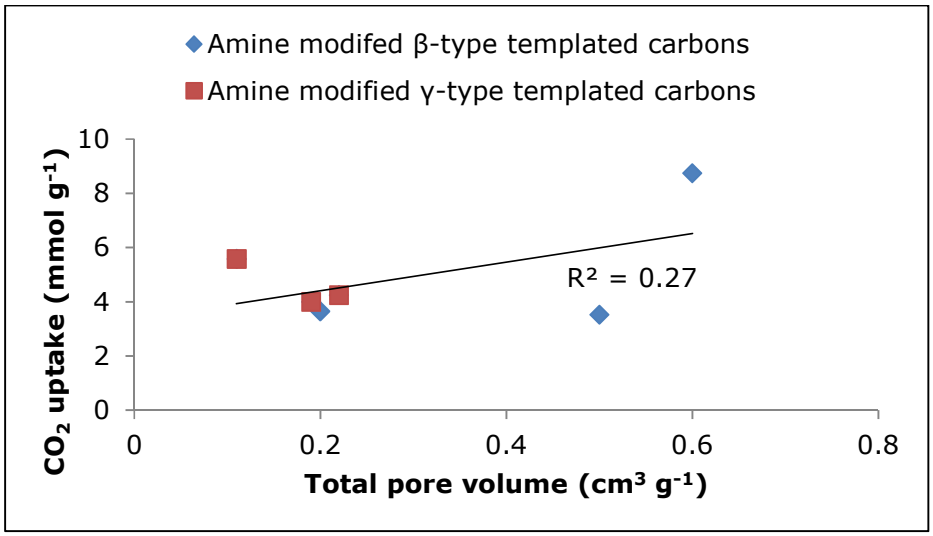

Figure 6.41. Correlation of equilibrium CO_2 uptakes at 4.1MPa with total pore volume for selected amine modified carbons.

6.5 Summary

In this chapter, the influence of surface modification on CO_2 uptake performance of three different modified adsorbents has been discussed. The influence of the textural properties of the adsorbents was also related to their CO_2 uptake capacities at ambient and high pressure conditions.

For the amine modified commercial activated carbon, the total pore volume was observed not to positively influence the CO_2 uptake capacities at both ambient and high pressure conditions. Whereas, the micropores and surface area of the adsorbents tend to positively influence the CO_2 uptake capacities at both ambient and high pressure conditions. For the oxidized phenolic resin activated carbons, their textural properties did not positively influence the CO_2 adsorption performance at ambient and high pressure conditions. Hence, no adsorption trend was recorded for the adsorbent with respect to the micropore volume, surface area and total pore volume. The textural properties did not positively influence the CO_2 uptake capacities of the amine modified templated carbon at both ambient and high pressure conditions. A change in kinetic characteristics was observed for the modified carbon. Diffusion-controlled reaction was observed to take place on the modified carbons in comparison to surface-controlled reaction observed for the unmodified carbons.

Generally, increased nitrogen loading and higher thermal stability, was observed on the modified materials compared to the unmodified ones. Also, increase in CO_2 uptake capacities was observed for all the modified adsorbents at high pressures than at ambient pressure conditions. While the unmodified adsorbents lost approximately 90% of their captured CO_2 at about 40 ^{o}C, the

modified adsorbents retained substantial amount of the adsorbate at similar temperature. Increased CO_2 adsorption ratio between 15% and 100% CO_2 stream, adsorption rate, CO_2 affinity, and better thermal stability were achieved on the amine modified adsorbents. The higher selectivity of these modified adsorbents at low pressure has been attributed to their narrower porosity and favourable surface chemistry.

The amine modified carbons showed lower CO_2 uptake capacities than their unmodified counterparts at ambient and higher pressures. This reduction has been attributed to the partial or total micropore blockage. This finding is in agreement with Plaza et al., (2011) when they evaluated ammonia modified activated biomass based carbon as adsorbents for CO_2. They recorded a higher CO_2 uptake for the activated samples than the aminated samples at pressures above 30 kPa. This was attributed to the presence of wider microporosity in the activated samples which was absent in the aminated samples.

General discussion

The CO_2 uptake of the respective carbons has been shown to depend greatly on the porosity. The CO_2 uptake capacities of carbons have been found to depend on total surface area and micropore volume at ambient conditions. However, at high pressure, the total pore volume has been found to relate to the total CO_2 uptake. Also, the properties of the carbons produced depend highly on the carbon synthesis technique. The pore structure of carbons obtained from a template is governed by the properties of the inorganic matrix; size of the interlayer spacing, water content of the matrix, and the carbonisation temperature. It was observed that the acetylene loading, the carbonisation temperature, and furfuryl alcohol positively influenced the properties of the synthesized carbons. However, Results have shown that the addition of PFA results in greater pore development in carbons synthesized from predominantly microporous zeolite templates, whilst being of no benefit when used for the predominantly mesoporous carbon.

Although the CO_2 uptake capacities of modified carbons were reduced compared to their unmodified counterparts, other properties like thermal stability and affinity for CO_2 increased after modification. While the reduction in CO_2 uptake was attributed to blocked micropores in the carbons, increased thermal stability and CO_2 affinity was attributed to the presence of functional groups and increased electrostatic interactions on the carbon surface after modification. Adsorption kinetics followed pseudo first order rate expression for the unmodified carbons with sorption rate being highest after three minutes of CO_2 adsorption. The reaction mechanism has been attributed to

surface or sorption controlled adsorption since the rate of CO_2 uptake is faster. For the modified carbons, adsorption kinetics followed pseudo-second-order rate expression with initial sorption rate being highest after two minutes. The reaction mechanism was observed to be diffusion controlled as the rate of CO_2 uptake was reduced due to reduced pore accessibility. However, process optimisation is key to robust adsorbents with high CO_2 adsorption capabilities for CCS application.

In summary, at ambient pressures, the carbons can be arranged in the following order based on performance; commercial activated carbons < templated carbons < amine modified activated carbon < oxidized phenolic resin carbons < amine modified templated carbon < phenolic resin carbons. At high pressures up to 4.1 MPa and 25 ^{o}C, the adsorbents can be arranged in the following order based on performance; commercial activated carbon < amine modified commercial activated carbon < amine modified templated carbon < oxidized phenolic carbon < phenolic resin carbon < templated carbon. Results presented in this thesis are promising and applicable to pre-combustion carbon capture as they show increased or improved CO_2 uptake compared to previous published data.

Chapter Seven

7 Conclusions

7.1 Overview

This study has provided insight into the field of CO_2 adsorption on carbon materials at ambient and high pressure. In addition, this thesis has explored the variables controlling sorption capacities of carbons. Chapter 4 and 5 provide understanding on the sorption of CO_2 on commercial activated carbon and templated carbons respectively, whereas, chapter 6 provides the influence of surface modification on CO2 adsorptions.

7.2 Templated carbon synthesis

The synthesis of templated carbon from acetylene CVD has been extensively investigated. Zeolite template is promising technique for synthesizing high surface area carbon materials with a narrow micropore distribution. The templated carbon preparation has also been adapted to produce a uniform product, facilitated by the use of acetylene as CVD gas and the use of a quartz reactor tube. Close control of the preparation parameters has allowed the controlled formation of templated carbons with 13-62 % carbon yield, surface areas of up to 2400 $m^2\ g^{-1}$, and a variety of pore structures ranging from micro to macropore. Micropore and mesopore structures obtained were in the range of 0.1-1.0 $cm^3\ g^{-1}$ and 0.1-0.38 $cm^3\ g^{-1}$ respectively.

7.3 Caron surface modification

The modification on carbon surfaces was achieved using well defined methods as specified in Section 3.3. Although, structural analysis of the modified carbons was not carried out, the porosity characterisation indicated that the pore structures were affected after modification. Also, the effect of carbon surface modification was observed on the templated carbons when the CO_2 adsorption kinetics changed from a surface-reaction controlled regime before modification to diffusion-controlled sorption regime after modification. The CO_2 sorption capacities were reduced after modification. However, the thermal stability, and CO_2 affinity of the carbon surface were improved.

7.4 Carbon vapour deposition rig development

The chemical vapour deposition rig has been developed for the carbonising zeolites at 600 and 700 ^{o}C. The apparatus has been rigorously calibrated and tested using several carbonisation runs. This evaluation was essential to prove this apparatus as a reliable method of CVD carbonisation. In order to achieve an accurate and repeatable result, an iterative process was used to determine the correct proportional integral derivative (PID) for the furnace control system. The apparatus has been shown to be a versatile apparatus, operating at ambient pressure and temperature reaching 1000 ^{o}C.

7.5 Ambient pressure CO_2 adsorption measurements

The carbons all displayed similar CO_2 sorption properties with uptakes ranging from 0.5 to 3.3 mmol g^{-1} at ambient pressure, showing a strong correlation with increasing micropore volume and surface area. This was supported by the observation that the majority of the CO_2 sorption was instantaneous.

7.6 High pressure CO_2 adsorption measurements

The carbons all displayed similar CO_2 sorption properties with uptakes ranging from 6.9 to 21.3 mmol g^{-1} at 25 ^{o}C and 4.1 MPa of pressure, and 10.3-21.1 mmol g^{-1} at 40 ^{o}C and 4.1 MPa, showing a strong correlation with increasing total pore volume. This was also supported by the observation that the CO_2 sorption was instantaneous. Summary of the maximum CO_2 uptake capacities of studied carbon is presented in Table 7.1.

Table 7.1. Summary of maximum CO_2 uptake of studied adsorbents at ambient and high pressure conditions.

Adsorbent	Ambient conditions CO_2 uptake ($mmolg^{-1}$)	High pressure conditions CO_2 uptake ($mmolg^{-1}$)	
	25 °C	25 °C	40 °C
Commercial activated carbon	2.4	6.6	-
Phenolic resin based carbon	3.3	12.2	-
Zeolite templated carbon	2.4	21.3	21.1
Oxidized phenolic resin carbon	2.9	10.6	10.3
Amine modified commercial activated carbon	2.7	6.5	-
Amine modified templated carbon	2.9	8.7	-

Chapter Eight

8 Further work

There are several areas that are worthy of additional research in this project. In addition to future work on carbon capture systems, several possible applications of templated carbons should be highlighted as avenues for future research.

8.1 CO_2 capture systems

- Further study on the kinetics of CO_2 adsorption on solid adsorbents.
- In addition to the fixed adsorption test conducted in this study, CO_2 adsorption in a fluidised bed should be undertaken if scale up is to be considered.

8.2 Templated carbon applications

- Production of templated carbon for application in methane separation.
- Activation and enhancement of templated carbon for application in hydrogen storage.
- Study on oxidation of templated carbons for application on CO_2 in gasification.
- Study on application of templated carbon for post combustion carbon capture.
- Study on application of templated carbons on hydrogen storage and separation of CO_2 and methane.

8.3 Recommendations

- Further study on the material's surface property should be undertaken to determine the total amount of basic sites on the surface of modified materials using Fourier-transform infrared (FTIR) spectroscopy, and X-ray Spectroscopy (XPS) to show the changes occurring in nitrogen species present.
- Obtaining CO_2 isotherm of carbons would be encouraged as this may provide further explanation of the pore structures.
- Adsorption kinetic models for high pressure CO_2 uptake should be undertaken as this gives better understanding of process design.
- Multi-cycle test on synthesized and modified materials should be encouraged to prove robustness, recyclability and reversibility of adsorbents.
- Study on the different ways to modify carbons for high pressure application should be undertaken.
- Study on structural effects of carbons and templates on CO_2 uptake should be undertaken.

9 References

Alcaniz-Monge, J. Carzorla-Amoros D. and Linares-Solano (1995). High Pressure CO_2 Adsorption on Activated Carbon Fiber. Alicante: University of Alicante, 331-334.

Alvarez, A. B. Fuertes, S. (2004). Template Synthesis of Mesoporous Carbons with Tailorable Pore Size and Porosity. *Carbon*, *42*(2), 433–436.

An, B. Feng, S. and Su, H. (2009). CO_2 Capture Capacities of Activated Carbon Fibre-Phenolic Resin Composites. *Carbon*, *47*(10), 2396–2405.

Anshul, Agarwal, Stephen, E. Zitney, and Lorenz, T. B. (2010). Superstructure-Based Optimal Synthesis of Pressure Swing Adsorption Cycles for Precombustion CO2 Capture. *Ind. Eng. Chem. Res*, *49*, 5066–5079.

APGTF, (2011). Cleaner Fossil Power Generation in the 21st Century: Maintainnig a Leading Role. *A Technology Strategy for Fossil Fuel Carbon Abatement Technology*. Rugby.

Arenillas, F. Parra, J. B. Ania, C. O. Pis, J. J. (2005). Surface Modification of Low Cost Carbons for their Application in the Environmental Protection. *Applied Surface Science*, *252*(3), 619–624.

Armandi, B. Bottero, I. Areán, C. Otero Garrone, E. Bonelli M. (2007). Synthesis and Characterization of Ordered Porous Carbons with Potential

Applications as Hydrogen Storage Media. *Microporous and Mesoporous Materials*, *103*(1-3), 150–157.

Armandi, M., Bonelli, B., Karaindrou, E. I., Areán, C. O., & Garrone, E. (2008). Post-synthesis Modifications of SBA-15 Carbon Replicas: Improving Hydrogen Storage by Increasing Microporous Volume. *Catalysis Today*, *138*(3-4), 244–248.

Atkins, Peter (1998). *Physical Chemistry 6th Edition*. New York: Freeman. Pp. 825-828.

Auerbach, S.M. Carrado, K.A. Dutta, P. K. (2003). *Handbook of Zeolite Science and Technology*. New York: Marcel Dekker, Inc.

Ávila-Orta V. J. Neira-Velázquez, M. G. Hernández-Hernández, E. Méndez-Padilla, M. G. Medellín-Rodríguez, F. J. Cruz-Delgado, C. A. (2009). Surface Modification of Carbon Nanotubes with Ethylene Glycol Plasma. *Carbon*, *47*(8), 1916–1921.

Aygün, A. Yenisoy-Karakaş S. Duman, I. (2003). Production of Granular Activated Carbon from Fruit Stones and Nutshells and Evaluation of their Physical, Chemical and Adsorption Properties. *Microporous and Mesoporous Materials*, *66*(2–3), 189–195.

Baerlocher Ch. Olson D.H., M. C. L. B. (2007). *Atlas of Zeolite Framework Types* (Sixth Revi.). Oxford: Elsevier.

Balooch, M., & Olander, D. R. (1975). Reactions of Modulated Molecular Beams with Pyrolytic Graphite. III. Hydrogen. *The Journal of Chemical Physics*, *63*(11), 4772.

Barata-Rodrigues, P.M. Moggridge, G.D. Mays, T. J. (2003). Structured Carbon Adsorbents from Clay, Zeolite, and Mesoporous Aluminisilicate Templates. *Carbon*, *4*, 2231–2246.

Barata-Rodrigues, P.M. Seaton, N.A. Moggridge, G.D. and Mays, T. J. (2002). Comparison of Porous Carbons Developed via Templating Technique. *Studies in Surface Science and Catalysis*, *144*, 139–146.

Barrer, R. M. (1978). *Zeolites and Clay Minerals as Sorbents and Molecular Sieves*. New York: Academic Press.

Barrett, Joyner, L.G., Halenda, P.P., E. P. (1951). Journal of American Chemical Society. *73*, 373–380.

Basile, A. and Julianelli, A. (2010). *Advanced Membrane Separation Processes and Technology for Carbon dioxide Capture in Power Plants* (pp. 203–220). Italy.

Bazargan, A., & McKay, G. (2012). A review – Synthesis of Carbon Nanotubes from Plastic Wastes. *Chemical Engineering Journal*, *195-196*, 377–391.

Bendosz, T. J. Jagiello, J. Schwarz, J. A. Putyera, K. (1994). Study of Carbon-smectite Composites and Carbons Obtained by In-situ Carbonisation of Polyfurfuryl Alcohol. *Carbon*, *4*, 659–664.

Biniak, S. Szymanski, G. Siedlewski, J. and Swiatkowski, A. (1997). The Characterisation of Activated Carbons with Oxygen and Nitrogen Surface Groups. *Carbon*, *35*(12), 1799–1810.

Blackman, J. M. Snape, C. Patrick, J. (2005). *High Pressure Hydrogen Storage on Carbon Materials for Mobile Applications*. *Department of Chemical and Environmental Engineering*. The University of Nottingham, Nottingham.

Blayden, H. E. & Patrick, J. W. (1967). Solid Complexes of Carbon and Sulphur—I. Sulphurised Polymer Carbons. *Carbon*, *5*(5), 533–544.

Bonjour, M. M. Francis, J. C. (2005). A TSA Process with Indirect Heating and Cooling: Parametric Analysis and Scaling-up to Practical Sizes. *Chemical Engineering and Processing*, *44*(9), 969–977.

Bourrelly, S. Llewellyn, P. L. Serre, C. Millange, F. Loiseau, T. & Férey, G. (2005). Different Adsorption Behaviours of Methane and Carbon Dioxide in the Isotypic Nanoporous Metal Terephthalates MIL-53 and MIL-47. *Journal of the American Chemical Society*, *127*(39), 13519–13521.

Brunauer, S. Deming, L.S. Deming, W.E. (1940). On a Theory of the Van der Waal Adsorption of Gases. *Journal of the American Chemical Society*, *62*, 1723–1732.

Budd, P. M. McKeown, N. B. & Fritsch, D. (2005). Free Volume and Intrinsic Microporosity in Polymers. *Journal of Materials Chemistry*, *15*(20), 1977.

Cameron, E. D. Sturgeon D. W. Rogerson J. W. and Senviratne. H. R. (2011). *Demonstration of an Oxyfuel Combustion System* Vol. 3, p. 47.

Caplan, A., Cornes, R and Silva, E. (2001). *Internationisation of Economic Policy Programme*. *Research Paper series* (p. 21). Leverhulme Centre.

Cazorla-Amorós, D. Ribes-Pérez, D. Román-Martínez, M. C. & Linares-Solano, A. (1996b). Selective Porosity Development by Calcium-catalyzed Carbon Gasification. *Carbon*, *34*(7), 869–878.

Cazorla-Amoros, D.J. Alcaniz-Monge and Linares-Solano A. (1996a). Characterization of Activated Carbon Fibers by CO2 Adsorption, *12*(11), 2820–2824.

Cejka, J., and Heyrovsky, H. J. (2005). *Zeolites and Ordered Mesoporous Materials: Progress and Prospects*. (H. J. Cejka, J., Ed.)*Stud. Surf. Sci. Catal* (Vol. 157). Amsterdam: Elsevier.

Cejka, J., Van Bekkum, H., Corma, A., Schuth, F. (2007a). *Studies in Surface Science and Catalysis: Introduction to Zeolite Science and Practice*. (F. Cejka, J., Van Bekkum, H., Corma, A., Schuth, Ed.) (3rd Revised). Oxford: Elsevier.

Chae, D. Y. Kim, J. Go, Y. Eddaoudi, M. Matzger, A. J. O'Keefe, M.; Yaghi, O. M. Siberio-Perez, H. K. (2004). No Title. *Nature*, *427*, 523.

Chen, Ranjeet K. Webley, Paul, Louis Singh (2007). Synthesis, Characterization and Hydrogen Storage Properties of Microporous Carbons

Templated by Cation Exchanged forms of Zeolite Y with Propylene and Butylene as Carbon Precursors. *Microporous and Mesoporous Materials*, *102*(1-3), 159–170.

Chen, C. Yang, J. Contreras, D.S. Clancy, Y.L. Lobkovsky, E.B. Yaghi, O.M. Dai, S. Angew, B. L. (2006). A Microporous Metal–Organic Framework for Gas-Chromatographic Separation of Alkanes. *Chem. Int. Ed.*, *45*, 1390.

Chen, J. Paul Wu, Shunnian Chong, Kai-Hau (2003). Surface Modification of a Granular Activated Carbon by Citric Acid for Enhancement of Copper Adsorption. *Carbon*, *41*(10), 1979–1986.

Cheu, K. Yun-Jong, Y. Soon-Haeng, C., K. Jong-Nam (1996). *Fundamentals of Adsorption*. (D. LeVan, Ed.) *Proc. Int. Conf*. Boston: Massachusetts: Kluwer Academic Publishers.

Chibowsk, I S. Patkowski J. and Grzadka E. (2009). Adsorption of Polyethyleneimine and Polymethacrylic Acid onto Synthesized Hematite. *J. Colloid Interf. Sci. 1*, 329.

Chingombe, B. Wakeman, R. J. Saha P. (2005). Surface Modification and Characterisation of a Coal-based Activated Carbon. *Carbon*, *43*(15), 3132–3143.

Choi, S. Drese, J. H. & Jones, C. W. (2009). Adsorbent Materials for Carbon Dioxide Capture from Large Anthropogenic Point Sources. *ChemSusChem*, *2*(9), 796–854.

Chue, K. T. Yoo Y. J. Cho S. H. Yang R. T. Kim J. N. (1995). Comparison of Activated Carbon and Zeolite 13X for CO_2 Recovery from Flue Gas by Pressure Swing Adsorption. *Ind. Eng. Chem. Res.*, *34*(2), 591–598.

Chunzhi, Shen C. A. G. Li, Ping Yu, Jianguo, Alirio Rodrodrigues, E. (2010). Adsorption Equilibrium and Kinetics of CO_2 and N_2 on Activated Carbon Beads. *Chemical Engineering Journal*, *160*, 398–407.

Clausse, J. Meunier, F. Bonjour, M. (2004). Adsorption of Gas Mixtures in TSA Adsorbers under Various Heat Removal Conditions. *Chemical Engineering Science*, *59*(17), 3657–3670.

Clayton, S.J. Stiegel, G.J. and Wimer, J. G. (2002). *Gasiification Technologies: Gasification Markets and Technologies – Present and Future*. US DOE Report, DOE/FE-0447.

Cobden, P.D. Van Beurden, P. Reijers H.Th.J. Elzinga G.D. Kluiters S.C.A. Dijkstra, J.W. Jansen, D. Van den Brink, R.W. (2007). Sorption-Enhanced Hydrogen Production for Pre-combustion CO_2 Capture: Thermodynamic Analysis and Experimental Results. *Int. J. Greenhouse Gas Control.*, *1*, 170 – 179.

Danafar, F. Fakhru'l-Razi, A. Salleh, M. A. M., & Biak, D. R. A. (2009). Fluidized Bed Catalytic Chemical Vapour Deposition Synthesis of Carbon Nanotubes—A review. *Chemical Engineering Journal*, *155*(1-2), 37–48.

Davidson, R. (2009), Post-combustion Carbon Capture – Solid Sorbents and Membranes. IEA Clean Coal Centre,

DECC, Change, Department of Energy andClimate Change (2011). *CCS Roadmap: Supporting Deployment of Carbon Capture and Storage in the UK* (p. 49). London: Department of Energy and Climate Change.

DECC. (2009). Climate Change Act 2008. (Department of Energy & Climate Change, Ed.). Department Of Energy and Climate change.

DECC. (2010). *UK Electricity Generation Costs Update*.

DECC. (2012a). Carbon Capture Projects. (D. of E. and C. Change, Ed.). DECC.

DECC. (2012b). Potential Cost Reductions in CCS in the Power Sector. (D. of E. and C. Change, Ed.). London: Mott MacDonald.

DECC. (2012c). Climate Change Act 2008. (D. of E. & C. Change, Ed.). Department Of Energy and Climate change.

Deng, S. (2006). *Sorbent Technology* (pp. 2825–2845). New Mexico.

DoE. (2011). CCS Legal and Regulatory Workshop. (D. of Energy, Ed.). Johannesburg: DoE.

Dong, H. Goto, M. Hirose, T, Lou F. (1990). *Separation and Purification Technology*, *15*, 31–40.

Donnet, J. B. (1968). The Chemical Reactivity of Carbons. *Carbon*, *6*(2), 161–176.

Drage, T.C. Pevida C., Plaza M.G., Rubiera F., Pis J.J., Snape C.E. and Tennison S., K. O. (2009). Developing Activated Carbon Adsorbents for Pre-combustion CO_2 Capture. *Energy Procedia*, *1*, 599–605.

Drage, T. C. Arenillas, A. Smith, K. M. Pevida, C., Piippo, S. & Snape, C. E. (2007). Preparation of Carbon Dioxide Adsorbents from the Chemical Activation of Urea-formaldehyde and Melamine-formaldehyde Resins. *Fuel*, *86*(1-2), 22–31.

Drage, Trevor C. Snape, Colin E. Stevens, Lee . Wood, Joseph Wang, Jiawei Cooper, Andrew I. Dawson, Robert Guo, Xiao Satterley, Christopher Irons, Robin (2012). Materials Challenges for the Development of Solid Sorbents for Post-combustion Carbon Capture. *Journal of Materials Chemistry*, *22*(7), 2815.

Drage, T. C. Arenillas, A. Smith, K. M. & Snape, C. E. (2008). Thermal Stability of Polyethylenimine Based Carbon Dioxide Adsorbents and its Influence on Selection of Regeneration Strategies. *Microporous and Mesoporous Materials*, *116*(1-3), 504–512.

Dreisbach, F. Keller, J.U. Staudt, R. (1999). High Pressure Adsorption Data of Methane, Nitrogen, Carbon dioxide and their Binary and Tertiary Mixtures on Activated Carbons. *Adsorption*, *5*, 215–227.

DTI. (2005). A Strategy for Developing Carbon Abatement Technologies for Fossil Fuel Use: Carbon Abatement Technologies Programme. Scottish Power, Shell and BP plc.

Dubinin, M. M. (1974). On Physical Feasibility of Brunauer's Micropore Analysis Method. *J. Coll. Interface Sci.*, *46*(1), 351–356.

Dubinin, M. M. (1980). Water Vapour Adsorption and the Microporous Structures of Carbonaceous Adsorbents. *Carbon*, *18*(5), 355–364.

Dubinin, M. M. (1981). Inhomogeneous Microporous Structures of Carbonaceous Adsorbents. *Carbon*, *19*(4), 321–324.

Dubinin, M. M. (1989). Fundamentals of the Theory of Adsorption in Micropores of Carbon Adsorbents: Characteristics of their Adsorption Properties and Microporous Structures. *Carbon*, *27*(3), 457–467.

Duong, D. Do (2008). Adsorption Analysis: Equilibria and Kinetics, Series on Chemical Engineering Vol.2, London, Imperial College Press, 346-518

Edward, S. Rubin Michael, B.P.I. Berkenpas, Anand B. Rao (2007). *Development and Application of Optimal Design Capability for Coal Gasification Systems: Oxygen-based Combustion Systems (Oxyfuels) with Carbon Capture and Storage (CCS)* (pp. 1–664). Pittsburgh: Carnegie Mellon University, Center for Energy and Environmental Studies, Department of Engineering and Public Policy.

Edward S. Rubin, Hari Mantripragada, Aaron Marks, Peter Versteeg, John Kitchin (2012), The outlook for improved carbon capture technology, Progress in Energy and Combustion Science, 1-42.

ERC. (2010). *Strong Solution for CO_2 capture: SEWGS* (p. 2). Netherland.

Fajula, F. Galarneau, A. & Renzo, F. D. (2005). Advanced Porous Materials: New Developments and Emerging Trends. *Microporous and Mesoporous Materials*, *82*(3), 227–239.

Figueiredo, M. C. A. and Ferraz, J. L. (1982). Textural Modification in Impregnated Active Carbons. *Studies in Surface Science and Catalysis*, *10*, 239–244.

Ferraz, J. L. and Figueiredo, M. C. A. (1982). Textural Modification in Impregnated Active Carbons. *Studies in Surface Science and Catalysis*, *10*, 239–244.

Fierro, V. Torné-Fernández, V. & Celzard, A. (2006). Kraft Lignin as A Precursor for Microporous Activated Carbons Prepared by Impregnation with Ortho-phosphoric Acid: Synthesis and Textural Characterisation. *Microporous and Mesoporous Materials*, *92*(1-3), 243–250.

Figueroa, Timothy Plasynski, Sean McIlvried, Howard Srivastava, Rameshwar D. José D Fout (2008). Advances in CO_2 Capture Technology-The U.S. Department of Energy's Carbon Sequestration Program. *International Journal of Greenhouse Gas Control*, *2*(1), 9–20.

Fogler, Ryan Hartman, L. and Scott, H (2007). Understanding the Dissolution of Zeolites. *Langmuir*, *23*, 5477–5484.

Frackowiak, E. Beguin, F. F. (2001). Carbon Materials for the Electrochemical Storage of Energy in apacitors. *Carbon*, *39*, 937–950.

Fuertes, A. B. (2004a). Synthesis of Ordered Nanoporous Carbons of Tunable Mesopore Size by Templating SBA-15 Silica Materials. *Microporous and Mesoporous Materials*, *67*(2-3), 273–281.

Fuertes, G. Centeno, T. A. Frackowiak, E., Lota, A. B. (2005). Templated Mesoporous Carbons for Supercapacitor Aapplication. *Electrochimica Acta*, *50*(14), 2799–2805.

García, Amelia Leon y Leon, Carlos A. Tascón, Juan M. D. Ana B Martínez-Alonso. (1998). Modification of the Surface Properties of an Activated Carbon by Oxygen Plasma Treatment. *Fuel*, *77*(6), 613–624.

García, S., Gil, M. V., Martín, C. F., Pis, J. J., Rubiera, F., & Pevida, C. (2011). Breakthrough Adsorption Study of a Commercial Activated Carbon for Pre-combustion CO_2 Capture. *Chemical Engineering Journal*, *171*(2), 549–

Gargiulo, N. Caputo, D. and Colella, C. (2007). Preparation and Characterization of Polyethylenimine-modified Mesoporous Silicas as CO_2 Sorbents. *Stud. Surf. Sci. Catal*, *170*, 1938.

Garsuch, Rita R. Witt, Susanne Klepel, Olaf, A. S. (2006). Adsorption Properties of Various Carbon Materials Prepared by Template Synthesis Route. *Microporous and Mesoporous Materials*, *89*(1-3), 164–169.

Gedeon, A. Massian, I P. B. F. (2008). *Zeolites and Related Materials: Trends Targets and Challenges (SET)*. (Gedeon A. Ed.) (p. 1442). Elsevier.

Gensterblum, Y., van Hemert, P., Billemont, P., Busch, A., Charriére, D., Li, D., Krooss, B. M., et al. (2009). European Inter-laboratory Comparison of High Pressure CO_2 Sorption Isotherms. I: Activated Carbon. *Carbon*, *47*(13), 2958–2969.

Gerard, David, and Wilson, J. E. (2007). *Carbon Capture and Sequestration: Integrating Technology, Monitoring and Regulation* (first edit. p. 269). Iowa: Blackwell Publishing.

Gil, M. V., Martínez, M., García, S. Rubiera, F. Pis, J. J. & Pevida, C. (2012). Response Surface Methodology as an Efficient Tool for Optimizing Carbon Adsorbents for CO_2 Capture. *Fuel Processing Technology*, *(In Press)*, 1–7.

Gil, A. and Grange, P. (1996). Application of the Dubinin-Radushkevich and Dubinin-Astakhov Equations in the Characterization of Microporous Solids. *Colloids and Surfaces A: Physicochemical and Engineering Aspects*, *113*(1-2), 39–50.

Gi-Moon, Nam Soek-Hyun Kang, Byung-Kwon Lee, and Dae-Ki Choi, Byung-Man Jeong (2005). Equilibrium Isotherm of CH_4, C_2H_6, C_2H_4, N_2, and H_2 on Zeolite 5A Using a State Volumetric Method. *J. Chem. Eng Data*, *50*, 72–76.

Golden, T.C. Sircar, S. (1990). Activated Carbon Adsorbent for PSA Driers. *Carbon*, *28*(5), 683–690.

Goodall, C. (2007). *How to Llive Low-carbon Life* (p. 319). Bath: Earthscan.

Gray, K. J. Fauth, D. Baltrus, J. P. Pennline, Henry, M. L. C. (2008). Performance of Immobilized Tertiary Amine Solid Sorbents for the Capture of Carbon Dioxide. *International Journal of Greenhouse Gas Control*, *2*(1), 3–8.

Gregory, P. Knowles Seamus W. Delaney, Alan L. Chaffee, J. V. G. (2005). Aminopropyl-functionalized Mesoporous Silicas as CO2 Adsorbents. *Fuel Processing Technology*, *86*(14-15), 1435–1448.

Guang-Ping, Hao Dan Qian, and An-Hui Lu, Wen-Cui Li (2010). Rapid Synthesis of Nitrogen-doped Porous Carbon Monolith for CO_2 Capture. *Material Views*, *22*, 853–857.

Guillot A., F. S. and Y. B. (1999). The Microporosity of Activated Carbon Fibre KF1500 Assessed by Combined CO_2 Adsorption and Calorimetry Techniques and by Immersion Calorimetry. *Adsorption Science & Technology*, *18*(1), 1–14.

Guoying, B. Zhao, A. (2010). Carbon dioxide Adsorption on Mesoporous Silica Surfaces Containing Amine-like Motifs. *Applied Energy*, *87*, 2907–2913.

Hameed, B. H., Din, T. M. & Ahmad, L. (2007). Adsorption of methylene blue onto bamboo-based activated carbon: kinetics and equilibrium studies. *Journal of hazardous materials*, *141*(3), 819–25.

Haring, H. W. (2007). *Industrial Gas Processing*. Weinheim, Germany: Wiley-VCH Verlag GmbH.

Harris, A. T. Deshpande, S. & Kefeng, X. (2009). Synthesis of Graphitic Carbon Particle Chains at Low Temperatures under Microwave Irradiation. *Materials Letters*, *63*(16), 1390–1392.

Harris P.J.F (1997) Structure of non-graphitic Carbons, International Materials Review, 42(5), 206-218.

Hartman R.L and Fogler, H. S. (2005). Reaction Kinetics and Mechanisms of Zeolite Dissolution in Hydrochloric Acid. *Ind. Eng. Chem. Fundam. Res.*, *44*, 7738.

Hassan, D. M. Raghavan, N. S. Ruthven, M. M. (1986). Air Separation by Pressure Swing Adsorption on a Carbon Molecular Sieve. *Chemical Engineering Science*, *41*(5), 1333–1343.

Haszeldine, R. S. (2009). Carbon Capture and Storage: How Green Can Black Be? *Science*, *325*, 1647–1652.

HCSTC (2006). *Meeting UK Energy and Climate needs: The Role of Carbon Captre and Storage* (Vol. 1, p. 81). London: House of Commons Science and Technology Committee.

Higman, C. (2010). *Gasification Processes and Synthesis Gas Treatment Technologies for Carbon dioxide Capture* (pp. 1–37).

Hines, A. L. L. Dural, N. H., Kuo, S. (1990). A New Analytical isotherm Equation for Adsorption on Heterogeneous Adsorbents. *Separation science Technology*, *25*, 869–888.

Ho, M. T., Allinson, G., & Wiley, D. E. (2006). Comparison of CO_2 separation options for geo-sequestration: are membranes competitive? *Desalination*, *192*(1-3), 288–295.

Ho, Y. & McKay, G. (1999). Pseudo-second Order Model for Sorption Processes. *Process Biochemistry*, *34*(5), 451–465.

Ho, Y. S. (2004). Citation review of Lagergren kinetic rate equation on adsorption reactions. *Scientometrics*, *59*, 171–177.

Ho, Y. S. (2006). Review of Second-order Models for Adsorption Systems. *Journal of Hazardous Materials*, *136*, 681–689.

Hong Dae Ho and Suh Myunghyun Paik (2012), Selective CO_2 adsorption in a metal–organic framework constructed from an organic ligand with flexible joints. Chem. Commun., 48, 9168–9170.

Horita, Kiyoshi and Takao Ohshima, Y. N. (1996a). Surface Modification of Carbon Black by Anodic Oxidation and Electrochemical Characterization. *Carbon*, *34*(2), 217–222.

Huang, H.Y. Chinin D. Munsom, C.L., Yanf, R. T. (2003). Amine-grated MCM-48 and Silica Xerogel as Superior Sorbents for Acidic Gas Removal from Natural Gas. *Ind. Eng. Chem. Res*, *42*, 2427–2433.

Hutton, H.D. Pocard, N. L. Alsmeyer, D.C. Schueller, O. J. A. Spontak, R. J. Huston, M. E. Huang, W. McCreery, R. L. Neenan, T. X. Callstrom, M. R.

(1993). Preparation of Nanoscale Platinum (0) Clusters in Glassy Carbon and their Catalytic Activity. *Chemistry of Materials*, *5*(12), 1727–1738.

IEA (2006). *Estimating the Future Trends in the Cost of CO_2 Capture Technologies*.

IEA. (2010). *CO_2 Emissions from Fuel Combustion*. *IEA Statistics* (Vol. 2010 Edit., p. 542).

IEA. (2011). CCS Legal and Regulatory Workshop. Johannesburg: DoE, IEA.

Imtiaz-Ul-Islam, M., Hong, L., & Langrish, T. (2011). CO_2 capture using whey protein isolate. *Chemical Engineering Journal*, *171*(3), 1069–1081.

IPCC. (2005). *Carbon Dioxide Capture and Storage* (p. 431). Cambridge: Intergovernmental Panel on Climate Change.

IPCC. (2005b) *Special Report on Carbon dioxide Capture and Storage*.

International Union of Pure and Applied Chemistry (IUPAC) (2012), Compendium of Chemical Terminology Gold Book, Version 2.3.2

Jaheon Kim, Banglin Chen, Theresa M. Reineke, Hailian Li, Mohamed Eddaoudi, David B. Moler, Michael O¢Keeffe, and Omar M. Yaghi, (2001). Assembly of Metal-Organic Frameworks from Large Organic and Inorganic Secondary Building Units: New Examples and Simplifying Principles for Complex Structures. J. Am. Chem. Soc., 123, 8239-8247.

Jasen, H. and Van Bekkum, R. J. J (1994). Amination and Ammoxidation of Activated Carbon. *Carbon*, *32*(8), 1507–1516.

Jeng, Hsin Chen Chung, Sung Tan David Shan, Hill Wong (1997). Adsorption and Desorption of Carbon Dioxide onto and from Activated Carbon at High Pressures. *Ind. Eng. Chem. Res.*, *36*, 2808–2815.

Jitong, Wang Huanhuan Zhou, Qingjun Chen, Xiaojun Liu and Licheng Ling, D. Lo. (2012). Surfactant Promote Solid Amine sorbents for CO_2 Capture. *Energy and Environmental Science*, *5*, 5742–5749.

Kaneko, Katsumi Kazunori Kakei, Takaomi Suzuki, and Sumio Ozeki, N. F. (1989). Enhancement of NO Dimerization by Micropore Fields of Activated Carbon Fibre. *Langmuir*, *5*, 960–965.

Kaneko, Masahiko Ogino, Keizo, Y. A. (1989). Adsorption Characteristics of Organic Compounds Dissolved in Water on Surface-Improved Activated Carbon Fibres. *Colloids and Surfaces*, *37*, 211–222.

Ke, G. (2009). Homogeneous Modification of Carbon Nanotubes with Cellulose Acetate. *Chinese Chemical Letters*, *20*(11), 1376–1380.

Kikkinides, E. S., Yang, R. T. (1993). Concentration and Recovery of CO_2 from Flue Gas by Pressure Swing Adsorption. *Ind. Eng. Chem. Res.*, *32*, 2714–2720.

King, A. (1937). Studies in Chemisorption on Charcoal. Part IX. The Influence of Temperature of Activation on the Sorption of Acids and Bases. *Journal of the Chemical Society*, 1489–1491.

Kline, H. S. and Fogler, W. E. (1981). Dissolution of Silicate Minerals by Hydrofluoric Acid. *Ind. Eng. Chem. Fundam.*, *20*(2), 155–161.

Knaebel, K. S. (1991). Pressure Swing Adsorption. (U. S. Patent, Ed.). United States of America: The Ohio State University.

Knapp, B. (1996). *Carbon*. (E. Walker, Ed.) (p. 56). Oxon: Atlantic Europe Publishing Company Limited.

Knappe, D.R.U., Matsui, Y., and Snoeyink, V. (1998). Predicting the Capacity of Powdered Activated Carbon for Trace Organic Compounds in natural Water. *Environ. Sci. Technol.*, *32*, 1694–1698.

Knowles, G. P. Delaney, S.W. and Chafee, A. L. (2005a). Amine-functionalised Mesoporous Silicas as CO_2 Adsorbents. *Stud. Surf. Sci. Catal.*, *156*, 887.

Knowles, G. P. Graham, J. V. Delaney, S. W., & Chaffee, A. L. (2005b). Aminopropyl-functionalized mesoporous silicas as CO_2 adsorbents. *Fuel Processing Technology*, *86*(14-15), 1435–1448.

Ko Mikyung Moon, Il Choi, Dae-ki, D. K. (2002). Analysis of Purge Gas Temperature in Cyclic TSA Process. *Chemical Engineering Science*, *57*(1), 179–195.

Kojima, T., & Harrison, B. (1994). *The Carbon dioxide Problem :The Integrated Energy and Environmental Policies for the 21st Century*. (B. Harrison, Ed.)*The Carbon dioxide Problem :The Integrated Energy and Environmental Policies for the 21st Century* (pp. 39–55). Yokyo: Agne Ahofu Publishing Inc.

Kozynchenko, Strello Volodymr Vasyljovch, Blackburn, Andrew John, O. P., & Tennison, S. R. (2001). Porous Carbon. (E. P. Specification, Ed.)*Freepatentsonline.com*. Europe: Mat & Separations Tech Int. Ltd (GB).

Krkljuš, I. (2011). *Correlation between the Microstructure of Porous Materials and the Adsorption Properties of H_2 and D_2*. Max-Planck-Institut für Intelligente Systeme.

Kwon, S. Fan, M. DaCosta, H. F. M. Russell, A. G. Berchtold, K. A. & Dubey, M. K. (2011). CO_2 Sorption. *Coal Gasification and Its Applications* (pp. 293–339). Boston: William Andrew Publishing.

Kyotani, T. (2006). Synthesis of Various Types of Nano Carbons Using the Template Technique. *The Chemical Society of Japan*, *79*(9), 1322–1337.

Kyotani, T., Nakazaki, S. Xu, W. H. & Tomita, A. (2001). Chemical Modification of the Inner Walls of Carbon Nanotubes by HNO_3 Oxidation. *Carbon*, *39*(5), 782–785.

Kyotani, Takashi Tomita, Akira and Ma, Z. (2003). Template Synthesis of Novel Porous Carbons Using Various types of Zeolite. *Carbon*, *41*, 1451–1459.

Leboda, R. (1993). Carbon-mineral Adsorbents- New types of Sorbents: Part II Surface Properties and Methods of their Modification. *Materials Chemistry and Physics*, *34*, 123–141.

Lee, Tack-Rae Ogale, Amod A. Kim, Myung-Soo, S. K. (2007). Surface and Structure Modification of Carbon Nanofibers. *Synthetic Metals*, *157*(16-17), 644–650.

Leitgeb, P. (1988). Pressure Spring Adsorption. (White, Ed.) *United States Patent*. Germany: Linde Aktiengesellschaft.

Liang, Y. (2003). *Carbon dioxide Capture from Flue Gas using Regenerable Sodium-Based Sorbent*. *Department of Chemical Engineering*. Loisiana State University and Agricultural and Mechnaical College, Loisiana.

Liu, Tong Li, Nan Wang, Peng Abulikemu, Gulizhaer, Qing-Song, Zheng (2010). Modification of Bamboo-based Activated Carbon Using Microwave Radiation and its Effects on the Adsorption of Methylene Blue. *Applied Surface Science*, *256*(10), 3309–3315.

Liu, C.Y. Sipöcz, N. Assadi, M. X. Bai, S. Chen, G. (2012). Characteristics of Oxy-fuel Combustion in Gas Turbines. *Applied Energy*, *89*(1), 387–394.

Liu, Y. Krastov, V.C. Larsen, R., Eddaoudi, M. (2006). *Chem. Commun.*, 1488.

Liu, Wenqiang An, H. Qin, C. Yin, J. Wang, G. Feng, B. & Xu, M. (2012). Performance Enhancement of Calcium Oxide Sorbents for Cyclic CO_2 Capture: A Review. *Industrial and Engineering Chemistry Research*, *51*, 1438–1463.

Loiseau, L. Volkringer, C. Marrot, J. Ferey, G. Haouas, M. Taulelle, F. Bourrelly, S. Llewellyn, P.L. Latroche, M. T. Lecroq (2006). MIL-96, A Porous Aluminium Trimesate 3D Structure Constructed from a Hexagonal Network of 18-Membered Rings and μ3-Oxo-Centered Trinuclear Units. *Journal of American Chemical Society*, *128*, 10223.

Lopez-Gonzalez, J. D. Moreno-Castilla C. Guerrero-Ruiz A., Rodriguez-Reinoso, F. (1982). Effect of Carbon-oxygen and Carbon-sulphur Surface Complexes on the Adsorption of Mercuric Chloride in Aqueous Solutions by Activated Carbons. *Journal of Chemical Technology and Biotechnology*, *32*(5), 575–579.

Love, G. D., Snape, C. E., Carr, A. D. & Houghton, R. C. 1995. Release of covalently-bound alkane biomarkers in high yields from kerogen via catalytic hydropyrolysis. *Organic Geochemistry,* 23**,** 981-986.

Lyubchik, R. Béguin, F. Benoit, S. B. (2002). Influence of Chemical Modification of Anthracite on the Porosity of the Resulting Activated Carbons. *Carbon*, *40*(8), 1287–1294.

Ma, Zhixin Tomita, Akira , Kyotani, T. (2002). Synthesis Methods for Preparing Microporous Carbons with a Structural Regularity of Zeolite Y. *Carbon*, *40*, 2367–2374.

Macario, A. Giordano, G. Iucolano, F. Caputo, D., A. K. (2005). Synthesis of Mesoporous Materials for Carbon dioxide Sequestration. *Microporous and Mesoporous Materials*, *81*(1-3), 139–147.

Maceiras, R. Alvarez, E. and Angeles, Cancela M. (2008). Effect of Temperature on Carbon dioxide Absorption in MonoethanolamineSolutions. *Chemical Engineering Journal*, *138*, 295–300.

Maier, G. (1998). Gas Separation with Polymer Membranes. *Angew. Chem. Int. Ed.*, *37*, 2960–2974.

Mall, I. D. Srivastava, V. C. Agarwal, N. K. & Mishra, I. M. (2005). Removal of Congo Red from Aqueous Solution by Bagasse Fly Ash and Activated Carbon: Kinetic Study and Equilibrium Isotherm Analyses. *Chemosphere*, *61*(4), 492–501.

Mandal, M. Biswas, A. K. Bandyopadhyay, S. S. Guha, B. P. (2001). Removal of Carbon dioxide by Absorption in Mixed Amines: Modelling of Absorption in Aqueous MDEA/MEA and AMP/MEA Solutions. *Chemical Engineering Science*, *56*(21-22), 6217–6224.

Maroto-Valer Zhong Zhang, Yinzhi, M. M. T. (2005). CO_2 Capture by Activated and Impregnated Anthracites. *Fuel Processing Technology*, *86*(14-15), 1487–1502.

Maroto-Valer; M. Mercedes. (2010). *Developments and Innovation in Carbon dioxide Capture and Storage Technology*. (M. M. Maroto-Valer, Ed.) (p. 335). New York: Woodhead Publishing.

Martin, Stockel Ev Clowes, Rob Adams, Dave J. Cooper, Andrew I. Pis, Jose J., Rubiera, Fernando, Pevida, Cova, C. F. (2011a). Hypercrosslinked Organic Polymer Networks as Potential Adsorbents for Pre-combustion CO_2 Capture. *Journal of Materials Chemistry*, *21*(14), 5475–5483.

Martín, C. F. García, S. Beneroso, D. Pis, J. J. Rubiera, F. & Pevida, C. (2012). Pre-combustion CO_2 Capture by means of Phenol–formaldehyde Resin-Derived Carbons: From Equilibrium to Dynamic Conditions. *Separation and Purification Technology*, *(In Press)*, 1–8.

Martín, C. F. Plaza, M. G. Pis, J. J. Rubiera, F. Pevida, C. & Centeno, T. A. (2010). On the Limits of CO_2 Capture Capacity of Carbons. *Separation and Purification Technology*, *74*(2), 225–229.

Masafumi, Matsumoto and Katsuhide, Murata Toshikiyo, H. (1994). Surface Modification of Carbon Whiskers by Oxidation Treatment. *Carbon*, *32*(1), 111–118.

Matsumura, Y. (1975). Production of Acidified Active Carbon by Wet Oxidation and its Carbon Structure. *Journal of Applied Chemistry and Biotechnology*, *25*(1), 39–56.

Mattisson, T., Johansson, M., Lyngfelt, A. (2004). Multicycle Reduction and Oxidation of different Types of Iron Oxide Particles–Application to Chemical-Looping Combustion. *Energy and Fuels*, *18*, 628–637.

Mattisson, T. Johansson, M. Lyngfelt, A. (2006). The use of NiO as an Oxygen Carrier in Chemical Looping Combustion. *Fuel*, *85*, 736–747.

Mazzoni, Robert Deithorn, T. and Anthony, F. (2011). Activated Carbons. Oakdale: TIGG Corporation.

McKeown, Neil B. Msayib, Kadhum J. Peter M. Budd, Carin E. Tattershall, Khalid Mahmood, Siren Tan, David Book, Henrietta W. Langmi, and Allan Walton, B. G. (2006). Towards Polymer-Based Hydrogen Storage Materials: Engineering Ultramicroporous Cavities within Polymes of Intrinsic Microporosity. *Angew. Chem. int. Ed.*, *45*, 1804–1807.

McMillan, W. G. and Teller, E. (1950). The Assumptions of the B.E.T. Theory. *J. of Phys. Chem*, *55*(1), 17–20.

Micromeritics. (2012). ASAP 2420 Software and Data Presentations. Norcross: Micromeritics.

Miller, B. (2011). Clean Coal Engineering Technology: CO_2 Capture and Storage. *Clean Coal Engineering*, 483–511.

Millward, Andrew R. A, Yaghi, O. M. (2008). Metal-Organic Frameworks with Exceptionally High Capacity for Storage of Carbon Dioxide at room Temperature. *Journal of the American Chemical Society*, *51*, 17998–17999.

MNA (2012). Carbon Capture and Storage: Clean Coal Technologies for Carbon Management. *National Mining Association*.

Mohammad, M. Hossain and Hugo, I. de L. (2008). Chemical-looping Combustion (CLC) for Inherent CO_2 Separations - A review. *Chemical Engineering Science*, *63*, 4433 – 4451.

Mohammad, Saleh Shafeeyan Amirhossein, Houshmand Arash Arami-Niya, Wan Mohd Ashri, Wan Daud (2011). Ammonia Modification of Activated Carbon to Enhance Carbon dioxide Sdsorption: Effect of Pre-oxidation. *Applied Surface Science*, *257*(9), 3936–3942.

Moreno-Castilla, C., Fernández-Morales, I., Domingo-Garcia, M., and López-Garzón, F. J. (1985). Carbon Molecular Sieves Produced by the Fixation of Sulphur Surface Complexes. *Chormatographia*, *20*(12), 709–712.

Mortier, J. W. (1982). *Compilation of Extra Framework Sites in Zeolite* (p. 71). Surrey: Butterworth Scientific Limited.

Nabais, Valente P. J. Ribeiro, M. Carrott, M. M. L. Menéndez, J. A., Carrott, J. M. (2004). Preparation and Modification of Activated Carbon Fibres by Microwave Heating. *Carbon*, *42*(7), 1315–1320.

Neimark, A. V. (1995). The Method of Indeterminate Lagrange Multipliers in Non Local Density Functional Theory. *Langmuir*, *11*(10), 4183–4184.

Olson, C. B. L. B. M. D. H. (2007). *Atlas of Zeolite Framework Types*. *Sixth Revices Edition* (p. 405). Amsterdam: Elsevier.

Noble, R.D., and Stern, S. A. (1995). Membrane Separations Technology. *Elsevier Science*, *84*.

Olivares-Marín, M., Maroto-valer, M. (2012). Development of Adsorbents for CO_2 Capture from Waste Materials: A Review. *Greenhouse Gases: Science and Technology*, *2*(1), 20–35.

Oosterkamp, A. and Ramsen, J. (2008), State-of-the-Art Overview of CO_2 Pipeline Transport with relevance to offshore pipelines.

OPSI. (2008). Climate Change Act 2008. Office of Public Sector Information.

Özge ˙Islegen, and Stefan Reichelstein (2011), Carbon Capture by Fossil Fuel Plants: An Economic Analysis. Management Science, 57(1), 21-39.

Ozkaya, B. (2006). Adsorption and desorption of phenol on activated carbon and a comparison of isotherm models. *Journal of hazardous materials*, *129*(1-3), 158–63.

Pachauri, A. (Eds.), and Reisinger, R. K. . (2007). Contribution of Working Groups I, II and III to the Fourth Assessment Report of the Intergovernmental Panel on Climate Change. (IPCC, Ed.). Geneva: IPCC.

Papirer, R. Donnet, J. B., Lacroix, E. (1996). Chemical Modifications and Surface Properties of Carbon Blacks. *Carbon*, *34*(12), 1521–1529.

Park, Z. Cote, A.P. Choi, J.Y. Huang, R. Uribe-Romo, F.J. Chae, H.K. O'Keefe, M. Yaghi, O.M., Ni, K. S. N. (2006). Exceptional Chemical and Thermal Stability of Zeolitic Imidazolate Frameworks. *Proc. Natl. Acad. Sci.*, *103*, 10186.

Parmentier, Valentin Gaslain, Fabrice Tosheva, Lubomira Ducrot-Boisgontier, Claire Möller, Janina Patarin, Joël Vix-Guterl, Cathie, J. V. (2009). Effect of the Zeolite Crystal Size on the Structure and Properties of Carbon Replicas Made by a Nanocasting Process. *Carbon*, *47*(4), 1066–1073.

Particulate Systems. (2011). *High Pressure Volumetric Analyzer* (p. 124).

Patrick, J., W. (1995). *Porosity in Carbons : Characterization and Applications*. (W. Patrick J. Ed.) (p. 331). London.

Peng-Xiang, Hou Hironnori, Orikasa, Kyotan, Takashi, Toshiaki, Y. (2005). An Easy Method for the Synthesis of Ordered Microporous Carbons by the Template Technique. *Carbon*, *43*, 2618–2641.

Granite, H. W. and Pennline, E. J. (2012). Photochemical Removal of Mercury from Flue Gas. *National Energy Technology Laboratory, United States Department of Energy*. Pittsburgh: Department of Energy.

Pevida, C. Plaza, M. G. Arias, B., Fermoso, J. Rubiera, F. & Pis, J. J. (2008a). Surface modification of activated carbons for CO_2 capture. *Applied Surface Science*, *254*(22), 7165–7172.

Pevida, T. C. Snape, C. E., Drage, C. (2008). Silica-templated Melamine-formaldehyde Resin Derived Adsorbents for CO_2 Capture. *Carbon*, *46*(11), 1464–1474.

Pirngruber, Stefania Louret, Sylvain Chaumonnot, Alexandra Delfort, Bruno, Gerhard, D. Cassiano-Gaspar (2009). Amines Immobilized on a Solid Support for Post-combustion CO_2 Capture-A Preliminary Analysis of the Performance in a VSA or TSA Process based on the Adsorption Isotherms and Kinetic Data. *Energy Procedia*, *1*(1), 1335–1342.

Plaza, C. Arenillas, A. Rubiera, F. Pis, J. J., Pevida, M. G. (2007). CO_2 Capture by Adsorption with Nitrogen Enriched Carbons. *Fuel*, *86*(14), 2204–2212.

Plaza, C. Martín, C. F. Fermoso, J. Pis, J. J. Rubiera, F. Pevida, M. G. (2010a). Developing almond shell-derived activated carbons as CO_2 adsorbents. *Separation and Purification Technology*, *71*(1), 102–106.

Plaza, M. G. García, S., Rubiera, F. Pis, J. J. & Pevida, C. (2010b). Post-combustion CO_2 Capture with A Commercial Activated Carbon: Comparison of Different Regeneration Strategies. *Chemical Engineering Journal*, *163*(1-2), 41–47.

Plaza, M. G. García, S. Rubiera, F. Pis, J. J. & Pevida, C. (2011). Evaluation of Ammonia Modified and Conventionally Activated Biomass Based Carbons

as CO_2 Adsorbents in Post-combustion Conditions. *Separation and Purification Technology*, *80*(1), 96–104.

Plaza, M. G. Pevida, C. Arias, B. Fermoso, J. Rubiera, F. & Pis, J. J. (2009). A Aomparison of Two Methods for Producing CO_2 Capture Adsorbents. *Energy Procedia*, *1*(1), 1107–1113.

Plaza, M. G. Pevida, C. Martín, C. F. Fermoso, J. Pis, J. J. & Rubiera, F. (2010). Developing Almond Shell-derived Activated Carbons as CO_2 Adsorbents. *Separation and Purification Technology*, *71*(1), 102–106.

Plaza, M.G. Arias, B. Fermoso, J. Arenillas, A Rubiera, F. and Pis, J. J. Pevida, C. (2008). Application of Thermogravimetric Analysis to the Evaluation of Aminated Solid Sorbents for CO_2 Capture. *Journal of Themal Analysis and Calorimetry*, *92*(2), 601–606.

Plaza, M.G. Arias, B. Fermoso, J. Casal, M.D. Martín, C.F. et al., Pevida, C. (2009). Development of Low-cost Biomass-based Adsorbents for Post-Combustion CO_2 Capture. *Fuel*, *88*(12), 2442–2447.

Plaza, M.G. Pevida, C. Rubiera. F Pis, J. J. (2010). Ammoxidation of Carbon Materials for CO_2 Capture. *Applied Surface Science*, *256*, 6843–6849.

Plaza Marta, Thurecht Kris, Pevida Cova, Rubiera Fernando, Pis J, Snape Colin Drage Trevor C (2012), Influence of oxidation upon the CO_2 capture performance of a phenolic-resin-derived carbon, *Carbon.*

Plazinski, Rudzinski W. Plazinska, A. W. (2009). Theoretical Models of Sorption Kinetics Including A Surface Reaction Mechanism: A Review. *Advances in Colloid and Interface Science*, *152*, 2–13.

Powell, C.E. and Qiao, G. G. (2006). Polymeric $C0_2/N_2$ Gas Separation Membranes for the Capture of Carbon Dioxide from Power Plant Flue Gases. *J. of polymer Science*, *279*, 1–49.

Marta Plaza; Kris Thurecht; Cova Pevida; Fernando Rubiera; J Pis; Colin Snape; Trevor C Drage (2012). Influence of oxidation upon the CO_2 capture performance of a phenolic-resin-derived carbon. Carbon (Under review)

Przepiórski, Beata Morawski, Antoni W., Jacek, T. (2002). Adsorption of Carbon dioxide On Phenolic Resin-based Carbon Spheres. *Applied Surface Science*, *196*(1-4), 296–300.

Rackley, S. A. (2010). *Carbon Capture and Storage* (p. 392). Oxford: Elsevier Inc.

Rai, P. B. & Singh, H. R. (1971). Carbon-sulphur Surface Complexes on Charcoal. *Carbon*, *9*(2), 123–134.

Rand, B. (1976). On the Empirical Nature of the Dubinin--Radushkevich Equation of Adsorption. *Journal of Colloid and Interface Science*, *56*(2), 337–346.

Ranjani V. Siriwardane, Ming-Shing Shen, and Ming-Shing, Shen (2003). Adsorption of CO_2, N_2, and O_2 on Natural Zeolites. *Energy & Fuels*, *17*, 571–576.

Raveendran, P. Wallen, S.L. Ikushima, Y. (2005). Polar Attributes of Supercritical Carbon dioxide. *Acc Chem Res.*, *38*(6), 478–485.

Rectisol, L. (2006). The Challenge Conditions for Capture. *7th European Gasification Conference*. Barcelona.

Rinker, E. B. Ashour, S. S. and Sandall, O. C. (2000). Absorption of Carbon Dioxide into Aqueous Blends of Diethanolamine and Methyldiethanolamine. *Ind. Eng. Chem. Res.*, *39*, 4346–4356.

Ritter, James A. Ebner, A. D. (2007). State-of-the- Art Adsorption and Membrane Separation Process for Hydrogen Production in the Chemical and Petrochemical Industries. *Separation and Purification Technology*, *42*(6), 1123–1193.

Rosi J. Eddaoudi, M. Chen, B. O'Keefe, M. Yaghi, O.M. Kim, N.L. (2005). Rod Packings and Metal−Organic Frameworks Constructed from Rod-Shaped Secondary Building Units. *Journal of American Chemical Society*, *127*, 1504.

Rouquerol, F, Sing, K. Rouquerol, J. (1999). *Adsorption by Powders and Porous Solids*. London: Academic Press.

Rowsell, J. L. C., & Yaghi, O. M. (2004). Metal–organic Frameworks: A New Class of Porous Materials. *Microporous and Mesoporous Materials*, *73*(1-2), 3–14.

Ruthven, D. M. (1984). *Principles of Adsorption and Adsorption Processes* (p. 433). Canada: John Wiley & Sons, Inc.

Samanta, A. Z., An S., George K. H. Sarkar, P. Gupta, R. (2012). Post-Combustion CO_2 Capture Using Solid Sorbents : A Review. *Ind. Eng. Chem. Res.*, *51*(4), 1438–1463.

Sayari A. Serna-Guerrero R. Belmabkhout, Y. (2011). Flue Gas Treatment via CO_2 Adsorption. *Chem. Eng. J.*, *171*, 760–774.

Schell, J. Casas, N. Mazzotti, M. (2009). CO_2 Capture for IGCC Plants by an Adsorption Process. *Energy Procedia*, *1*, 655–660.

Schuth Ferdi, Keneth S.W. Sing, and Jen Weikamp (2002). *Handbook of Porous Solids Vol. 1* (p. 184). Weinhein: WILEY-VCH Verlag GmbH

Seredych, Martin Bandosz, Teresa J. M. van der M. (2009). Effects of Surface Chemistry on the Reactive Adsorption of Hydrogen Cyanide on Activated Carbons. *Carbon*, *47*(10), 2456–2465.

Sevilla, Antonio B. Fuertes, Marta (2012). CO_2 Adsorption by Activated Templated Carbons. *Journal of Colloid and Interface Science*, *366*(1), 147–154.

Shaikjee, A. & Coville, N. J. (2012). The Synthesis, Properties and Uses of Carbon Materials with Helical Morphology. *Journal of Advanced Research*, *3*(3), 195–223.

Shan, Shu-quan Zhang, Wen-hui, Xiao-mei, Z. (2008). Effect of Surface Modification of Activated Carbon on its Adsorption Capacity for NH_3. *Journal of China University of Mining and Technology*, *18*(2), 261–265,274.

Shuji, Himeno Shoichi, F., & and Toshiya, K. (2005). High-Pressure Adsorption Equilibria of Methane and Carbon Dioxide on Several Activated Carbons. *J. Chem. Eng*, *50*, 369–376.

Sioshansi, F. (2010). Generating Electricity in a Carbon Constraint World (Lackner S.). Elsevier Inc.

Siriwardane, R. V. Shen, M.-S. Fisher, E. P. & Losch, J. (2005). Adsorption of CO_2 on Zeolites at Moderate Temperatures. *Energy & Fuels*, *19*(3), 1153–1159.

Siriwardane, R., Shen, M., Fisher, E., & Losch, J. (2012). *CO_2 Capture Utilizing Solid Sorbents* (pp. 1–5). Morgantown.

Smith, C. L. (2009). *Practical Process Control: Tuning and Troubleshooting*. New Jersey: John Wiley & Sons, Inc.

Soonchul, Kwon Herbert, F.M. DaCosta, Armistead G. Russell, Kathryn A. Berchtold, Manvendra K. dDUbey, M. F. (2011). *Coal Gasificastion and Its Applications*. (10C., Ed.) *CO_2 Sorption*. Elsevier Inc.

Speyer, R. F. (1994). *Thermal Analysis of Materials* (p. 285). New York: Marcel Sekker Inc.

Stern, S. (2002). Polymers for Gas Separation: the Next Decade. *J. Membrane Sci.*, *94*, 1–65.

Stoeckli, A. G. and F. (2001). Reference Isotherm for High Pressure Adsorption of CO_2 by Carbons at 273K. *Carbon*, *39*, 2059–2064.

Su X. S. Lv, Lu Zhou, Zuocheng, F. Z. (2004). Synthesis and Characterization of Microporous Carbons Templated by Ammonium-form Zeolite Y. *Carbon*, *42*(14), 2821–2831.

Su, Jianhuang Yu, Yaoshan Lv, Lu Lee, Jim Yang Zhao, X. S. Fabing, Zeng (2005). Template Synthesis of Microporous Carbon for Direct Methanol Fuel Cell Application. *Carbon*, *43*(11), 2366–2373.

Szeto, K.P. Tilset, M. Bjorgen, M. Prestipino, C. Zecchina, A. Lamberti, C. Bordiga, S. Lillerud, K. C. (2006). A Thermally Stable Pt/Y-Based Metal−Organic Framework: Exploring the Accessibility of the Metal Centers with Spectroscopic Methods Using H_2O, CH_3OH, and CH_3CN as Probes. *Joural of Physical Chemistry B.*, *110*, 21509.

TA Instruments (2009). Thermogravimetric Analysis: Basic Theory & Applications Training. Herts: TA Instruments.

Tabe-Mohammadi, A. (1999). A Review of the Application of Membrane Separation Technology in Natural Gas Treatment. *Sep. Sci. Technol.*, *34*(10), 2095–21 11.

Takada, M. Kumagai, H. Sanada, Y., Nakahara, T. (1996). Surface Modification and Characterization of Carbon Black with Oxygen Plasma. *Carbon*, *34*(9), 1087–1091.

Tao, Zhu Dae, Ki Choi, Kyung Ho, Row and Seil, Yang (2010). Korean J. Chem. Eng. 27 (6), 1910-1915.

Thomas, D. C., Benson, S. M. (2005). *Carbon Dioxide Capture for Storage in Deep Geological Formations- Results from the CO_2 Capture Project*. (D. C. Thomas, Ed.) (volume 1., p. 660). Elsevier.

Tlili, Georges Vallières, Cécile, N. G. (2009). Carbon dioxide Capture and Recovery by means of TSA and/or VSA. *International Journal of Greenhouse Gas Control*, *3*(5), 519–527.

TSB. (2009). Carbon Abatement Technologies. Swindon: Technology Strategy Board .

Tsubokawa, S. and Yoshikawa N. (1996). Grafting of Polymers with Controlled Molecular Weight onto Carbon Black Surface. *Polymer Journal*, *28*(4), 317–322.

UNFCCC. (2009). Copenhagen Accord. Copenhagen: United Nations Framework Convention on Climate Change.

USEPA. (2006). Environmental Footprints and Costs of Coal-Based Integrated Gasification Combined Cycle and Pulverized Coal Technologies. Washington: USEPA.

Wang, J. Stevens, L. Drage, T. & Wood, J. (2012). Preparation and CO_2 Adsorption of Amine Modified Mg-Al LDH via Exfoliation Route. *Chemical Engineering Science*, 68(1): p. 424-431.

Wang, Mei-xian Wang, Cheng-yang Chen, Ming-ming Wang, Yan-su Shi, Zhi-qiang Du, Xuan Li, Tong-qi Hu, Zi-jun (2010). Preparation of High-performance Activated Carbons for Electric Double Layer Capacitors by KOH Activation of Mesophase Pitches. *New Carbon Materials*, *25*(4), 285–290.

Weihong, Gao David, L. and Tomasko, D. B. (2004). High-Pressure Adsorption of CO_2 on NaY Zeolite and Model Prediction of Adsorption Isotherms. *Langmuir*, *20*, 8083–8089.

WEO (2010). World Energy Outlook. (Energy, Ed.). Paris: IEA.

Willis, R., & LLC, U. O. P. (2010). *Carbon Dioxide Removal from Flue Gas Using Microporous Metal Organic Frameworks* (pp. 1–110). Illinois: Honeywell Company.

WNN. (2010). Roadmap gives options for 2050 target. *World Nuclear News*.

WRI. (2012). *Carbon Capture and Storage* (p. 2).

Xiao, P. Wilson, S. Singh, R., Webley, P., Xiao, G. (2009). Novel Adsorption Process for Carbon dioxide Capture within IGCC Process. *Energy Procedia*, *1*, 630–638.

Yagi, T., Shibuya H., and S. T. (1992). Application of Chemical Absorption Process to CO_2 Recovery from Flue Gases Generated in Power Plants. *Energy Conversion and Management*, *33*, 349–355.

Yan, X. Zhang, L. Zhang, Y. Qiao, K., Yan, Z. & Komarneni, S. (2011). Amine-Modified Mesocellular Silica Foams for CO_2 Capture. *Chemical Engineering Journal*, *In Press,*

Yang, H. Xu Z., Fan M. Gupta R. Slimane R. B. Bland A.E. and Wright, I. (2008). Progress in Carbon dioxide Separation and Capture: A Review. *J Environ Sci. China*, *20*, 14–27.

Yazaydýn A. Ozgur, Annabelle I. Benin, Syed A. Faheem, Paulina Jakubczak, John J. Low, Richard R. Willis, and Randall Q. Snurr (2009). Enhanced CO_2 Adsorption in Metal-Organic Frameworks via Occupation of Open-Metal Sites by Coordinated Water Molecules. *Chem. Mater.* 2009, *21,* 1425–1430.

Yoko, I Sho-ichi Komai, Shin-ichi Hattori, Tadashi Murata, Shizuaki, T. I. (2005). Chemical Modification of Carbon Nanotubes with Organic Hydrazines. *Carbon*, *43*(14), 2869–2874.

Yokoyama, T. (2004). Separations Technology VI: New Perspectives on Very Large-Scale Operations. *Japanese R&D on large scale CO_2 capture', in Fell*

C and Keller G E I1 (eds), ECI Symposium Series Volume RF'3 (p. Paper 7). New York: Engineering Conferences International.

Yuh-Shan Ho, (2004) Citation Review of Largergren Kinetic Rate Equation on Adsorption Reaction, Scientometics 59(1), 171-177.

Zelenak V. Halamova D. Cejka J. Zukal A Murafa N. Goerigk G. Badanicova M. (2008). Amine-modified Ordered Mesoporous Silica: Effect of Pore Size on Carbon dioxide Capture. *Chemical Engineering Journal*, *144*, 336–342.

Zelenák, D. Gaberova, L. Bloch, E. Llewellyn, P. Halamova, V. (2008). Amine-Modified SBA-12 Mesoporous Silica for Carbon dioxide Capture: Effect of Amine Basicity on Sorption Properties. *Microporous and Mesoporous Materials*, *116*(1-3), 358–364.

ZEP. (2011). *The Costs of CO_2 Capture*.

Zhang, J. Webley, P. A. & Xiao, P. (2008). Effect of Process Parameters on Power Requirements of Vacuum Swing Adsorption Technology for CO_2 Capture from Flue Gas. *Energy Conversion and Management*, *49*(2), 346–356.

Zhang, Z. Xu, M. Wang, H. & Li, Z. (2010). Enhancement of CO_2 Adsorption on High Surface Area Activated Carbon Modified by N_2, H_2 and Ammonia. *Chemical Engineering Journal*, *160*(2), 571–577.

Zhang, Z. Xian, S. Xi, H. Wang, H. & Li, Z. (2011). Improvement of CO_2 Adsorption on ZIF-8 Crystals Modified by Enhancing Basicity of Surface. *Chemical Engineering Science*, *66*(20), 4878–4888.

Zhang, Zhang, W., Chen, X., Xia, Q., Li, Z.,, Z. (2010a). Adsorption of CO_2 on Zeolite 13X and Activated Carbon with Higher Surface Area. *Separation Science and Technology*, *45*, 710–719.

Zhuxian, Yang Xuezhong Sun, and Robert Mokaya, Y. X. (2006). Preparation and Hydrogen Storage Properties of Zeolite-Templated Carbon Materials Nanocast via Chemical Vapour Deposition: Effect of the Zeolite Template and Nitrogen Doping. *J. Phys. Chem. B*, *110*, 18424–18431.

10 Appendices

10.1 Appendix 1: Adsorption/desorption isotherms for templated carbons

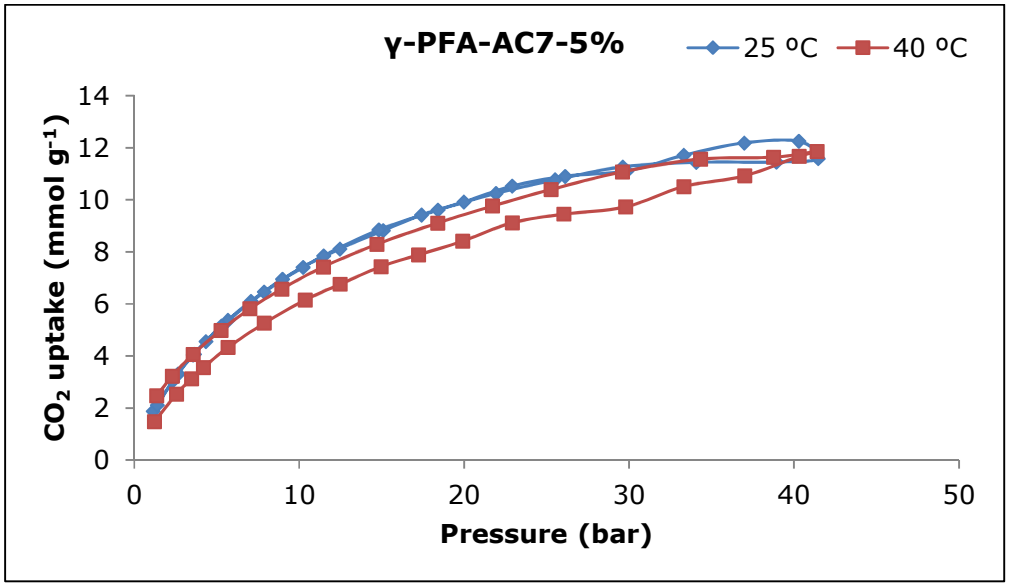

Figure 10.1. CO_2 uptake of γ-PFA-AC7-5% at 25 and 40 ^{o}C at high pressure.

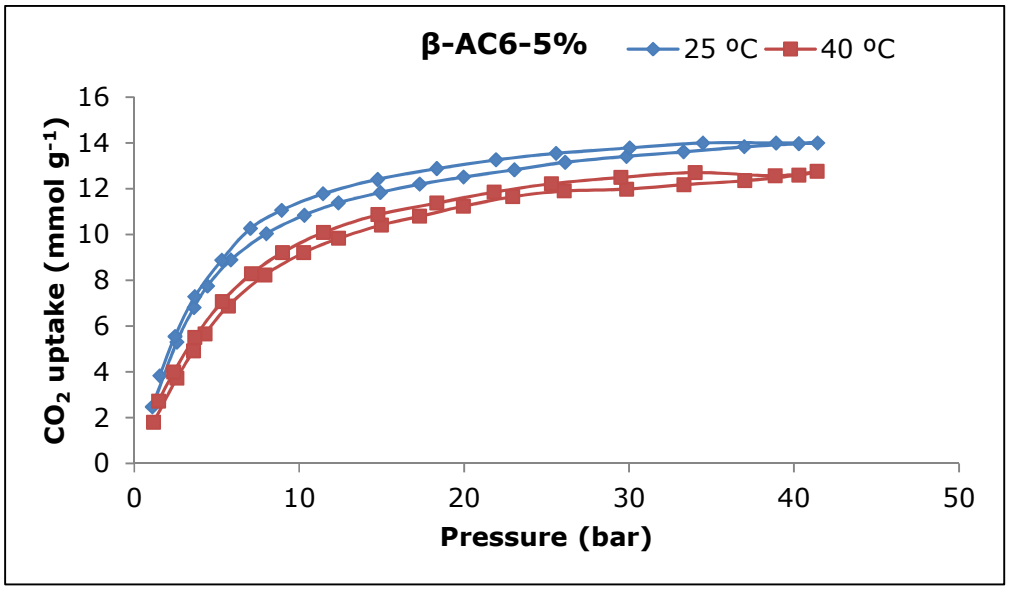

Figure 10.2. CO_2 uptake of β-AC6-5% at 25 and 40 ^{o}C at high pressure.

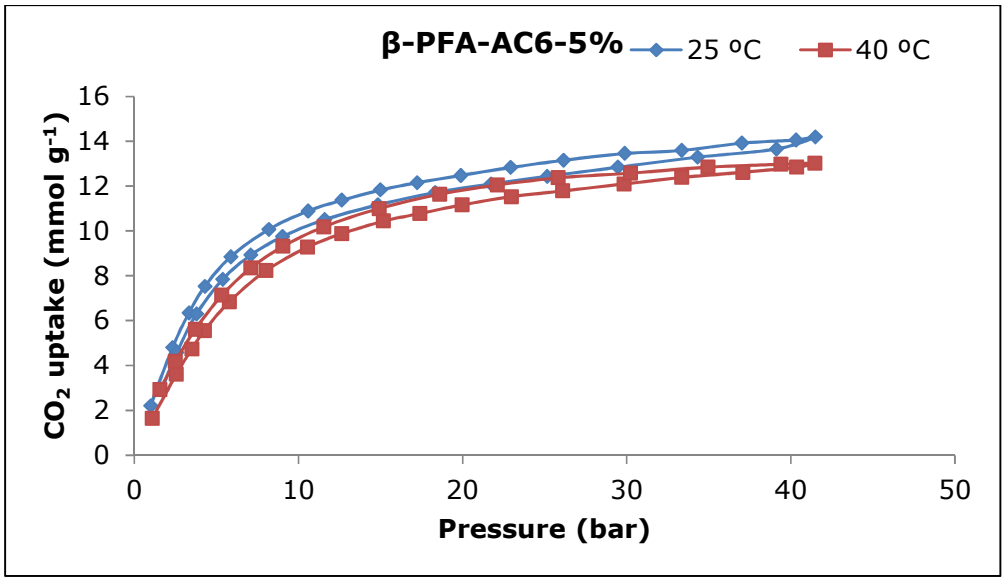

Figure 10.3. CO_2 uptake of β-PFA-AC6-5% at 25 and 40 ^{o}C at high pressure.

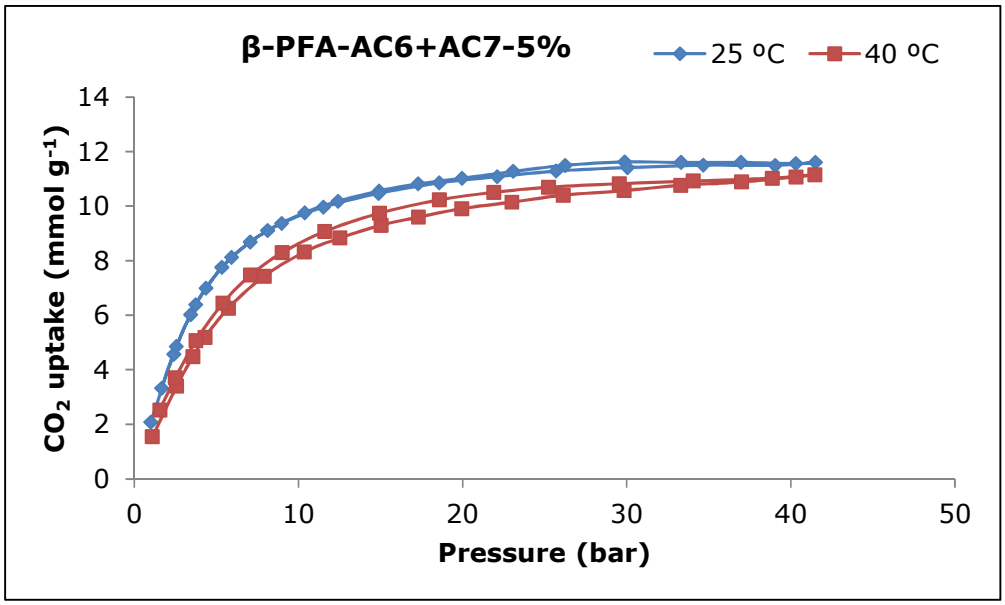

Figure 10.4. CO_2 uptake of β-PFA-AC6+AC7-5% at 25 and 40 °C at high pressure.

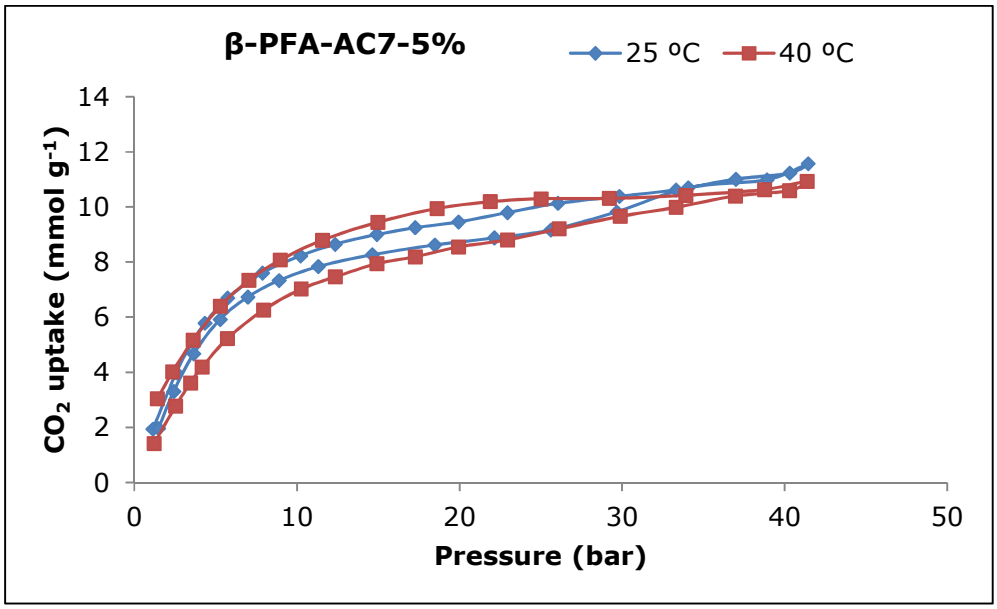

Figure 10.5. CO_2 uptake of β-PFA-AC7-5% at 25 and 40 °C at high pressure.

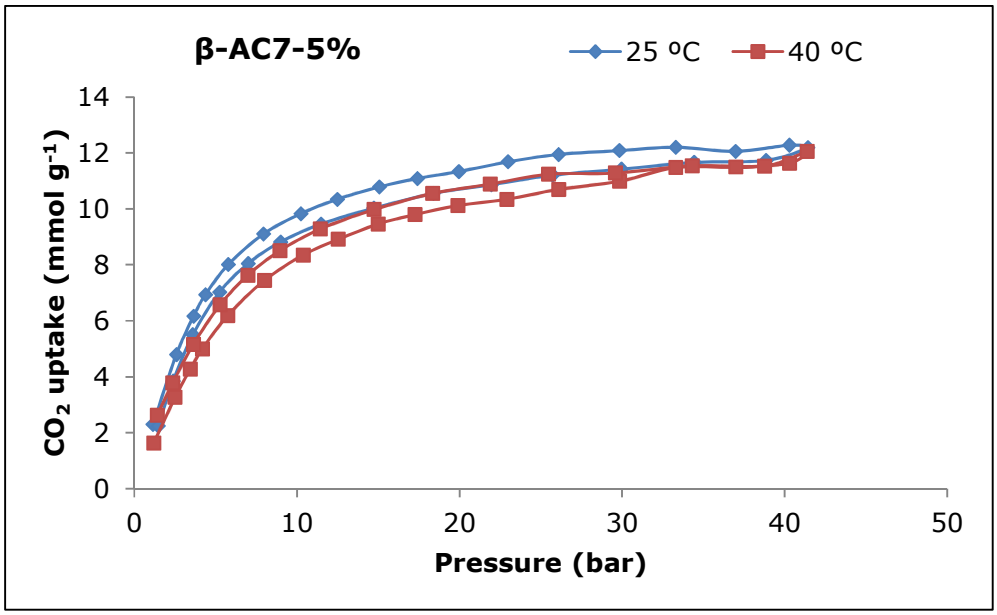

Figure 10.6. CO_2 uptake of β-AC7-5% at 25 and 40 °C at high pressure.

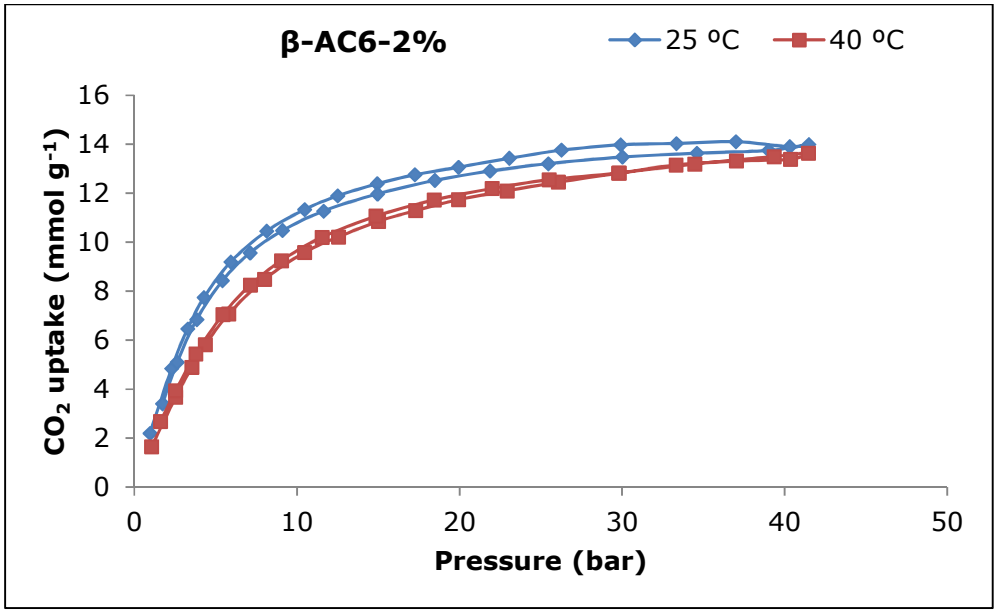

Figure 10.7. CO_2 uptake of β-AC6-2% at 25 and 40 °C at high pressure.

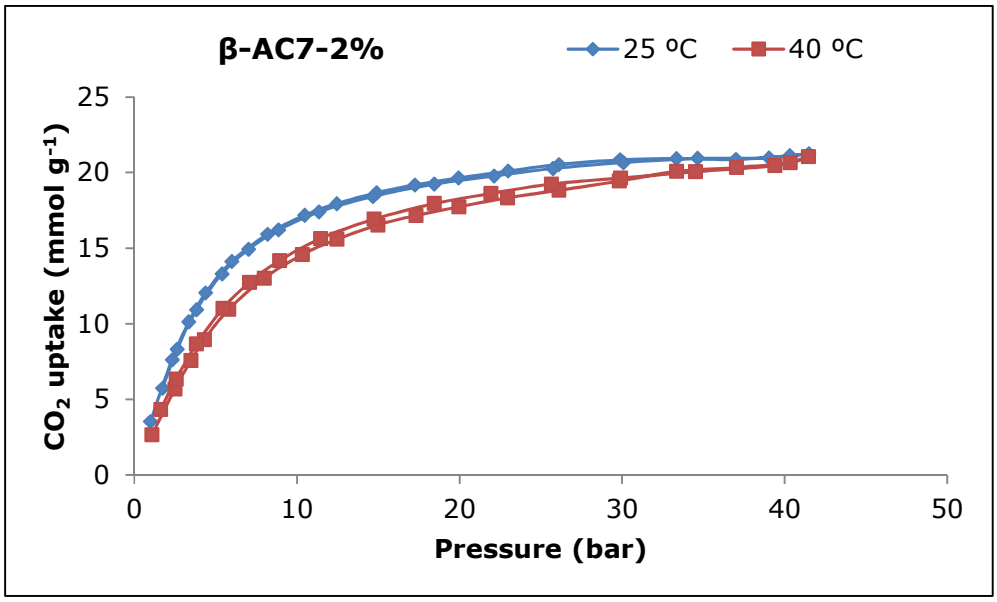

Figure 10.8. CO_2 uptake of β-PFA-AC7-2% at 25 and 40 ^{o}C at high pressure.

10.2 Appendix 2: Adsorption/desorption isotherms for oxidized carbons

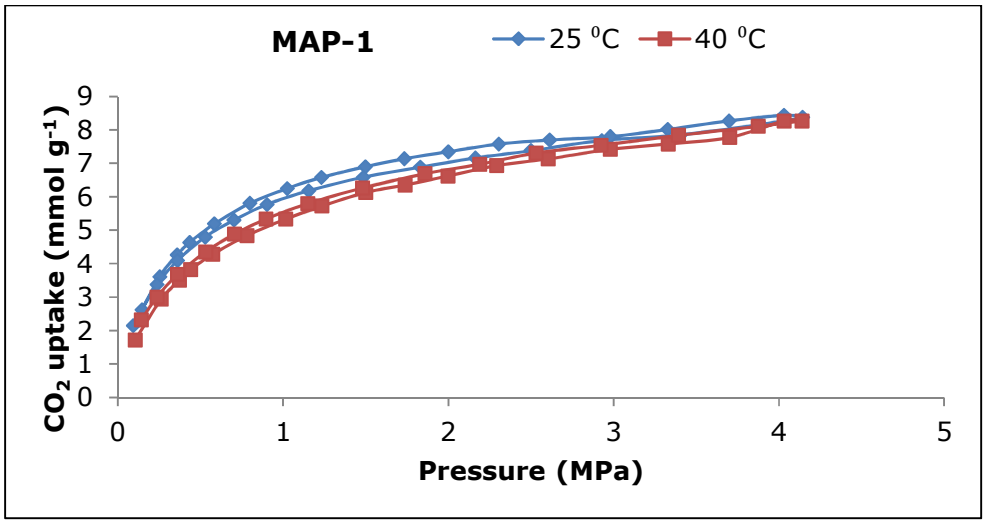

Figure 10.9. CO_2 adsorption isotherms for MAP-1 carbons at 25 and 40 °C and pressures up to 4.1 MPa.

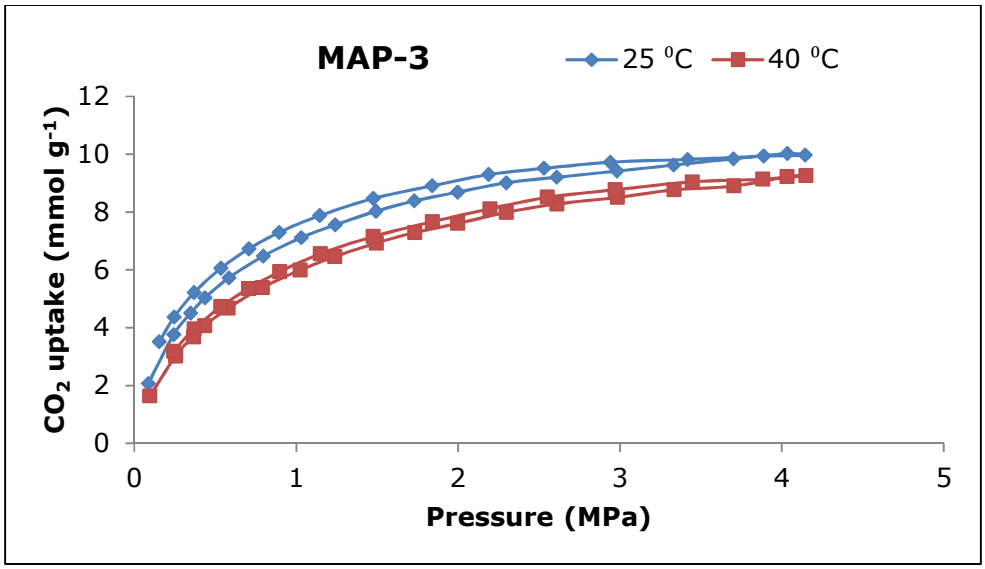

Figure 10.10. Adsorption isotherms for MAP-3 carbons at 25 and 40 °C and pressures up to 4.1 MPa.

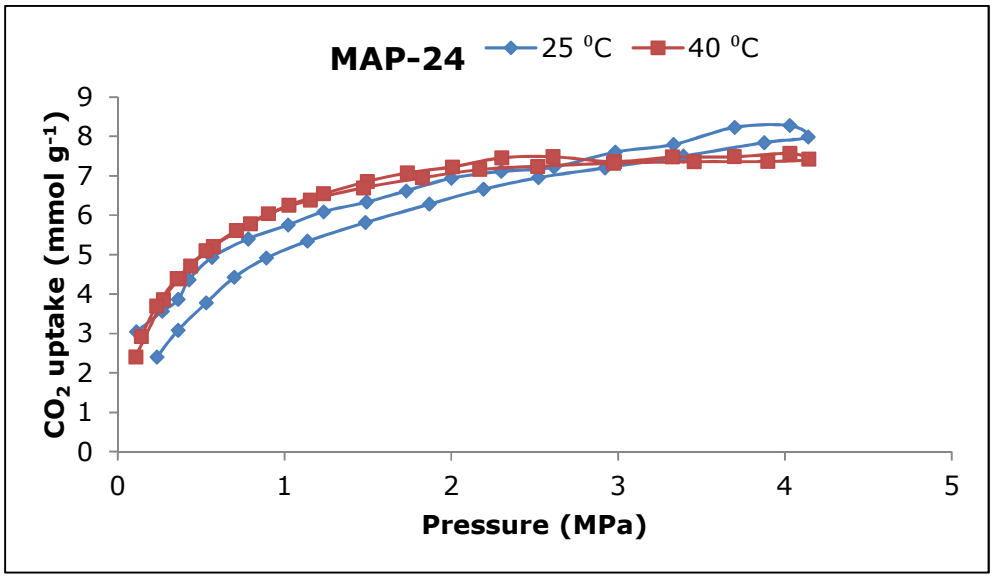

Figure 10.11. Adsorption isotherms for MAP-24 carbons at 25 and 40 °C and pressures up to 4.1 MPa.

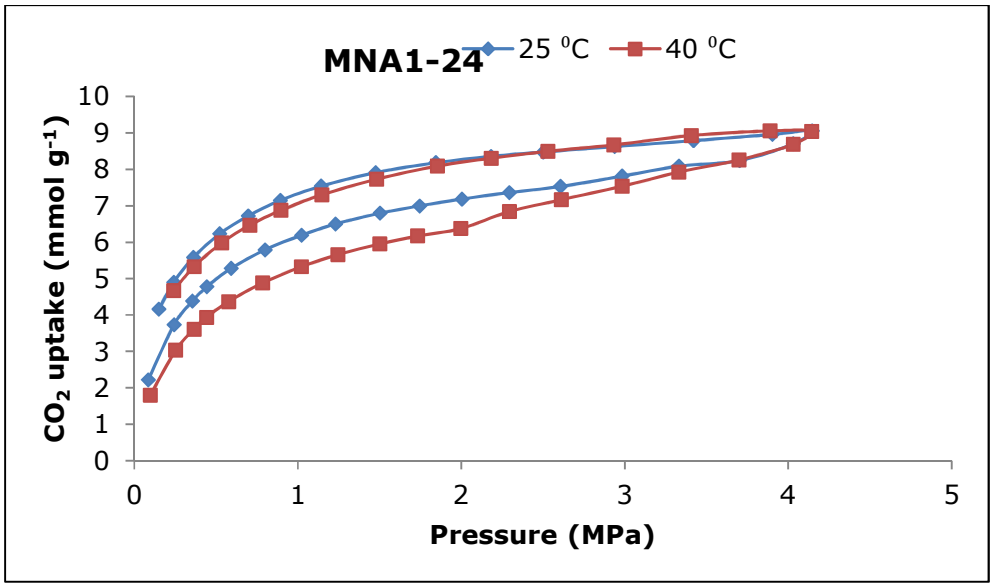

Figure 10.12. Adsorption isotherms for MNA1-24 carbons at 25 and 40 °C and pressures up to 4.1 MPa.

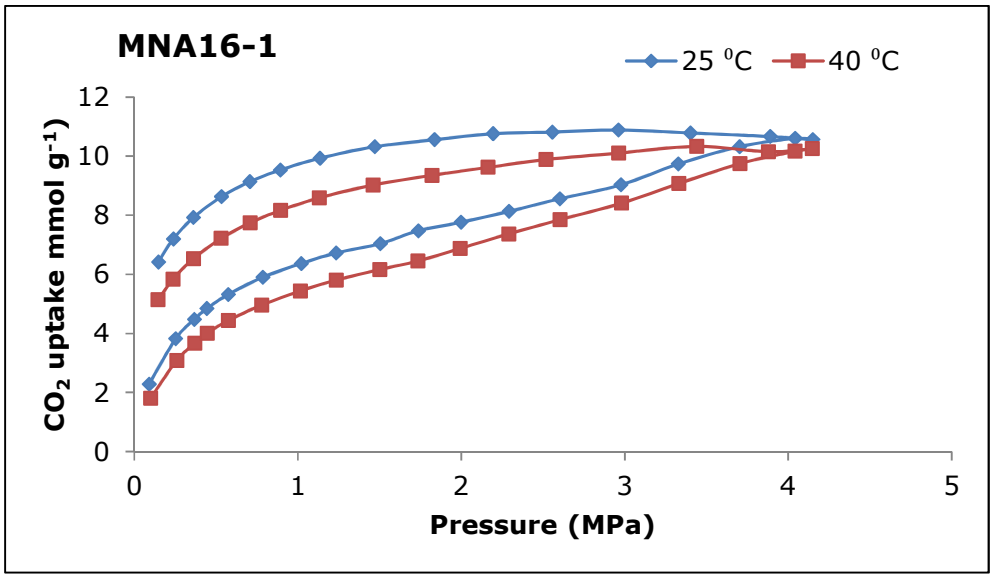

Figure 10.13. Adsorption isotherms for MNA16-1 carbons at 25 and 40 °C and pressures up to 4.1 MPa.

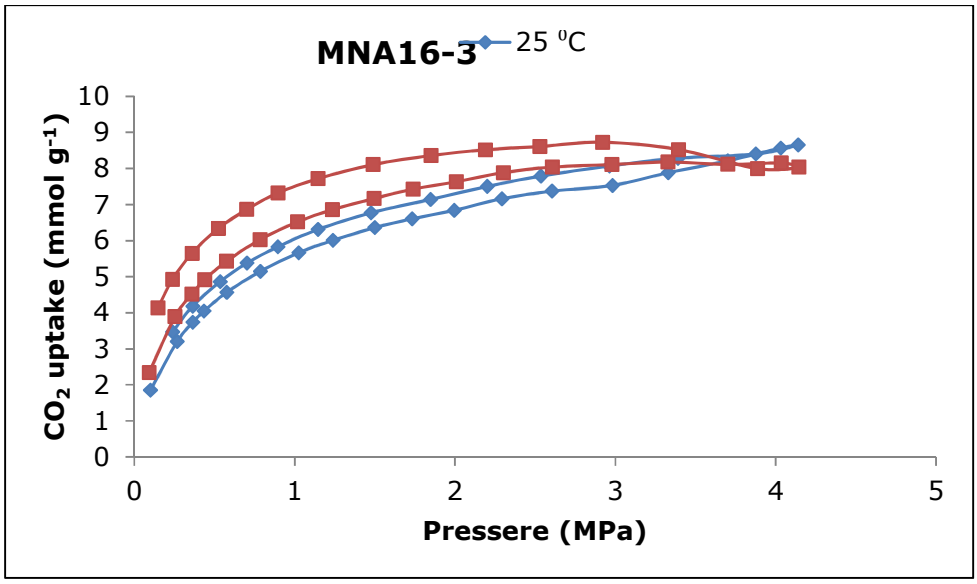

Figure 10.14. Adsorption isotherms for MNA16-3 carbons at 25 and 40 °C and pressures up to 4.1 MPa.

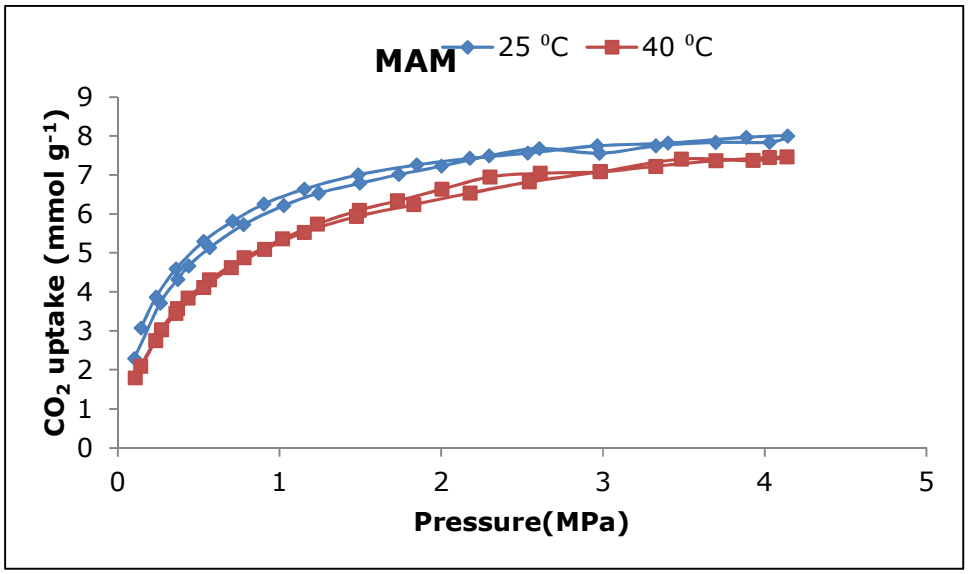

Figure 10.15. Adsorption isotherms for MAM carbons at 25 and 40 °C and pressures up to 4.1 MPa.